



## City Research Online

### City, University of London Institutional Repository

---

**Citation:** Moore, P. J. (1989). Adaptive digital distance protection. (Unpublished Doctoral thesis, City University)

This is the accepted version of the paper.

This version of the publication may differ from the final published version.

---

**Permanent repository link:** <https://openaccess.city.ac.uk/id/eprint/35123/>

**Link to published version:**

**Copyright:** City Research Online aims to make research outputs of City, University of London available to a wider audience. Copyright and Moral Rights remain with the author(s) and/or copyright holders. URLs from City Research Online may be freely distributed and linked to.

**Reuse:** Copies of full items can be used for personal research or study, educational, or not-for-profit purposes without prior permission or charge. Provided that the authors, title and full bibliographic details are credited, a hyperlink and/or URL is given for the original metadata page and the content is not changed in any way.

CONTENTS

CHAPTER 1 INTRODUCTION

1.1 Introduction ..... 21  
1.2 Scope of the thesis ..... 27

CHAPTER 2 BASIC STRUCTURE OF THE DIGITAL DISTANCE RELAY

SIMULATION

2.1 Introduction **ADAPTIVE DIGITAL** ..... 31  
2.2 Relay specifications **DISTANCE PROTECTION** ..... 32  
2.3 Relay setting ..... 37  
2.3.1 Setting strategy ..... 37  
2.3.2 Precision of analogue to digital converter ..... 38  
2.3.3 Equalisation of converted voltage and current values ..... 39  
2.3.4 Current clipping ..... 40  
2.4 Functional structure of the simulation ..... 41  
2.4.1 Formation of the normal current ..... 41  
2.4.2 Cable voltage and current transducers ..... 42  
2.4.3 Data acquisition system ..... 43  
2.4.4 Data processing ..... 44

Submitted by Philip John Moore

For the degree of Ph.D.

Department of Electrical, Electronic and Information  
Engineering

City University, Northampton Square, London EC1V 0HB

April 1989

2.5 Application of the distance relay system ..... 45  
2.5.1 The line equation ..... 47  
2.5.2 Evaluating the line resistance and reactance ..... 48  
2.6 Methods of forming solutions to the line equation ..... 49  
2.6.1 Orthogonal component method ..... 49

## CONTENTS

### CHAPTER 1 INTRODUCTION

1.1 Introduction .....	21
1.2 Structure of the thesis .....	27

### CHAPTER 2 BASIC STRUCTURE OF THE DIGITAL DISTANCE RELAY SIMULATION

2.1 Introduction .....	31
2.2 Relay specification .....	32
2.3 Relay setting .....	32
2.3.1 Setting strategy .....	32
2.3.2 Precision of analogue to digital converter ...	33
2.3.3 Equalisation of converted voltage and current values .....	34
2.3.4 Current clipping .....	35
2.4 Functional components of the simulation .....	36
2.4.1 Formation of the neutral current .....	36
2.4.2 Relay voltage and current transducers .....	36
2.4.3 Anti-aliasing filter .....	37
2.4.4 Time decimation .....	38
2.4.5 Analogue clipping .....	38
2.4.6 Analogue to digital conversion .....	39
2.5 Simulation of the primary system .....	40

### CHAPTER 3 IMPEDANCE MEASUREMENT

3.1 Introduction .....	42
3.2 Basic theory .....	42
3.2.1 The line equation .....	42
3.2.2 Evaluating the line resistance and reactance .	43
3.3 Methods of forming solutions to the line equation ..	44
3.3.1 Orthogonal component method .....	44

## Contents

3.3.2 Enhanced orthogonal component method .....	45
3.3.3 Time spaced solution method .....	46
3.4 Choice of solution extraction technique .....	47
3.4.1 Effect of non-power system frequencies .....	47
3.4.2 Practical considerations .....	49
3.4.3 Method used in the simulation .....	50

## CHAPTER 4 THE RELAY DIGITAL FILTERING FUNCTION

4.1 Introduction .....	51
4.2 Relay filtering requirements .....	51
4.2.1 Travelling wave noise .....	51
4.2.2 Exponential offsets .....	53
4.2.3 Extraneous noise .....	54
4.2.4 Harmonics .....	55
4.3 The prefilter .....	55
4.4 The signal averager .....	58
4.5 Current derivative .....	61

## CHAPTER 5 FAULT EVALUATION

5.1 Introduction .....	64
5.2 Relay characteristic and counting strategy .....	64
5.3 Effect of fault inception angle .....	67
5.3.1 Statement of the problem .....	67
5.3.2 Prevention of overreaching .....	68
5.4 Earth fault elements .....	69
5.4.1 General description .....	69
5.4.2 Residual compensation factor .....	70
5.4.3 Residual current restraint .....	72
5.5 Phase fault elements .....	73
5.5.1 General description .....	73
5.5.2 Phase element restraint .....	74

## Contents

5.6 Close-up faults .....	75
5.6.1 Introduction .....	75
5.6.2 Relay directionality .....	76
5.6.3 Current clipping on close-up faults .....	79
5.7 Miscellaneous functions .....	81
5.7.1 Relay reset .....	81
5.7.2 Invoking the averager .....	81
5.7.3 Low current restraint .....	83
 <b>CHAPTER 6 HIGH RESISTANCE EARTH FAULTS</b>	
6.1 Introduction .....	84
6.2 Relay adaptation .....	87
6.3 Methods of estimating the swivelling angle $\theta$ .....	89
6.3.1 Introduction .....	89
6.3.2 Method 1: assuming $Z_{sq0}$ to be zero .....	89
6.3.3 Method 2: assuming $Z_{sq0}$ and $Z_{sq0}$ to be equal .	90
6.3.4 Method 3: assuming $i_{p0}$ to be in phase with $i_f$	90
6.4 Initial performance studies of $\theta$ estimators .....	91
6.5 Detailed performance studies of $\theta$ estimators .....	93
6.5.1 Relay implementation .....	93
6.5.2 Relay performance for methods 2 and 3 .....	95
6.6 Conclusion .....	97
 <b>CHAPTER 7 POWER SWINGS AND THREE-PHASE FAULTS</b>	
7.1 Introduction .....	98
7.2 Three-phase faults .....	99
7.3 Power swings .....	100
7.3.1 Causes of a power swing .....	100
7.3.2 Effect of power swings on distance relays ...	101
7.3.3 Zones of protection .....	102
7.3.4 Conventional method of power swing blocking .	103

## Contents

7.3.5 A new method of power swing blocking .....	105
7.3.6 Description of algorithm for new PSB method .	107
7.3.7 Performance of new PSB method .....	108
7.4 Conclusion .....	109

## CHAPTER 8 RESULTS

8.1 Introduction .....	110
8.2 Relay accuracy .....	110
8.3 Relay operating time .....	114
8.3.1 Single phase to earth faults .....	114
8.3.1.1 100km line length .....	114
8.3.1.2 250km line length .....	117
8.3.1.3 Effect of prefault load angle .....	118
8.3.1.4 Detailed effect of fault angle .....	119
8.3.2 Phase to phase faults .....	120
8.3.3 Three-phase faults .....	121
8.4 Relay fault resistance coverage .....	122

## CHAPTER 9 SUMMARY AND PROPOSALS FOR FURTHER WORK

9.1 Introduction .....	127
9.2 Summary .....	127
9.3 Proposals for further work .....	136

## 13 Published work

## REFERENCES

## APPENDICES

1	Relationship between primary and secondary impedances .....	138
2	Derivation of the required number of bits of the analogue to digital converter .....	139
3	Derivation of scaling factors for relay voltage and current transducers .....	140
4	Digital simulation of the anti-aliasing filter ....	141
5	Derivation of the recursive digital implementation of a simple R-C circuit .....	142
6	Programmable parameters for primary system simulations .....	143
7	400kV line configuration .....	144
8	Formulation of the current derivative .....	145
9	Derivation of the residual compensation factor ....	147
10	Relationship between D and the current magnitude ..	148
11	Impedance measured by relay for single phase to earth fault .....	150
12	220kV line configuration .....	151
13	Parameters for power swing study .....	152
14	Behaviour of $\sigma$ during three-phase fault conditions	153
15	Published work .....	156

<b>REFERENCES</b> .....	173
-------------------------	-----

## LIST OF ILLUSTRATIONS

- Figure 2.1 Current clipping when CSM = 1.0.
- Figure 2.2 Schematic diagram of relay simulation.
- Figure 2.3 Anti-aliasing filter circuit.
- Figure 2.4 Magnitude responses for real and simulated anti-aliasing filters (a=real, b=simulated).
- Figure 2.5 Arrangement of analogue to digital conversion components.
- Figure 2.6 Primary system model.
- Figure 3.1 Solution formation using orthogonal filters.
- Figure 3.2 Phase, magnitude and impulse responses for 6 point, half cycle, sine function based orthogonal filter.
- Figure 3.3 Phase, magnitude and impulse responses for 6 point, half cycle, cosine function based orthogonal filter.
- Figure 3.4 Magnitude responses for 12 point, full cycle, sine and cosine function based orthogonal filters.
- Figure 3.5 Solution formation by time spacing.
- Figure 3.6 Error in inductance measurement versus power system frequency.
- Figure 4.1 Travelling wave frequency versus distance to fault for small and large source impedances.
- Figure 4.2 Voltage waveforms for 'a' phase to earth fault (Fault angle=90°, fault position=80% of line length, source SCL=5GVA).
- Figure 4.3 Frequency response of a 80 point, full cycle sine wave based impulse response.

## Illustrations

- Figure 4.4 Phase, frequency and impulse responses for the prefilter.
- Figure 4.5 Frequency response of the averager when the window is fully extended to a length of 16 points.
- Figure 4.6 Illustrative operation of the averager for heavily distorted waveforms on 250km line (Fault angle =  $90^\circ$ , fault position = 80% of line length, source SCL = 5GVA, fault type = 'a' phase to earth).
- Figure 4.7 Frequency responses for three methods of formulating the current derivative.
- Figure 4.8 'a' phase line current (a) and its derivative calculated using Equation 4.8 (b) and Equation 4.9 (c) [Line length = 100km, source SCL = 5GVA, fault type = 'a' phase to earth, fault distance = 80km, harmonic level = 5% 7th].
- Figure 5.1 Relay quadrilateral characteristic.
- Figure 5.2 Illustrative operation of the relay counting strategy ('a' to earth element).
- Figure 5.3 Effect of fault inception angle on the convergence of the measured resistance and reactance values.
- Figure 5.4 Relay overreach for fault inception angle of  $40^\circ$  [Source SCL = 5GVA, fault position = 80% of line length, prefault full load exporting from relay point, line length = 100km].

## Illustrations

- Figure 5.5 Extent of overreach for 100km line length with prefault full load exporting ('a' to earth faults).
- Figure 5.6 Calculation of  $d(D.X)/dt$ .
- Figure 5.7 Prevention of overreach by modifying the counter increment (same fault as Figure 5.4).
- Figure 5.8 Percentage error in impedance measurement versus the argument of the residual compensation factor,  $K_{Res}$ .
- Figure 5.9 Percentage error in impedance measurement versus the load angle for 100km line.
- Figure 5.10 Illustrative operation of the relay showing the effect of the residual current function  $D_0$ .
- Figure 5.11 Flow chart for the algorithm used to restrain the phase elements in the presence of non pps current.
- Figure 5.12 Operation of the relay for close-up forward fault.
- Figure 5.13 Operation of the relay for close-up reverse fault.
- Figure 5.14 Effect of clipping on the quantised 'a' phase line current and the measured impedance.
- Figure 6.1 Resistive earth fault on a single phase transmission system.
- Figure 6.2 Sequence component diagram of a two ended system for single phase to earth fault.

## Illustrations

- Figure 6.3 Impedance measured by 'a' phase to earth element for resistive 'a' phase to earth fault at the reach point.
- Figure 6.4a Impedance measured by faulted earth element (Local SCL = 2GVA, remote SCL = 2GVA).
- Figure 6.4b Impedance measured by faulted earth element (Local SCL = 20GVA, remote SCL = 2GVA).
- Figure 6.4c Impedance measured by faulted earth element (Local SCL = 20GVA, remote SCL = 20GVA).
- Figure 6.4d Impedance measured by faulted earth element (Local SCL = 2GVA, remote SCL = 20GVA).
- Figure 6.5 Fixed and adaptive relay characteristics (Adaptive characteristic shown for pre-fault importing load flow).
- Figure 6.6 Performance of 3 methods of estimating the swivel angle on a 10km, 220kV line (Local SCL = 2GVA, remote SCL = 20GVA, full load importing).
- Figure 6.7 Performance of 3 methods of estimating the swivel angle on a 10km, 220kV line (Local and remote SCL's = 20GVA, full load importing).
- Figure 6.8 Component parts of impedance measured by earth element for resistive earth fault at the reach point.
- Figure 6.9 Reach point accuracy of relay, for resistive earth fault, using 2 methods of estimating  $\theta$  (Local SCL = 2GVA, remote SCL = 20GVA).

## Illustrations

- Figure 6.10 Estimation of swivel angle, and its component parts, using method 2 ( $\alpha=1.0$ ) on a 10km, 220kV line (Local SCL = 2GVA, remote SCL = 20GVA, full load importing).
- Figure 6.11 Reach point accuracy of relay, for resistive earth fault, using method 2 ( $\alpha=1.0$ ), on a 10km, 220kV line with  $2.8^\circ$  phase error between primary voltages and currents (Local SCL = 2GVA, remote SCL = 20GVA).
- Figure 7.1 Flow chart for the detection of three-phase faults using the phase elements.
- Figure 7.2 400kV system configuration used to study power swings.
- Figure 7.3 Relay behaviour during power swing.
- Figure 7.4 Locus of impedance measured by relay during power swing.
- Figure 7.5 Zones of protection based on quadrilateral characteristics.
- Figure 7.6 Behaviour of relay with new method of power swing blocking.
- Figure 7.7 Flow chart of algorithm used to differentiate between three-phase faults and power swings.
- Figure 7.8 Flow chart for the detection of three-phase faults including power swing blocking.
- Figure 8.1 Earth fault operating times for 400kV, 100km line cases.
- Figure 8.2 Earth fault operating times for 400kV, 250km line cases.
- Figure A6.1 Impulse response of simulated AA filter.

## Illustrations

- Figure 8.3 Effect of prefault load flow on earth fault operating times for 400kV, 100km line cases.
- Figure 8.4 Earth fault operating time versus fault inception angle for 400kV, 100km line cases.
- Figure 8.5 Phase fault operating times for 400kV, 100km line cases.
- Figure 8.6 Three-phase fault operating times for 400kV, 100km line cases.
- Figure 8.7a Resistive earth fault coverage for adaptive relay on 220kV, 10km line (Local SCL = 2GVA, remote SCL = 2GVA).
- Figure 8.7b Resistive earth fault coverage for adaptive relay on 220kV, 10km line (Local SCL = 20GVA, remote SCL = 2GVA).
- Figure 8.7c Resistive earth fault coverage for adaptive relay on 220kV, 10km line (Local SCL = 20GVA, remote SCL = 20GVA).
- Figure 8.7d Resistive earth fault coverage for adaptive relay on 220kV, 10km line (Local SCL = 2GVA, remote SCL = 20GVA).
- Figure 8.8 Resistive earth fault coverage for fixed characteristic relay on 220kV, 10km line (Local SCL = 2GVA, remote SCL = 20GVA).
- Figure 8.9 Resistive earth fault coverage for adaptive relay on 400kV, 100km line (Local SCL = 5GVA, remote SCL = 50GVA).
- Figure 8.10 Resistive earth fault coverage for fixed characteristic relay on 400kV, 100km line (Local SCL = 5GVA, remote SCL = 50GVA).
- Figure A4.1 Impulse response of simulated AA filter.

## Illustrations

Figure A14.1 Variation of  $\hat{\sigma}$  versus fault angle for each phase element.

Figure A14.2 Variation of  $\hat{\sigma}_{\max}$  versus fault angle for different values of SCL.

Figure A14.3 Variation of  $\hat{\sigma}_{\max}$  versus a) Load angle and b) Fault position.

## LIST OF TABLES

Table 8.1	Distribution of reach point accuracy.
Table 8.2	System conditions resulting in 91% accuracy.
Table 8.3	System conditions resulting in 92% accuracy.
Table 8.4	System conditions resulting in 93% accuracy.
Table 8.5	System conditions resulting in 94% accuracy.
Table 8.6	System conditions resulting in 95% accuracy.
Table 8.7	System conditions resulting in 97% accuracy.
Table 8.8	System conditions resulting in 101% accuracy.
Table 8.9	System conditions resulting in 102% accuracy.

## ACKNOWLEDGEMENTS

It was my good fortune, whilst carrying out the work described in this thesis, to be surrounded by so many excellent friends and colleagues who, in one way or another, helped me greatly. It would, of course, be impossible to acknowledge everyone individually, but there are several people who I would like to extend my deepest thanks to.

I was supervised during this project by Professor Allan T Johns, without whose excellent guidance and spirited enthusiasm I would surely have never achieved what is described herein.

My colleagues in the Power System Research Group were a constant source of inspiration and, in particular, I would like to thank fellow project member [REDACTED] [REDACTED] for his comradeship, and [REDACTED] [REDACTED], for his invaluable assistance in all aspects of the many different computers and programs that were used for this project.

This work was co-operatively sponsored by the SERC and GEC Measurements plc, Stafford, to both of whom I am deeply grateful. GECM also provided me with a wealth of knowledge on the subject of power system protection, in the form of many interesting discussions with their engineers; I would especially like to thank [REDACTED] [REDACTED] [REDACTED] [REDACTED] [REDACTED]

Finally I would like to thank [REDACTED] for her patience and understanding during my absence from home whilst spending many late nights and weekends in the laboratory.

## DECLARATION

This thesis describes the simulation of an adaptive digital distance relay suitable for transmission line protection on line applications up to 250km in length.

The relay calculates the line impedances by solving the first order differential line equation. To remove travelling wave distortion and transformer noise, the relay incorporates an adaptive filtering arrangement. This allows the relay to provide accurate impedance measurement for faulted waveforms which provide discrimination for faulted waveforms which provides discrimination for faulted waveforms for more distorted waveforms.

## COPYRIGHT DECLARATION

I grant powers of discretion to the University Librarian to allow this thesis (ADAPTIVE DIGITAL DISTANCE PROTECTION) to be copied in whole or in part without further reference to me. This covers only single copies made for study purposes, subject to normal conditions of acknowledgement.

The relay incorporates a novel power swing blocking feature where power swings and three-phase faults are reliably distinguished by using a novel arrangement for filter transients which are not present for three-phase faults but not for single phase faults. This arrangement gives the advantage that the power swing period will be determined. A study on part of a 500kV system shows that the relay

Results are presented for reach point accuracy and operating time for single phase to earth, phase to phase and three phase faults, where particular emphasis has been placed on the effect of harmonics, source short circuit impedance, fault location and fault inception angle. Fault coverage is comprehensively investigated and results compare the differences between adaptive and fixed characteristic relays for short and medium line length applications.

P.J.MOORE

LONDON 1989

## ABSTRACT

This thesis describes the simulation of an adaptive digital distance relay suitable for transmission line protection on line applications up to 250km in length.

The relay calculates the line impedance by solving the first order differential line equation. To remove travelling wave distortion and transducer noise, the relay incorporates an adaptive filtering arrangement. This allows the relay to provide ultra-high-speed operation for faulted waveforms which do not require extensive filtering, yet provides discrimination and very-high-speed operation for more distorted waveforms.

To improve the reach point accuracy and fault resistance coverage for high resistance earth faults, the earth element characteristics, which are based on quadrilaterals, are adapted to the prospective fault condition by swivelling the characteristics according to the postfault zero sequence current. It is shown that the resistive to reactive reach ratio of the relay may be set to 3 without gross overreaching of the relay or particular reference to the line application.

The relay incorporates a novel power swing blocking feature where power swings and three-phase faults are reliably differentiated by checking for filter transients which are shown to be always present for three-phase faults but not for power swings. This arrangement gives the advantage that faults occurring during the power swing period will be detected by the relay. A study on part of a 400kV system subjected to a power swing shows that the relay successfully blocks.

Results are presented for reach point accuracy and operating time for single phase to earth, phase to phase and three-phase faults, where particular emphasis has been placed on the effect of harmonics, source short circuit level, prefault loading and fault inception angle. Fault resistive coverage is comprehensively investigated and results compare the difference between adaptive and fixed characteristic relays for short and medium line length applications.

## SYMBOLS AND ABBREVIATIONS USED IN THE THESIS

### Abbreviations

AA = Anti-aliasing

ADC = Analogue to digital converter.

CSM = Current setting multiplier.

CT = Current transformer.

CVT = Capacitor divider voltage transformer.

DFT = Discrete fourier transform.

FFT = Fast fourier transform.

FIR = Finite impulse response.

IIR = Infinite impulse response.

ISA = Ideal swivelling angle.

OC = Orthogonal component.

PSB = Power swing blocking.

QL = Quantisation level.

SCL = Short circuit level.

SIR = System impedance ratio =  $Z_S/Z_1$ .

SH = Sample and hold.

TSS = Time spaced solution.

VT = Voltage transformer.

nps = Negative phase sequence.

pps = Positive phase sequence.

zps = Zero phase sequence.

### Symbols

0,1,2 = relating to zero, positive or negative phase  
sequence (subscripts).

$4\Omega_{sec}$  =  $4\Omega$  secondary value, i.e. as seen by the relay.

$4\Omega_{pri}$  =  $4\Omega$  primary value, i.e. in the primary system.

a,b,c,n = relating to phases a,b,c or neutral (subscripts).

D = Determinant of current matrix (see Equation 3.3).

$h$  = Sampling interval.

INC = Counter increment.

$i_r'$  =  $di_r/dt$ .

$i_{res}$  = Residual current.

$k, n$  = Integer variables.

$K_{res}$  = Residual compensation factor.

$L$  = Inductance.

$R$  = Resistance.

$R_f$  = Fault resistance.

$R_0, X_0$  = Reverse reach point resistance and reactance.

$R_r, X_r$  = Forward reach point resistance and reactance.

$V_a$  = 'a' phase voltage vector.

$v_a$  = instantaneous value of 'a' phase voltage.

$v_a(n)$  =  $v_a$  written explicitly in time sampled form.

$v_r, i_r$  = Voltages and currents measured by relay.

$X$  = Reactance.

$X_m$  = Directional reactance.

$Z_l$  = Line impedance.

$Z_s$  = Source impedance.

$\alpha$  = Proportional position on transmission line ( $0 \leq \alpha \leq 1$ ).

$\alpha_r$  = Reach point value of  $\alpha$ .

$\theta$  = Swivelling angle of relay characteristic.

$\sigma$  = Normalised value of reactance derivative (see

Equation 7.1).

$\omega$  = Angular power system frequency.

CHAPTER I  
INTRODUCTION

1.1 INTRODUCTION

The field of digital distance protection is by no means a new area of research; numerous publications have already resulted. Early papers in this field were concerned with the feasibility of using computers for real time protection such as Mann [1] and McInnes and Harrison [2]. As the use of computers became widespread for various functions, more elaborate techniques were developed. For example, Sanjhar and Cory [3] described a technique of digital distance protection which incorporated a digital filtering technique which eliminated low order noise system harmonics. Hope and Unamathavan [4] described impedance measurement techniques which employed orthogonal filters to facilitate impedance calculation. More recently, the frequency response of such techniques was examined by Hope et al [5] who began to use a Fourier series approach to separate the orthogonal components and who were also concerned with the operating time of the relay and how it influenced the algorithm implementation. It became apparent that the filtering employed in digital relays greatly influenced the operating time, and, since high sampling rates implied expensive hardware, a compromise between analogue and digital filtering had to be found, as described by Sanjhar and Cory [6]. Inevitably, the cost of hardware dropped and, in response, sampling rates increased. Johns and Hartle [7] described an ultra-high-speed protection relay which worked at a sampling frequency of 48KHz. Further to this, the

This thesis is dedicated to my parents,  
for sharing my aspirations.

## CHAPTER 1

### INTRODUCTION

#### 1.1 INTRODUCTION

The field of digital distance protection is by no means a new area of research; numerous publications have already resulted. Early papers in this field were concerned with the feasibility of using computers for real time protection such as Mann [1] and McInnes and Morrison [2]. As the use of computers became accepted for protection functions, more elaborate techniques for impedance measurement resulted. Ranjbar and Cory [3] described a technique of digital distance protection which incorporated a digital filtering technique which eliminated low order power system harmonics. Hope and Umamaheswaran [4] described various impedance measurement techniques which employed orthogonal filters to facilitate impedance calculation, but, importantly, began examining the frequency response of each technique. This work was extended by Hope et al [5] who began to use a Fourier series approach to forming the orthogonal components and who were also concerned with the operating time of the relay and how it influenced the algorithm implementation. It became apparent that the filtering employed in digital relays greatly influenced the operating time, and, since high sampling rates implied expensive hardware, a compromise between analogue and digital filtering had to be found, as described by Ranjbar and Cory [6]. Inevitably, the cost of hardware dropped and, in response, sampling rates increased. Johns and Martin [7] described an ultra-high-speed protection relay which worked at a sampling frequency of 4kHz; further to this, the

digital filtering was based on travelling wave noise considerations and not on harmonic rejection. Now that hardware existed for realistic protection schemes, other considerations developed and Jeyasurya and Smolinski [8] investigated various algorithms with respect to the transient response of the impedance measurement at the fault inception. Alegria et al [9], and many others, considered the use of Kalman filtering, which although computationally complex, provided a faster impedance convergence time when compared against a Fourier filter technique.

Hence, at the time of writing, digital protection is now a mature area. However, a new science of 'adaptive protection' is now emerging. To differentiate 'adaptive protection' from existing protection equipment, which may be described as fixed protection, a definition, due to Horowitz et al [10], is given here:

"Adaptive protection is a protection philosophy which permits and seeks to make adjustments to various protection functions in order to make them more attuned to prevailing power system conditions".

This definition must be interpreted advisedly, since, it could be argued, that an overcurrent relay having an inverse characteristic could be described as adaptive in so much as the operating time is a function of the overload condition and it is clearly advisable to remove severe overloads in a shorter time than marginal overloads. Thus, adaptive protection as used in this context refers to a philosophy which enables a protection relay to operate in a

fashion which is superior to existing fixed protection relays.

Horowitz et al [10] describe the potential benefits of applying adaptive principles to the area of transmission system protection and in particular show how adaptivity may be achieved in multi-terminal transmission line protection, transformer protection and auto-reclosing schemes. Rockefeller et al [11], again in the field of transmission protection, concentrate more in the area of distance protection and show how improved system reliability arises from providing the distance protection with information from a central system impedance model. The concept of an adaptive distribution protection system using a digital overcurrent relay is developed by Shah et al [12] where the time-current characteristic of such a relay is adapted to the relevant loading condition. It is shown that not only an improved protection response would result from adopting this adaptive scheme, but there is also an economic advantage in doing so.

One common characteristic of these adaptive protection schemes, and indeed an implication of the previously stated definition, is that an adaptive relay is provided with more information than was previously supplied to a given relaying function. In its simplest form, this may be achieved by stand-alone relays to which data is transmitted from a central computer prior to the fault as proposed by Rockefeller [11]; the operation of the relay does not require the data during the fault. A more complicated arrangement of providing relays with extra data lies in the

concept of a hierarchical substation computer system, as described by Phadke in Chapter 5 of reference 13.

Doubtlessly, within time, concepts such as these will increasingly find their way into the substation environment. However, at the present time, there is still an important role to be played by an adaptive protection relay which is not provided with any more information than its fixed counterpart. Such an adaptive relay may be classed as an 'independent stand-alone' in so much as its adaptive features derive, not from any outside controlling influence, but from a more detailed analysis of the existing information presented to it.

It will be apparent that the field of adaptive protection per se has arisen due to the advent of cheaper and more powerful microprocessors [14], and through the development of better media through which computers are able to communicate with each other. The most relevant example of this latter point is the growth of fibre optic communications [15]. Thus, with respect to better microprocessors, the independent stand-alone relay can now be capable of extensively processing the information presented to it, and through this, providing a protection function which is superior to existing fixed relays.

The independent stand-alone adaptive relay has the benefit that it may be installed in place of an existing relay at this point in time, i.e. there is no requirement to wait for the advent of the hierarchical substation computer concept. A further attraction of the stand-alone adaptive relay will exist if it is shown that the relay may be

placed in service without any specific reference to the system it is protecting, i.e. the relay is application independent. It is an independent stand-alone adaptive distance relay which is the topic of this thesis.

The adaptivity of the relay to be described here lies in three areas. Firstly, the relay has an adaptive filtering function which allows it to be applied to line applications of up to 250km without any adjustment; for strong source situations, the relay is capable of ultra-high-speed operation, the benefits of which are well known [16]. Secondly, the relay is provided with adaptive earth elements which adjust, under high resistance earth fault conditions, to give relay operation which is discriminative, i.e. is not prone to gross overreaching or underreaching, and affords good fault resistance coverage. A study of a wide variety of system configurations have shown that the adaptive earth elements are not unduly sensitive to the particular configuration. Both this first and second point exemplify the idea of the relay being application independent. Thirdly, the relay is able to reliably differentiate between three-phase faults and power swings to an extent that its performance under power swing conditions is superior to conventional distance relays with power swing blocking. This third feature, although not being described overtly as an adaptive function, does embody the basic principle of the independent stand-alone relay in that it achieves power swing blocking through greater analysis of the information presented to it.

A recent paper by Zhang and Chen [17] described the

application of adaptive principles to a distance relay in the context of, what is described here as being, independent and stand-alone. Without decrying some of interesting features of this paper, the following criticisms are levied. Firstly, the authors devoted much attention to an adaptive sampling interval with the aim of reducing the error in reactance measurement under power system frequency variations. Had the authors realised that the fundamental problem was in their choice of impedance measuring algorithm then it would be apparent that there is no need for adaptive sampling in a distance relay. The algorithm described in this thesis is completely insensitive to small variations in the power system frequency. This criticism is not meant to imply that the field of adaptive sampling is irrelevant since it clearly does have implications for others protection areas, e.g. volt/hertz relays [18]. Secondly, the adaptive earth elements are set with reference to the source impedances of the line application. This detracts from the idea of adaptive protection being application independent, unlike the work described herein.

Zhang and Chen's paper [17] does however have the distinction of being the first published work which is entirely directed to the field of stand-alone adaptive digital distance protection, although several authors have specifically addressed the problem of high resistance faults [19,20,21]. The primary objective of the work described in this thesis is to make a significant step forward in this field.

## 1.2 STRUCTURE OF THE THESIS

A brief description of the Chapters contained within this thesis is given here.

Chapter 2 states the desired relay specifications and outlines the structure of the relay simulation with respect to the hardware that the simulation is emulating. The relay setting strategy is discussed in relation to the resolution of the analogue to digital converter and the need for an adjustable setting on the current inputs. A brief description of the primary power system simulations used to test the relay are included.

The algorithm used to evaluate the line impedance from the sampled voltage and current samples is described in Chapter 3. Three approaches to solving the first order differential line equation are discussed and evaluated by considering the presence of non-power system frequencies on the input measurands. It is shown that a time spaced solution approach to solving the line equation is the best method.

Following on from the impedance measurement, the necessity for digitally filtering the input measurands, and an optimal arrangement of digital filters for achieving the best compromise between rejection of non-power system frequencies and speed of the post-fault impedance convergence is described in Chapter 4. It is shown that an arrangement of a finite impulse response prefilter applied to the voltage and current waveforms, and a variable length adaptive signal averager applied to the measured resistance and reactance values is capable of producing satisfactory impedance measurements from heavily corrupted primary

system waveforms. A discussion on techniques for evaluating the current derivative, as required by the impedance measurement algorithm, is also described in this Chapter.

Chapter 5 describes how the relay, having calculated the line impedance, then evaluates whether or not the impedance represents a fault for which a trip action is required. This is achieved by the use of a quadrilateral characteristic and a counting strategy which is dependent on the position of the measured impedance within the characteristic. It is described how three residually compensated elements are provided for the detection of earth faults, and similarly, three elements are used to detect phase faults. The detection of three-phase faults is discussed in Chapter 7. An important aspect of Chapter 5 is the effect that the fault inception angle has on the trajectory of measured impedance. It is shown that overreaching is a possibility for some values of fault inception angle and a technique for completely eliminating overreaching due to this effect is proposed. This technique involves adapting the counting strategy to reflect the certainty of the impedance measurement. Finally, the Chapter describes the operation of the relay under forward and reverse close-up fault conditions.

The description of the earth elements in Chapter 5 only covers the basic fixed characteristic element which will not provide satisfactory relay operation under high resistance earth fault conditions. The concept of an adaptive earth element is introduced in Chapter 6. Chapter 6 begins with an evaluation of the errors of impedance

## Chapter 1

measurement under resistive earth fault conditions and describes how an adaptation of the earth element characteristic may enhance relay operation under such conditions. The key to the adaptation involves swivelling part of the characteristic through an angle which is a function of the primary system parameters. The rest of the Chapter is devoted to finding the best method of estimating the swivelling angle and it is shown that a simple approach involving a function of the residual current gives the best method of estimation.

Chapter 7 investigates the area of power swings and shows how a distance relay may unnecessarily operate under power swing conditions which result in the measured impedance passing through the relay characteristic. Due to the similarity, as perceived by the relay, between three-phase faults and power swings, a technique is proposed which enables the relay to differentiate between these two conditions. Although techniques already exist for blocking distance relay operation during power swings, the new technique proposed here has the advantage that the relay can detect, and trip for, developing faults which may occur during the power swing period. Results are presented for a power swing simulation study on a 400kV system configuration which show that the relay blocks in an ideal manner for severe power swings which result in pole slips.

Chapter 8 is entirely devoted to the results of the new adaptive relay when subjected to single phase to earth, phase to phase clear of ground and three-phase fault types. Particular attention is placed on the reach point accuracy,

## Chapter 1

relay operating time and high resistance fault coverage. The effect of fault inception angle, prefault load flow, fault position, harmonics and system parameters, i.e. line length and source short circuit levels, are considered. It is shown that the relay accuracy is to within the specifications given in Chapter 2 and that the relay is capable of ultra-high-speed operation. The operating area of the relay under high resistance earth faults is presented for both 400kV and 220kV systems and a comparison between adaptive and fixed characteristic relays is made where it is shown that the adaptive characteristic affords superior operation in terms of overreaching and fault resistance coverage.

Chapter 9 concludes the thesis and provides a summary of the work described herein. Several proposals for further work are presented.

Throughout the thesis, a distinction is made between primary and secondary values. Primary values refer to the actual voltages and currents which are present in the power system being protected (this is sometimes referred to as the primary system). Secondary values refer to voltages and currents which are fed into the relay device, i.e. primary values which have been transformed to levels suitable for

## CHAPTER 2

### BASIC STRUCTURE OF THE DIGITAL DISTANCE RELAY SIMULATION

#### 2.1 INTRODUCTION

The relay to be described in the forthcoming Chapters has been simulated on a microVAX II computer using the FORTRAN programming language. The purpose of this Chapter is to, firstly, describe the relay specifications and setting strategy and examine how these influence the design of the relay and, secondly, describe how some of the more basic components of the simulation have been realised digitally. Finally, a section is included to describe the simulation of the primary system.

Great care has been taken throughout this work to ensure that the simulation emulates, as closely as possible, realistic hardware. The hardware is assumed to consist of a 16 bit microprocessor complete with ROM, RAM and all other necessary peripherals enabling communication with the outside world. Since this thesis describes work which is mainly of an algorithmic nature, no great detail is presented here of the specific hardware requirements; a competent discourse on digital relay hardware may be found in references 13 and 22.

Throughout the thesis, a distinction is made between primary and secondary values. Primary values refer to the actual voltages and currents which are present in the power system being protected (this is sometimes referred to as the primary system). Secondary values refer to voltages and currents which are fed into the relay device, i.e. primary values which have been transformed to levels suitable for

relaying. Since the transformation ratios of the voltage and current are not necessarily the same, an impedance in the primary system will differ in magnitude when expressed in secondary quantities. Appendix 1 describes the relationship between primary and secondary impedances and gives details of the transformation ratios used throughout the thesis.

## 2.2 RELAY SPECIFICATION

The operating limits of the relay are given below:

Setting impedance (secondary ohms): 0.5 - 240  $\Omega$

Minimum input to relay (V and I): 1V and 0.25A

Maximum line length: 250km

Operating time: < 10ms for 75% of reach

Accuracy:  $\pm 5\%$  for SIR's up to 30

$\pm 10\%$  for SIR's 30 - 60

an addition  $\pm 5\%$  allowed for 5% harmonic level

Overvoltage factor: 1.8

Sampling frequency: 4kHz

Power system frequency (50Hz nominal): 47 - 53Hz

Additionally, the following specifications are relevant to the simulation:

Minimum source SCL: 0.5GVA

Maximum source SCL: 50GVA

## 2.3 RELAY SETTING

### 2.3.1 Setting Strategy

In a conventional static distance relay, the input voltage and current signals are scaled in order to adjust the reach point position on the line which the relay is protecting. A

relay of this type operates by effectively comparing the scaled voltage/current quotient with a fixed reference impedance; the true impedance presented to the relay is never actually evaluated. The impedance of the line between the relaying position and the reach point is referred to as the **setting impedance**.

With a true algorithmic microprocessor based relay, scaling the input measurands in this fashion is no longer necessary since the relay calculates an actual impedance value and thus the reach point setting may be implemented in software. To answer fully the question of relay setting, it is necessary to consider how the input measurands are converted to digital values, i.e., how many bits of analogue to digital converter precision are required and at what point are the converted current and voltage values equalised in magnitude.

### 2.3.2 Precision of analogue to digital converter

The precision, or number of bits required, of the analogue to digital converter (ADC) is a function of the dynamic range of the input voltage and current signals. In deciding on the precision required, the current channel was taken to be the limiting measurand since, unlike the voltage, it is possible to have a fully offset current input for faults occurring with an inception angle close to zero. Appendix 2 shows that at least 15 bits are required to resolve the dynamic range of the current channel adequately. Commercially, only 14 or 16 bit devices are available, so it would be necessary to use a 16 bit converter in order to effect correct relay operation without any adjustable

scaling. However, since the simulation was being used to facilitate the development of hardware, the use of a 16 bit ADC was rejected for the following reasons:

- a) at the project inception there were no realistically priced 16 bit ADC's available on the market, and,
- b) the use of a 16 bit ADC would necessitate a signal to noise ratio of 96dB on the analogue input stages of the relay. In view of the relay being situated in the electrically harsh environment of a substation, a 96dB signal to noise ratio was considered to be unrealistic on both practical and economic grounds.

Hence, the approach taken was to use a 14 bit ADC with a switchable current setting multiplier. The arrangement of the multiplier setting with respect to the setting impedance is given below:

Current setting multiplier	Setting impedance range
X1.0	4 - 240 $\Omega_{sec}$
X0.25	0.5 - 4 $\Omega_{sec}$

Note that there are situations where the current will exceed the range of the ADC, this is dealt with in section 2.3.4.

### 2.3.3 Equalisation of converted voltage and current values

From the specifications given in section 2.2, it can be seen that the minimum voltage and current signals for correct operation of the relay correspond to an impedance of 4 $\Omega_{sec}$ . Since this is the limiting point of relay operation, in order to afford the required accuracy, the

quantised voltage and current signals internal to the relay are equalised at this point. Thus, if the accuracy is acceptable at the point of minimum voltage and current, then the accuracy will be at least as good under any other condition. Hence, with this setting strategy and knowledge of the overvoltage factor, the relationship between secondary signals and their quantised counterparts may be derived as described in Appendix 3.

#### 2.3.4 Current Clipping

Section 2.3.2 showed that under the most arduous conditions of the minimum setting impedance, i.e. the largest magnitude of current, the ADC will correctly digitise the input measurands. However, since this analysis has been based on the setting impedance, it is only pertinent to faults at the reach point, where the accuracy must necessarily be high. Attention must now be paid to faults occurring within the protected zone of the relay where, although accuracy need not be so great, the relay must still operate correctly.

Faults that occur close to the busbar where the source capacity is large are at risk of the current magnitudes exceeding the limits of the ADC and thus leading to clipping. It can be shown that with a current setting multiplier (CSM) of 0.25, even with a fault on the busbar in the protected zone, the relay will not clip. However, with the CSM set at 1.0, current clipping will occur for close-up faults. This is shown in Figure 2.1 which shows that current clipping is a function of the distance to fault and the source SCL. With the CSM set at 1.0, the

minimum setting impedance is  $4\Omega_{sec}$ , which at 400kV corresponds to 23km of line. Since current clipping can occur only up to 16km distant from the relay, it can be seen that the incidence of current clipping always occurs under a fault situation. This fact will be exploited for close-up faults where it is only necessary to detect the presence of current clipping in order for the relay to trip.

## 2.4 FUNCTIONAL COMPONENTS OF THE SIMULATION

A schematic diagram of the simulation is shown in Figure 2.2, where each functional part of the simulation has been represented in a block. The blocks titled 'Pre-filter' and 'Impedance measurement & Protection algorithms' form the bulk of the thesis, so no explanation of these blocks will be given in this section. A detailed discussion of the remaining blocks will now follow.

### 2.4.1 Formation of the neutral current

This block is not part of the relay since in practice a relay is provided with a neutral current direct from a separate CT. However, for the purposes of this simulation, the input to it, i.e. the simulation of the primary system, is assumed to consist of the 3 phase voltages,  $v_a$ ,  $v_b$  and  $v_c$ , and the 3 line currents,  $i_a$ ,  $i_b$  and  $i_c$ , all expressed in secondary values. Thus, it is necessary to calculate the neutral current  $i_n$  by the vector summation of the line currents, hence,

$$i_n = i_a + i_b + i_c$$

### 2.4.2 Relay voltage and current transducers

These devices account for the secondary voltage and current

signals being transformed down to a low voltage level suitable for manipulation by the relay electronics. This low voltage level will be referred to as the **relay signal voltage** level and is assumed to be  $\pm 10V$ . In the case of the current, the transducer is assumed to act as a trans-resistance, i.e. the current is converted into a corresponding voltage. In reality these transducers would also isolate the relay from the substation environment. The frequency responses of these transducers are assumed to be ideal. Details of the scaling factors used to convert between secondary values and the relay low voltage values are given in Appendix 2.

### 2.4.3 Anti-Aliasing Filter

The purpose of the anti-aliasing filter is to remove high frequency components on the input measurands before the signals reach the analogue to digital converter. If this is not done, frequencies which are greater than half the sampling frequency of the relay may be 'folded' down to lower frequencies and affect the operation of the relay. A more detailed explanation of this effect may be found in reference 10. The relay samples at 4kHz and hence the anti-aliasing filter must remove all frequencies above 2kHz. In order to simulate this device accurately, the input data must be sampled at a rate of at least twice the relay sampling rate of 4kHz. In the simulation, the input data to the anti-aliasing filter is sampled at 8kHz allowing the filter to act on frequencies in the range 2-4kHz.

The circuit diagram of the anti-aliasing filter used for this work is shown in Figure 2.3. The filter was modelled

as a finite impulse response (FIR) filter [23-26] by using the impulse invariant technique as described in Appendix 4. The frequency domain magnitude responses of the real and simulated filter, calculated using an FFT program, are shown in Figure 2.4. It can be seen that the simulation is reasonably accurate with the simulated hf rejection inferior to that of the analogue circuit. Whilst the hf rejection properties of the simulated filter are not ideal in the range 2-4kHz, the hf rejection becomes better for frequencies close to 4kHz. This is a desirable property, since it is only frequencies close to 4kHz which will be folded down to frequencies close to 50Hz and potentially affect relay operation.

#### 2.4.4 Time Decimation

This process is also not part of the relay, but accounts for the change in sampling frequency that is necessary to accurately simulate the anti-aliasing filter as described in section 2.4.3. Thus, in order to change the sampling frequency (a process known as time decimation [26]) from 8kHz to 4kHz, every other sample in a discrete time series is discarded. Thus, the time series input,

$x(0), x(1), x(2), x(3), x(4), x(5), x(6), x(7), x(8), x(9)$   
would become,

$x(0), x(2), x(4), x(6), x(8)$

after decimation.

#### 2.4.5 Analogue Clipping

This stage of the simulation accounts for input signals which, having passed through the relay input transducers, have values greater than the relay signal voltage levels of

$\pm 10V$ . It is assumed that a protection circuit exists to prevent damage to the relay electronics in this event, and will, hence, clip such signals. Thus, the output of this stage is bounded in the range  $-10V$  to  $+10V$ .

#### 2.4.6 Analogue to Digital Conversion

Figure 2.5 shows the detailed arrangement of the components comprising the box labelled 'ANALOGUE TO DIGITAL CONV.' in Figure 2.2. It can be seen that the input signals are multiplexed before being applied to a sample and hold (SH) amplifier and, finally, the analogue to digital converter (ADC). The SH amplifier is used to prevent signal variation during the finite conversion time of the ADC.

From a simulation point of view, this arrangement of the conversion components may be considered as an ideal ADC, where the relay signal voltage values are linearly mapped to the corresponding digital value. Thus, with a 14 bit ADC, an analogue value of  $+10V$  will be converted to a digital value of  $2^{13}-1$ , or  $+8191$ . In the simulation, all analogue values are represented by floating point arithmetic, whilst integer arithmetic is used for digitally converted values.

Whilst the whole of the A to D conversion process was considered to be ideal, a mention needs to be made of the conversion time of the ADC. This was taken to be  $25\mu s$  which is relatively small compared to the sampling interval of  $250\mu s$ , at  $4kHz$ . Due to the sequential sampling arrangement of Figure 2.5, within any one sampling interval, the POW of the first signal to be sampled will lag that of the last signal by  $150\mu s$ . For  $50Hz$  signals, this can lead to an

apparent phase error of  $2.7^\circ$  between the first and last samples. This effect was not modelled since it is possible, and will be necessary in the hardware realisation, to compensate for it using a simple linear interpolation technique.

## 2.5 SIMULATION OF THE PRIMARY SYSTEM

The primary system input to the relay simulation, i.e. the signals  $i_a$ ,  $i_b$ ,  $i_c$ ,  $v_a$ ,  $v_b$  and  $v_c$  in Figure 2.2, come from one of two digital simulations of faulted power networks. In both simulations the primary system was simulated as a two ended model as shown in Figure 2.6. The voltage and current signals are calculated, at a 8kHz sampling rate, for the relay location, at busbar P. A description of the parameters which can be programmed into the primary system simulations is given in Appendix 6.

There were two programs used to simulate the primary system, these were:

- a) A simulation based on the work of Johns and Aggarwal [27]. This is a frequency-domain simulation based on a distributed parameter model and models the effects of non-ideal transposition of the conductors and travelling wave distortion of the signals. Details of the line configuration are given in Appendix 7. The primary system voltage transducer is modelled, in the frequency domain, as a CVT [28]. The primary system current transducer is assumed to be ideal. This simulation will be referred to as the **distributed parameter model**.

b) A frequency-domain simulation based upon a lumped parameter model. This simulation is essentially a rudimentary form of the distributed parameter model where the lines are assumed to be ideally transposed and no account is made of travelling waves. The simulation also models the effect of harmonics. Both the voltage and current transducers of the primary system are assumed to be ideal. This simulation will be referred to as the lumped parameter model.

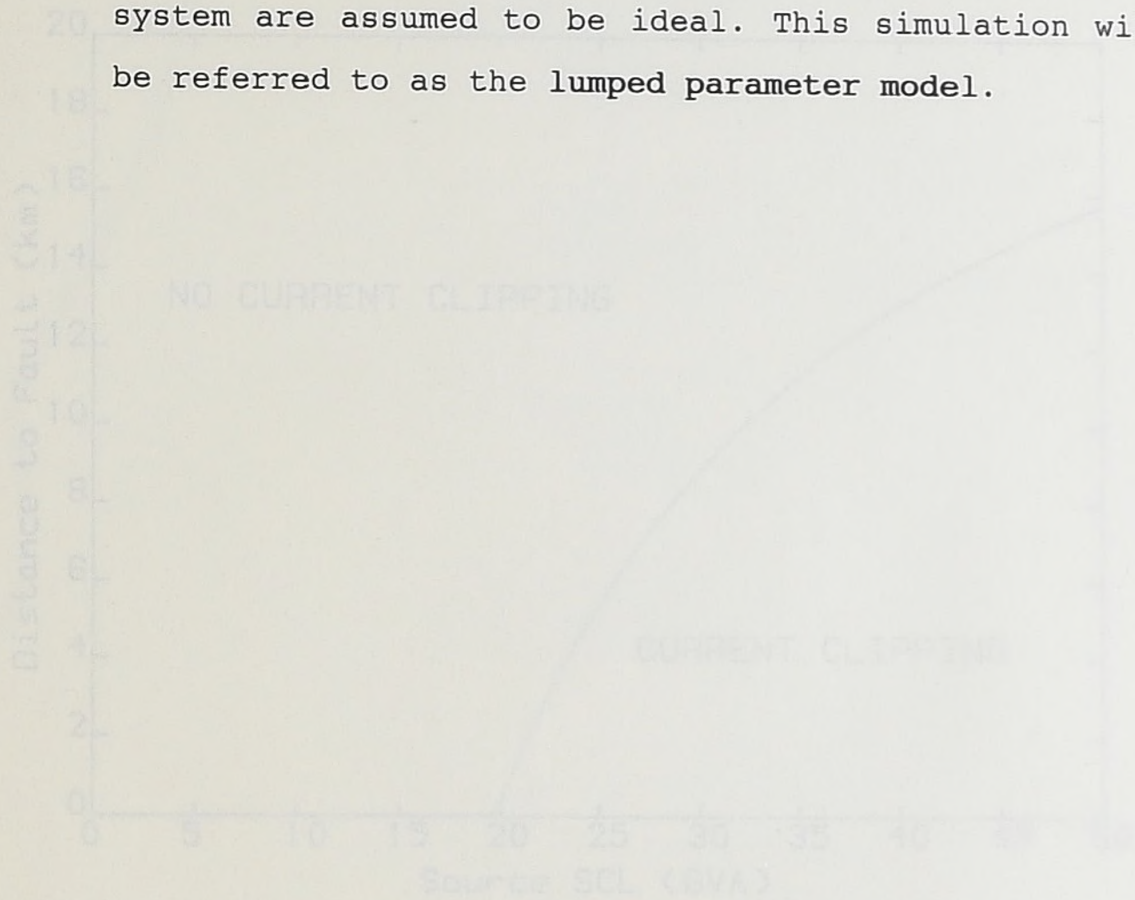


Figure 2.1 Current clipping when  $OSM = 1.2$

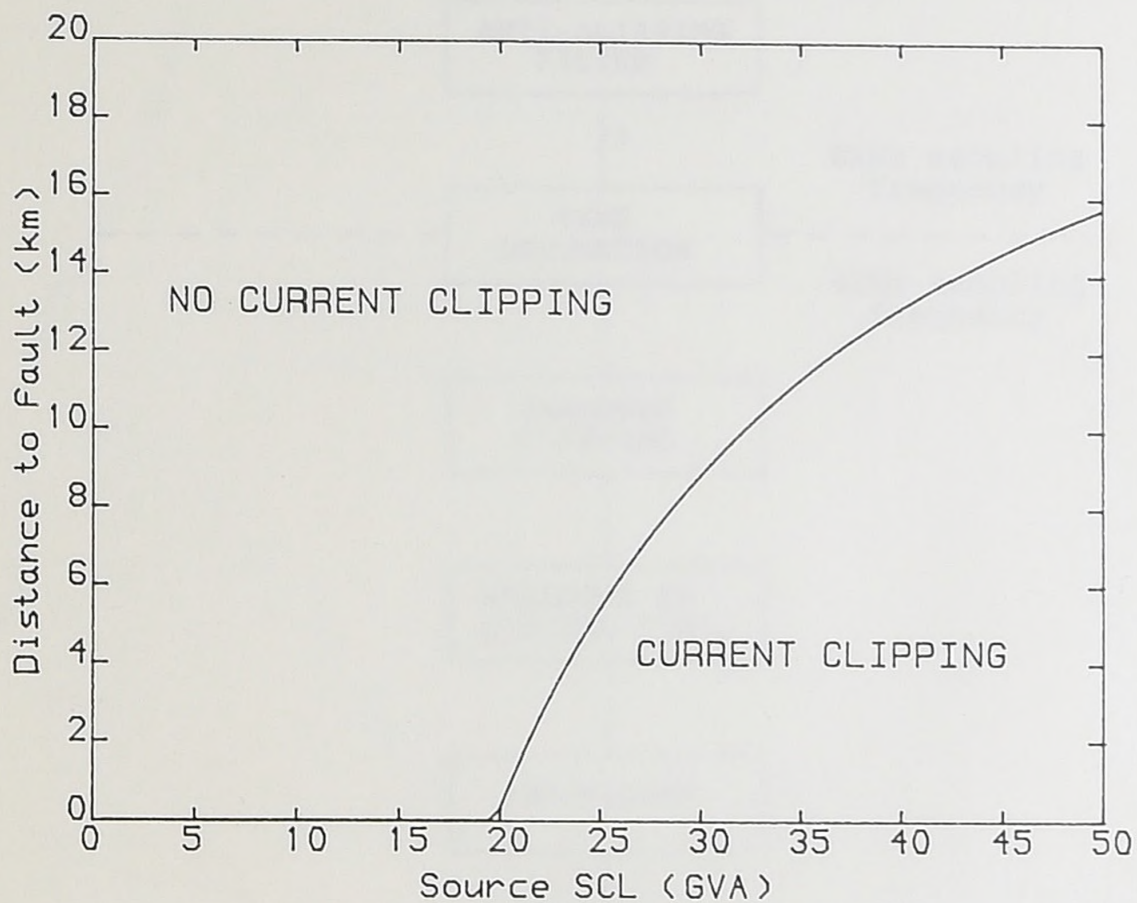


Figure 2.1 Current clipping when CSM = 1.0

Figure 3.2 Schematic Diagram of Relay Algorithm

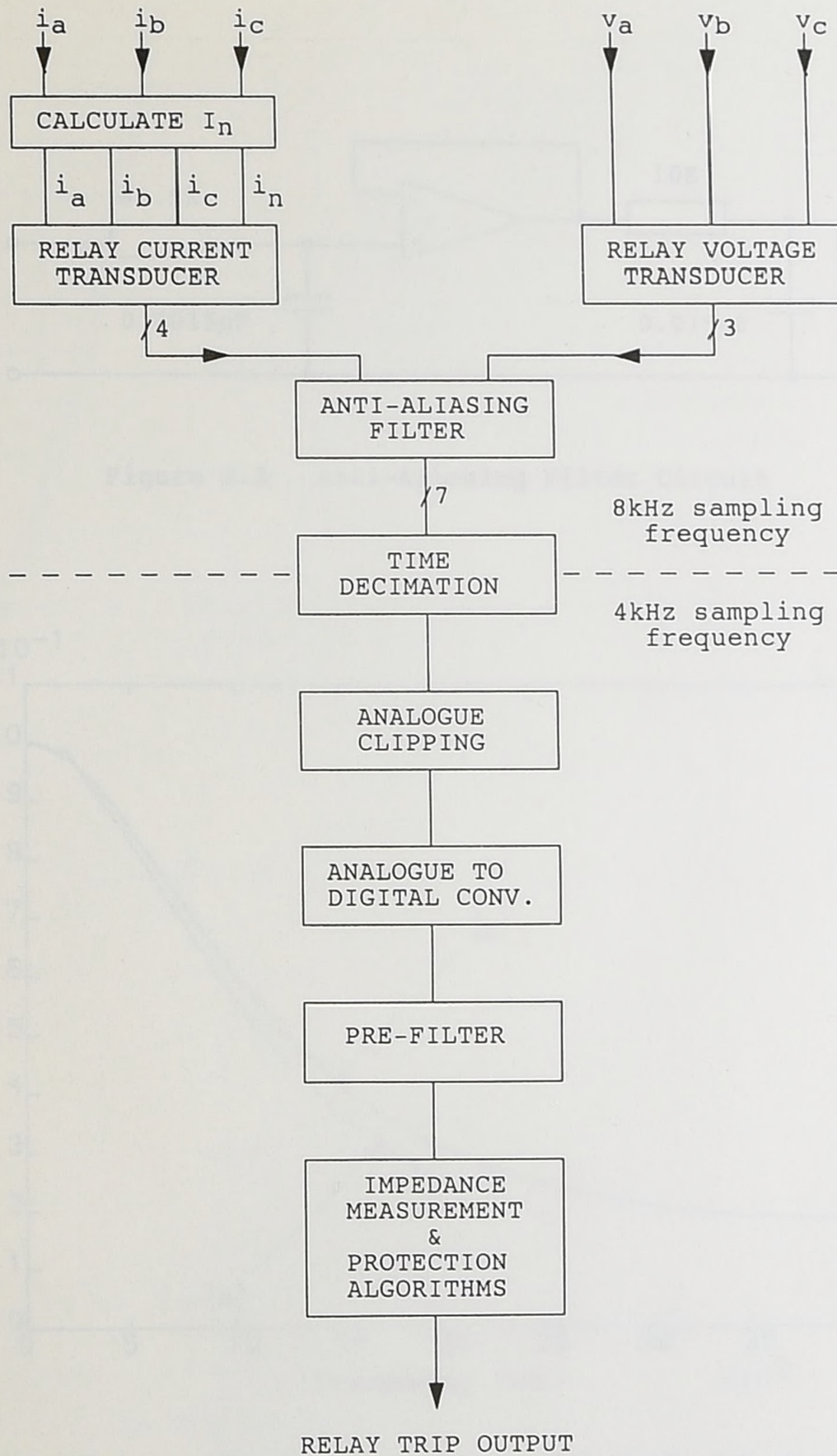


Figure 2.2 Schematic Diagram of relay simulation

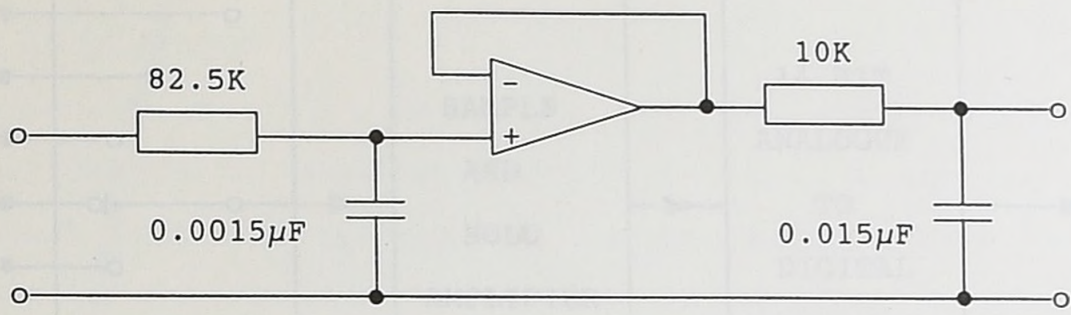


Figure 2.3 Anti-Aliasing Filter Circuit

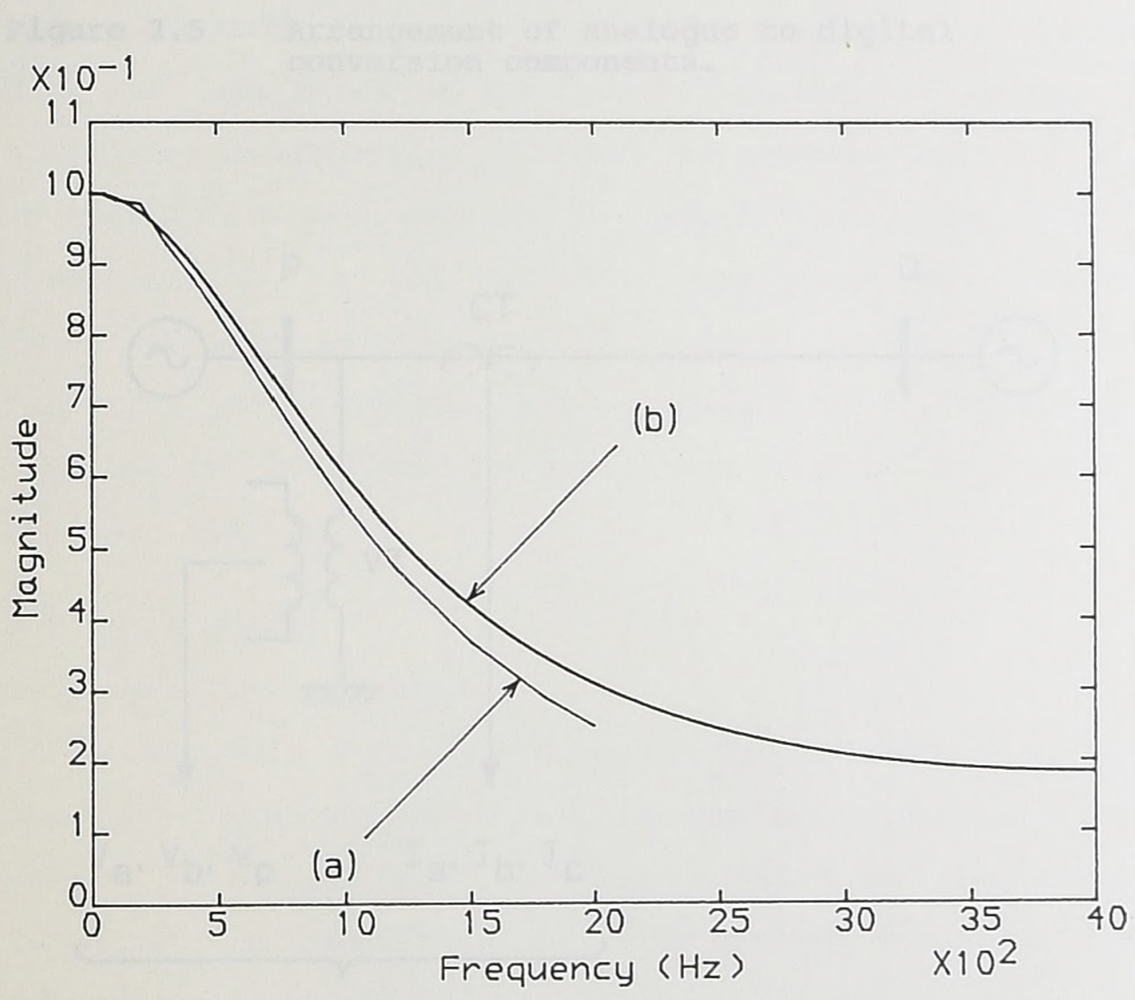


Figure 2.4 Magnitude responses for real and simulated anti-aliasing filters (a=real, b=simulated).

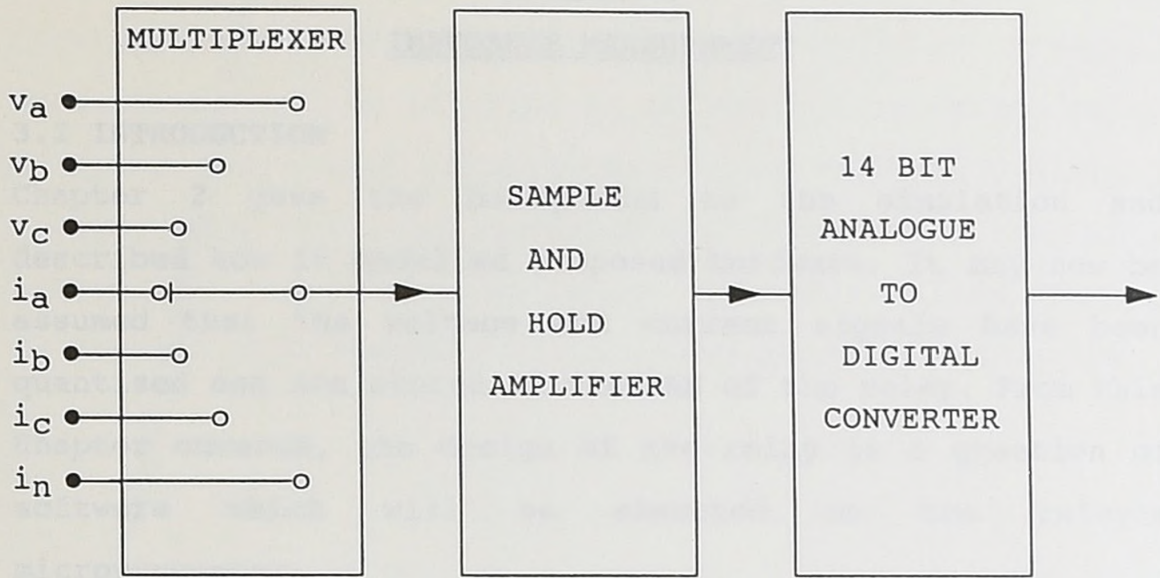


Figure 2.5 Arrangement of analogue to digital conversion components.

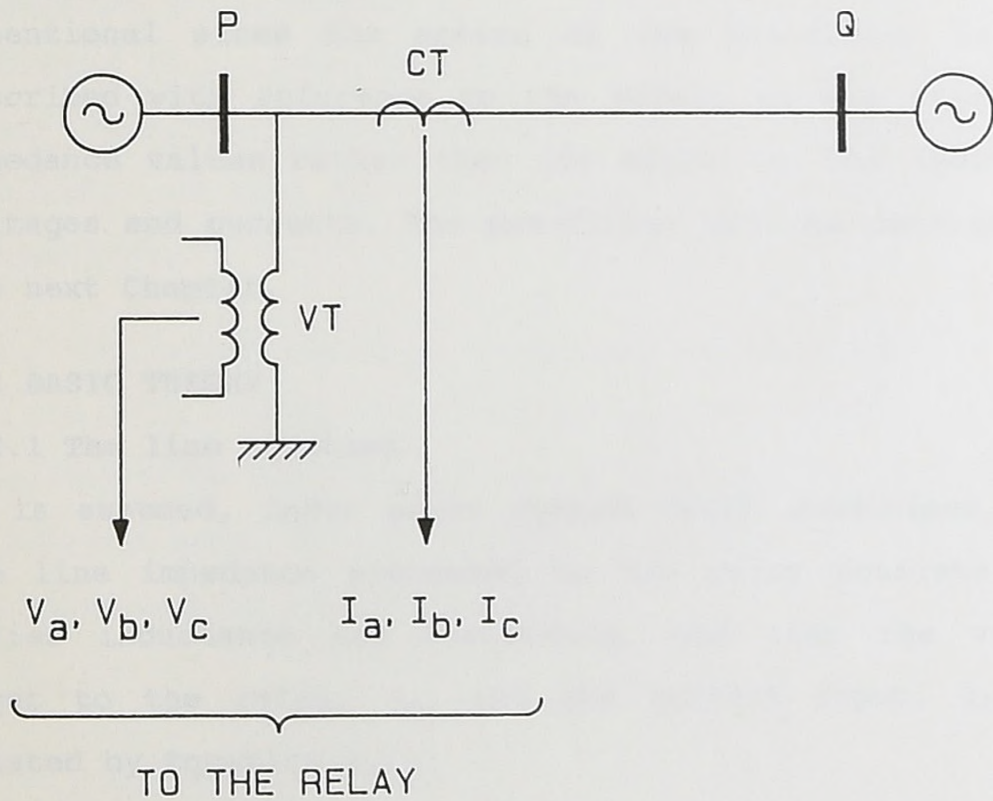


Figure 2.6 Primary system model

## CHAPTER 3

### IMPEDANCE MEASUREMENT

#### 3.1 INTRODUCTION

Chapter 2 gave the background to the simulation and described how it modelled proposed hardware. It may now be assumed that the voltage and current signals have been quantised and are stored in the RAM of the relay. From this Chapter onwards, the design of the relay is a question of software which will be executed on the relay's microprocessor.

With reference to Figure 2.2, this chapter is concerned with the last block of the simulation, on the subject of 'impedance measurement'. It will be noticed that, so far, no mention has been made of the 'pre-filter' block. This is intentional since the action of the pre-filter is best described with reference to its effect on the calculated impedance values rather than its effect on the individual voltages and currents. The pre-filter will be described in the next Chapter.

#### 3.2 BASIC THEORY

##### 3.2.1 The line equation

It is assumed, under power system fault conditions, that the line impedance presented to the relay consists of a series inductance and resistance, and thus the voltage input to the relay,  $v_R$ , and the current input,  $i_R$ , are related by Equation 3.1:

$$v_R = R.i_R + L.i_R' \quad \dots\dots\dots 3.1$$

where R and L represent the resistance and inductance from

the relay to the fault point, and  $i_r' = di_r/dt$ . It is problematic whether this assumption is true under unfaulted situations, so long as there is no possibility of the relay tripping under such situations. In the case of a lightly loaded, long line, the impedance will doubtlessly contain a substantial capacitive component. However, as the Chapter on results will justify, no relay maloperation will occur.

Since there is one controlling equation, 3.1, and two unknowns, R and L, it is necessary to find two solutions to Equation 3.1. Whilst a lot of literature has been written on the subject of impedance measurement for power system protection [1-4,7-9,29,30], all the approaches described essentially solve Equation 3.1 by providing two linearly independent solutions from the sampled data. Two approaches to providing solutions to Equation 3.1 will be discussed in the next Section, but, for the purposes of the basic theory, it will be assumed that the two solutions are available and they will be denoted by subscripts 1 and 2 respectively.

### 3.2.2 Evaluating the line resistance and reactance

The analysis, described by Johns and Martin [7], used to form equations for the resistance (R) and the reactance (X) is adopted here. In matrix form, Equation 3.1 and its two solutions may be expressed as:

$$\begin{bmatrix} v_{r1} \\ v_{r2} \end{bmatrix} = \begin{bmatrix} i_{r1} & i_{r1}' \\ i_{r2} & i_{r2}' \end{bmatrix} \begin{bmatrix} R \\ L \end{bmatrix} \dots\dots\dots 3.2$$

Thus, premultiplying both sides by the inverse of the current matrix gives:

$$\begin{bmatrix} R \\ L \end{bmatrix} = \frac{1}{D} \begin{bmatrix} i_{r2}' & -i_{r1}' \\ -i_{r2} & i_{r1} \end{bmatrix} \begin{bmatrix} v_{r1} \\ v_{r2} \end{bmatrix} \quad \dots\dots\dots 3.3$$

$$\text{where } D = i_{r1} \cdot i_{r2}' - i_{r1}' \cdot i_{r2} \quad \dots\dots\dots 3.4$$

Hence, equations for R and X may be stated as:

$$R = [v_{r1} \cdot i_{r2}' - v_{r2} \cdot i_{r1}'] / D \quad \dots\dots\dots 3.5$$

$$X = \omega L = \omega [v_{r2} \cdot i_{r1} - v_{r1} \cdot i_{r2}] / D \quad \dots\dots\dots 3.6$$

where  $\omega$  = angular power system frequency

However, since digital division places a large burden on the relay processor, the D terms are cross multiplied in Equations 3.5 and 3.6 and the R and X values evaluated as a product of D:

$$D \cdot R = [v_{r1} \cdot i_{r2}' - v_{r2} \cdot i_{r1}'] \quad \dots\dots\dots 3.7$$

$$D \cdot X = D \cdot \omega L = D \cdot \omega [v_{r2} \cdot i_{r1} - v_{r1} \cdot i_{r2}] \quad \dots\dots\dots 3.8$$

Thus, when it is necessary to compare the measured line impedance with the setting impedance, the values given by Equations 3.7 and 3.8 are compared with the setting impedance multiplied by D, which in turn is evaluated by Equation 3.4.

### 3.3 METHODS OF FORMING SOLUTIONS TO THE LINE EQUATION

#### 3.3.1 Orthogonal component method

In this method, two solutions are derived from a single input signal by filtering the signal simultaneously with two orthogonal filters, as depicted in Figure 3.1, where the discrete signal  $x$  is resolved into the orthogonal components  $x_1$  and  $x_2$ . The property of orthogonal filters is that their outputs differ in phase by  $90^\circ$ , i.e. the outputs

are orthogonal. Johns and Martin [7] used orthogonal filters based on 6 point half cycle sine and cosine functions, detailed analyses of the phase, magnitude and impulse responses of these filters are shown in Figures 3.2 and 3.3 respectively. Notice how the filters, although exhibiting perfect orthogonality, have differing magnitude responses. Orthogonal filters may be derived from any pair of functions which have the same general wave shape, one of which is symmetrical and the other is anti-symmetrical. By reference to Figures 3.2 and 3.3, it can be seen that symmetry about the mid point of the impulse response leads to a  $0^\circ$  phase shift whilst anti-symmetry about the mid point gives a  $90^\circ$  phase shift. Hence, orthogonal filters are not solely restricted to sine and cosine functions and it is possible to base filters on square and triangular waves [4].

It is worth noting that historically, filtering based on square wave functions, or Walsh functions, was widely researched [31] since it saved microprocessors from having to execute, what was then, lengthy multiplication instructions. However, at present times, microprocessors exist that can execute a multiplication instruction in the same time that it takes to execute an add instruction [14] and thus the necessity for using Walsh functions, and their associated limitations, are avoided.

This method of solution formation will be referred to as the **basic orthogonal component (OC) method**.

### 3.3.2 Enhanced orthogonal component method

An improvement to the efficiency of the orthogonal method

may be gained by recognition of the fact that the output from the cosine based filter of Figure 3.3 can be considered to be the derivative of the sine based filter of Figure 3.2. Since it is necessary to form derivatives of both orthogonal components of current, a substitution of the form:

$$i_{r1}' = -i_{r2}$$

$$i_{r2}' = i_{r1}$$

may be used to obviate the need for an additional calculation of the current derivative. It will be shown in Section 4.4 that the current derivative calculation is detrimental to the overall relay filtering both in terms of frequency response and group delay.

Use of the substitutions given above add an additional constraint to the orthogonal filters that their gains at power system frequency be equal. The filters of Figures 3.2 and 3.3 have this property (at 50 Hz) but a comparison of the scales on the magnitude response graphs show the cosine based orthogonal filter to have a magnitude response greatly in excess of its sine based counterpart. A move to using orthogonal filters based on full cycle sine and cosine functions gives no significant benefit as shown in Figure 3.4 where the magnitude responses of 12 point orthogonal filters, each having unity gain at 50 Hz, are plotted on the same graph.

### 3.3.3 Time spaced solution method

An alternative solution formation method which does not necessarily imply orthogonality of the solutions, but which

does give linear independence, is to use different points on the wave of the sampled data. Hence, the sampled voltage and current values are stored in the RAM of the relay and the two solutions are derived by using, firstly, the most recent sample, and secondly, a sample that was stored 'k' samples previous; such solutions may be described as 'time spaced'. Figure 3.5 shows the formation of two solutions from the sampled signal x, where previous sampled values of x are stored.

The optimum value of 'k' is related to the precision of the microprocessor and the ADC. A value of  $k=1$  would require great precision from both in order to sufficiently discriminate between points on wave of  $4.5^\circ$  apart and ensure linear independence of the two solutions. Conversely, a large value of k, say 20, whilst giving linear independence largely irrespective of precision, would introduce large group delays into the impedance measurement process and thus lead to a longer relay operating time. Empirical tests on the simulation with a 14 bit ADC and 16 bit microprocessor revealed that  $k=6$  gave correct impedance measurement under all specified conditions. This corresponds to  $27^\circ$  spacing of the solutions for a power system frequency of 50Hz sampled at 4kHz.

### **3.4 CHOICE OF SOLUTION EXTRACTION TECHNIQUE**

#### **3.4.1 Effect of non-power system frequencies**

Figure 3.6 shows the effect of varying the power system frequency, with respect to the accuracy of the inductance measurement, for the three methods of solution formation

discussed in the previous section. The responses were evaluated by feeding a primary system input into the simulation which corresponded to a  $10\Omega_{sec}$   $188^\circ$  fault at the rated voltage. The power system frequency was then varied and the mean value of the inductance measurement observed. Notice that all three graphs of Figure 3.6 have different x axis scales.

Figure 3.6 b) shows that the enhanced OC method is only accurate at exactly power system frequency; this is a result of setting the gains of the orthogonal filters equal at 50Hz as discussed in Section 3.3.2. The specified range of power system frequencies, given in Section 2.1, for which the relay must correctly operate is 47-53Hz. The enhanced OC method gives an error of -7% at 47Hz and +7% at 53Hz. Thus this method is unsuitable for use since it will tend to overreach when the power system frequency is low and underreach when the frequency is high.

Figures 3.6 a) and c) show that the remaining two methods of solution formation give virtually error free inductance measurement within the frequency range of the power system. The basic OC method, Figure 3.6 a), shows a large increase in error when the system frequency exceeds 70Hz. Whilst, at first sight, it may appear unrealistic to evaluate the response of the method for higher than normal system frequencies, this analysis does highlight a basic defect in the basic OC method.

The reason that the basic OC method goes into error is due to the cosine based orthogonal filter having a large gain for frequencies greater than 50Hz. With close reference to

Figure 3.3, it can be seen that the gain at 100Hz is approximately 6 times greater than the gain at 50Hz, and, in general, signals in the range 80 to 1000Hz will have gains exceeding the 50Hz gain. Thus, any signal which is convolved with this filter, even though it has passed through the analogue input stages of the relay without clipping, is at risk of exceeding the relay microprocessor word length of 16 bits, i.e. the signal can overflow. The relevance of this effect is not in the abstract case of a power system frequency of, say, 80Hz, but of a normal system frequency signal that is corrupted by harmonics or travelling wave noise. Clearly, there is a risk of overflow in these situations which will lead to an incorrect impedance measurement and, ultimately, to maloperation of the relay.

The time spaced solution (TSS) method does not suffer from any overflow problems of this nature since the two solutions may be considered to have equal, unity gain frequency responses. Figure 3.6 c) shows that the error in evaluating the inductance for the TSS method does not exceed +1.5% in the frequency range 30-500Hz. Thus, this method will exhibit good immunity to power system noise components which obey the fundamental line equation (Equation 3.1), e.g. harmonics.

#### 3.4.2 Practical considerations

Since the enhanced OC method gives such gross errors for non power system frequencies, it will not be considered further. In terms of efficiency, the TSS method is simpler to implement on a microprocessor than the OC method since

it only requires manipulation of 2 of the sampled values as opposed to 6 if the filters of figures 3.2 and 3.3 were used. Since it is necessary to form 2 solutions to a total of 9 signals, i.e. 3 voltages, 3 currents and 3 current derivatives, the saving in processing time is appreciable.

### 3.4.3 Method used in the simulation

The TSS method was used throughout the simulation for the following reasons:

- 1) It has an inherently good frequency response.
- 2) There is no risk of overflow of the solutions irrespective of the spectrum of the input signal.
- 3) It is relatively simple to implement.

Figure 3.1 Solution formation using orthogonal filters.

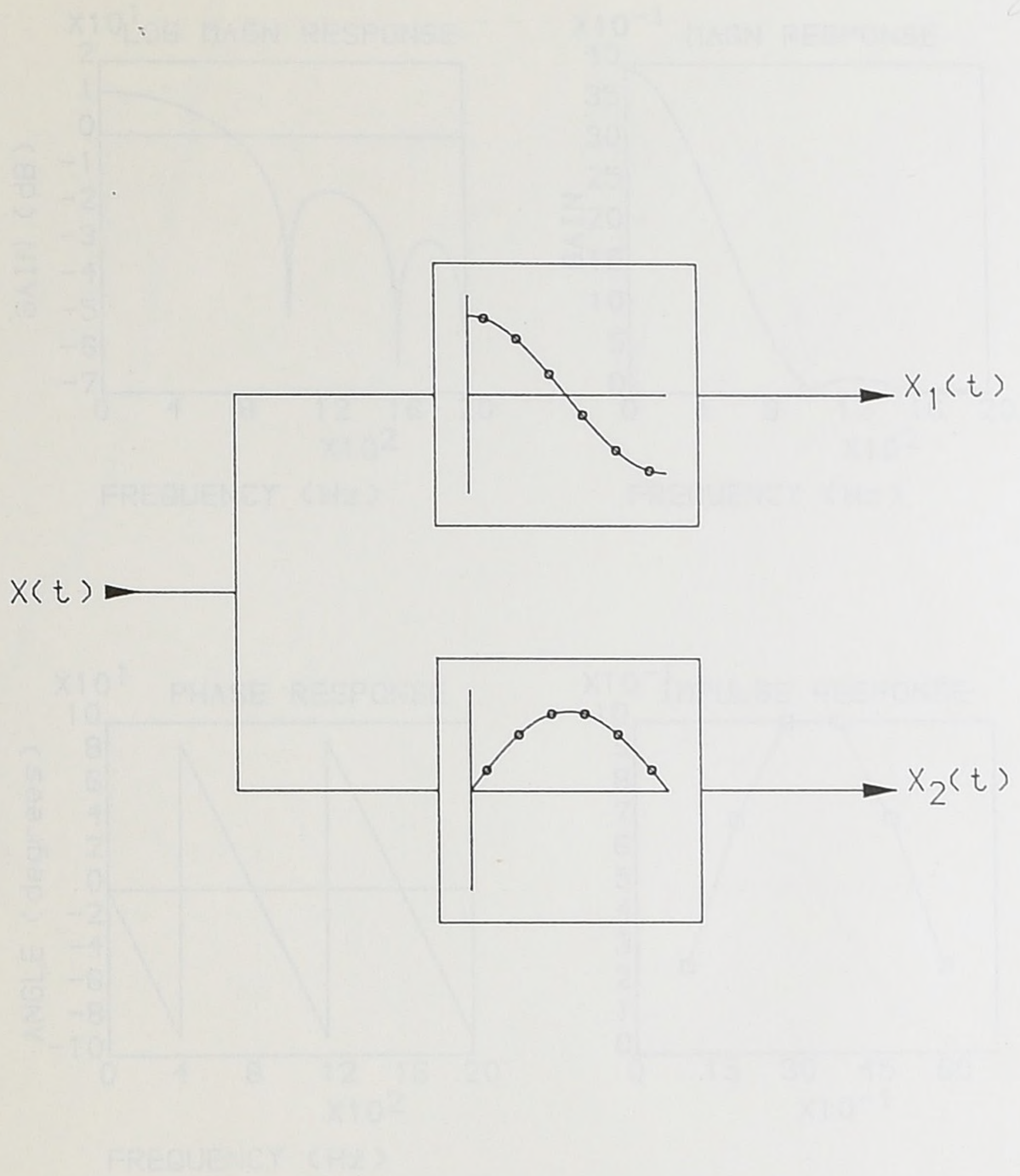


Figure 3.1 Solution formation using orthogonal filters.

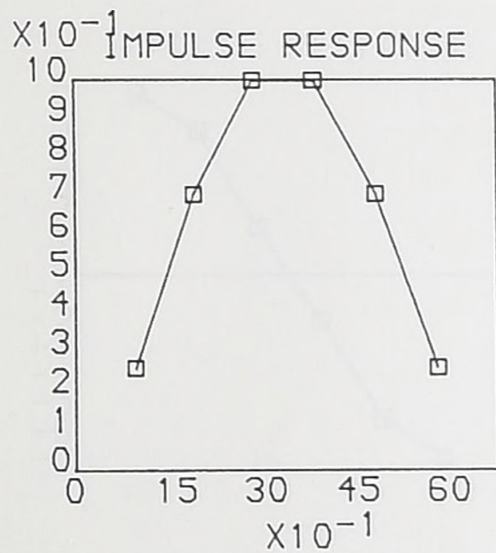
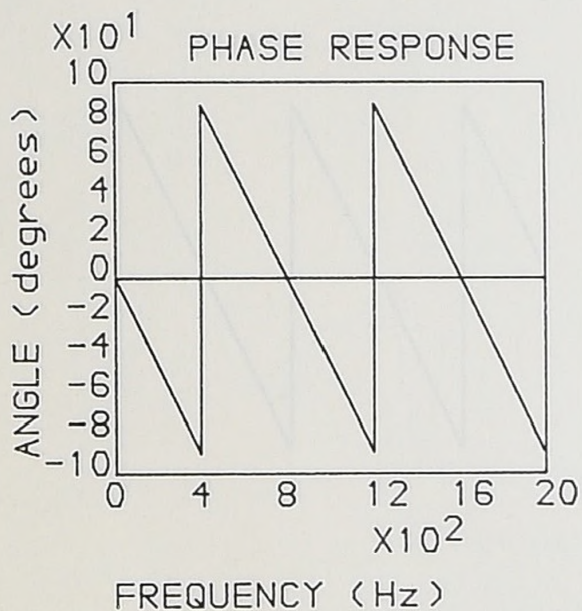
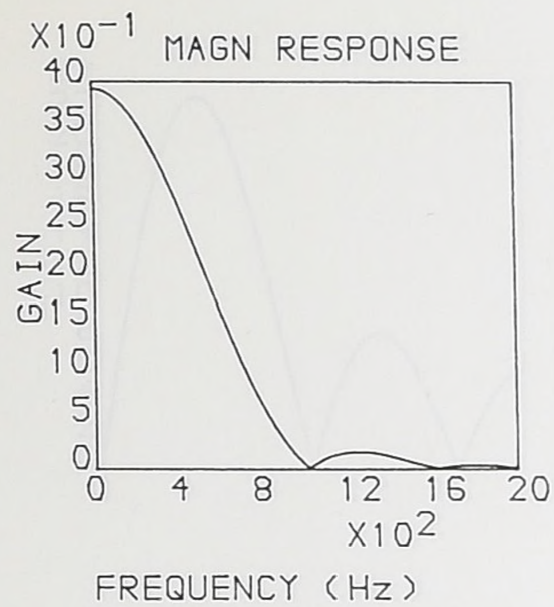
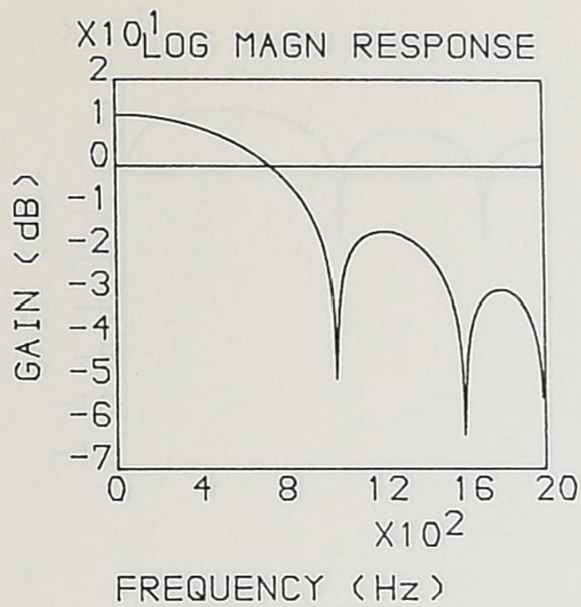


Figure 3.2 Phase, magnitude and impulse responses for 6 point, half cycle, sine function based orthogonal filter.

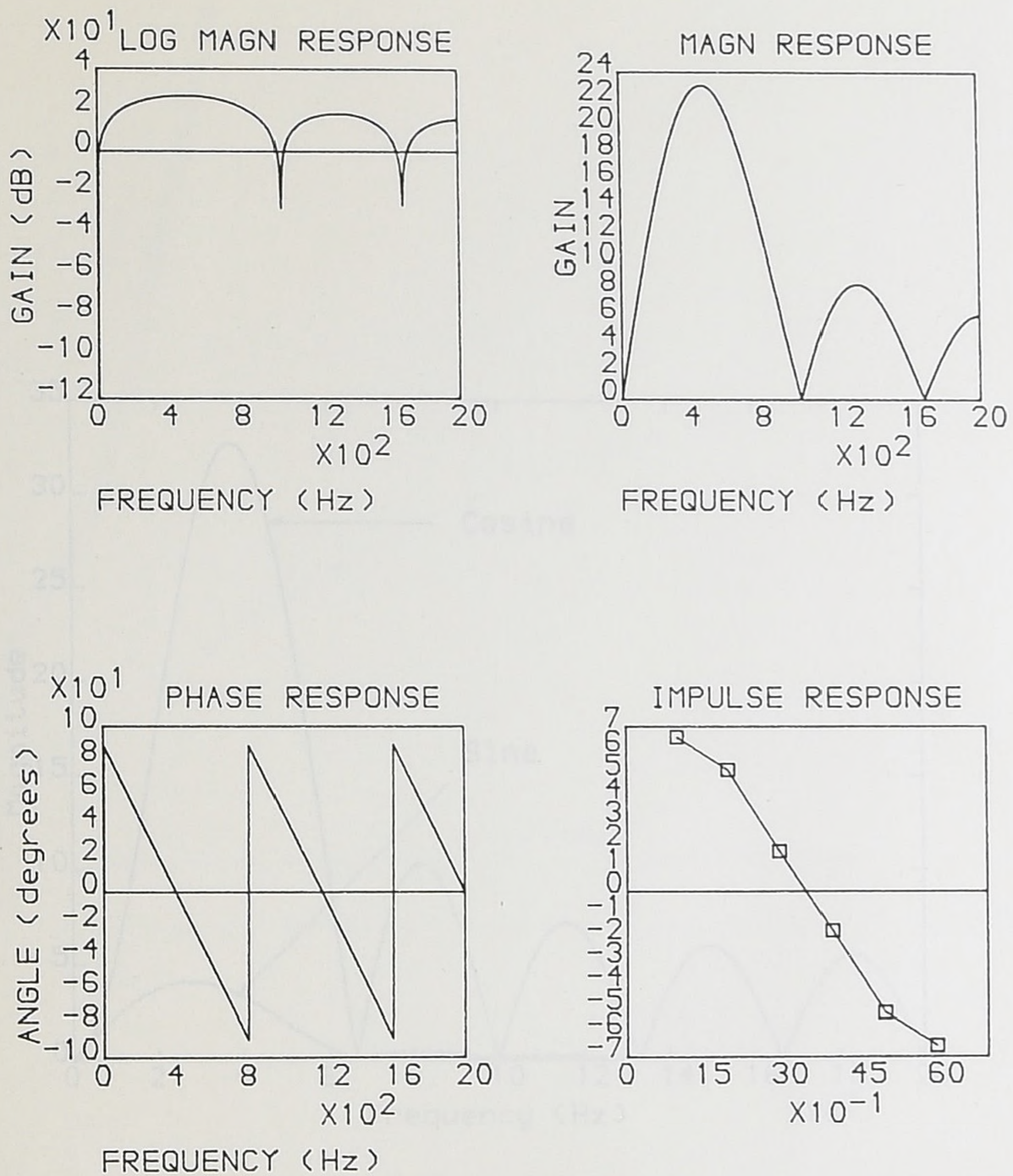


Figure 3.3 Phase, magnitude and impulse responses for 6 point, half cycle, cosine function based orthogonal filter.

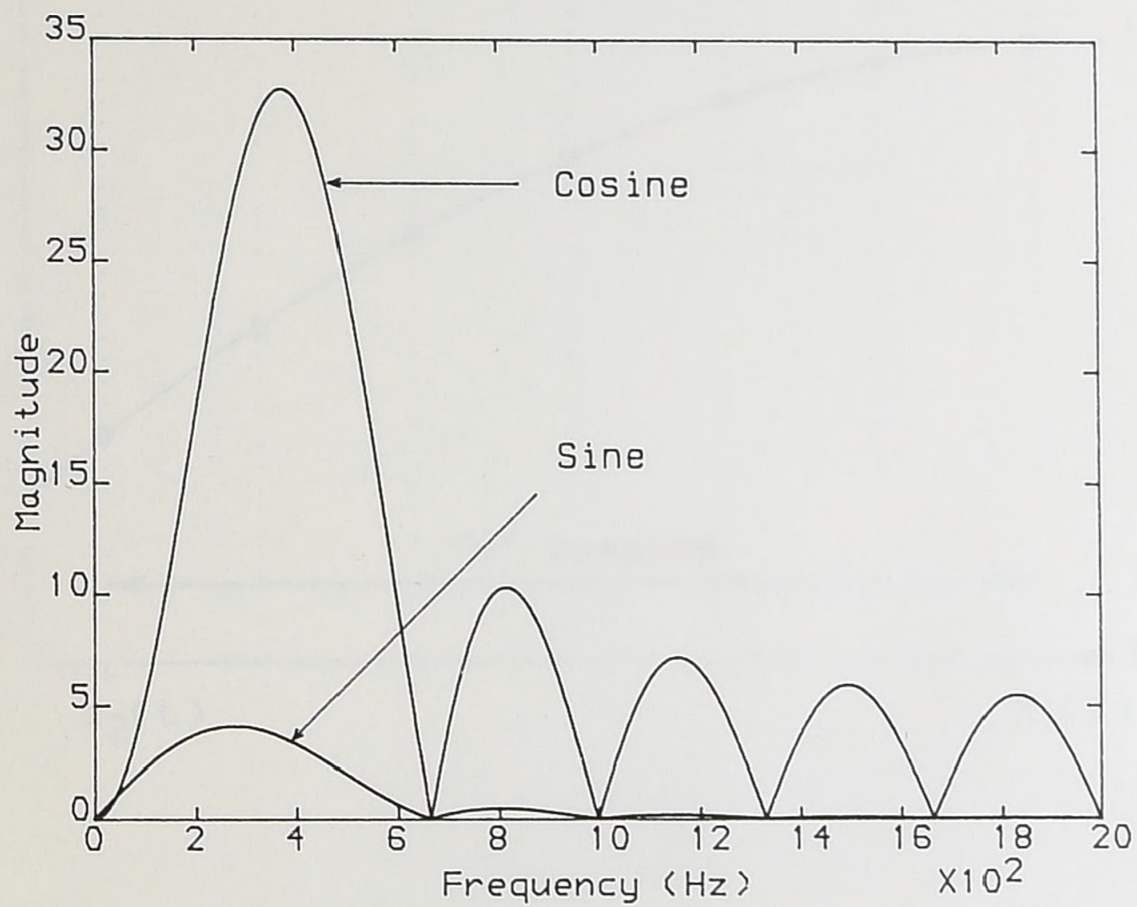


Figure 3.4 Magnitude responses for 12 point, full cycle, sine and cosine function based orthogonal filters.

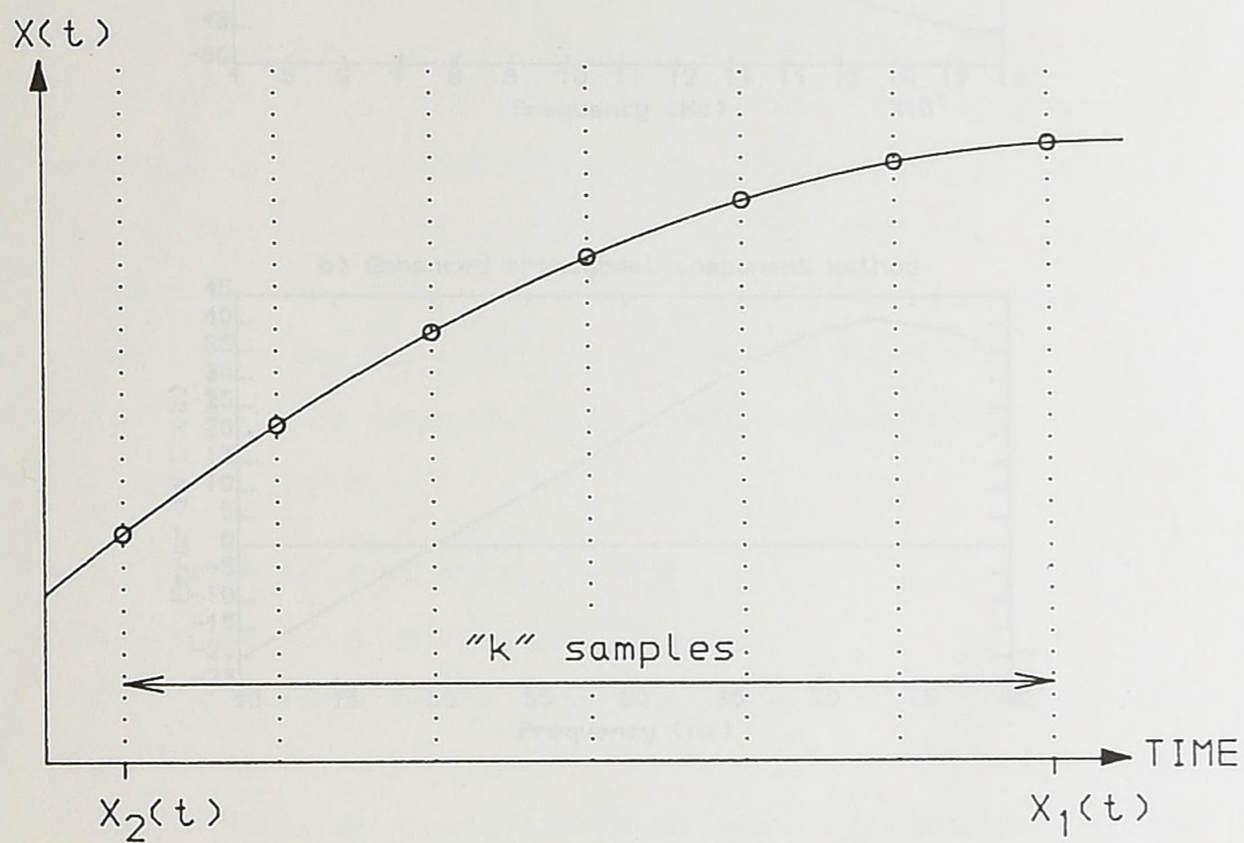


Figure 3.5 Solution formation by time spacing.

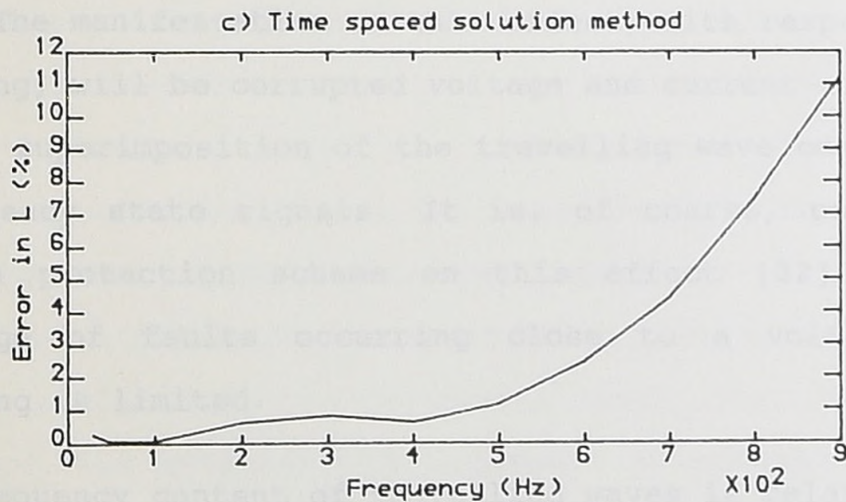
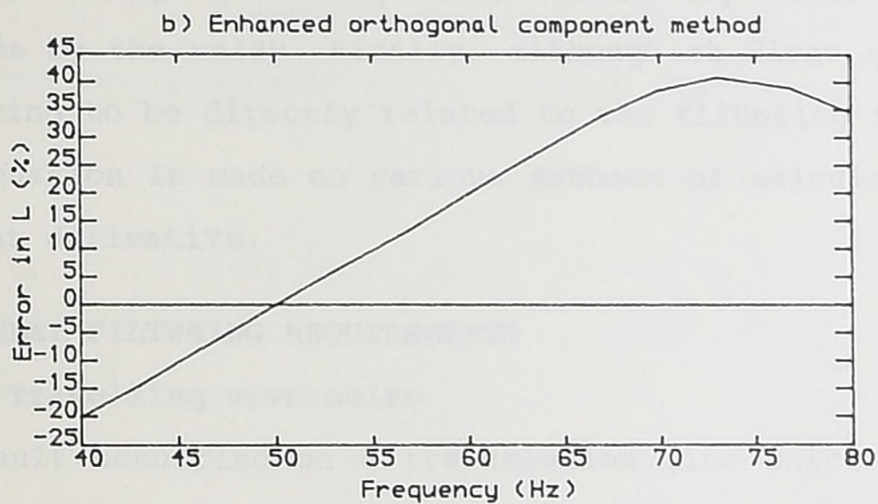
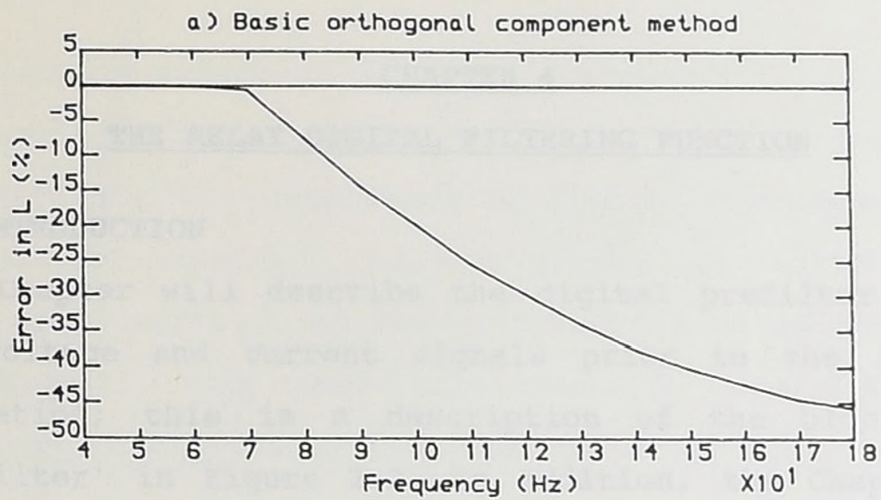


Figure 3.6 Error in inductance measurement versus power system frequency.

## CHAPTER 4

### THE RELAY DIGITAL FILTERING FUNCTION

#### 4.1 INTRODUCTION

This Chapter will describe the digital prefilter used on the voltage and current signals prior to the impedance evaluation; this is a description of the block marked 'prefilter' in Figure 2.2. In addition, the Chapter will describe an adaptive filter which is used to directly filter the impedance components before any fault decision is made by the relay. Finally, although at first sight not appearing to be directly related to the filtering function, a discussion is made on various methods of calculating the current derivative.

#### 4.2 RELAY FILTERING REQUIREMENTS

##### 4.2.1 Travelling wave noise

Any fault occurring on a transmission line which causes a voltage discontinuity will result in a travelling wave which propagates from the fault point to the end of the line. The manifestation of this effect, with respect to the relaying, will be corrupted voltage and current signals due to the superimposition of the travelling wave component on the steady state signals. It is, of course, possible to base a protection scheme on this effect [32], but the coverage of faults occurring close to a voltage zero-crossing is limited.

The frequency content of travelling waves is related to the distance to the fault and the nature of the source impedance at the line end. Swift [33] showed that the range of expected frequencies for faults of this nature can be

evaluated by assuming, firstly, a transition time,  $\tau$ , for the wave to travel from the fault point to the source, and secondly, two limiting cases of source impedance. With a small source impedance, i.e. a strong bus, the travelling wave, upon incidence at the source, will be reflected with an opposite sign and the dominant travelling wave frequency,  $f_{\text{noise}}$ , will be given by:

$$f_{\text{noise}} = \frac{1}{2\tau} \text{ Hz} \quad \dots\dots\dots 4.1$$

When the source impedance is large, the wave is reflected with the same sign and  $f_{\text{noise}}$  is given by:

$$f_{\text{noise}} = \frac{1}{4\tau} \text{ Hz} \quad \dots\dots\dots 4.2$$

Clearly, the transit time,  $\tau$ , is related to the distance to the fault,  $d$ , and the speed of propagation,  $c$ , which is assumed to be the velocity of light:

$$\tau = \frac{d}{c} \quad \dots\dots\dots 4.3$$

Figure 4.1 shows the dominant travelling wave frequency plotted against distance to fault for the two source situations described above. It may be inferred from this graph that for, say, a 100km line, the expected distribution of the travelling wave frequencies will be in the range 700 - 1400Hz. However, inferences of this nature are to be discouraged since it makes the assumption that the relaying end is synonymous with the source; in practice, the relay may be separated by another length of transmission line before the source is reached, and thus, the expected frequency range will be modified. Furthermore, the aim of this project is to evolve a distance relay

capable of use on any line up to 250km in length; it is not intended to have one relay with the filtering designed for a 100km line, and another suitable for 250km lines. Figure 4.1 shows that, for the maximum line length of 250km, it is necessary to incorporate filtering which can attenuate frequencies as low as 300Hz.

Using the distributed parameter simulation described in Section 2.5, two illustrations of travelling wave distortion are presented. Figure 4.2 a) shows the 'a' phase voltage at the relaying point for a solid 'a' phase to earth fault occurring at 80% along a 100km line. Figure 4.2 b) shows a similar case but with the line length of 250km. Notice the difference in the dominant travelling wave frequencies for the different line lengths.

#### 4.2.2 Exponential Offsets

Offsets may arise in either the current or voltage signals. In the case of the current, an exponential offset is induced if a fault occurs at any POW other than the angle of the combination of the line and source impedances. The severest cases of exponential offset on the current occur for faults close to a zero crossing. The inclusion of any fault resistance will have the effect of dampening the offset abruptly. Offsets on the voltage can be associated with large magnitude current offsets, but also occur due to the action of the CVT [34], particularly in situations where the primary system voltage is greatly reduced by a fault. In terms of the action of the relay, the current offset should not lead to any maloperation since it is a legitimate solution to the line equation. Since, however,

the line equation is an approximation to a true distributed parameter transmission line, and that the CT, although assumed perfect for this work, will to some extent distort the offset, it was considered prudent to filter any dc component from the input current signals to the relay.

Any offsets occurring on the voltage signal due to CVT transients will lead to impedance measurement errors since the voltage signal in this situation does not solve the line equation. Thus it is necessary to filter the dc component from the voltage signals. This reinforces the case for dc blocking of the current signals since it would be impractical to filter both voltage and current signals with anything other than the same filter. The use of two different filters, one each for the voltage and current, would introduce impedance measuring errors due to the differing phase and magnitude responses of each filter. Whilst it is possible to compensate for this effect with respect to the power system frequency, it would not be practical to compensate for harmonics.

#### 4.2.3 Extraneous noise

Within this category falls switching noise generated from either the protected line or adjacent lines. Since noise of this nature tends to involve spikes with fast rising edges, its corresponding frequency spectrum will be in the high frequency range and is unlikely to involve frequencies lower than 300Hz. Thus, any externally generated noise will be assumed not to impose any more limitations on the relay filtering requirements above those stated in Section 4.2.1.

#### 4.2.4 Harmonics

There has, in the past, been much attention paid to filtering frequency components, from digital relay measurands, which are harmonically related to the power system frequency [6]. Using the impedance measurement algorithm described in Chapter 3, harmonics which are integer multiples of the system frequency will not cause the impedance estimates to be corrupted since the harmonics will obey the governing, lumped parameter, line equation. Even allowing for the fact that a transmission line is composed of distributed parameters, results have shown that no particular attention need be made to the design of the filtering for harmonic rejection.

#### 4.3 THE PREFILTER

The prefilter acts on the voltage and current signals before the impedance is evaluated. From Section 4.2, the voltage and current signals entering the relay are required to be filtered so that the dc component and frequencies above 300Hz are removed. Ideally, the prefilter will have a frequency domain function which blocks dc, has a peak at 50Hz and gives sufficient rejection for frequencies above 250Hz. However, it will be shown that this is not possible.

One consideration when designing the prefilter is the group delay since this will affect the relay operating time. A FIR filter structure was chosen for the prefilter, rather than an IIR filter [26], since the group delay is known and equal to the length of the impulse response. It was stated in Chapter 2 that the maximum desired operating time of the relay should be less than 10ms for faults within 75% of the

reach. Allowing time for the group delay of the anti-aliasing filter and time for the protection algorithm to make the fault decision, the maximum allowable time for the prefilter impulse was set at 6ms. Thus, for a FIR filter working at a 4kHz sampling rate, this corresponds to a maximum filter length of 24 points.

An effective method of designing optimal FIR filters is by the use of the 'Remez Exchange' algorithm [26]. In this method, the pass and stop bands of the frequency spectrum are specified and an optimisation criterion is formulated such that the worst case deviation of the error between the impulse response and the desired frequency response transformation is minimised. The minimisation process is performed iteratively using the Remez multiple exchange algorithm. The use of the Remez exchange, however, did not produce satisfactory results due to the stop band at dc, and the pass band at 50Hz, being very close together. Note, of course, that the description of 'close together' is entirely relative, but, with a total frequency spectrum of 2kHz, the difference between dc and 50Hz only represents 2½% of the available spectrum. Since the filter length was limited to 24 points, the Remez algorithm was unable to fit an impulse response to the specified frequency spectrum with the required degree of rejection above 300Hz.

Since the Remez Exchange failed to provide a basis for designing the prefilter, a different approach was taken and a study was made of the mechanism by which a Discrete Fourier Transform (DFT) performs the time to frequency transformation. Note that the DFT is usually numerically

evaluated using the Fast Fourier Transform (FFT) [26,35] which is a more computationally efficient algorithm than the DFT; the results in either case are identical. The DFT calculates the spectral content of, say, the 50Hz component of a discretely sampled time series by convolving the series with firstly a sampled 50Hz sine wave, and secondly, a sampled 50Hz cosine wave. This process is similar to the orthogonal component method of solution formation discussed in Chapter 3. The resulting values from the convolutions are the real and imaginary components of the 50Hz phasor. The reason that the DFT was studied in relation to the prefilter, was that, with the exception of the dc component, the frequency response of every spectral component evaluated by the DFT has a zero at dc. Figure 4.3 shows the magnitude response in the frequency domain for a filter based on the 50Hz sine component of the DFT; the impulse response for a 4kHz sampling frequency is a sine wave consisting of 80 points, i.e. 20ms in length. It will be noted that the 50Hz component represents the highest gain in the spectrum and that the dc component is blocked. However, the penalty for such an ideal filter is that the group delay is 20ms and is thus unsuitable for this application. It can now be seen that a compromise between the frequency response of the prefilter and its length must be met.

The approach taken for the prefilter, was to use a simple 12 point sine wave based impulse response, the details of which are shown in Figure 4.4. It can be seen that between 50Hz and 650Hz, any spectral content will be amplified rather than attenuated. The philosophy behind the use of

this filter is that only faults which present a threat to stability of the system need to be cleared fast. Faults falling into this category will occur close to large sources and, from Figure 4.1, will generate travelling wave frequencies which are, in general, higher than 650Hz. Thus, stability threatening faults will be cleared quickly since the prefilter has a short group delay. Faults which occur at, say, the mid section of long lines are less of a threat to stability since there is a substantial amount of line impedance in the fault path. These faults will generate a lower travelling wave frequency which the prefilter will be unable to attenuate. The next Section will describe an adaptive filter which is used in conjunction with the prefilter to provide attenuation of frequencies less than 650Hz.

#### 4.4 THE SIGNAL AVERAGER

Section 4.3 described the prefilter used in the relay and eluded to some of its limitations. This Section describes a signal averager which is used to provide the extra filtering function, required of the relay, but not produced by the prefilter. In contrast to the prefilter, the averager acts on the impedance estimates rather than the voltage and current signals. Also, unlike the prefilter, the averager is only used when there is a potential fault situation. Thus the averager may be described as an adaptive filter. If the relay considers the power system to be unfaulted, then the averager is not invoked.

Mathematically, the operation of the averager may be described by the following equation:

$$YAV(n+k) = \sum_{i=0}^m \frac{Y(n+k-i)}{m+1} \dots\dots\dots 4.4$$

where  $m = k$  if  $k \leq 15$ , and,  $m = 15$  if  $k > 15$ .  $Y(n)$  is the input signal and  $YAV(n)$  is the output averaged version of the input.

The operation of the averager can be described by likening it to a 'window', through which the input data is viewed. If the window is 5 samples in length, then the output is the sum of the 5 input samples divided by 5, i.e. the average or geometric mean of the input samples. When the averager is invoked, the window length is set to 1 and this length increases by 1 at every new sample point. 16 samples after invocation, the window remains fixed at a length of 16 and then 'follows' the input data, i.e. at any time after this the window will contain the most recent sample and the 15 previous samples. When the averager is no longer required, the window length is reduced, by 1 sample at a time, until it has contracted to a length of 1.

The averager is invoked when a potential fault situation arises and, conversely, is disabled when the power system is in an unfaulted condition. The exact method of deciding when these two situations are in force will be described in the next Chapter. However, for the present, it may be assumed that the averager is invoked if any impedance sample falls within the characteristic and, is disabled if the impedance is consistently outside the characteristic.

The advantage of using the averager is that, assuming it is invoked after the group delay of the prefilter and hence

only uses post-fault data, there is no group delay associated with its use. Thus, in situations where the relay can discriminate a fault using only the prefilter, the use of the averager will have no effect on the relay operation time. However, for faults which result in heavily corrupted impedance estimates, the relay will be able to discriminate after the averager has extended its window length to a position where the filtering effect is sufficient to remove the noise from the signals.

Figure 4.5 shows the magnitude response of the averager when its window is at the fully extended length of 16 points. Note that dc, which is the pertinent relaying information of the impedance estimates, is the highest point on the magnitude response curve. Note also, that in conjunction with the prefilter, the relay filtering process as a whole is now capable of attenuating frequencies as low as 250Hz. Thus it can be seen that by using a fixed prefilter on the voltage and current samples and an adaptable filter on the impedance estimates, the relay can operate quickly for relatively uncorrupted faults, yet still have the capability to discriminate 'noisy' fault situations.

When applying the averager to the impedance estimates, it is necessary to average D.X, D.R and D separately and hence three averagers are required for each impedance estimate. It will be recalled from Chapter 3 that steps are taken to avoid the need for digital division. However, the averager will not present any burden in this direction since it is only ever necessary to divide the sum of the input samples

by an integer in the range 1 to 16. This division may be converted to a multiplication by prestoring the reciprocals of the integers 1 to 16.

The action of the averager is shown in Figure 4.6 where the measured reactance for a voltage maxima, 'a' phase to earth fault occurring at 200km from the relay on a 250km line is shown with, and without, the averager. The 'a' phase voltage for this fault is shown in Figure 4.2 b). It can be appreciated that the relay would not readily be able to discriminate whether the fault is in or outside of the characteristic when the averager is not used. Note that the X value, rather than the D.X value, is presented for clarity; since both the D.X and the D terms are averaged separately, the presentation of results in this form is an accurate representation of the operation of the relay.

#### 4.5 CURRENT DERIVATIVE

Chapter 3 discussed the necessity to form derivatives of the line current in order to solve the line equation. This Section will describe the formulation of the current derivative and its effect on the relay filtering.

Three formulas for the current derivative were investigated. The first formula, used by Johns and Martin [7], calculates the derivative of the sampled current signal,  $i(n)$ , as:

$$i'(n) = \frac{i(n) - i(n-1)}{h} \dots\dots\dots 4.7$$

where  $h$  is the time between samples. The advantage of this method is that it does not require any information ahead of

the most recent sample. However, it can be seen that the derivative is most accurate at the point mid way between the two samples rather than at sample 'n'. Hence, a better approximation would be:

$$i'(n) = \frac{i(n+1) - i(n-1)}{2h} \quad \dots\dots\dots 4.8$$

However, since this requires the use of the 'n+1'th point, this imposes an increase of one sample in the group delay of the relay. The final method uses four samples in total; two samples either side of the point in interest:

$$i'(n) = \frac{1}{12h} \cdot \{i(n-2) - 8i(n-1) + 8i(n+1) - i(n+2)\} \dots 4.9$$

The derivation of Equation 4.9 is shown in Appendix 8. It is also shown in Appendix 8 that the inherent error associated with Equation 4.8 is of the order of  $h^2$ , whilst for Equation 4.9 the error is of the order of  $h^4$ .

Since Equations 4.7, 4.8 and 4.9 may be considered to be impulse responses, their frequency domain functions may be found by the use of the FFT. Figure 4.7 shows the magnitude responses for these three equations. Note that Equation 4.7 gives an undesirable effect on the filtering since it has the tendency to amplify every frequency greater than 50Hz; for this reason it will be considered no further. Of the remaining two methods, Equation 4.8 shows a slightly better frequency response in terms of the hf gain. In either case, the gain rolls off after a maximum of about 1kHz. Since this maximum occurs at a position in the frequency spectrum which is well attenuated by the prefilter, there is little difference in the filtering performance of either Equation

4.8 or Equation 4.9.

A benefit of using Equation 4.9 is that, assuming the bottom line ' $12h$ ' term to be cross multiplied out of the expression, the magnitude of the current and its derivative are approximately equal without any loss of precision. This effect becomes important when the input current signal level is small. This effect is illustrated in Figure 4.8 which shows the 'a' phase current and its derivative, calculated using both methods, when the relay was subjected to an 'a' to earth fault at 80% of a 100km line with a SIR of 1 and 5% of 7th harmonic superimposed on the source. Note the larger magnitude of the derivative when Equation 4.9 is used and note also that the harmonic level is increased more or less equally in both cases.

Since Equation 4.9 has an inherently smaller error term than Equation 4.8, Equation 4.9 was adopted as the method of current derivative formulation used in the relay. Although the group delay is increased by two samples for Equation 4.9, as opposed to an increase of one sample for Equation 4.8, it was considered that the better precision for small signals outweighed the extra group delay.

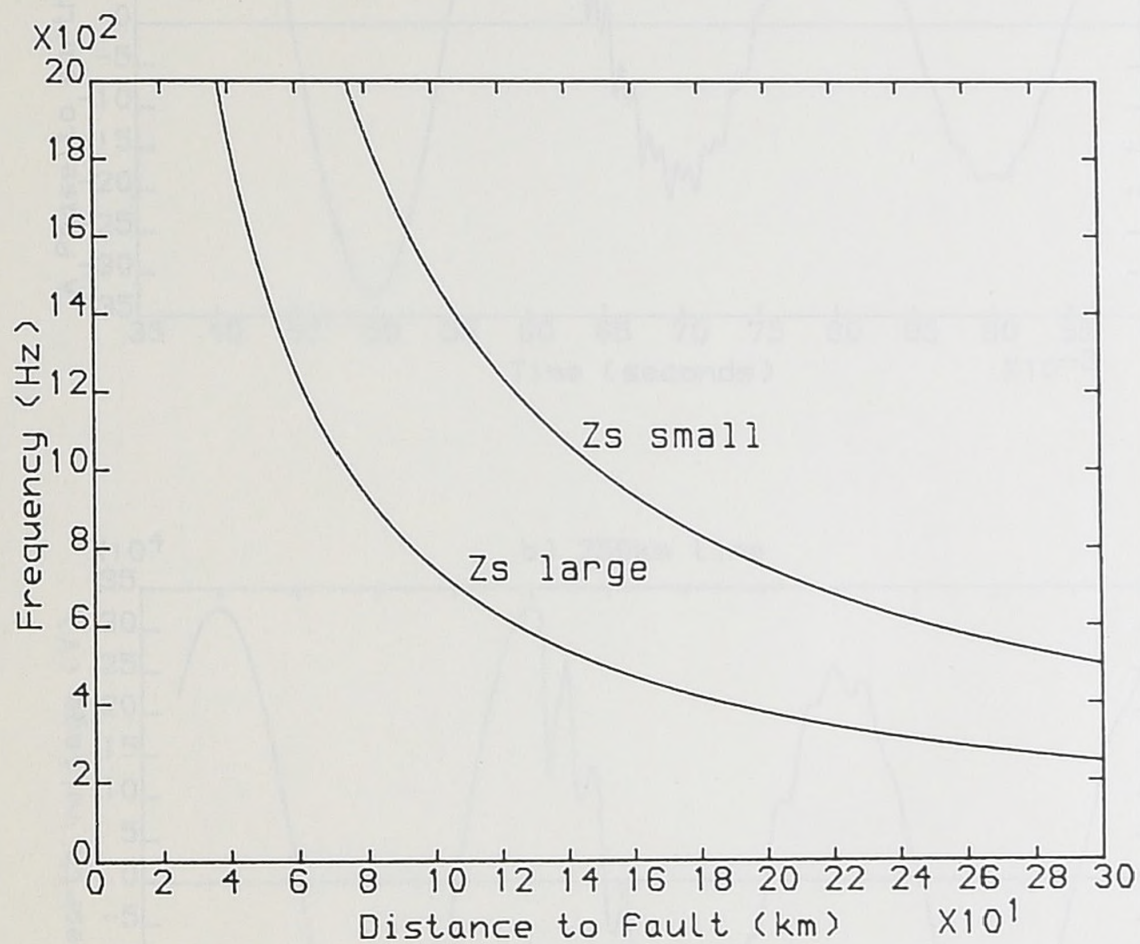


Figure 4.1 Travelling wave frequency versus distance to fault for small and large source impedances.

Figure 4.2 Voltage waveforms for B phase to earth fault (Fault angle = 30°, Fault position = 90% of line length, Source MVA = 5000)

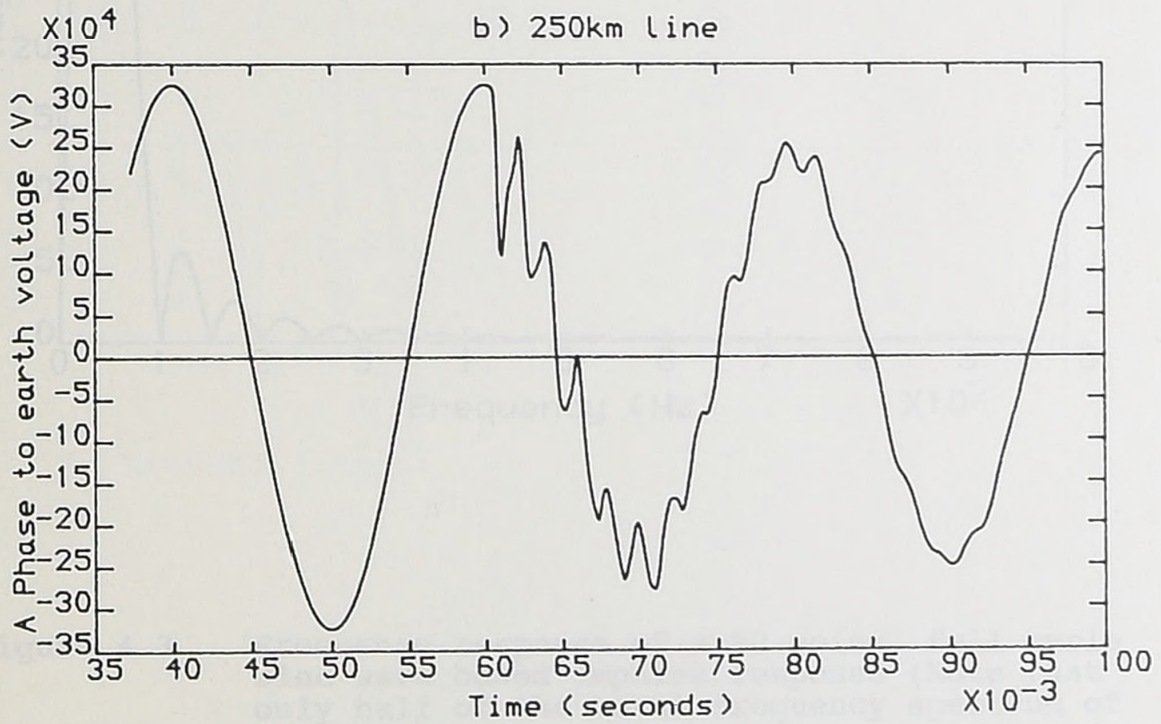
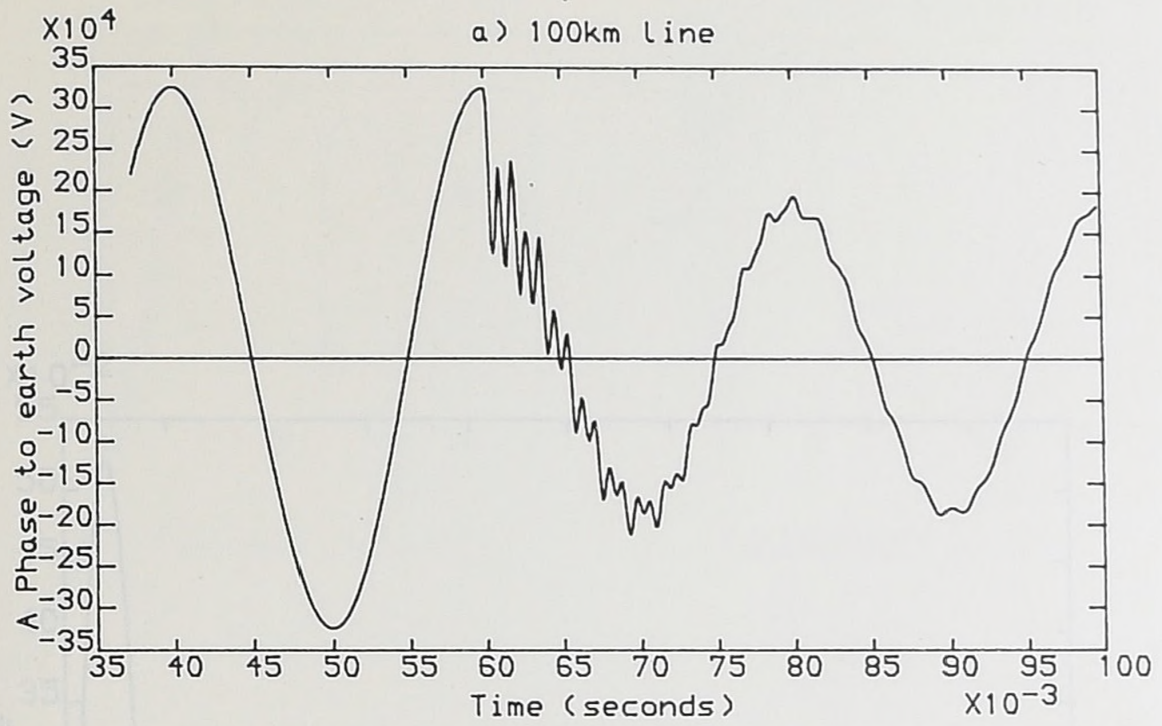


Figure 4.2 Voltage waveforms for A phase to earth fault (Fault angle =  $90^\circ$ , Fault position = 80% of line length, Source SCL = 5GVA).

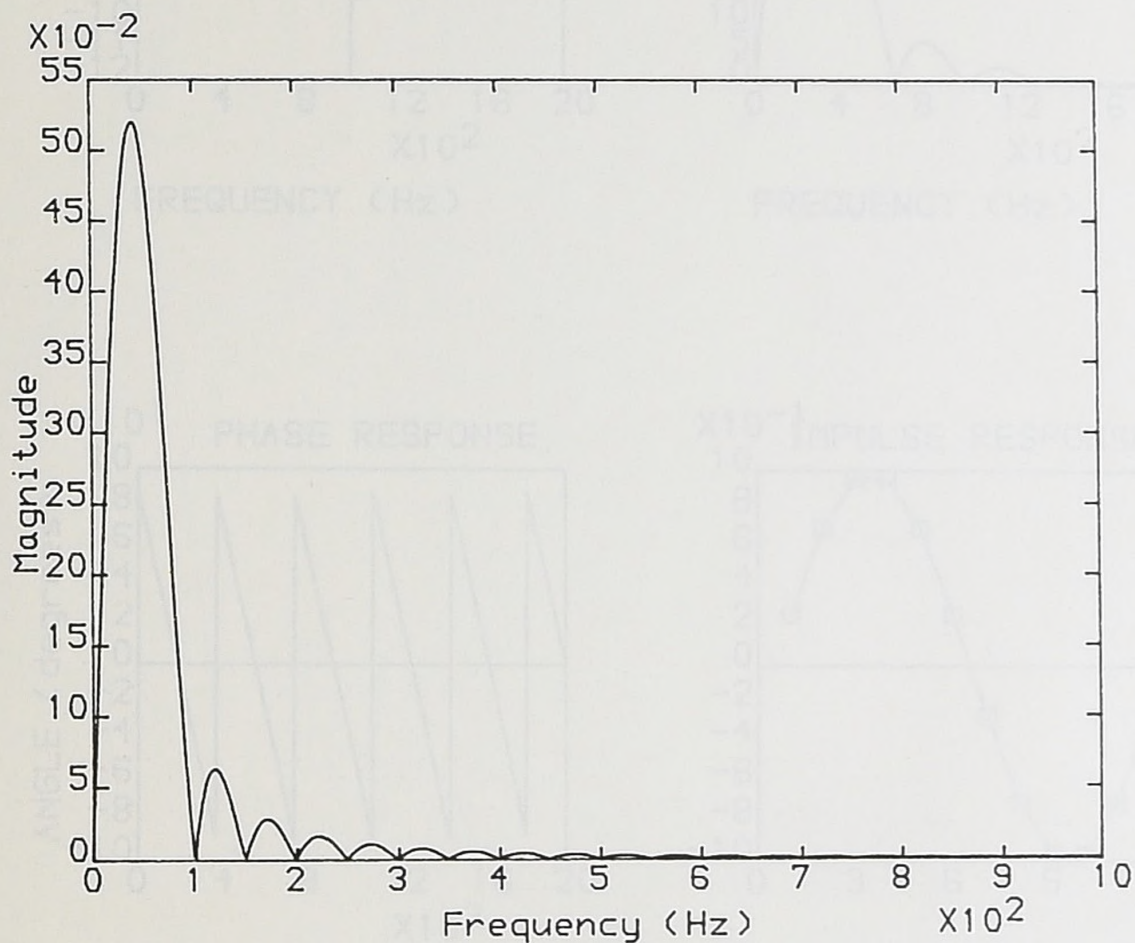


Figure 4.3 Frequency response of a 80 point, full cycle sine wave based impulse response (Note that only half of the total frequency spectrum of 0 - 2kHz is shown for clarity).

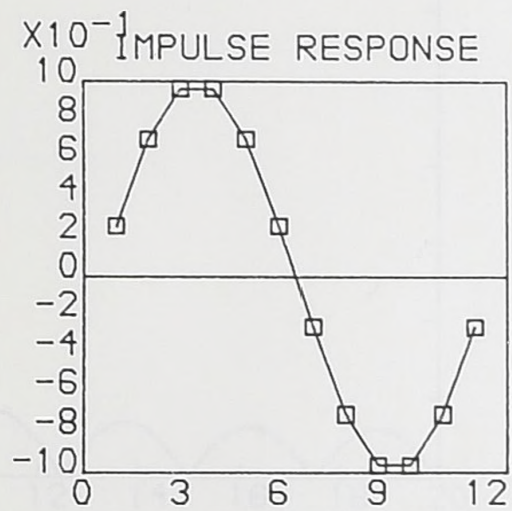
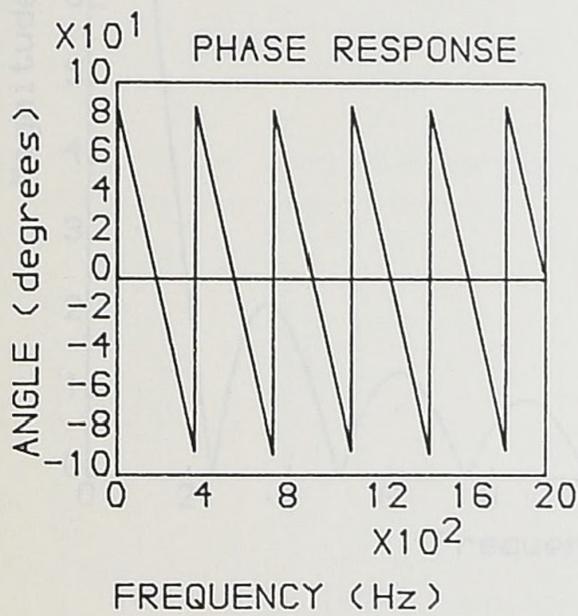
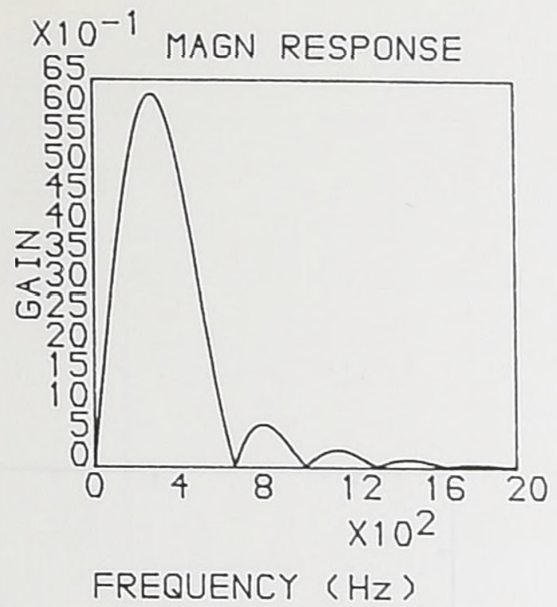
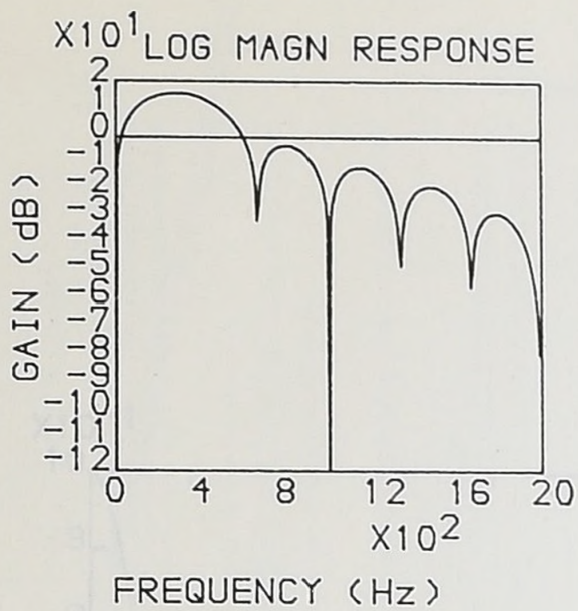


Figure 4.4 Phase, frequency and impulse responses for the prefilter.

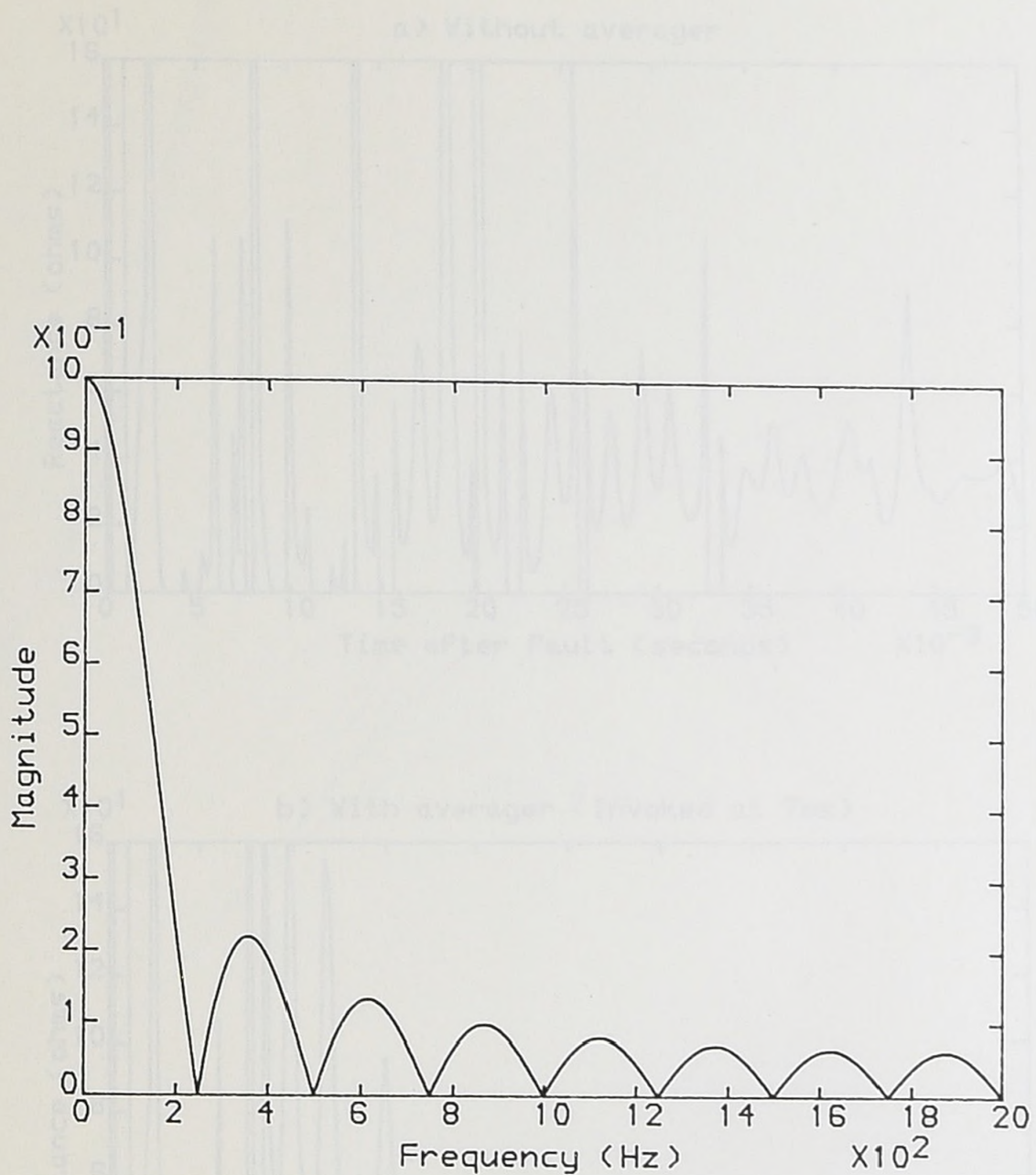


Figure 4.5 Frequency response of the averager when the window is fully extended to a length of 16 points.

Figure 4.6 Illustrative operation of the averager for heavily distorted waveforms on 230kV line. (Fault angle=99°, Fault position=80% of line length, Source SW-SCVA, Fault type=A-earth).

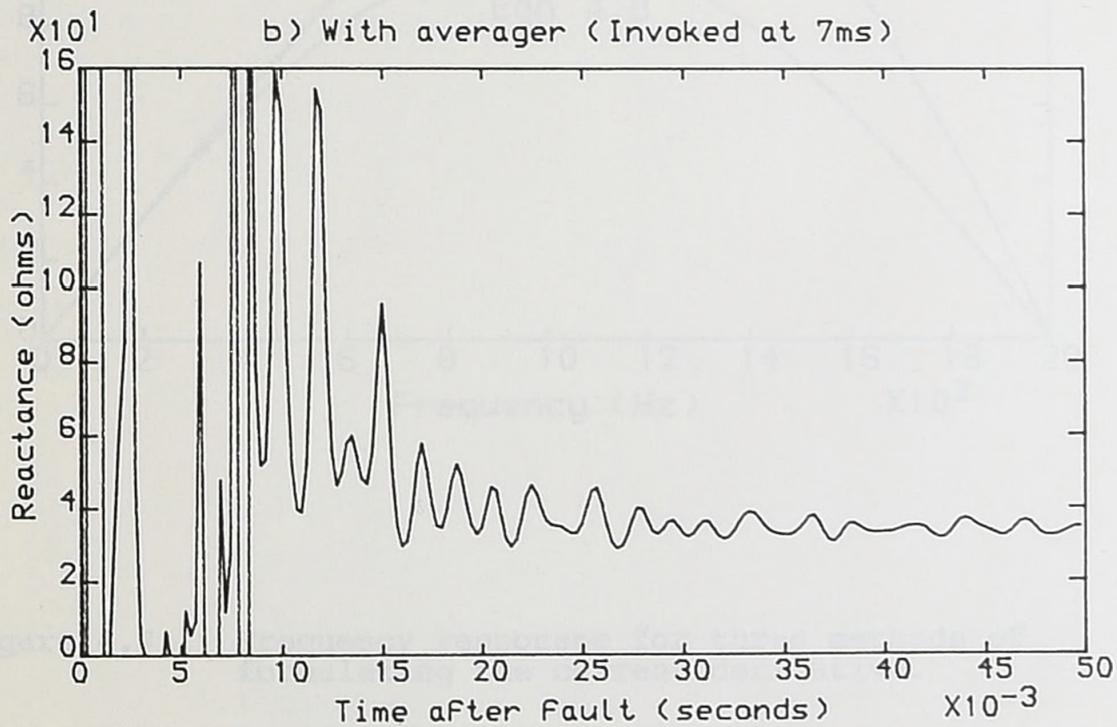
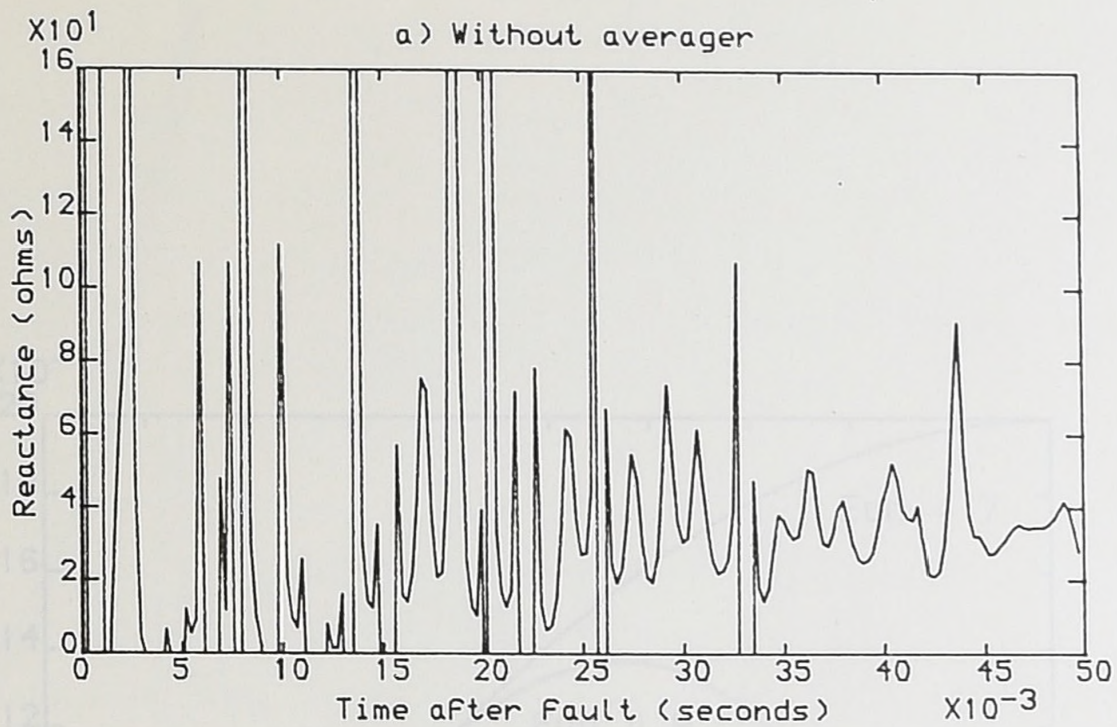


Figure 4.6 Illustrative operation of the averager for heavily distorted waveforms on 250km line. (Fault angle=90°, Fault position= 80% of line length, Source SCL=5GVA, Fault type=A-earth).

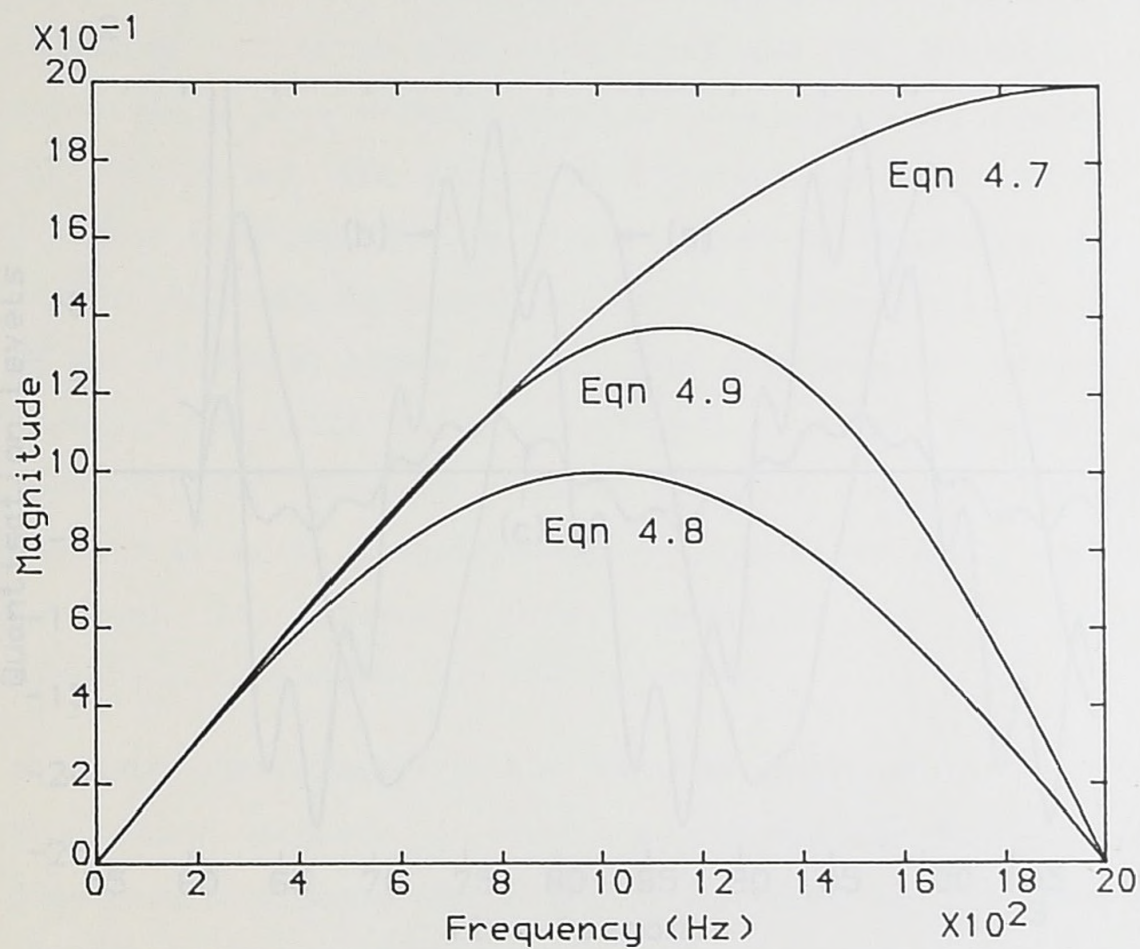


Figure 4.7 Frequency responses for three methods of formulating the current derivative.

Equation 4.7 (Eq. 4.7) and Equation 4.8 (Eq. 4.8) are based on the assumption that the source SCL = 40VA, Fault base = A phase to earth, Fault distance = 50km, Harmonic = 5% 7th 1.

CHAPTER 4  
FAULT EVALUATION

4.1 INTRODUCTION

Previous Chapters have described how the impedance estimates are calculated from the voltage and current signals, and, how filtering is employed to render the estimates such that they are not corrupted by

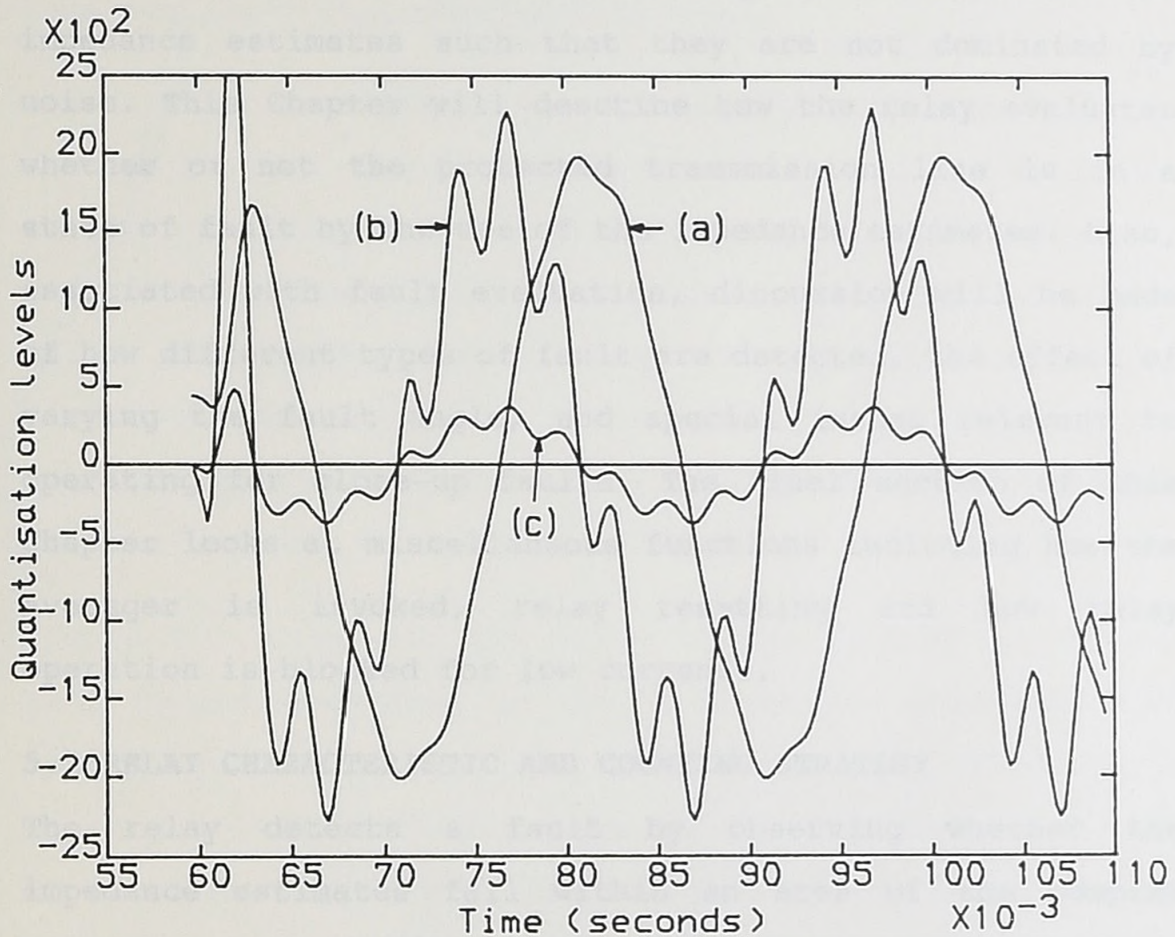


Figure 4.8 A phase line current (a) and its derivative calculated using Equation 4.8 (b) and Equation 4.9 (c) [ Line length = 100km, Source SCL = 5GVA, Fault type = A phase to earth, Fault distance = 80km, Harmonic = 5% 7th ].

## CHAPTER 5

### FAULT EVALUATION

#### 5.1 INTRODUCTION

Previous Chapters have described how the impedance estimates are calculated from the voltage and current signals, and, how filtering is employed to render the impedance estimates such that they are not dominated by noise. This Chapter will describe how the relay evaluates whether or not the protected transmission line is in a state of fault by the use of the impedance estimates. Also, associated with fault evaluation, discussion will be made of how different types of fault are detected, the effect of varying the fault angle, and special issues relevant to operating for close-up faults. The final section of this Chapter looks at miscellaneous functions including how the averager is invoked, relay resetting and how relay operation is blocked for low currents.

#### 5.2 RELAY CHARACTERISTIC AND COUNTING STRATEGY

The relay detects a fault by observing whether the impedance estimates fall within an area of the complex impedance plane called the **characteristic**. Since the filtering used in calculating the impedance estimates is not perfect, the single occurrence of the measured impedance being within the characteristic is not sufficient to identify a fault. Thus, a counting strategy is employed where a counter is incremented every time the impedance is within the characteristic. When the counter reaches a preset level, the relay signals a fault. Figure 5.1 shows the quadrilateral characteristic used in the simulation.

Note that this characteristic is **fixed**, i.e. the boundaries of the characteristic do not vary with time. In the next Chapter, which describes the coverage of faults with significant fault resistance, the characteristic will be seen to vary. However, for the present it will be assumed that faults do not encompass large fault resistances and thus the fixed characteristic is used.

Due to the line angle of a 400kV transmission line being in the region of  $85^\circ$ , the reactance value (X), with due respect to the numerical conditioning of the algorithm, will always be more inherently accurate than the resistance value (R). Thus, the counting strategy is weighted in favour of the X values rather than the R values. The boundary of the characteristic on the positive reactance side is referred to as the **reach point**.

Figure 5.1 shows how the value of the counter increment, INC, varies according to the area of the characteristic inside which a particular sample estimate of measured impedance lies. INC is set to +9 for impedances measured within the first 80% of the characteristic, and decreases to a value of +1 for impedances close to the reach point. Faults beyond the reach point result in INC assuming a value of -1 for impedances close to the reach point, decreasing to -9 for impedances far away from the reach point. The change in INC as the fault falls near the reach point contributes to ensuring correct reach point accuracy. There is no need to grade the counter increment values towards the negative reactive boundary since reverse faults are blocked by the directional reactance check which is

described in Section 5.6.2.

The characteristic boundaries, shown in Figure 5.1, refer to positive phase sequence (pps) impedance values. The positive reactive reach point setting value,  $X_R$ , is normally set to 80% of the estimated total line reactance. Since the line impedance can never be known with great certainty, setting the reach point at 80% of the line ensures that overreaching for faults on the next line is minimised. The characteristic allows a constant value of fault resistance,  $R_R$ , throughout the protected area, by tilting the positive resistive limit by the line angle,  $Z_{ang}$ . Since the relay has directionality, and can discriminate between forward and reverse faults, it is permissible to allow negative reactive and resistive limits,  $-X_0$  and  $-R_0$ , to facilitate accurate discrimination for faults close to the relaying point.

The relay flags a trip when the counter reaches a value of 45. To assist the relay resetting process, the counter is allowed to reach a maximum count of 90 after a trip has occurred.

Note that in the case of, say, comparing the X value against the reach point reactance  $X_R$ , the relay actually compares  $D.X$  against  $D.X_R$  to preclude the need for digital division as discussed in Chapter 3.

The operation of the counting strategy is illustrated in Figure 5.2 which shows the X, R, counter and relay trip flag for the first 10ms after an 'a' phase to earth fault, 20km from the relay on a 100km line. The fault inception

angle was  $90^\circ$  and the source SCL was 5GVA.

### 5.3 EFFECT OF FAULT INCEPTION ANGLE

#### 5.3.1 Statement of the problem

Figure 5.3 shows the variation of the R and X values as the impedance changes from the unfaulted system state at full load to a single phase to earth fault. Three curves are shown in each graph of Figure 5.3 corresponding to fault inception angles of  $0^\circ$ ,  $30^\circ$  and  $90^\circ$ . Note how the different fault inception angles lead to different trajectories of the impedance from the unfaulted to the faulted state. This variation in the impedance estimate is due to the group delay of the prefilter. As the transition is made from pre-fault to post-fault, the prefilter transiently contains both pre-fault and post-fault information and thus leads to the described impedance variation. Clearly, changing the fault angle will change the information held in the prefilter during the group delay and hence lead to different impedance trajectories.

Figure 5.4 shows the operation of the relay for an 'a' phase to earth fault which occurred just beyond the reach point of the relay, i.e., the fault was slightly beyond the protected area of the relay. It can be seen from Figure 5.4 that the X value, after the group delay, falls just outside of the reactive reach point. However, due to the variation of R and X during the prefilter group delay, the counter reaches a value of 45 before R and X have converged on their post-fault values and so the relay incorrectly flags a fault.

It is worth noting that, since the maximum value of INC is 9, and the trip value of the counter is 45, the relay can flag a fault in 5 samples or 1.25ms. It will be recalled from Chapter 4 that the prefilter has an impulse response of 3ms and hence there is great opportunity for overreaching by this process.

Figure 5.5 shows the extent of overreach versus fault angle for 'a' phase to earth faults on a 100km line. The prefault power transfer was full load exporting from the relay point. The relay was set to protect 80% of the line length, but, with fault angles between 30° and 45°, the fault could be beyond the end of the line before the relay stopped operating. It was discovered that the specific range of fault angles which lead to overreaching varies with prefault loading.

### 5.3.2 Prevention of overreaching

In order to prevent overreaching of the relay via the fault angle effect, a method of modifying the counter increment INC, described in Section 5.2, to reflect the certainty of the X value estimate was developed. The basis of the method is to compare the rate of change of D.X values with the reach point boundary value  $D.X_r$  and then to alter INC accordingly. Figure 5.6 shows how the  $d(D.X)/dt$  value is calculated;  $d(D.X)/dt$  is the difference between two D.X values spaced INTV samples apart but INTD samples from the most recent value of D.X.

Overreaching is prevented by modifying the value of INC in the following way:

```

if  $|d(D.X)/dt| > |D.X_r/2|$  then INC = 0
if  $|D.X_r/2| > |d(D.X)/dt| > |D.X_r/4|$  then INC = INC/4
if  $|D.X_r/4| > |d(D.X)/dt| > |D.X_r/8|$  then INC = INC/2
if  $|D.X_r/8| > |d(D.X)/dt|$  then INC unchanged

```

Due to the indeterminate nature of  $D.X$  during the prefilter group delay, it is virtually impossible to perform any formal analysis on the calculation of  $d(D.X)/dt$  in order to optimise the values of INTV and INTD. Instead, an empirical study involving detailed examination of the behaviour of  $D.X$  during various fault angles and test runs in excess of 10,000 faults revealed that the optimum setting of INTV is 6 samples and INTD is 3 samples.

Figure 5.7 shows the operation of the relay, for the same fault as Figure 5.4, with the modified counter increment. Note how the counter value becomes 'frozen' during part of the prefilter group delay and thus does not reach a value of 45 or cause the relay to trip. The penalty for using this technique is that the relay operation time is slightly increased by, depending on the fault angle, up to 1.5ms. However, the advantage it brings is that the relay is completely immune to overreaching due to fault angle effects.

## 5.4 EARTH FAULT ELEMENTS

### 5.4.1 General Description

The relay contains three earth fault elements to detect faults occurring between a line conductor and the earth for any of the three phases. Each of the elements calculates its own impedance, as described in Chapter 3, and utilises its own characteristic with increment counter modification

to prevent overreaching due to the fault angle effect, as described in Section 5.3. In the case of the 'a' phase to earth element, in order to calculate the correct impedance, the following substitutions are made into Equation 3.3:

$$\begin{aligned} V_r &= V_a \\ i_r &= i_a + K_{res} \cdot i_{res} \end{aligned} \quad \dots\dots\dots 5.1$$

where  $K_{res}$  is the residual compensation factor and,

$$i_{res} = i_a + i_b + i_c$$

#### 5.4.2 Residual Compensation Factor

From symmetrical component theory, the current flowing in an earth fault flows through all three sequence impedance network and, in order to correctly measure the positive phase sequence impedance between the relay and the fault, it is necessary to compensate by adding part of the residual current to the line current as shown in Equation 5.1. In Appendix 9 it is shown that the residual compensation factor,  $K_{res}$  is given by,

$$K_{res} = 1/3 \cdot [(Z_{10}/Z_{11}) - 1]$$

However, in general,  $K_{res}$  will be a complex number and thus, to give perfect residual compensation, it will be necessary to alter the phase and the magnitude of the residual current,  $i_{res}$ . For the 400kV line configuration given in Appendix 7, the sequence components of the line are:

$$\begin{aligned} Z_{11} &= 0.0175 + j0.31 \quad \Omega_{pri} \text{ km}^{-1} \\ Z_{10} &= 0.1080 + j0.88 \quad \Omega_{pri} \text{ km}^{-1} \end{aligned}$$

And hence,

$$K_{res} = 0.61825 + j0.00234 = 0.61925 \angle -5.6^\circ$$

Generally, for an overhead transmission line, the angle of  $K_{res}$  is small;  $K_{res}$  only assumes large angles for circuits incorporating a significant length of cable.

Since it would be inherently easier to assume  $K_{res}$  to be a real number, a computer program was developed, based on a symmetrical components model of a two ended transmission line, to assess the influence of the argument of  $K_{res}$  on the measured impedance. Figure 5.8 shows how the error in the reach point values of X and R varies with the argument of  $K_{res}$  assuming no pre-fault power flow. Note the difference in the y-axis scales; if  $K_{res}$  is real, the X measurement error is only -0.3% whilst for R an error of nearly +60% occurs. Taking  $K_{res}$  to be real, Figure 5.9 shows the impedance measurement error versus load angle. In this graph it will be observed that the R measurement varies little with load but the X error is at its worst value of -1.2% when the line is pre-fault exporting at full load. Load angle is defined as the angle by which the voltage at the relay end busbar leads the voltage at the remote end busbar. Thus, a positive load angle implies that power is being exported from the relay busbar.

This investigation revealed that the maximum error in the X measurement was -1.2%, and, since the parameters of an overhead transmission are not known to within -1.2% accuracy, it was considered acceptable to make the assumption that  $K_{res}$  was real and accept the error. The

error in the R measurement was not considered to be significant since the R measurement is influenced by arc resistance and, in general, does not reflect the true line resistance. Furthermore, the operation of the relay is biased towards X measurements when the limit of the relay operation, i.e. the reach point, is considered. Further discussion on fault resistance is made in Chapter 6.

Note that it would be relatively simple to provide complex residual compensation by time shifting the residual current to the correct angle. However, this would extend the group delay of the total impedance measuring process and lead to a longer relay operation time, although, due to the small time shifts involved, this effect would not be very significant.

#### 5.4.3 Residual current restraint

Since an earth fault is always accompanied by the presence of residual current, to prevent the earth elements operating for any fault clear of ground, the elements are restrained by checking for the presence of residual current, thus helping towards overall relay discrimination. This is accomplished by calculating a value of  $D$ , as described in Equation 3.4, by substituting  $i_{res}$  for  $i_r$ ; this value will be referred to as  $D_0$ . In Appendix 10, it is shown that

$$D = \omega \cdot I_{max}^2 \cdot \sin\phi$$

where  $\phi$  is the angular displacement between the solutions to the line equation, and  $I_{max}$  is the peak value of the current. Appendix 10 also relates the actual value of  $D$  to

$I_{max}$  measured in secondary amperes:

$$I_{max} = 0.002828 \cdot \sqrt{D} \quad A_{sec}$$

Thus, the value of  $D_0$  may be related to the secondary residual current.

To restrain the earth elements, the value of  $D_0$  is compared against a threshold,  $D_0THR$ . The outcome of the comparison adjusts the counter increment,  $INC$ , as follows:

if  $D_0 < D_0THR$  then  $INC = 0$

if  $D_0 \geq D_0THR$  then  $INC$  is unaltered

Since the relay cannot trip unless the counters reach a level of 45, the earth elements are restrained from operating unless there is sufficient residual current present. The value of  $D_0THR$  used was 8,000 which corresponds to a secondary residual current of 0.25A.

Figure 5.10 shows the behaviour of  $D_0$ ,  $X$  and the trip counter for an 'a' phase to earth fault occurring at 40km from the relay on a 100km line. The source SCL was 5GVA, the fault angle was  $90^\circ$  and there was full load exporting prior to the fault. Figure 5.10 illustrates that using this method of residual current restraint, there is no increase in the relay operating time since  $D_0$  exceeds its threshold value well before the  $X$  measurement has converged to its post-fault value. Note that  $D_0THR$  is not shown in Figure 5.10 since it is so small compared with the value of  $D_0$ .

## 5.5 PHASE ELEMENTS

### 5.5.1 General description

The phase elements detect faults existing between any two

phases of the transmission line. Thus, three elements exist to detect faults between a-b, b-c and c-a phases. The elements operate, similar to the earth elements, via the use of their own characteristic. In order to calculate the impedance for the, say b-c element, the following substitutions are made into Equation 3.3:

$$V_R = V_b - V_c$$

$$i_R = i_b - i_c$$

and hence the relay measures the mean impedance of the two lines up to the fault point. Note that since the difference in the line currents is used, it does not matter whether the line currents have been residually compensated or not.

#### 5.5.2 Phase element restraint

To prevent the phase elements operating for faults and system conditions which do not involve an imbalance in the line currents, e.g. three-phase faults and power swings (which are discussed in Chapter 7), a test is made for the presence of non positive phase sequence current. Ideally, for phase faults, the presence of negative phase sequence current would be detected. However, to detect nps current, it is necessary to delay the line currents by  $60^\circ$ , thus incurring an extra 3.33 ms group delay on the operation of the phase element. Since this would lead to increased relay operating time, an alternative approach was sought.

In order to detect the presence of non pps current, a test is made on the D values, which, as discussed earlier, are related to the square of the magnitude of the line currents. The D values calculated for the phase fault

elements will be referred to as  $D_{ab}$ ,  $D_{bc}$  and  $D_{ca}$ . In addition, the mean value,  $D_{mean}$ , of  $D_{ab}$ ,  $D_{bc}$  and  $D_{ca}$  is also calculated. The technique for restraining phase element operation involves comparing  $D_{mean}$  with the difference between each of  $D_{ab}$ ,  $D_{bc}$  and  $D_{ca}$  in turn. If the difference is less than  $D_{mean}$ , then the system is relatively balanced, and so the phase elements are restrained; if the difference exceeds  $D_{mean}$ , the elements are enabled. Figure 5.11 shows the algorithm used for phase element operation. This method of phase element restraint has been tested and found to work satisfactorily for all expected unbalanced system conditions for which the phase elements are not required to operate.

Note that earth faults may also enable the phase elements since earth faults also result in considerable imbalance of the line currents. However, since the resistive reach point of the characteristic, i.e.  $R_r$  in Figure 5.1, is set smaller for the phase elements than for the earth elements, phase faults generally not encompassing as much fault resistance as earth faults, then the likelihood that the phase elements will operate for earth faults is minimised.

## 5.6 CLOSE-UP FAULTS

### 5.6.1 Introduction

This section examines the operation of the relay when subjected to faults close to the busbar on which the relay is situated. There are two potential problems associated with the use of digital distance relays under these situations. Firstly, if the fault occurs very close to the relay, then the primary voltage will collapse and it is

important that the relay maintains correct directionality. Secondly, if the source local to the relay has a large SCL, then the resulting current may be of a sufficient magnitude to cause clipping at the input to the relay ADC.

### 5.6.2 Relay directionality

There are two situations which can result in the primary voltage at the relay point being reduced to virtually zero. These are faults occurring just in front of the relay, in which case the relay should trip, or faults occurring just behind the relay, in which case the relay should block. Note that in each case the relay will measure R and X values of zero, which, by reference to Figure 5.1, will fall within the relay characteristic. Faults occurring behind the relay location are referred to as reverse faults; faults in front of the relay are referred to as forward faults.

In order to maintain correct directionality for voltage collapse faults, the relay calculates a value of reactance which is based upon the post fault current and the pre fault voltage. This reactance will be referred to as the directional reactance,  $X_m$ , and is calculated for all the elements. Thus, taking Equation 3.8 and transforming it into discrete sampled form, gives

$$D(n).X(n) = D(n).\omega[v_{R2}(n).i_{R1}(n) - v_{R1}(n).i_{R2}(n)] \dots\dots\dots 5.2$$

and hence,

$$D(n).X_m(n) = D(n).\omega[v_{R2}(n-p).i_{R1}(n) - v_{R1}(n-p).i_{R2}(n)] \dots\dots\dots 5.3$$

where  $p = k.N$ ,  $N =$  number of samples per power system

frequency cycle (for 50Hz = 80 at 4kHz sampling frequency), and,  $k$  = integer number of pre fault cycles used in calculating  $X_m$ .

Hence, it is necessary for the relay to store previous values of all three phase voltages in order that  $X_m$  can be calculated on all the elements. These stored voltages will be referred to as the memory voltages.

Since the memory voltage gives information of the phase and magnitude of the busbar voltage before the fault occurred, it follows that the polarity of  $X_m$  should be positive for faults occurring in front of the relay, and negative for faults behind the relay. Thus, in order to polarise the relay, a further test on the operation of any of the elements described in Section 5.4, is that  $X_m$  should be positive.

When the memory voltage has run out,  $X_m$  will tend to the same value as  $X$ . Since this value may be zero, the detection of the polarity of  $X_m$  is made around a small positive limit rather than zero, and thus the test made on  $X_m$  is that it must exceed the directional reactance limit,  $X_0$ , as shown in Figure 5.1. This is a criteria for setting INC greater than zero; if  $X_m$  is less than  $X_0$ , INC is set to -9. If  $X_m$  were compared with zero, it is possible that maloperation could occur due to  $X_m$  alternating between small positive and negative values.

The behaviour of  $X_m$ ,  $X$  and the trip counter is typically as shown in Figures 5.12 and 5.13 for forward and reverse faults respectively. In both cases the relay is protecting a 100km line with local and remote SCL's both set at 5GVA.

Both faults are 'a' phase to earth occurring at a fault angle of  $90^\circ$ . For Figure 5.12 the fault is on the busbar just in front of the relay, and, for Figure 5.13, the fault is just behind the relay. Both Figures relate to the operation of the 'a' phase to earth element.

For the forward fault, Figure 5.12, it can be seen that the reactance converges to zero after the fault.  $X_m$ , however, remains above the directional limit,  $X_0$ , for as long as the memory voltage is available, which, in this case is one cycle. Thus, the relay operates correctly for this case and the trip counter exceeds the trip level, thus causing a relay trip, at 7.5 ms after the fault was applied. It can be seen that when the memory voltage expires,  $X_m$  converges towards zero, thus invalidating the directional check and hence, the trip counter falls back to zero.

In Figure 5.13, the reverse fault causes  $X_m$  to assume a negative value, below  $X_0$ , and the trip counter remains unchanged, even though the reactance is at zero and hence in the characteristic. Note that when the memory voltage runs out,  $X_m$  goes to zero, which is still less than  $X_0$ , and so the trip counter stays at zero and the relay remains blocked.

The length of the memory voltage will be affected by the relay application and the attitude of the utility running the power system. If it were required to ensure that the relay maintains correct directionality in the event of breaker failure, a memory voltage of 16 cycles in length would not be uncommon.

### 5.6.3 Current clipping on close-up faults

It was shown in Section 2.3.4 how current clipping could occur if the current setting multiplier (CSM) is set to 1 with a distance to fault of 16km or less, and a maximum source SCL of 50GVA. Under this condition, the minimum length of line protected would be 23km, and thus, no clipping would occur at the reach point.

Hence, there is no possibility of overreach due to current clipping since the relay operates normally at the reach point. However, the effect of current clipping was investigated to ensure that correct relay operation occurs for all faults.

Clipping has been observed to occur only on close-up three-phase faults since the fault current for a three-phase fault is larger than for earth or phase faults. This is because only the positive phase sequence impedances are involved in a three-phase fault. Also, the position of the fault at which clipping begins to occur is sensitive to the X:R ratio of the source.

Detection of three-phase faults will be discussed in Chapter 7. However, for the present, it may be assumed that three-phase faults are detected through the phase elements. Figure 5.14 shows the effect of current clipping for a three-phase fault occurring 10km from the relay with a local source SCL of 50GVA and an X:R ratio of 20. The fault inception angle was  $0^\circ$  with respect to the 'a' phase voltage. Figure 5.14a shows  $i_a$  after it has been quantised by the ADC. Note how, due to the exponential offset, the peak values of  $i_a$  are clipped at the maximum positive ADC

value of 8191. Figures 5.14b and c show the R and X values for the a-b element; note the ensuing discontinuities in these values.

However, despite the corrupted measurements, the element indicated a trip signal at 11.5ms after the fault. Thus it can be seen that the incidence of current clipping only leads to an increase in operation time; clearly, even with a fault on the busbars, the relay will operate after the exponential has decayed.

In order to understand why the operating time is increased under current clipping conditions, it is necessary to explain why the R and X values become corrupted. Investigations showed that the prefilter was the primary cause of the corruption since, with reference to Figure 4.4, it can be seen that the prefilter has a zero at dc. Hence, when the current is clipped by the ADC, the resulting waveform contains a dc component, e.g. between 7 and 12ms in Figure 5.14a, and the output of the prefilter falls to zero thus causing the discontinuities in R and X. Furthermore, from Figure 4.4, the length of the impulse response of the prefilter is 3ms, and thus any signal which displays a dc characteristic equal to or exceeding 3ms in length will cause the undesired effect. However, a dc level for less than 3ms will cause less corruption since the prefilter output will not necessarily fall to zero. This is illustrated in Figure 5.14 between 28 and 30ms where the current is briefly clipped but the X and R values are only minimally affected.

Therefore, it has been established that:

- a) Clipping can only occur for a situation where the fault is within the relay's protected area, and,
- b) The relay will operate correctly if the extent of clipping does not exceed the prefilter IR of 3ms.

Thus, a method of increasing relay operating speed for severe current clipping conditions is to detect the occurrence of 3ms of contiguous clips and trip the relay without delay. This method has been implemented and leads to overall acceptable tripping times for close-up faults involving clipping.

## 5.7 MISCELLANEOUS FUNCTIONS

### 5.7.1 Relay reset

After the relay has tripped, and the fault has been removed by the circuit breaker, the relay must reset its trip contact. This is achieved by examining the trip counters for all the elements of the relay. When the fault is removed, the faulted element(s) trip counter(s) will count down, from their maximum values of 90, to zero, as shown in Figure 5.12. After the relay has detected that the trip counters of all the elements have been at zero for 10ms, the relay resets its trip contact.

### 5.7.2 Invoking the averager

The use of signal averagers to improve the frequency domain function of the impedance estimates was described in Section 4.4. For each element it was shown to be necessary to use three separate averagers; one each for D.X, D.R and D. However, now that the concept of  $X_m$  has been introduced, it can be seen that each element, in fact, requires a group

of four averagers, the additional averager being used for  $D.X_m$ . Thus, in totality, the relay uses 24 averagers.

A group of averagers are invoked simultaneously when a potential fault situation is detected. The condition used for this detection is that an impedance estimate has entered the characteristic, or, more specifically, the counter increment value, INC, of that element is greater than zero before the fault angle modification is applied, as discussed in Section 5.3.2. However, since certain fault angles can cause the unmodified INC value to exceed zero at the beginning of the prefilter group delay, an extra 2ms delay is incorporated before the averagers take effect. This ensures that the averagers are not applied before the impedance estimates have converged to their post-fault values.

Note that the state of any of the four averagers in an element will always be the same, e.g. they will all be either disabled or all invoked. However, the averagers of different elements operate independently, e.g. the 'a' earth element averagers may be invoked but the 'b' earth element averagers may be disabled.

Having been invoked, a group of averagers will count up to their maximum window length of 16 samples irrespective of any other condition. To disable a group of averagers, firstly, the window length must be at 16, and secondly, the trip counter must have been zero for the previous 4ms. When disabled, the averagers reduce their window length, one sample at a time, until the window length is 1, at which point they have no effect.

5.7.3 Low current restraint

If the secondary current flowing into the relay falls below 0.25A, then the current is not within the specifications given in Section 2.2, and thus, the relay should be restrained from operating. This is achieved, for every element, by ensuring that the value of D calculated is greater than 8,000. From Appendix 10, this will be seen to correspond to a secondary value of 0.25A. If a D value is below 8,000, then the INC value of that element remains at zero irrespective of the measured impedance.

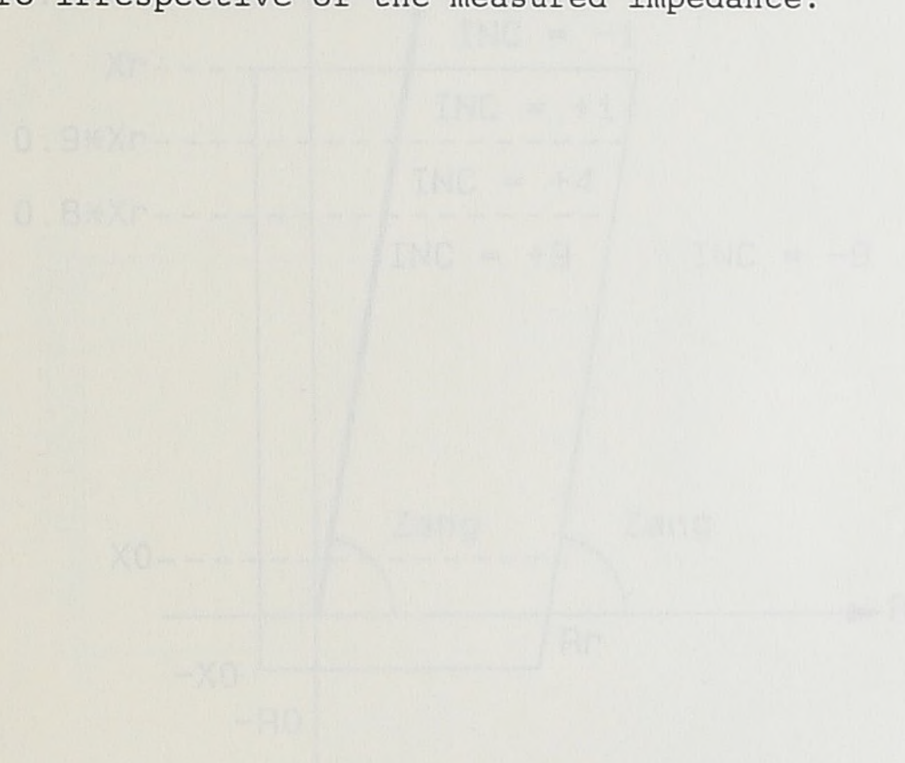


Figure 5.1 Relay quadrilateral characteristics

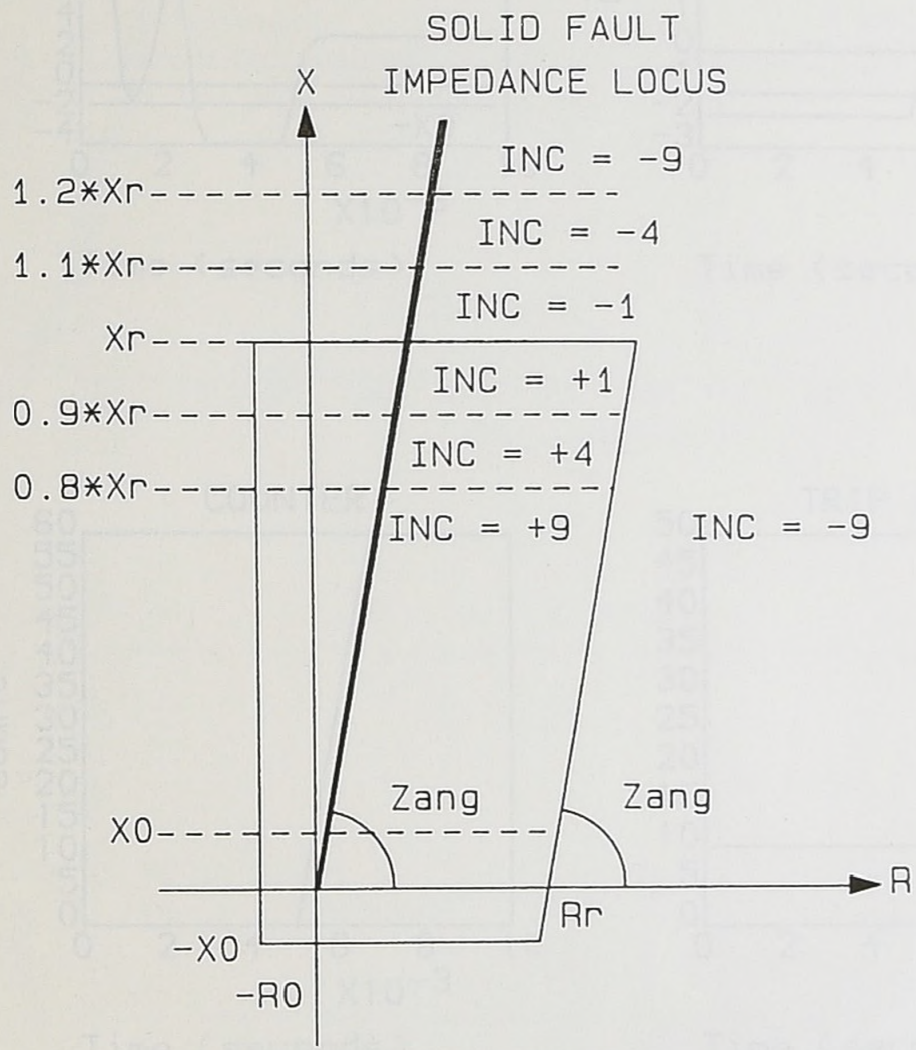


Figure 5.1 Relay quadrilateral characteristic.

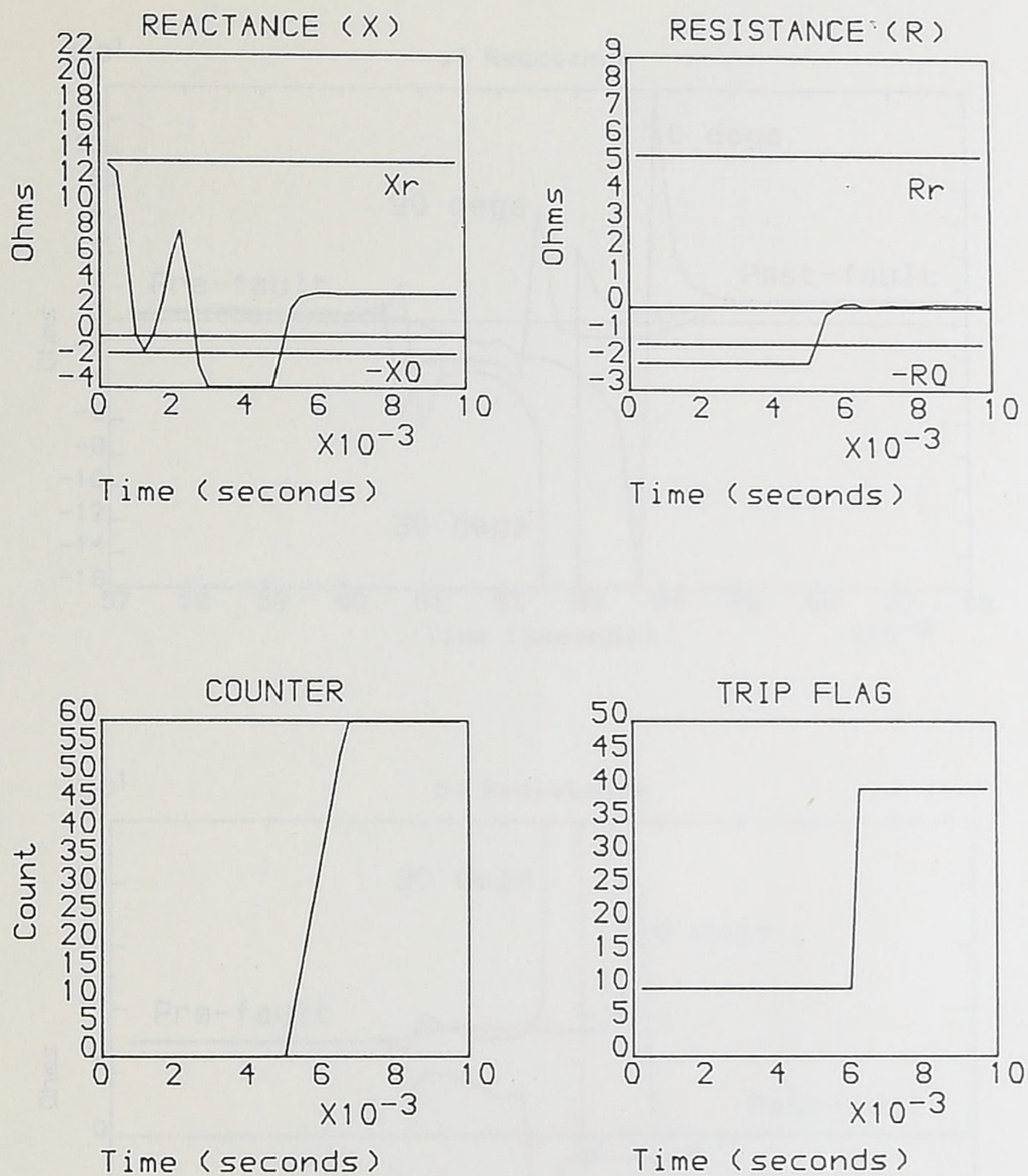


Figure 5.2 Illustrative operation of the relay counting strategy ('a' to earth element).

Figure 5.3

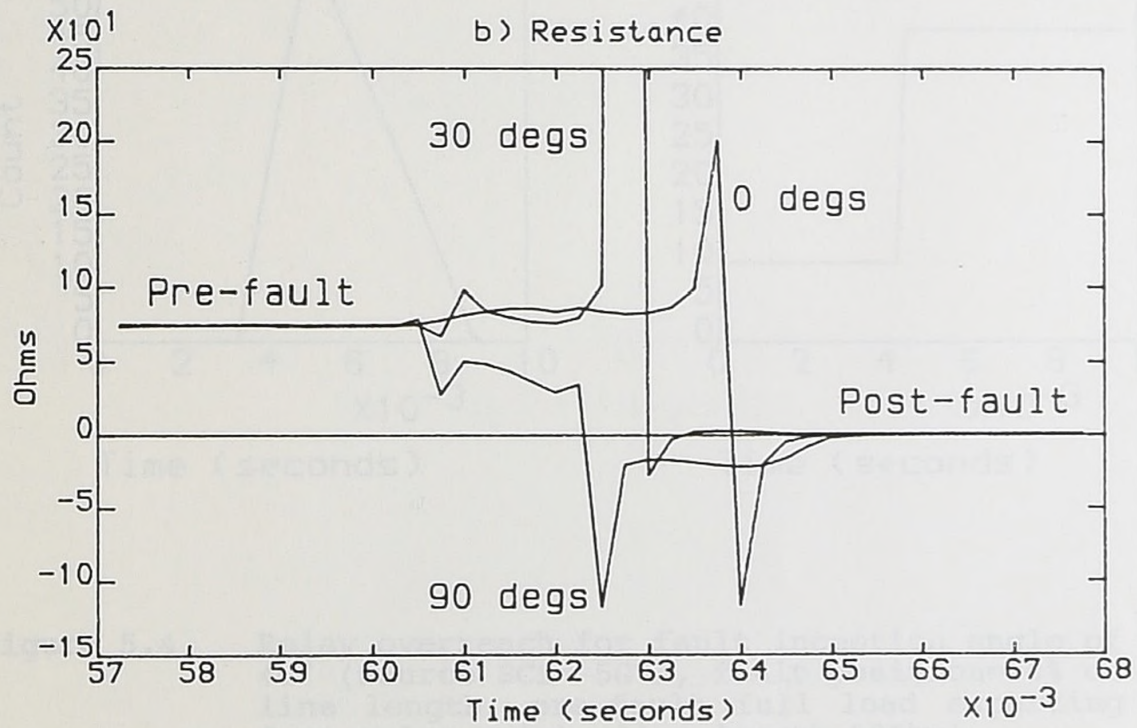
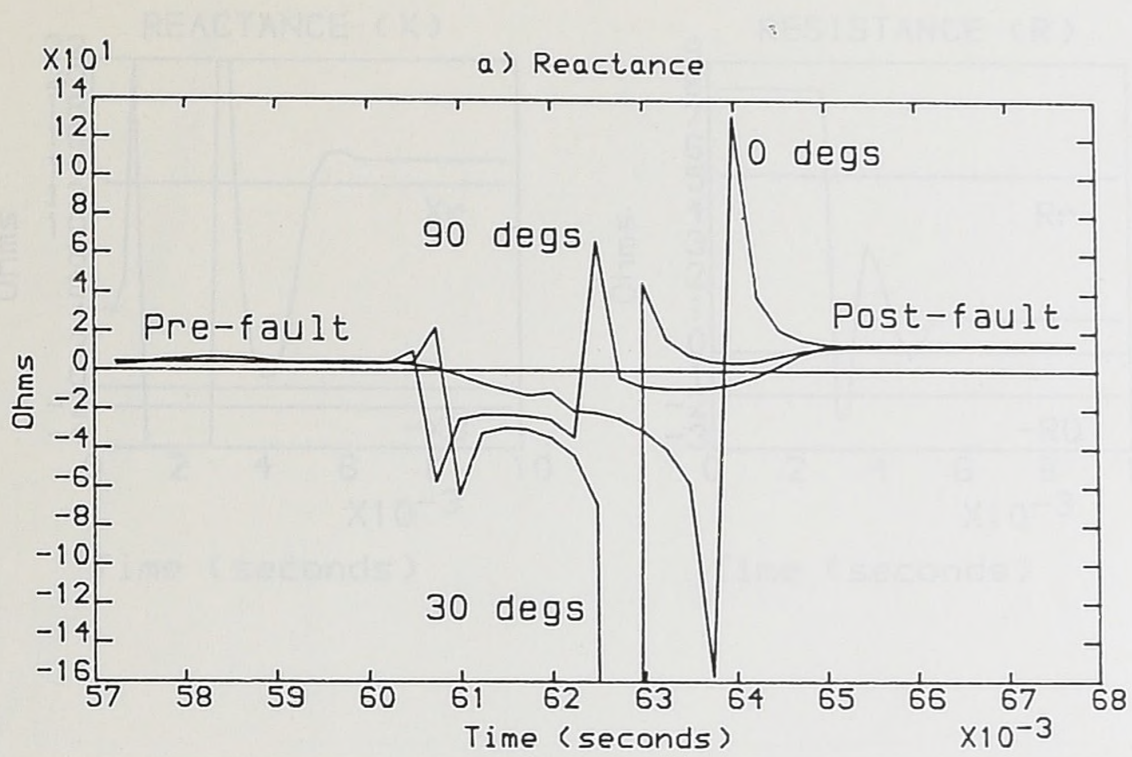


Figure 5.3 Effect of fault inception angle on the convergence of the measured resistance and reactance values.

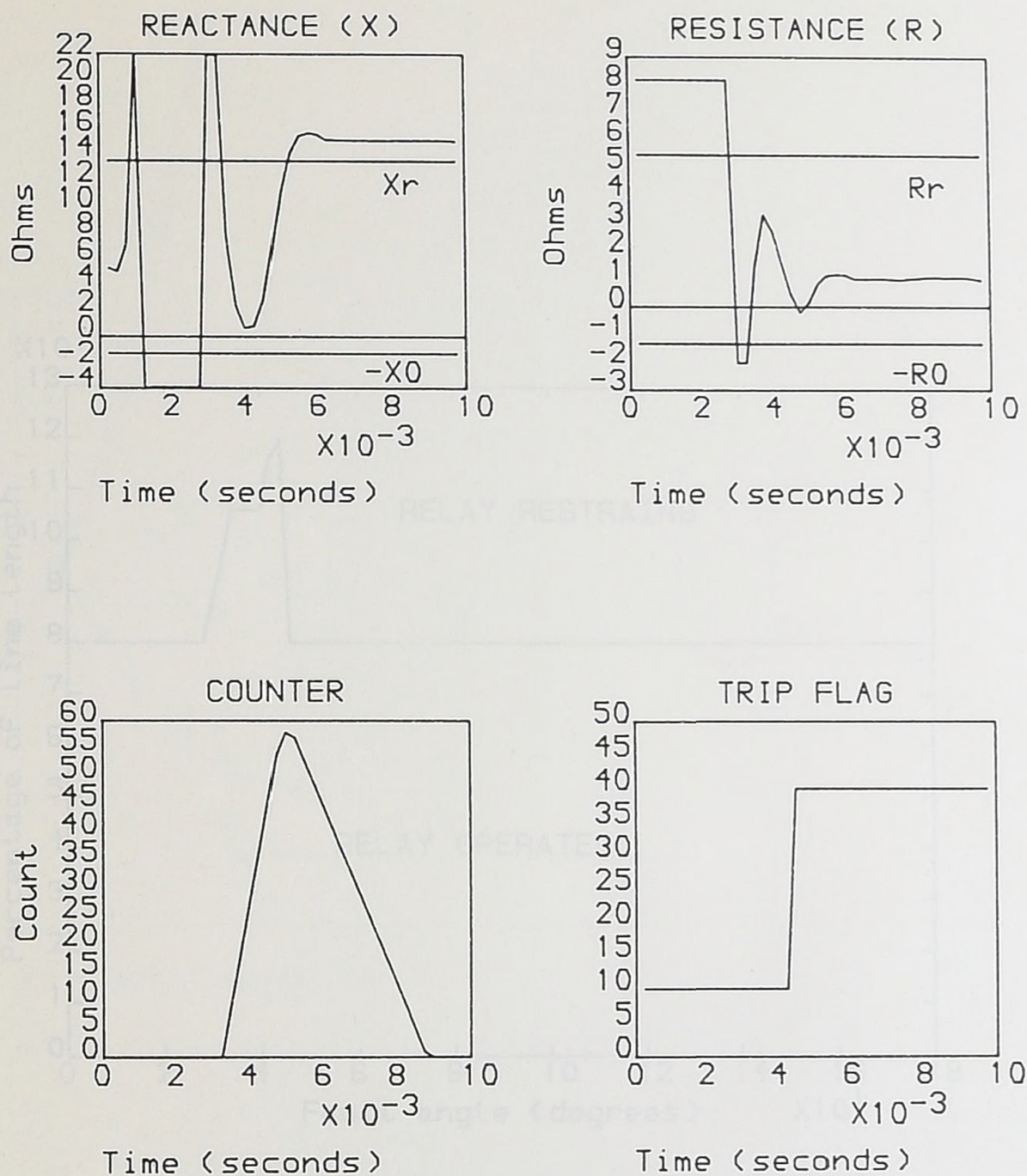


Figure 5.4 Relay overreach for fault inception angle of  $40^\circ$  (Source SCL= 5GVA, fault position=80% of line length, pre-fault full load exporting from relay point, line length=100km).

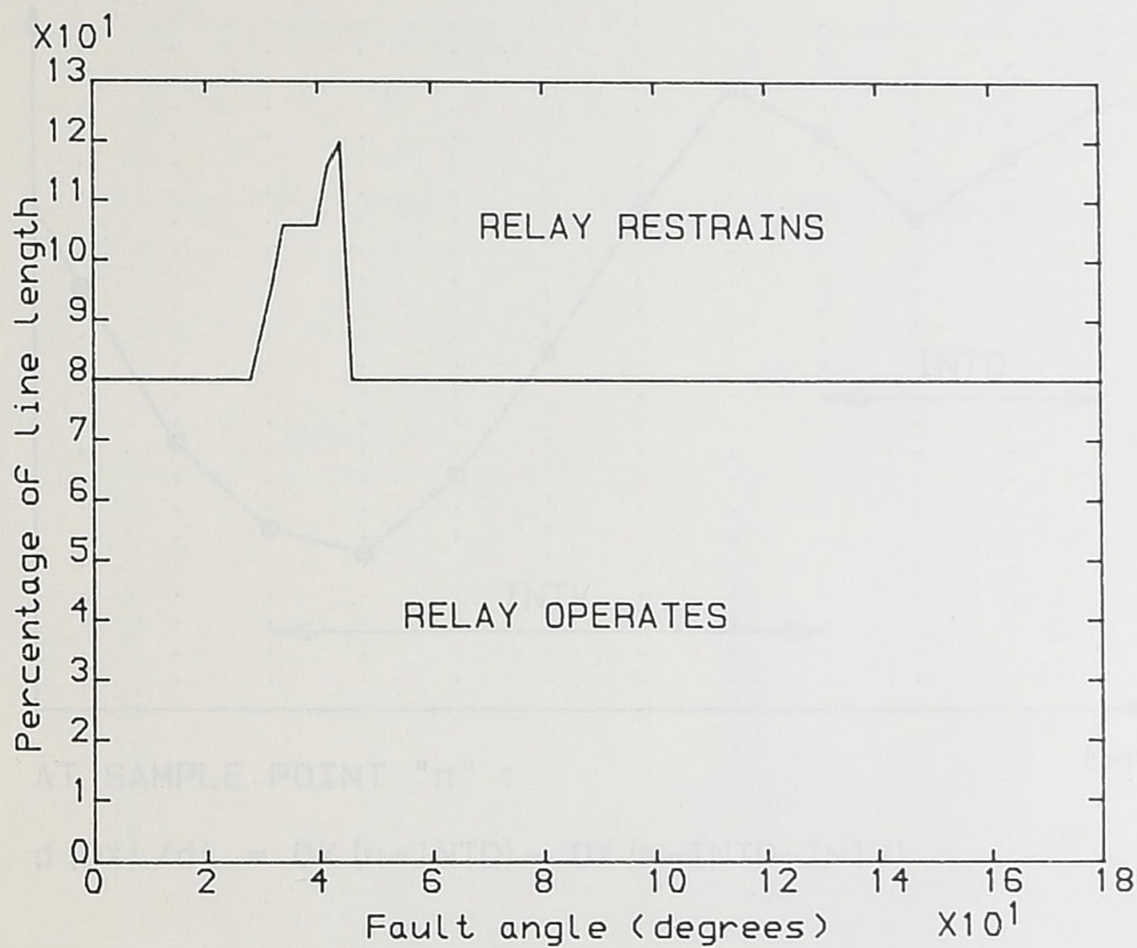
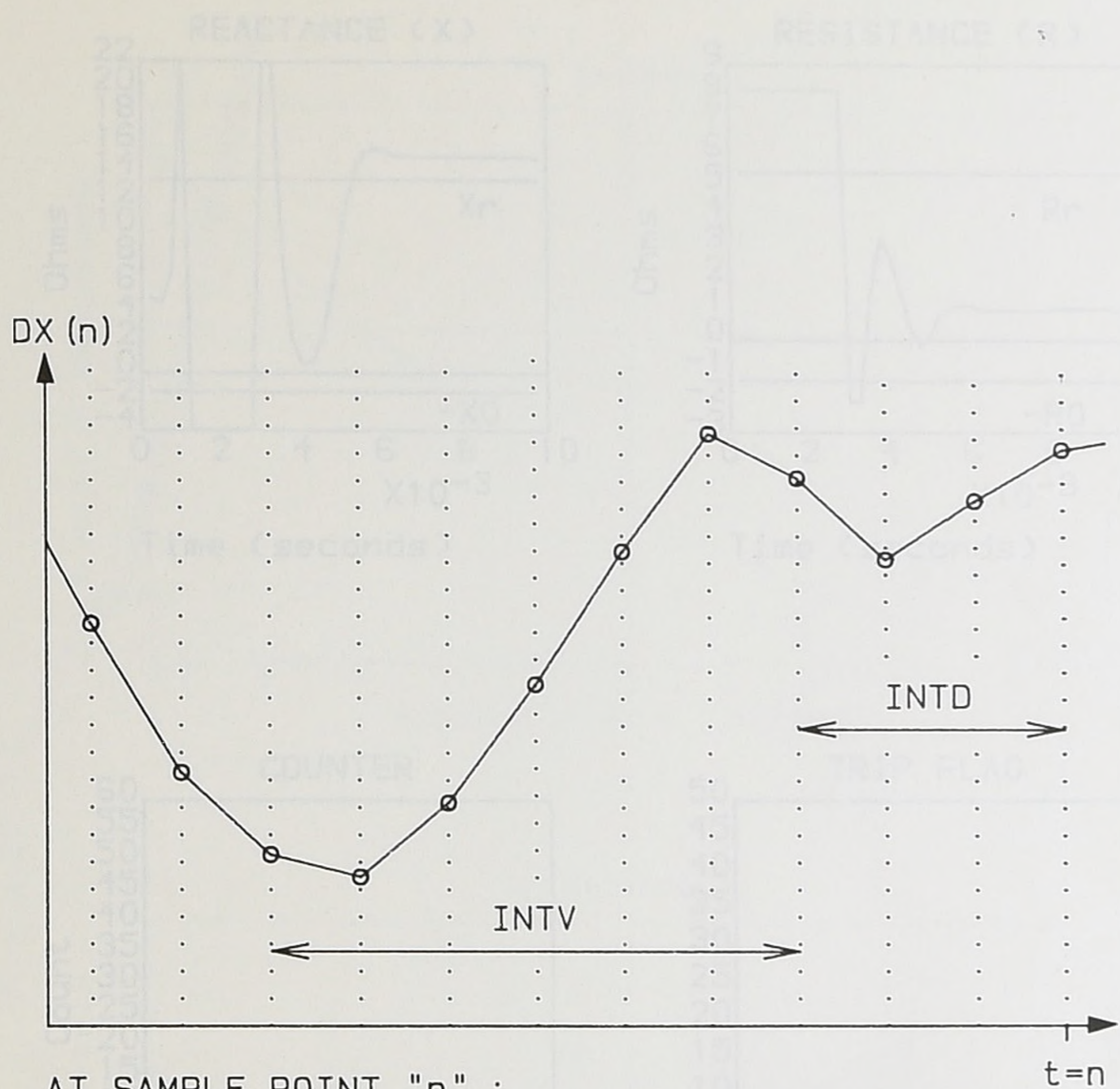


Figure 5.5 Extent of overreach for 100km line length with pre-fault full load exporting ('a' to earth faults).



$$d(DX) / dt = DX (n-INTD) - DX (n-INTD-INTV)$$

Figure 5.6 Calculation of  $d(D.X)/dt$ .

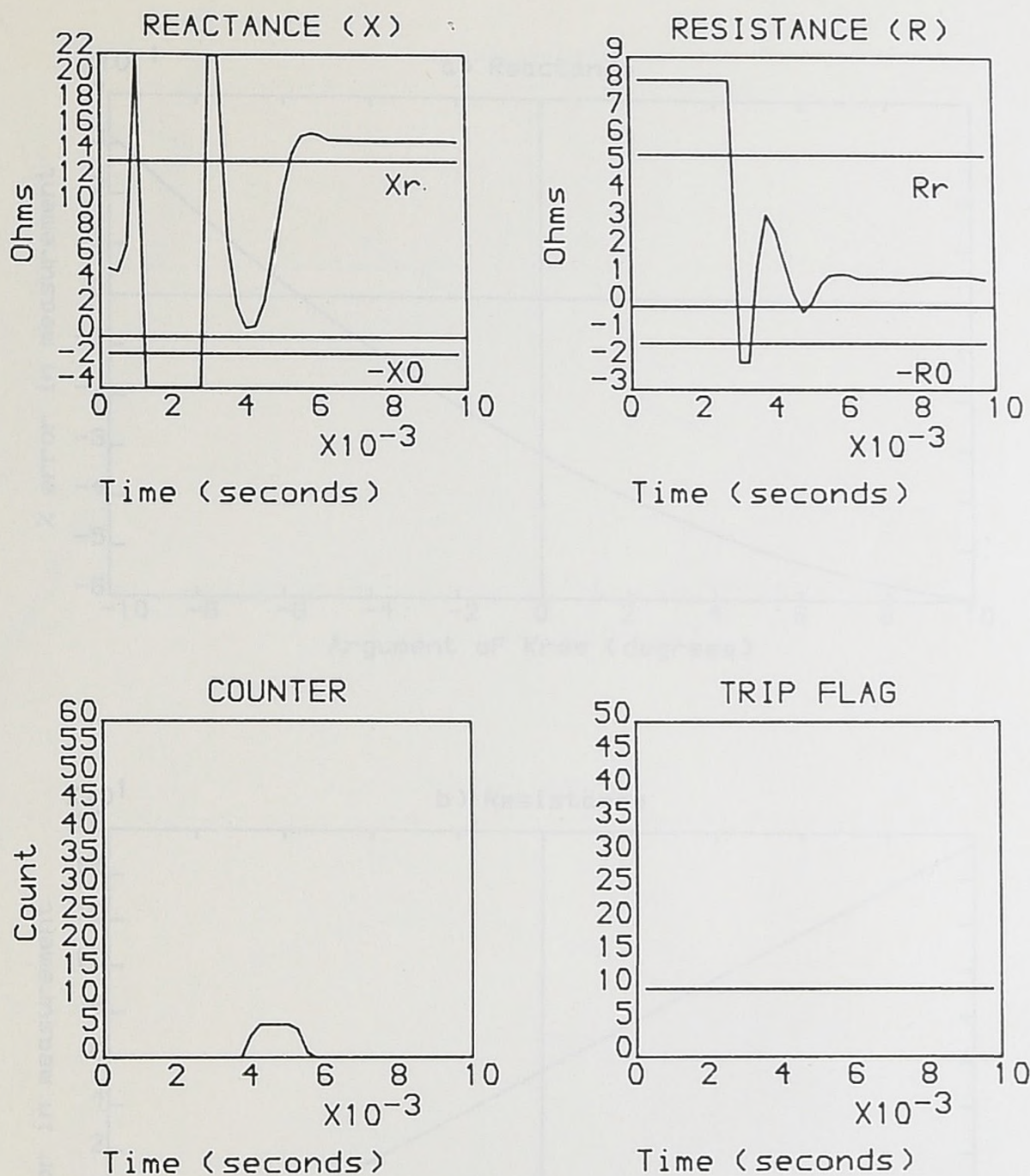


Figure 5.7 Prevention of overreach by modifying the counter increment (same fault as Figure 5.4).

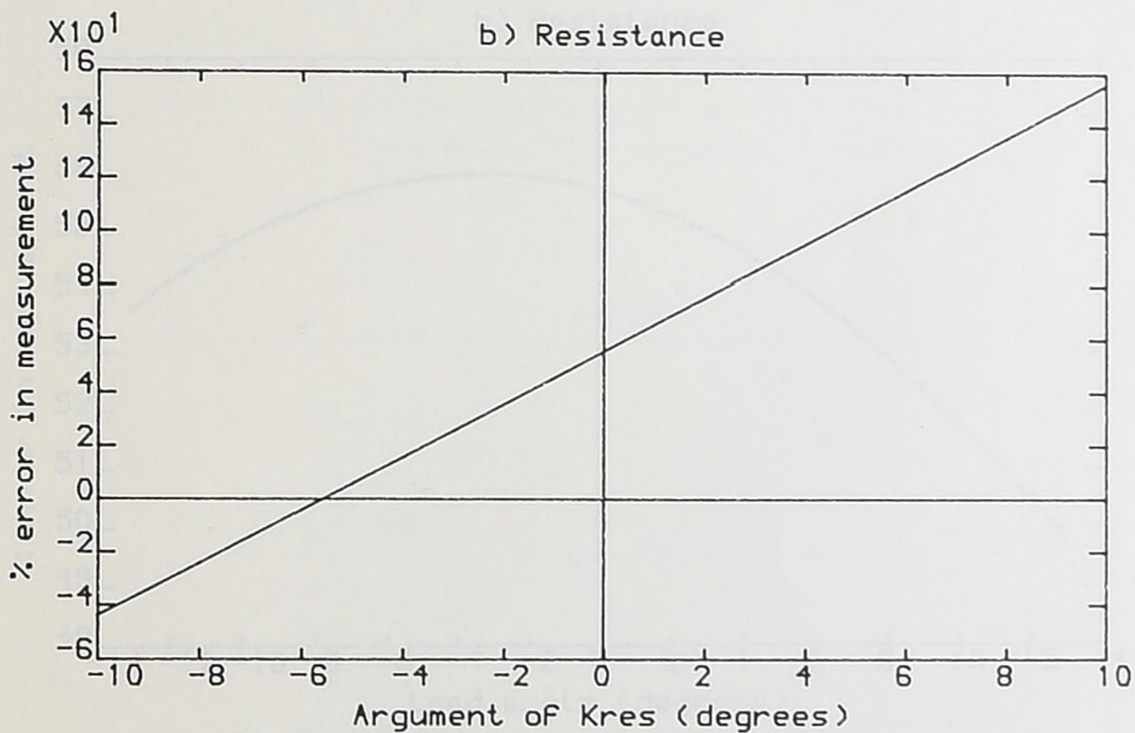
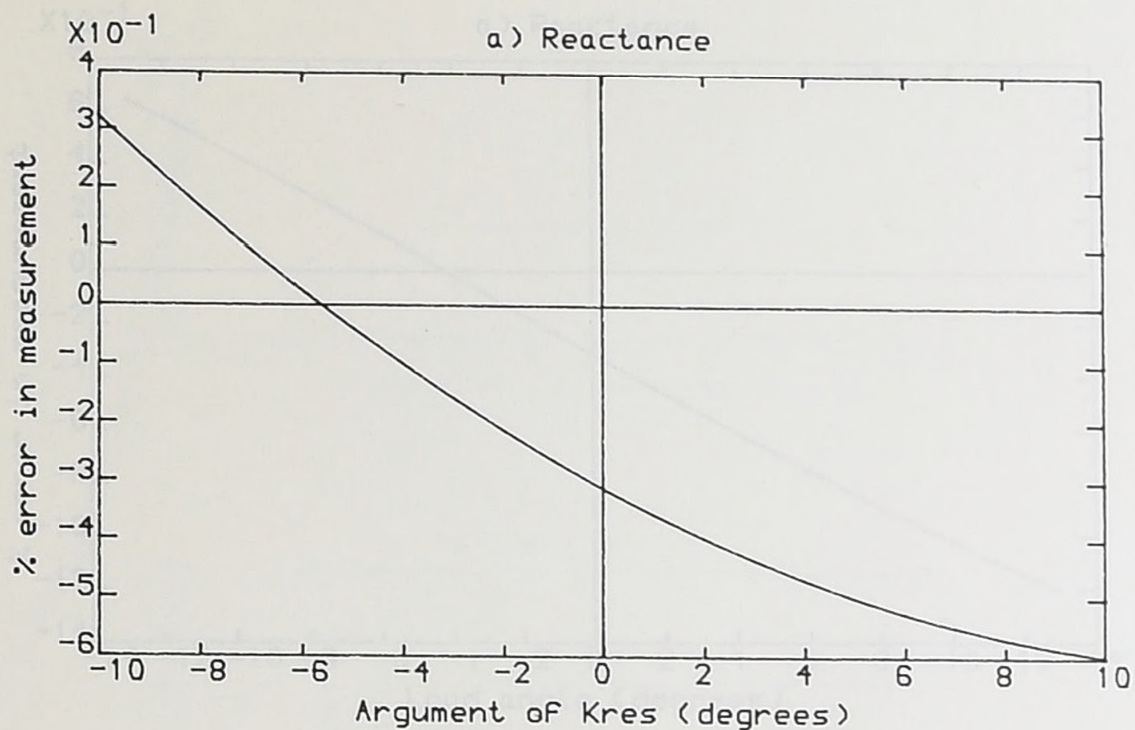


Figure 5.8 Percentage error in impedance measurement versus the argument of the residual compensation factor,  $K_{res}$ .

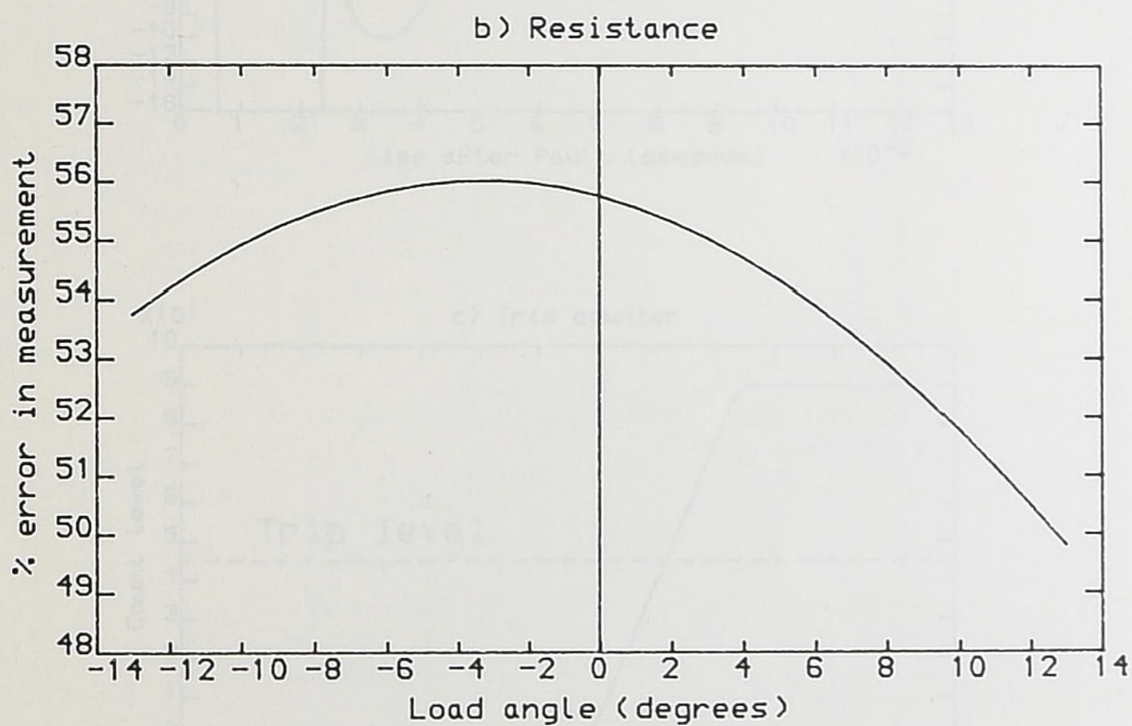
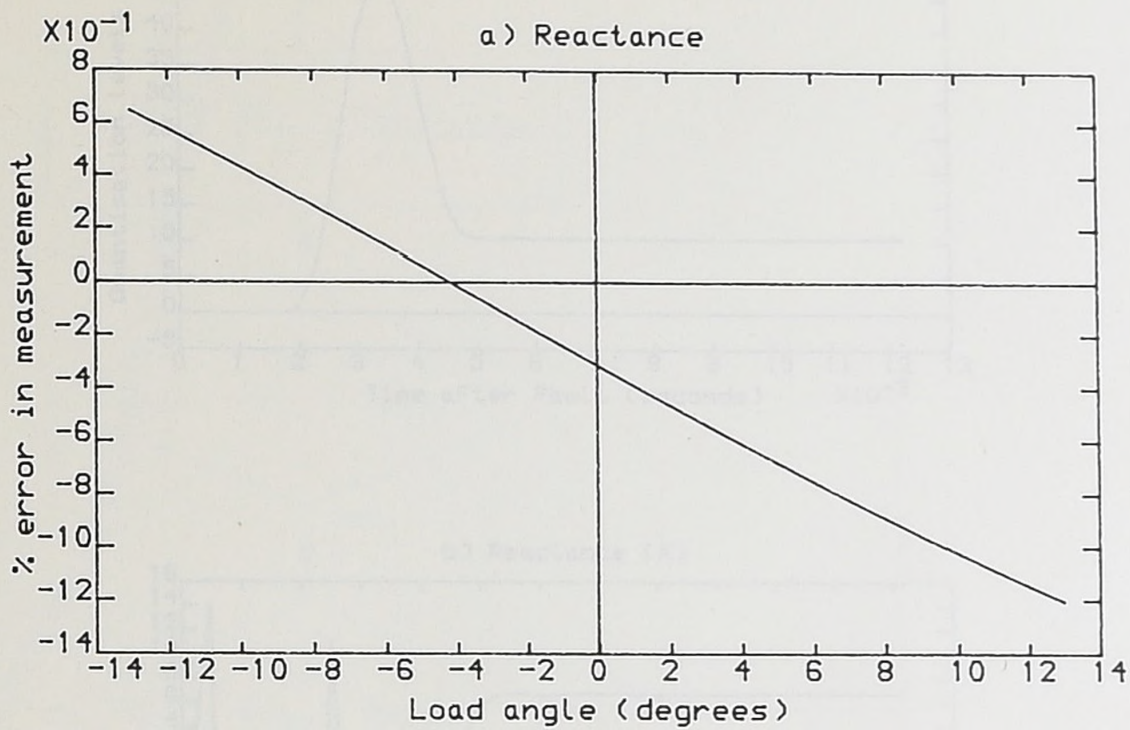


Figure 5.9 Percentage error in impedance measurement versus the load angle for 100km line.

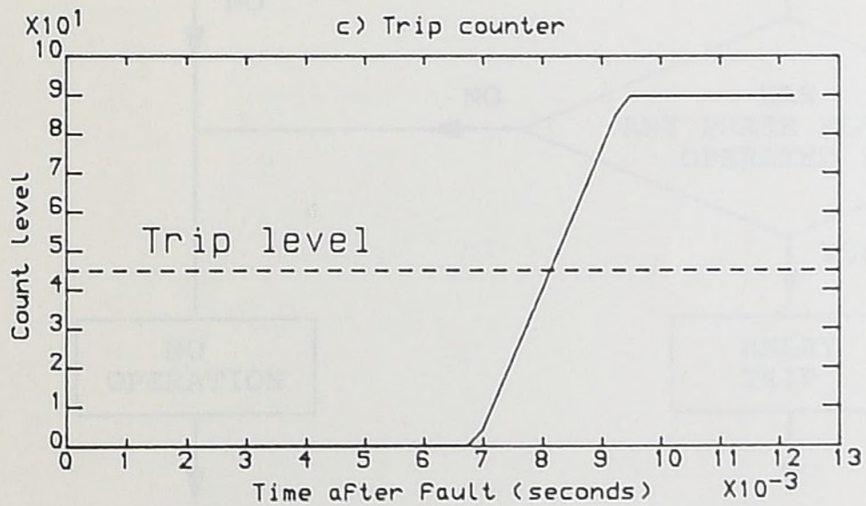
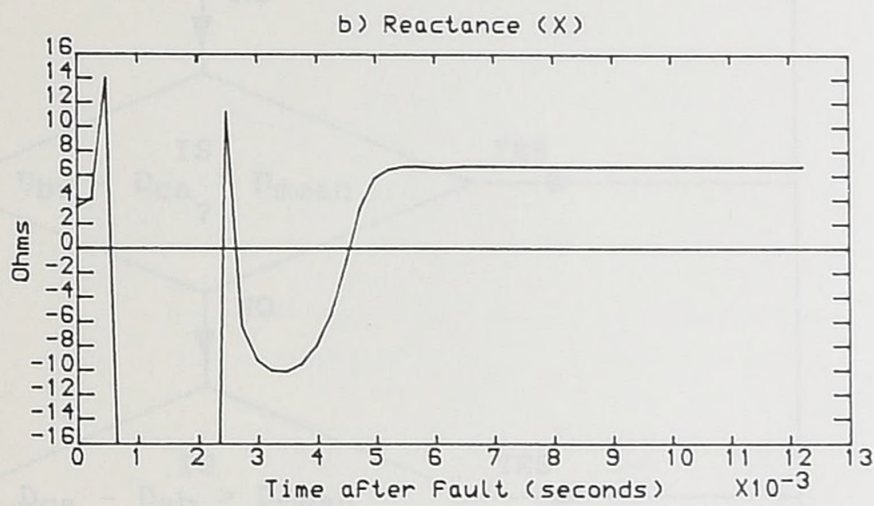
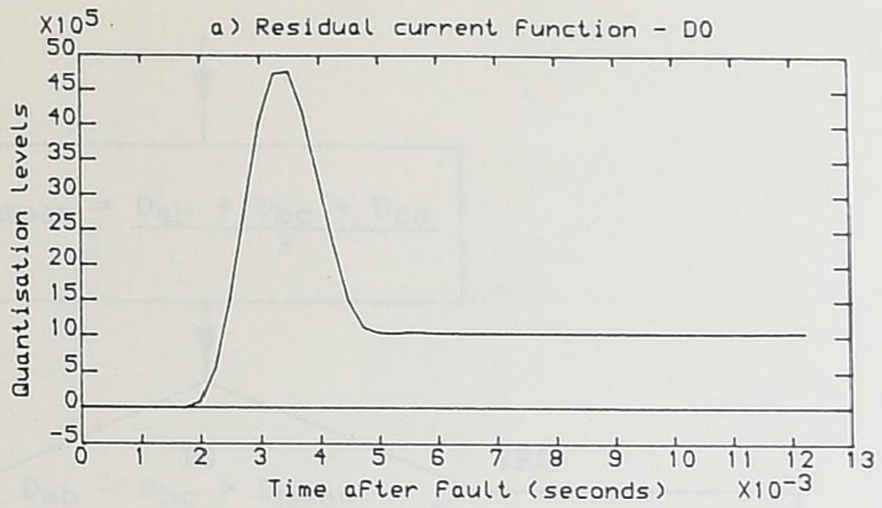


Figure 5.10 Illustrative operation of the relay showing the effect of the residual current function, D0.

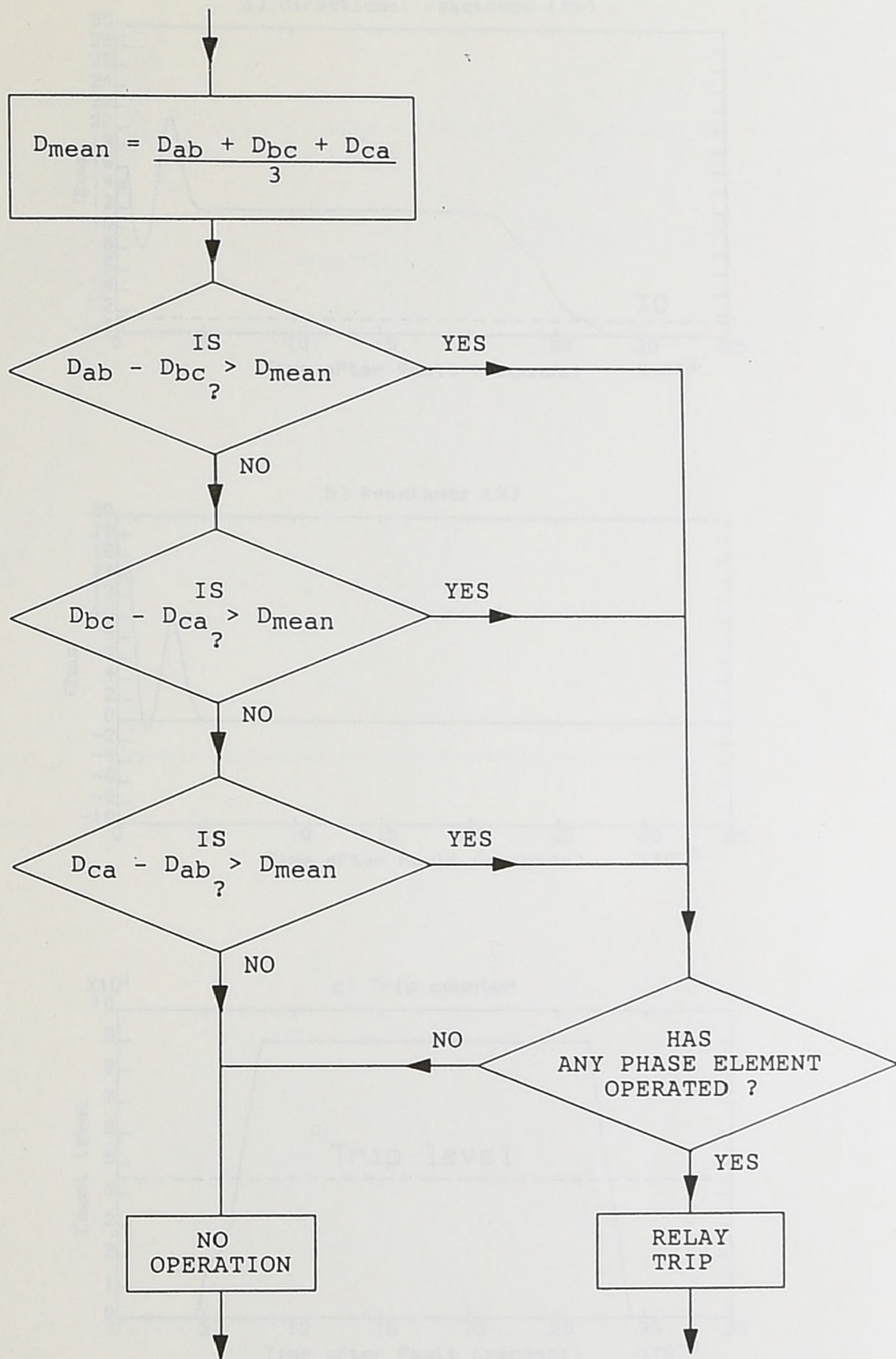


Figure 5.11 Flow chart for the algorithm used to restrain the phase elements in the presence of non pps current.

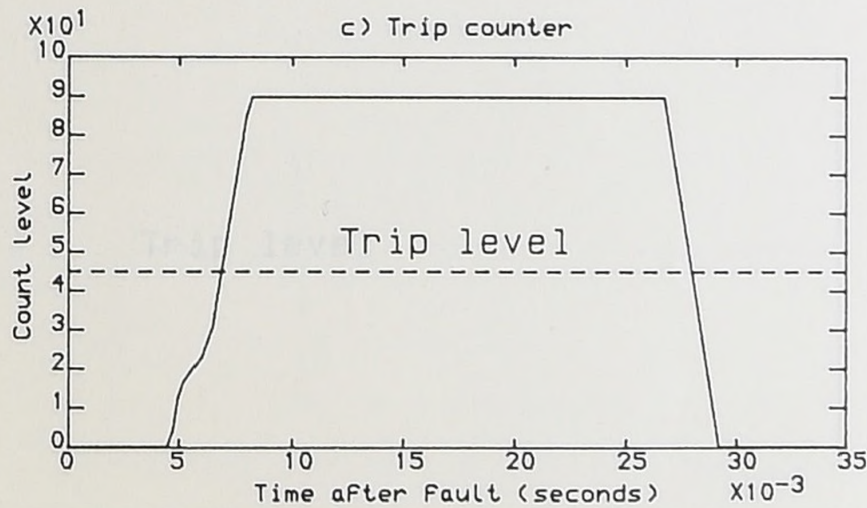
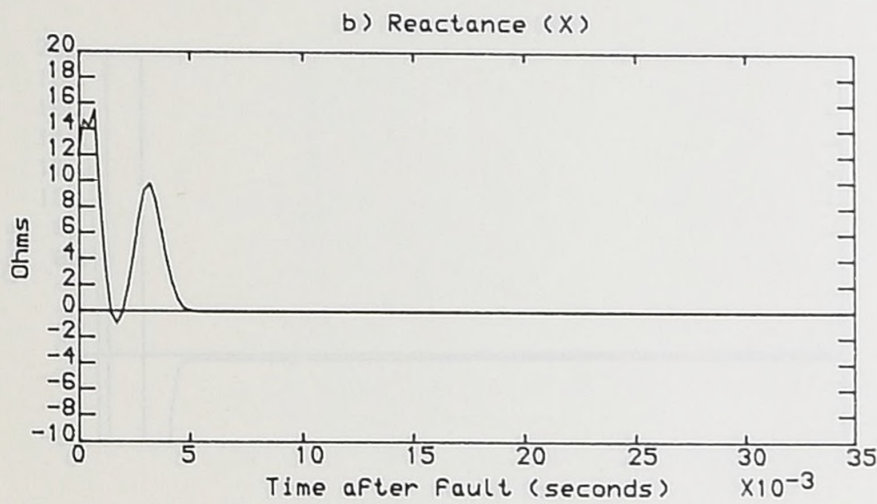
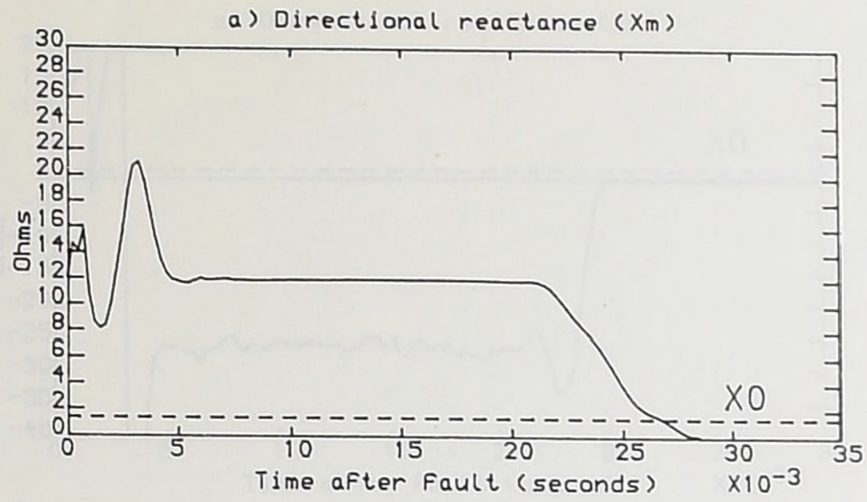


Figure 5.12 Operation of the relay for close-up forward fault.

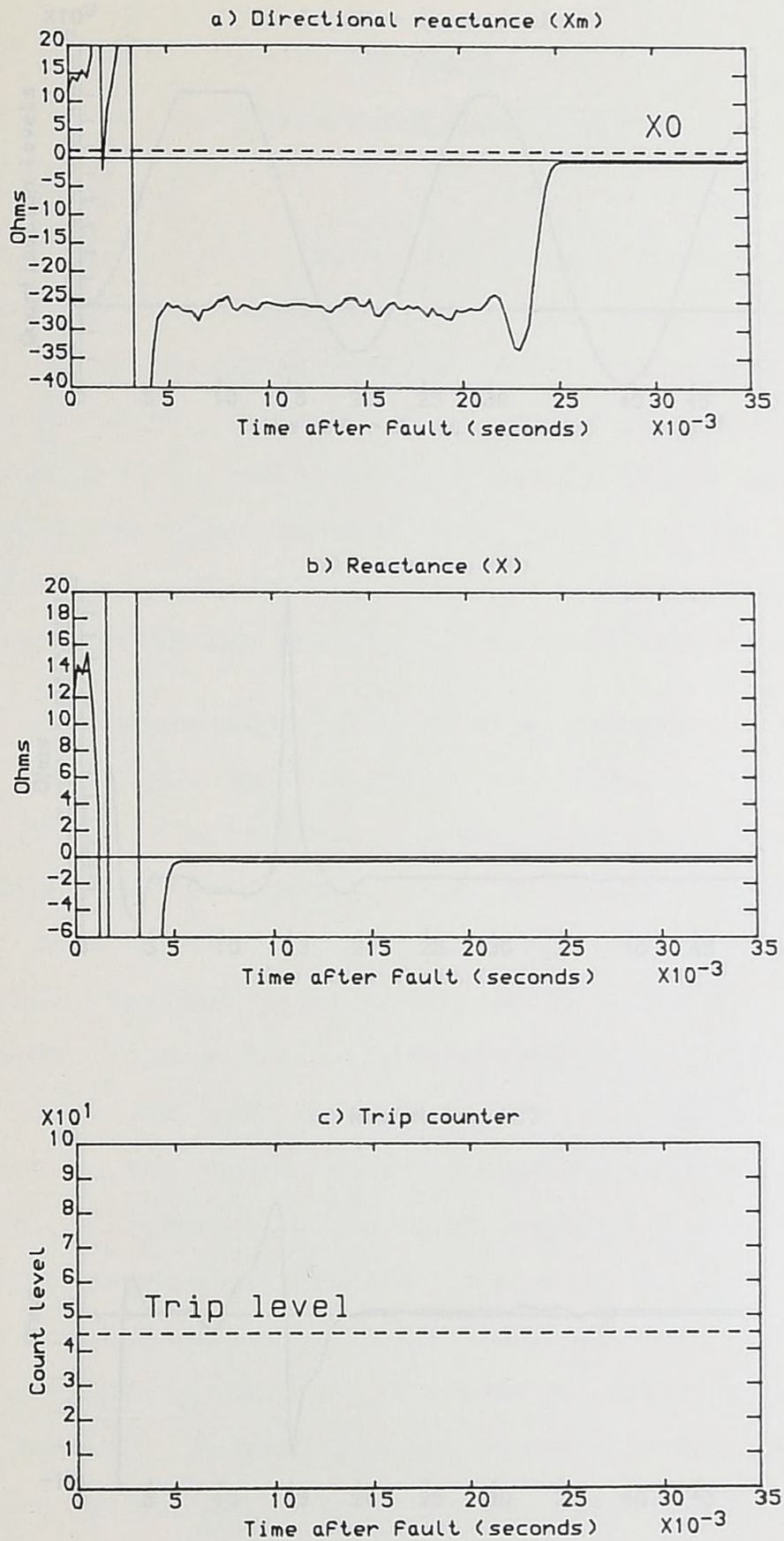


Figure 5.13 Operation of the relay for close-up reverse fault.

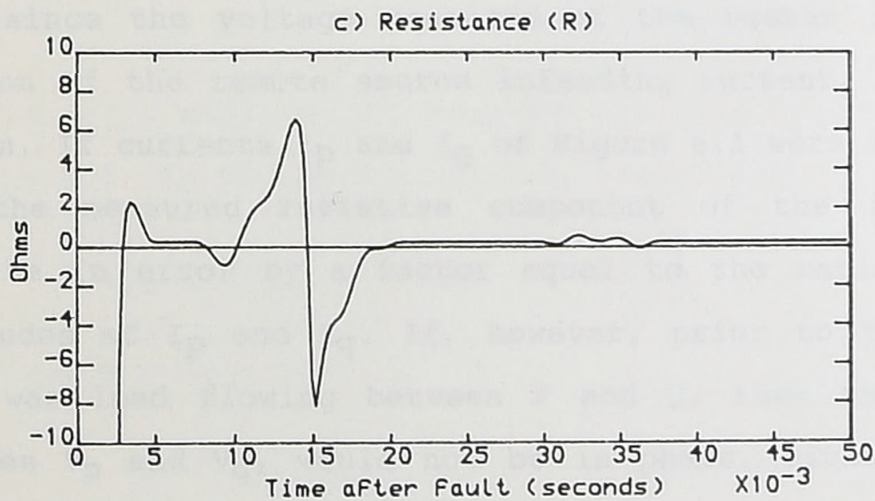
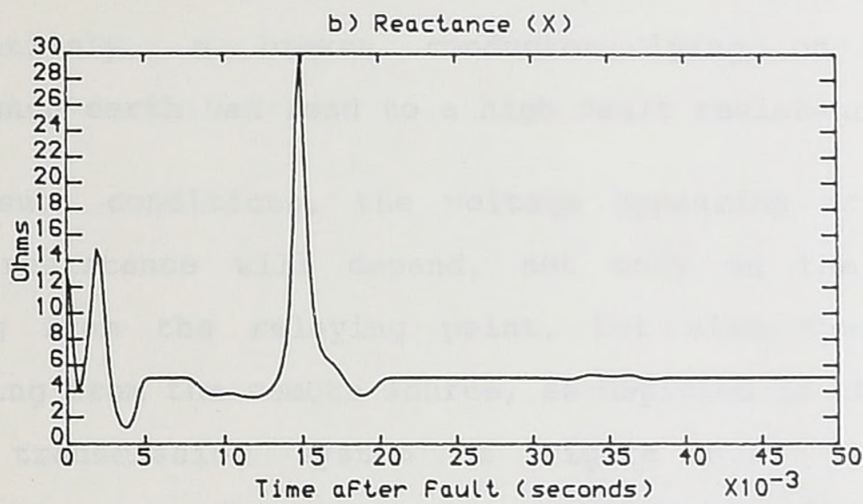
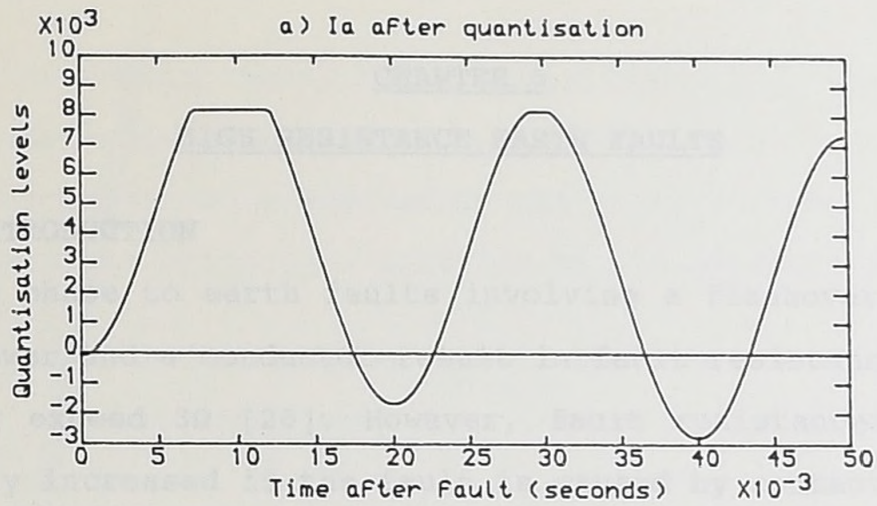


Figure 5.14 Effect of clipping on the quantised 'a' phase line current and the measured impedance.

CHAPTER 6HIGH RESISTANCE EARTH FAULTS**6.1 INTRODUCTION**

Single phase to earth faults involving a flashover between the tower and a conductor result in fault resistances which rarely exceed  $3\Omega$  [20]. However, fault resistances may be greatly increased if the fault is caused by contact between a conductor and vegetation; this usually occurs towards the middle of the line, at the lowest point of the catenary. Alternatively, a broken conductor lying on a high resistance earth can lead to a high fault resistance.

Under such conditions, the voltage appearing across the fault resistance will depend, not only on the current feeding from the relaying point, but also the current infeeding from the remote source, as depicted in the single phase transmission system of Figure 6.1. Thus, the impedance measured by the relay at P, being the ratio of the busbar voltage to the line current, will clearly be in error since the voltage measured at the busbar is now a function of the remote source infeeding current, which is unknown. If currents  $I_p$  and  $I_q$  of Figure 6.1 were in phase, then the measured resistive component of the impedance would be in error by a factor equal to the ratio of the magnitudes of  $I_p$  and  $I_q$ . If, however, prior to the fault there was load flowing between P and Q, then the busbar voltages  $V_p$  and  $V_q$ , would not be in phase, either before the fault or during it. Thus,  $I_p$  and  $I_q$  would now not be in phase and so the impedance measured at P would be in error on both the resistive and reactive components.

Thus, in faults involving a relatively high resistance where there is infeed from the remote end of the line, the apparent impedance presented to the relay will be in error, the extent of which is a function of the prefault loading.

This general result may be equally applied to a three phase system; the sequence component diagram for a single phase to earth fault including fault resistance is shown in Figure 6.2. It is shown in Appendix 11, that for, say, an 'a' phase to earth fault involving fault resistance, the impedance measured,  $Z_{meas}$ , by the residually compensated 'a' phase to earth element is given by,

$$Z_{meas} = \alpha Z_{11} + \frac{3 \cdot i_f \cdot R_f}{i_a + K_{res} \cdot i_{res}} \dots\dots\dots 6.1$$

Where, it can be seen from Figure 6.2, that  $i_f$  is the current flowing through the fault resistance. Figure 6.3 shows  $Z_{meas}$  in the complex plane, assuming that  $\alpha$  corresponds to the reach point of the relay. Clearly the relay will be prone to either overreaching or underreaching depending on the sign of angle  $\theta$ .

For clarity, when  $\alpha$  corresponds to the reach point, Equation 6.1 can be more succinctly stated as,

$$Z_{meas} = Z_{reach} + Z_{rf} \dots\dots\dots 6.2$$

where  $Z_{reach} = \alpha Z_{11}$  and,

$$Z_{rf} = \frac{3 \cdot i_f \cdot R_f}{i_a + K_{res} \cdot i_{res}} \dots\dots\dots 6.3$$

High resistance earth faults have attracted the attention of many authors [19-21], and, in pursuing this work, it was

felt that an application study which produces severe cases of impedance measurement error should be chosen. Johns and El-Alaily [19] described their work on the development of a relay capable of protecting for resistive earth faults with reference to a 10km, 220kV unearthed transmission line. This was shown to be a demanding situation for the protection and so it is used here as the application study in preference to the 400kV configuration used elsewhere. Details of the system are given in Appendix 12.

Using the 220kV system, studies were made of the expected impedance to be measured by an ideally residually compensated earth element. Figures 6.4a) to d) show the results of  $Z_{meas}$  for all combinations of strong (20GVA) and weak (2GVA) sources, all combinations of prefault loading and fault resistances from 0 to  $10\Omega_{pri}$ . For comparison purposes, each of Figures 6.4a) to d) shows the fixed quadrilateral characteristic set with  $X_R = 3.1\Omega_{pri}$  and  $R_R = 6.2\Omega_{pri}$ . It can be seen from these Figures that  $Z_{meas}$  is highly dependent on the prefault load transfer; angle  $\theta$  of Figure 6.3 can be seen to be positive for prefault importing and negative for prefault exporting load conditions.

Under no load conditions, the reactive component of  $Z_{meas}$  is approximately correct since the contributions, from ends P and Q, to the current in the fault resistance are approximately in phase. However, in all situations except when the remote source is much smaller than the local source, the value of the resistive component of  $Z_{meas}$  is greatly in error. In the situation where the remote source

is greater than the local source, Figure 6.4d), it can be seen that the measured resistance is 5 times larger than the actual fault resistance. Thus, even when there is no error in the reactance measurement, a scalar error of the resistance measurement is seen to exist which increases as the ratio of the remote to local SCL exceeds unity.

## 6.2 RELAY ADAPTATION

Using the fixed quadrilateral characteristic described in Chapter 5, substantial overreaching of the relay may be expected to occur for high resistance faults with prefault exporting load flow; conversely, prefault importing conditions will lead to underreaching. In order that the relay maintains correct operation in these conditions, it is desirable that the quadrilateral characteristic is, in some form, **adapted** to suit the prospective fault characteristic.

Since the fault resistance is not known, nor is it likely to be estimated, then the magnitude of  $Z_{rf}$  of Equations 6.3 and 6.2 is also not known. However, if an estimation of the current flowing through the fault resistance,  $i_f$ , were made, then the argument of  $Z_{rf}$  could be estimated since the denominator of Equation 6.3 is known;  $R_f$  only affects the magnitude. Thus, a method of adapting the quadrilateral characteristic to enhance operation for high resistance faults would be to swivel the upper reactance line through an angle  $\theta$  given by,

$$\theta = \arg \left[ \frac{i_f}{i_a + K_{res} \cdot i_{res}} \right] \dots\dots\dots 6.4$$

An illustration of this method of adapting the characteristic is shown in Figure 6.5 where the part of the characteristic lying to the right of the imaginary axis from its intersection with the solid fault impedance locus has been swivelled by the angle  $\Theta$ . In this Figure, the characteristic has been adapted to enhance the coverage of high resistance faults occurring after prefault importing load flow; the swivelling angle  $\Theta$  is positive.

In order to effect this adaptation of the characteristic, it can be seen necessary to form an estimate of the swivelling angle  $\Theta$ , which in turn is a function of an estimate of the fault current,  $i_f$ . The next Section will describe methods used in this estimation, but, it should be emphasised that attempts to estimate  $\Theta$  will always involve an inherent error since the optimal value of  $\Theta$  is a function of the remote source. Note that this protection scheme is, of course, a non-unit type so no real-time information of the remote source can be assumed. Some earlier work in this area [20,21] describe methods of remote source infeed compensation which assume a value for the remote source impedance, usually in the form of distribution factor for one of the sequence networks. It is assumed here that the relay has no *appriori* knowledge of the remote source; the relay is expected to, ideally, function correctly in any of the configurations shown in Figures 6.4a) to d) without knowing which configuration it is in.

### 6.3 METHODS OF ESTIMATING THE SWIVELLING ANGLE $\theta$

#### 6.3.1 Introduction

This section will describe three methods used for estimating  $\theta$ . Two of the methods described make use of the fact that the local zero sequence source impedance,  $Z_{sp0}$ , may be found, during the fault, from the following equation,

$$Z_{sp0} = -v_{p0}/i_{p0} \dots\dots\dots 6.5$$

which may be verified by reference to Figure 6.2. Note that  $i_{p0}$ , which is equal  $i_{res}/3$ , is already available to the relay, being used for residual compensation,  $v_{p0}$  is readily calculated by summing the phase voltages at each sampling interval:

$$v_{p0} = v_a + v_b + v_c \dots\dots\dots 6.6$$

#### 6.3.2 Method 1: assuming $Z_{sq0}$ to be zero.

In this method, recognition is given to the fact that the worst case error in the impedance measurement occurs when the remote SCL is large and hence the remote source impedance is small. In this method, the remote source impedance is assumed to be zero. Thus, with reference to the zero sequence network of Figure 6.2, by equating the voltages on either side of the fault point, the following expression may be derived for  $i_f$ ,

$$i_f = i_{p0} \cdot \frac{(Z_{sp0} + Z_{sq0} + Z_{l0})}{(Z_{sq0} + (1-\alpha)Z_{l0})} \dots\dots\dots 6.7$$

And, in this method, by putting  $Z_{sq0} = 0$ ,  $i_f$  is estimated by,

$$i_f = i_{p0} \cdot \frac{(Z_{sp0} + Z_{l0})}{(1-\alpha)Z_{l0}} \dots\dots\dots 6.8$$

Note that  $Z_{l0}$  must be known since it is used in calculating the residual compensation factor;  $i_{p0}$  and  $Z_{sp0}$  are available to the relay as discussed earlier. Thus,  $\theta$  may be estimated from Equation 6.4 by substituting for  $i_f$  given in Equation 6.8.

**6.3.3 Method 2: assuming  $Z_{sp0}$  and  $Z_{sq0}$  to be equal**

This method, which complements method 1, is to assume that the local and remote source impedances are equal. Thus, following the same analysis as method 1, but replacing  $Z_{sq0}$  with  $Z_{sp0}$  in Equation 6.7,  $i_f$  may be expressed as,

$$i_f = i_{p0} \cdot \frac{(2Z_{sp0} + Z_{l0})}{(1-\alpha)Z_{l0} + Z_{sp0}} \dots\dots\dots 6.9$$

And thus  $\theta$  may be calculated, by using Equation 6.4 substituted for the value of  $i_f$  given in Equation 6.9.

**6.3.4 Method 3: assuming  $i_{p0}$  to be in phase with  $i_f$**

In this method it is assumed that the argument of the impedances on either side of the fault point of the zero sequence network of Figure 6.2 are equal. This then leads to the fact that  $i_{p0}$  and  $i_{q0}$ , and hence  $i_f$ , are in phase. Thus replacing  $i_f$  with  $i_{p0}$  in Equation 6.4 gives the following expression for  $\theta$ ,

$$\theta = \arg \left[ \frac{i_{p0}}{i_a + K_{res} \cdot i_{res}} \right] \dots\dots\dots 6.10$$

Note that this method will give perfect characteristic adaptation in a homogeneous system where the arguments of

the source and line impedances are equal. In a real system, however, this may not be so and thus its reliability is based upon a simplifying assumption, as are methods 1 and 2. This method, in different forms, has been previously applied for improving the resistive earth fault performance of distance relays [17,19].

#### 6.4 INITIAL PERFORMANCE STUDIES OF $\theta$ ESTIMATORS

In order to investigate the potential performance of the three methods of estimating  $\theta$ , without resorting to a fully implemented relay simulation, an initial study was conducted to evaluate the accuracy of the estimations. Illustrative results of study are shown in Figures 6.6 and 6.7.

These Figures show how  $\theta$  varies with the fault position for a resistive single phase to earth fault on the 220kV application system where the fault resistance and local and remote SCL's remain constant. Each graph of these Figures shows the ideal swivel angle (ISA) which is the angle that the upper reactance line of the characteristic should be swivelled through so that this line now intersects the point of measured impedance. The ISA of the fault locus is formed, in the complex impedance plane, by drawing a line from the point of measured impedance to intersection of the reach point of relay with the solid fault impedance locus. The ISA is then measured as the angle between this line and a line parallel with the resistive axis. It therefore follows from this, that if the estimated value of  $\theta$  exceeds the ISA, then the relay will operate. Clearly, the ideal case will show  $\theta$  exceeding the ISA up to the reach point

and the situation being reversed beyond the reach point.

Figure 6.6 shows the behaviour of the  $\theta$  estimating methods for the worst case error of the measured impedance; the local source SCL is 2GVA, the remote SCL is 20GVA and there is full prefault load flow importing to P. With a resistance of  $10\Omega_{pri}$ , method 1 is seen to result in overreaching whilst methods 2 and 3 do not allow relay operation until the fault is 15% of the line length from the relay location. When the fault resistance is reduced to  $1\Omega_{pri}$ , method 1 still affords overreaching, beyond the remote busbar, whilst methods 2 and 3 allow relay operation up to nearly the reach point.

Figure 6.7 shows the situation when both local and remote SCL's are 20GVA and, again, with full prefault load into P. When  $R_f$  is  $10\Omega_{pri}$ , all methods can be seen to lead to overreaching. However, it was discovered that if the value of  $\alpha$  in Equation 6.9, the equation used to estimate  $i_f$  in method 2, is increased towards 1, then the tendency to overreach is diminished. It can be seen from Figure 6.7 that method 2 ( $\alpha=1$ ) now gives satisfactory operation with the relay ceasing to operate for faults beyond the mid point of the line. When  $R_f$  is  $1\Omega_{pri}$ , all methods are seen to give correct reach point operation and little penalty is seen to exist for changing the value of  $\alpha$  in Equation 6.6.

Note that making  $\alpha = 1$  in Equation 6.9 considerably simplifies the mathematics of method 2 since the  $Z_{l0}$  term disappears from the denominator, thus the expression for  $i_f$  in method 2 becomes,

$$i_f = i_{p0} \cdot \frac{(2Z_{sp0} + Z_{l0})}{Z_{sp0}} \dots\dots\dots 6.11$$

From the results of the initial performance studies, it was concluded that method 1 showed little promise as an estimator of  $\theta$  due to its inability to promote correct relay operation even in the case of fault resistances as small as  $1\Omega_{pri}$ .

**6.5 DETAILED PERFORMANCE STUDIES OF  $\theta$  ESTIMATORS**

**6.5.1 Relay implementation**

A more detailed study of the performances of methods 2 and 3 was conducted by realising a full relay implementation of both these methods and then testing the reach point accuracy using simulated time series data of resistive single phase to earth faults.

In order to effect the real time adaptation of the relay characteristic, it is much simpler, in terms of the processing complexity, to adapt the measured impedance such that it may be compared against the fixed characteristic described in Chapter 5, than to swivel the lines of the characteristic, as shown in Figure 6.5b). Note that, whichever approach is used, the operation of the relay will be the same in either case. Hence, with reference to Figure 6.8, if the measured impedance is  $Z_{meas}$  and the impedance of the line at the reach point is  $Z_{reach}$ , then the following expression is used to form  $Z_R$ , the impedance used in comparison with the characteristic,

$$X_R = X_{meas} - (R_{meas} - R_{reach}) \cdot \tan\theta \dots\dots\dots 6.12$$

$$R_R = R_{meas} \dots\dots\dots 6.13$$

Equations 6.12 and 6.13 are only used if  $R_{meas}$  exceeds  $R_{reach}$ , otherwise  $Z_{meas}$  is entered into the fault evaluation algorithm unadapted.

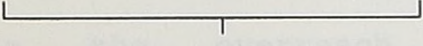
Thus, it necessary to derive  $\tan\theta$ . For method 3, this is accomplished by finding the real and imaginary components of the quotient  $i_{p0}/(i_a + K_{res}\cdot i_{res})$  as expressed in Equation 6.10. By treating  $i_{p0}$  as a voltage, the quotient can be enumerated as an impedance by using the impedance measurement technique described in Chapter 3. The resistance and reactance values from this calculation thus represent the real and imaginary values of the quotient.  $\tan \theta$  is then easily evaluated by dividing the imaginary component by the real component. This is one situation where a digital division cannot be avoided.

For method 2,  $\tan \theta$  is not so easily evaluated since it is necessary to find the argument of  $i_f/(i_a + K_{res}\cdot i_{res})$  where  $i_f$  is given by Equation 6.11. From Equations 6.11 and 6.5, it can be written,

$$\frac{i_f}{i_a + K_{res}\cdot i_{res}} = \frac{i_{p0}\cdot Z_{l0} - 2\cdot v_{p0}}{i_a + K_{res}\cdot i_{res}} \cdot \frac{1}{Z_{sp0}} \dots\dots 6.14$$

Therefore,  $\theta$  may be evaluated as,

$$\theta = \arg \left[ \frac{i_{p0}\cdot Z_{l0} - 2\cdot v_{p0}}{i_a + K_{res}\cdot i_{res}} \right] - \arg \left[ Z_{sp0} \right] \dots 6.15$$



TERM 1



TERM 2

Again, the impedance measurement approach is used for evaluating the real and imaginary components of TERM 1 and

TERM 2. It is necessary for this method to provide a tangent function look-up table for finding values of TERM 1 and TERM 2, and finding the tangent of the difference between them.

### 6.5.2 Relay performance for methods 2 and 3.

Using a lumped parameter model of the 220kV 10km line described in Appendix 12, relay simulations incorporating characteristic adaptation methods 2 and 3 were tested for reach point accuracy with fault resistances up to  $1.6\Omega_{pri}$ . The local SCL was 20 GVA and the remote SCL was 2GVA for these tests. For both methods the characteristic was set with the reactive reach point at 80% of the line and a resistive to reactive reach ratio of 3. The results of these tests are shown in Figure 6.9 ; the curves depicted in the graphs represent, for a given fault resistance, the fault position at which the relay begins to restrain.

In Figure 6.9a), it can be seen that method 3 gives reasonably accurate reach point response with a maximum overreach to 82% of the line length being observed for the prefault full load exporting condition with fault resistances in excess of  $1\Omega_{pri}$ . This performance is within the  $\pm 5\%$  accuracy specification, given in Section 2.2, for SIR's of up to 30; this application has an SIR of 6. It was discovered that, using this method, increasing the resistive to reactive reach ratio to a value greater than 3 resulted in the overreach exceeding the relay specifications.

The results shown in Figure 6.9b) for method 2, however, show that substantial overreaching of the relay, in excess

of 90% of the line length, occurs for fault resistances in the range  $0.6 - 0.8\Omega_{pri}$  with pre-fault full load exporting. Within this range of resistances, the relay is observed to overreach for all conditions of loading.

The results for method 2 were quite surprising since the initial performance studies suggested that this method would allow better fault resistance coverage than method 3. Investigations into the failure of method 2 to provide better accuracy showed that the 16 bit precision of the relay microprocessor was the predominant cause of error. This level of precision resulted in considerable errors in the estimation of  $\theta$ . As an illustration of the problems of implementing method 2, the two terms involved in the formation of  $\theta$ , TERM 1 and TERM 2 of Equation 6.15, are shown, as a function of the fault position, in Figure 6.10. Note, for comparison, that the system condition shown in this Figure is the same as shown in Figure 6.6b). It can be seen from Figure 6.10 that  $\theta$  is estimated in method 2 from the difference of two, relatively large in magnitude, terms. Thus errors involved in the evaluation of these two terms can result in an even larger error occurring in  $\theta$ .

Further to the basic problem of estimating  $\theta$  using method 2, it was also discovered that this method is very sensitive to small phase differences existing between the voltage and current signals on the faulted phase. Figure 6.11 shows results to the same faults shown in Figure 6.9b) except that, in the primary system simulation, all the phase voltages have been shifted forward in time by  $+2.8^\circ$  with respect to the line currents. Notice how the position

of the overreach has been moved; method 3 showed little sensitivity to the same faults. This effect was considered important since, even if the relay was implemented with, say, a 32 bit processor to overcome the precision problems, any phase error existing between primary system voltages and currents could affect the relay performance. The drift in performance of a CVT could account for such a phase error.

## 6.6 CONCLUSION

This Chapter has described how the relay can adapt itself to the potentially onerous conditions of high resistance earth faults by swivelling the characteristic in the complex impedance plane. Three methods have been described for estimating the optimum swivelling angle such that the relay does not overreach. It was shown that two of the methods did not reliably estimate the swivelling angle and hence, did not lead to relay performance of the required accuracy. The method which proved to give satisfactory results makes the assumption that the arguments of the line impedance and the local and remote source impedances of the zero sequence network of the fault are equal. It was found possible to set the relay with a resistive to reactive reach ratio of 3 using this method. Thus, this method is adopted for further analysis.

Figure 6.1 Resistive earth fault on a single phase transmission system

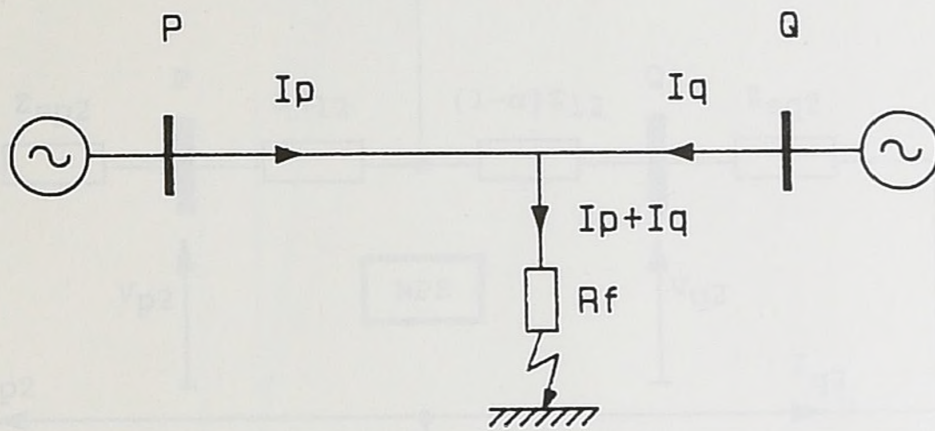


Figure 6.1 Resistive earth fault on a single phase transmission system.

Figure 6.2 Sequence component diagram of a two ended system for single phase to earth fault.

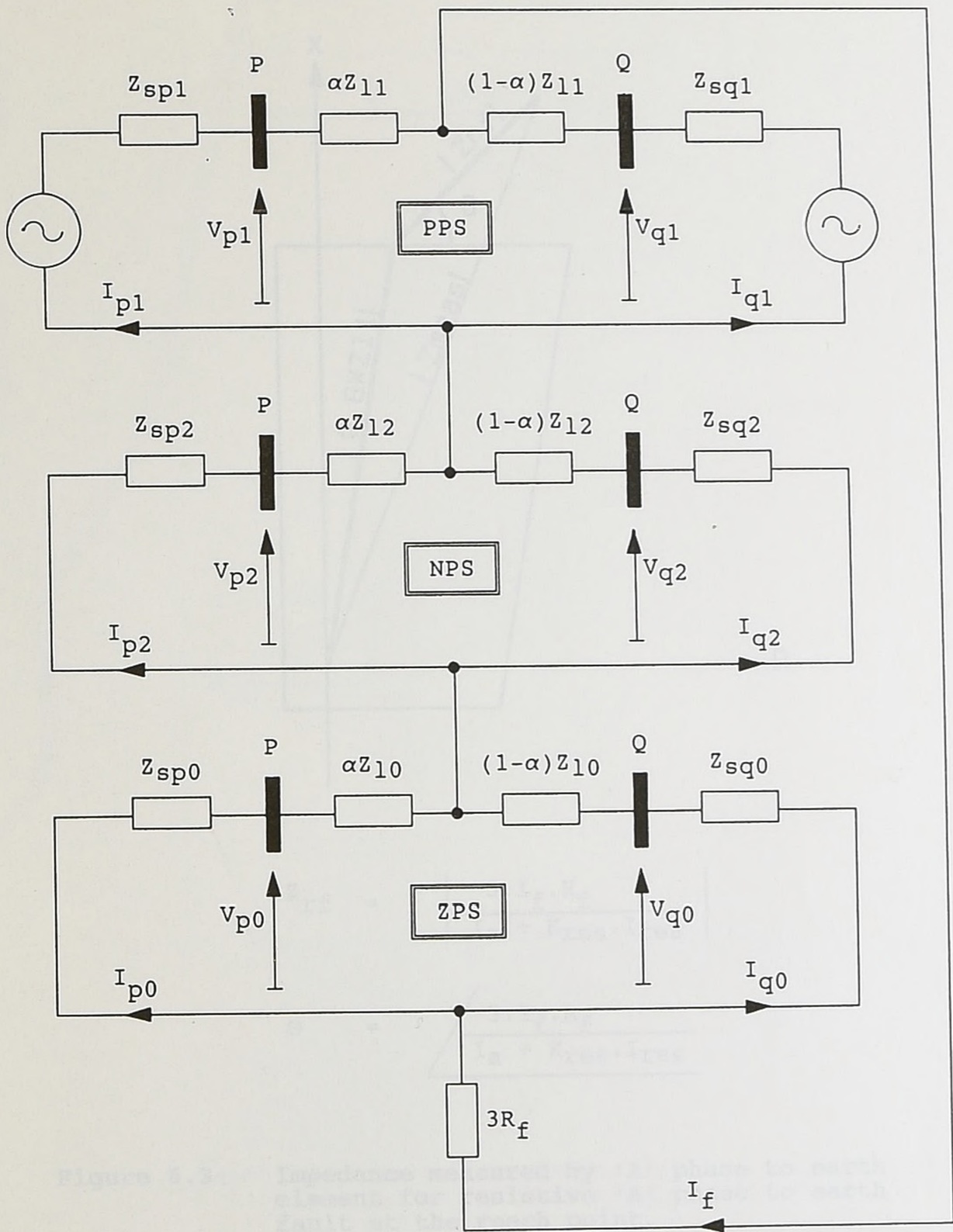
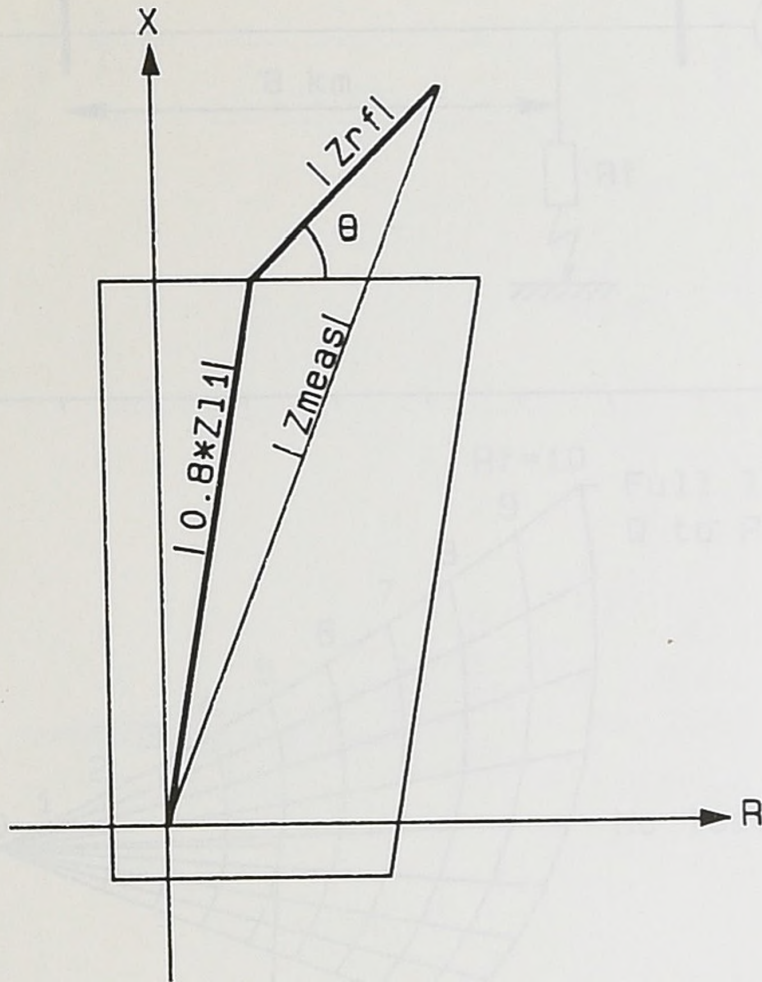


Figure 6.2 Sequence component diagram of a two ended system for single phase to earth fault.



$$Z_{rf} = \left| \frac{3 \cdot I_f \cdot R_f}{I_a + K_{res} \cdot I_{res}} \right|$$

$$\theta = \frac{3 \cdot I_f \cdot R_f}{I_a + K_{res} \cdot I_{res}}$$

Figure 6.3 Impedance measured by 'A' phase to earth element for resistive 'A' phase to earth fault at the reach point.

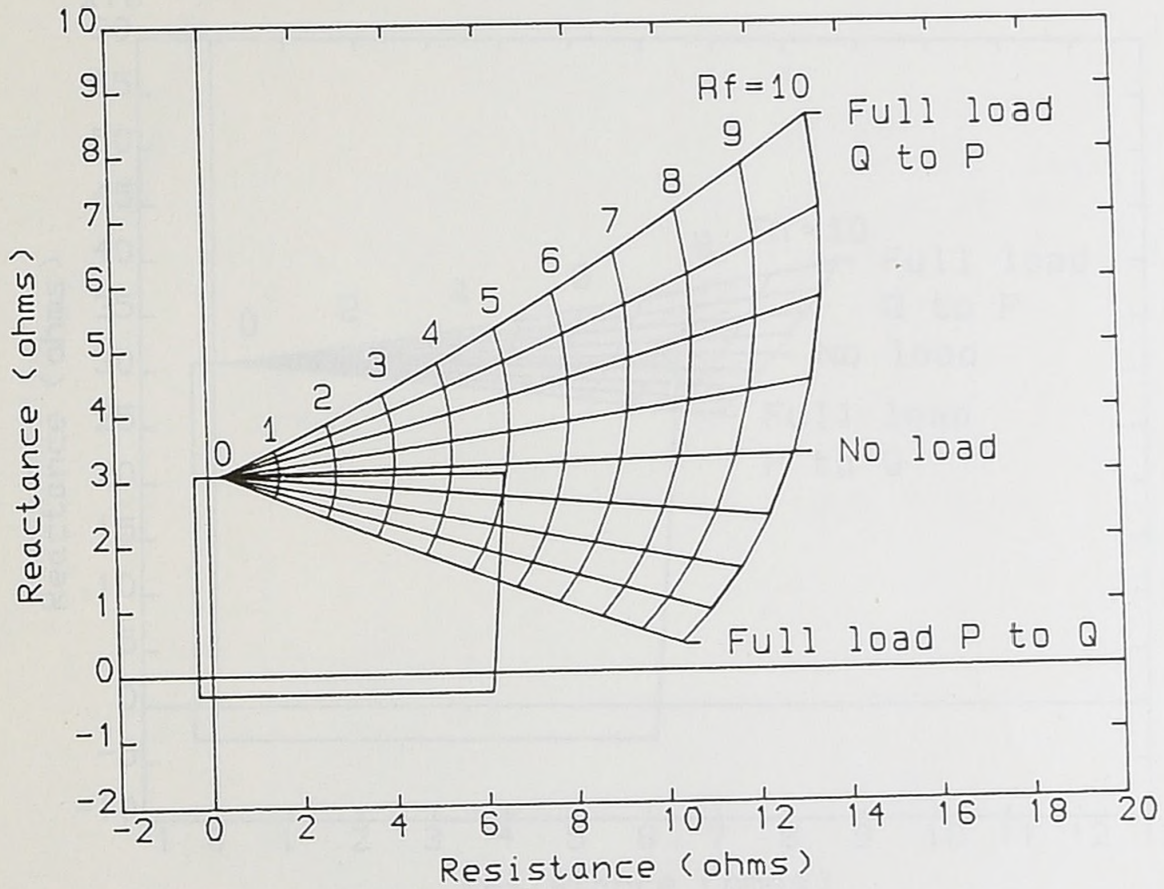
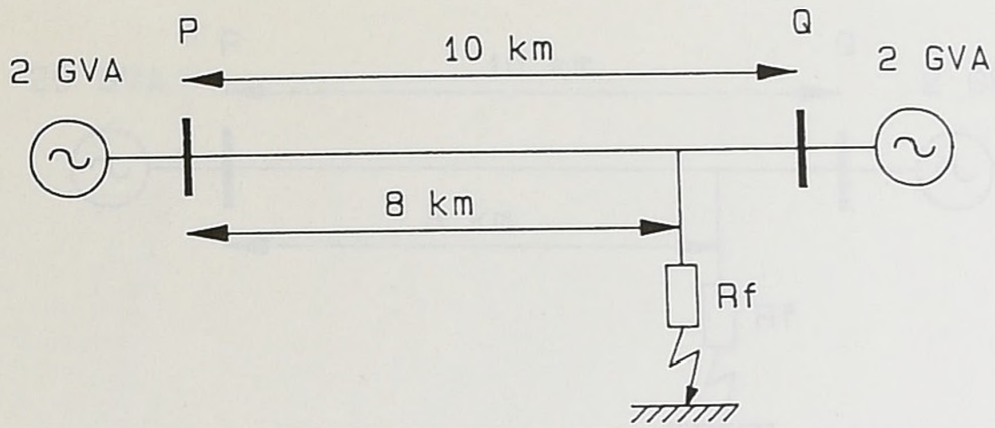


Figure 6.4a) Impedance measured by faulted earth element (Local SCL = 2GVA, remote SCL = 2GVA).

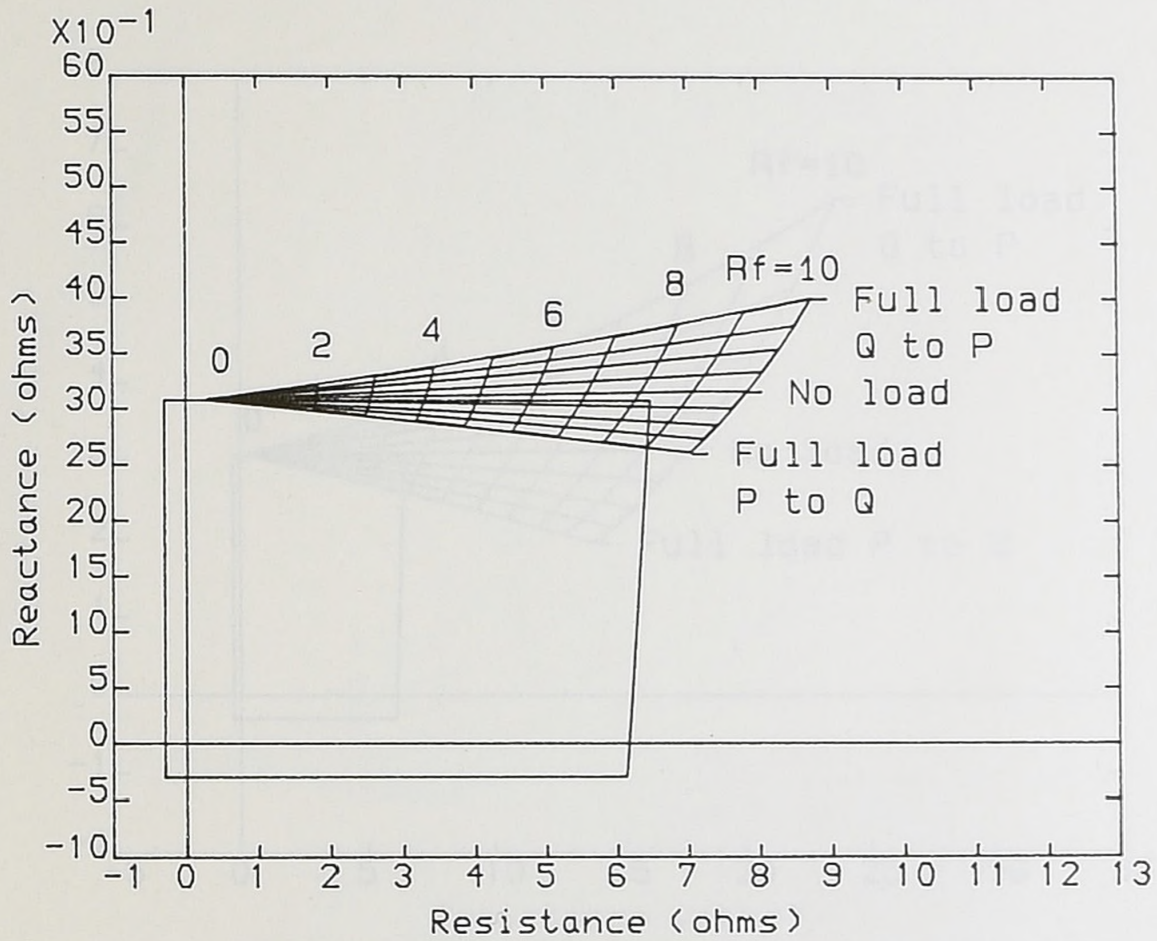
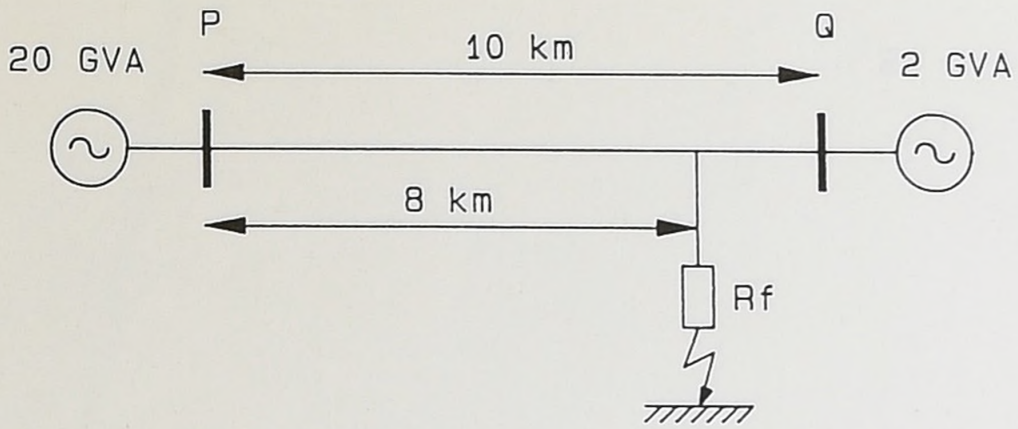


Figure 6.4b) Impedance measured by faulted earth element (Local SCL = 20GVA, remote SCL = 2GVA).

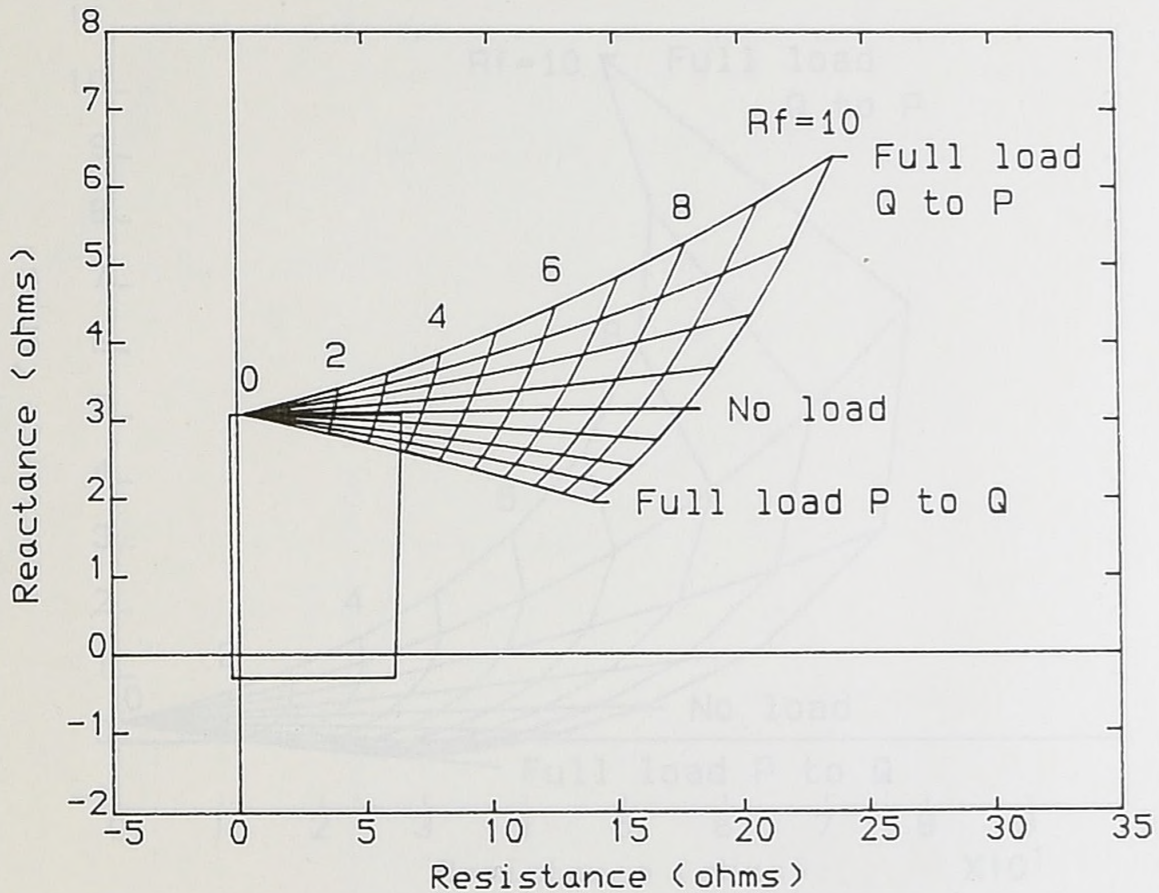
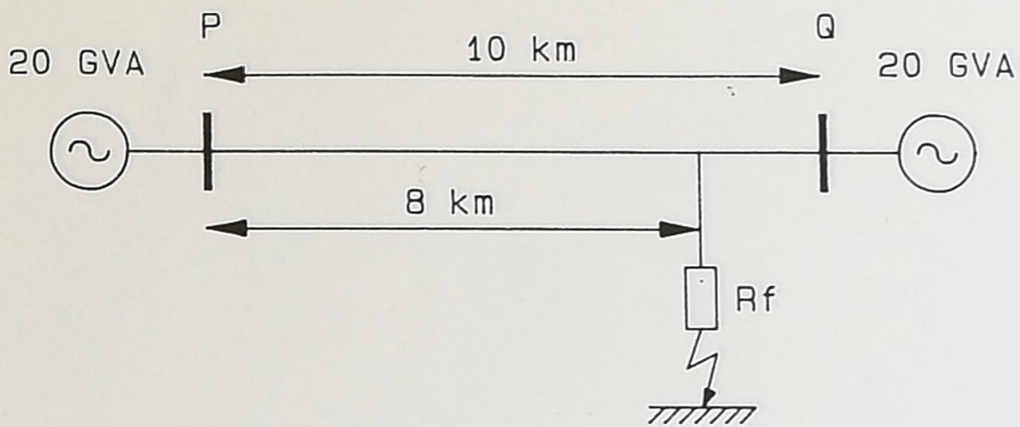


Figure 6.4c) Impedance measured by faulted earth element (Local SCL = 20GVA, remote SCL = 20GVA).

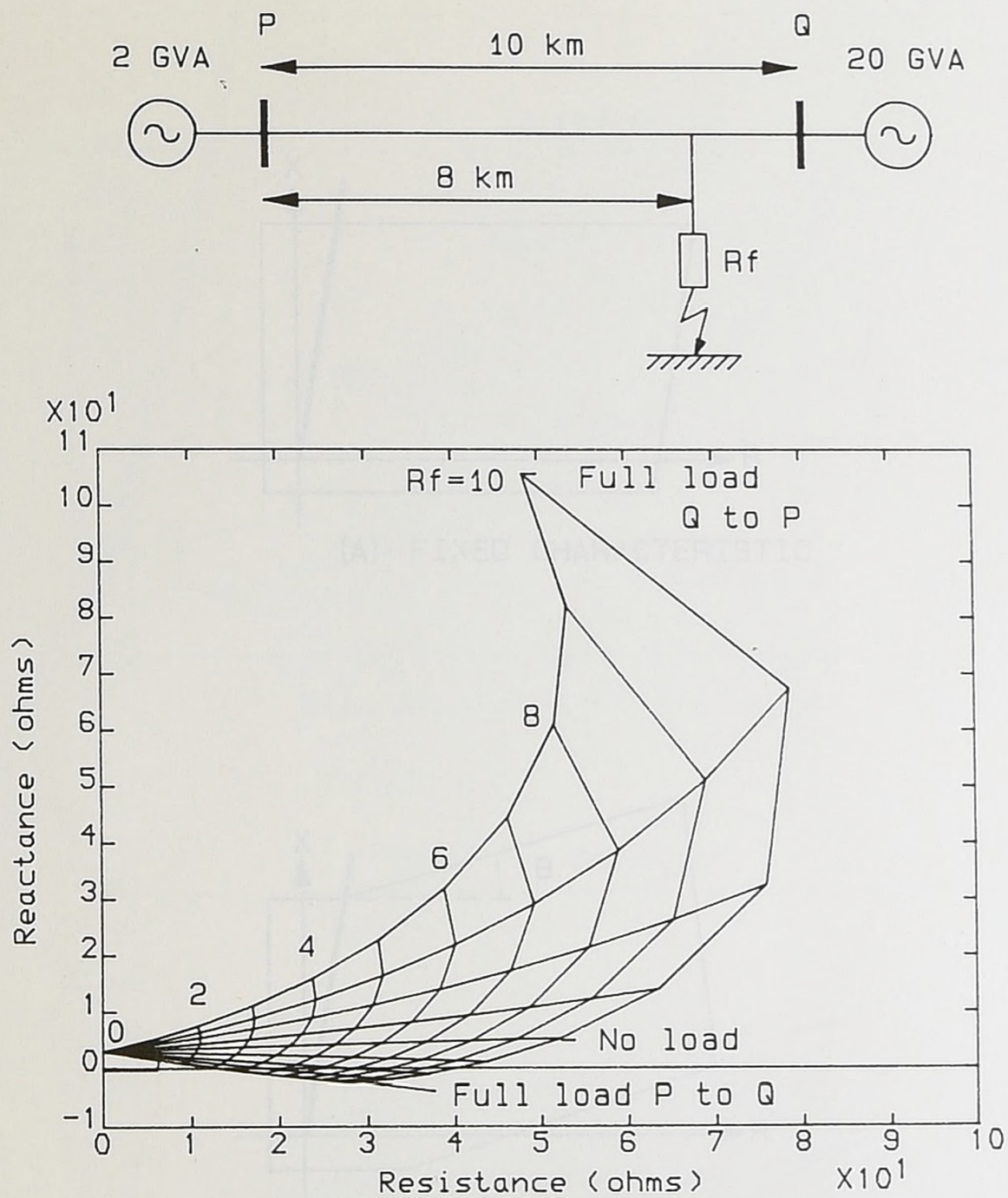


Figure 6.4d) Impedance measured by faulted earth element (Local SCL = 2GVA, remote SCL = 20GVA).

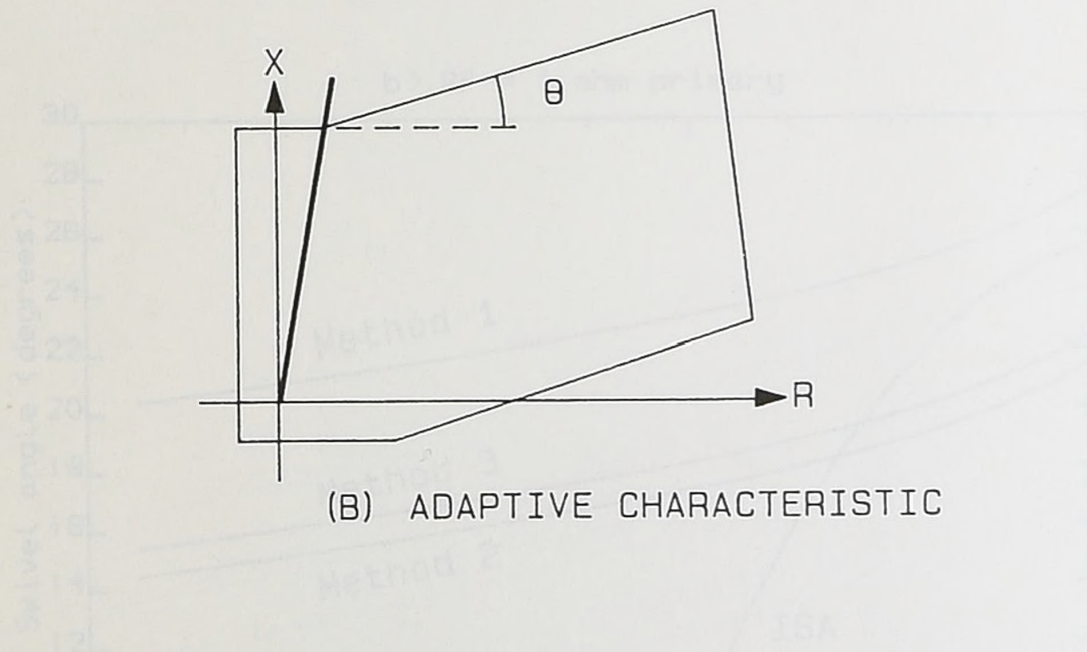
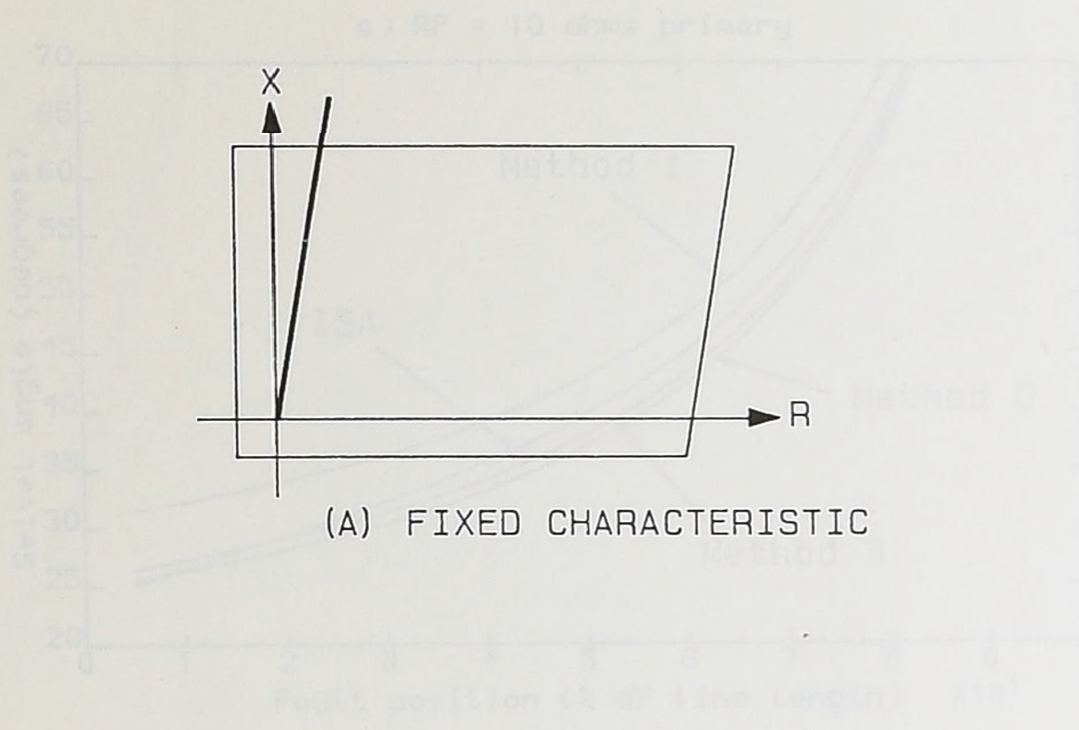


Figure 6.5 Fixed and adaptive relay characteristics (Adaptive characteristic shown for prefault importing load flow).

Figure 6.6 Performance of 3 methods of estimating the swivel angle on a 10km 120kV line. (Load SCL = 20VA, reactance 811-200VA, full load importing)

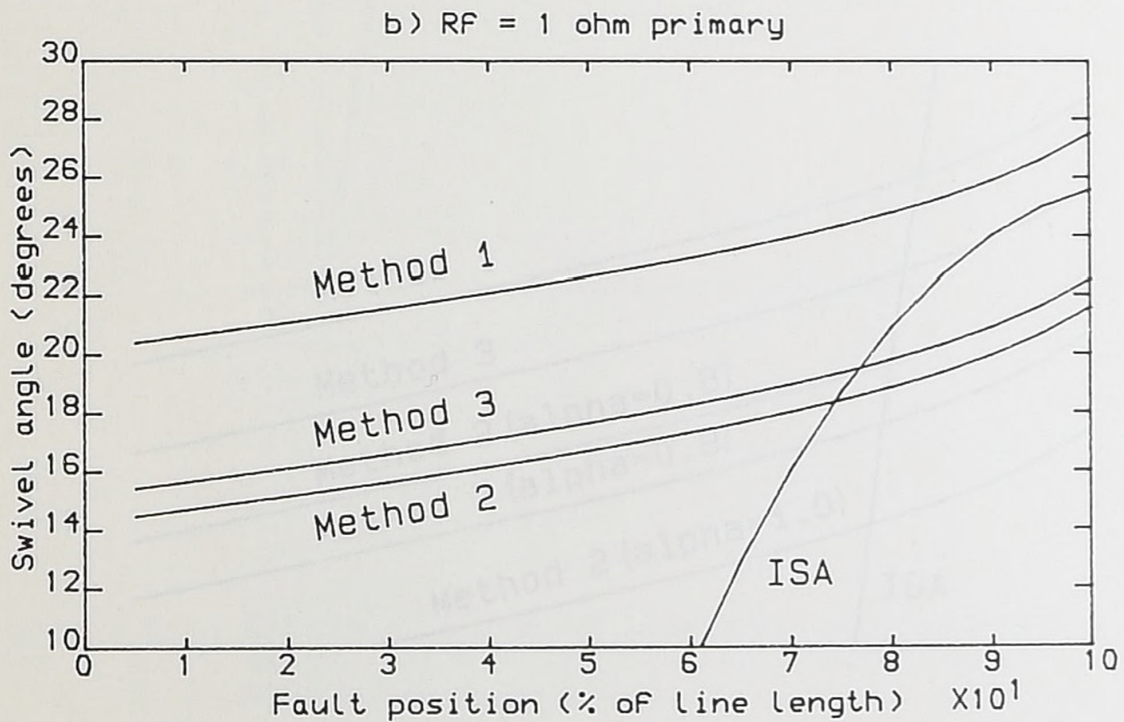
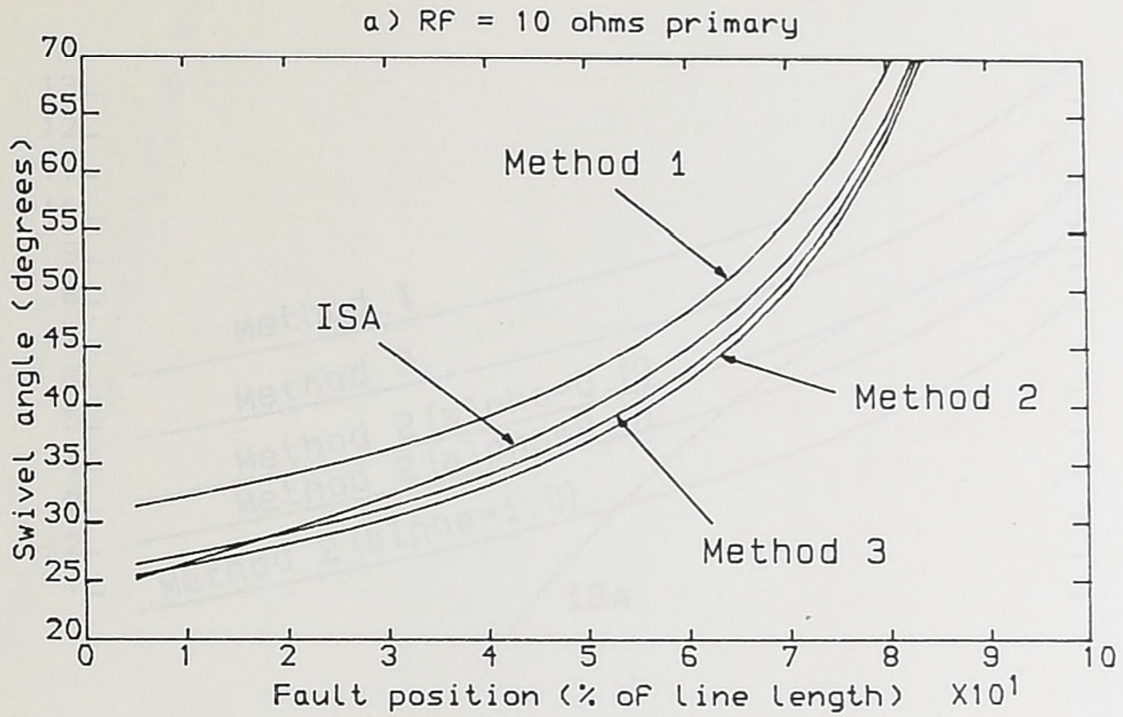


Figure 6.6 Performance of 3 methods of estimating the swivel angle on a 10km 220kV line. [Local SCL=2GVA, remote SCL=20GVA, full load importing]

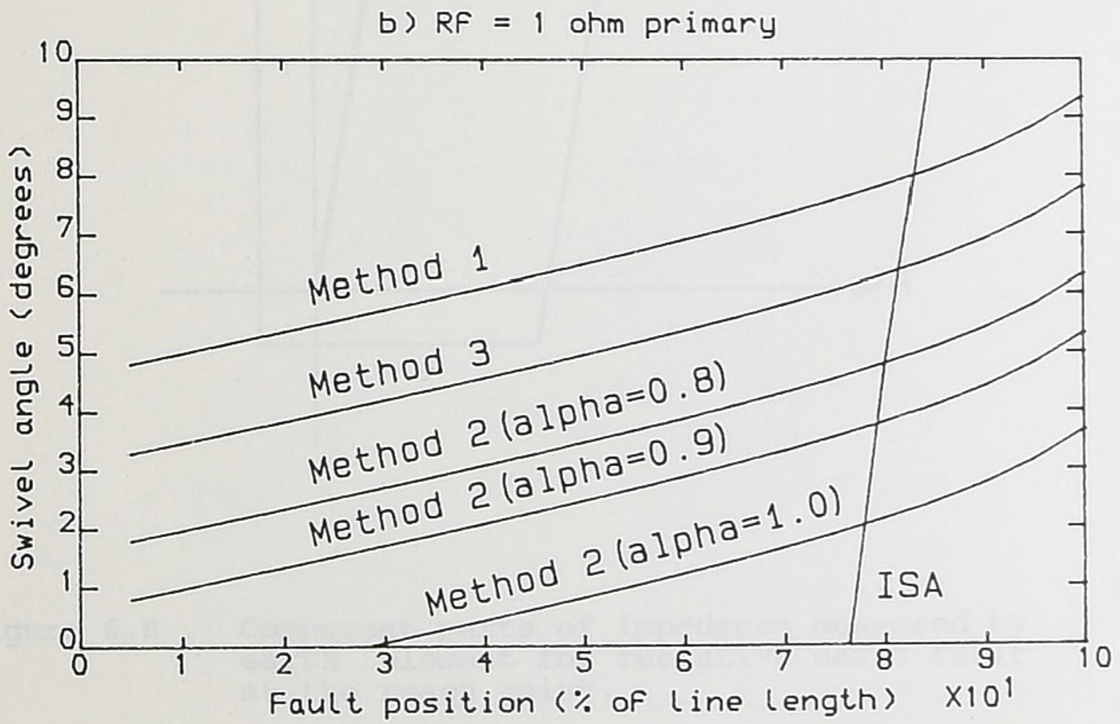
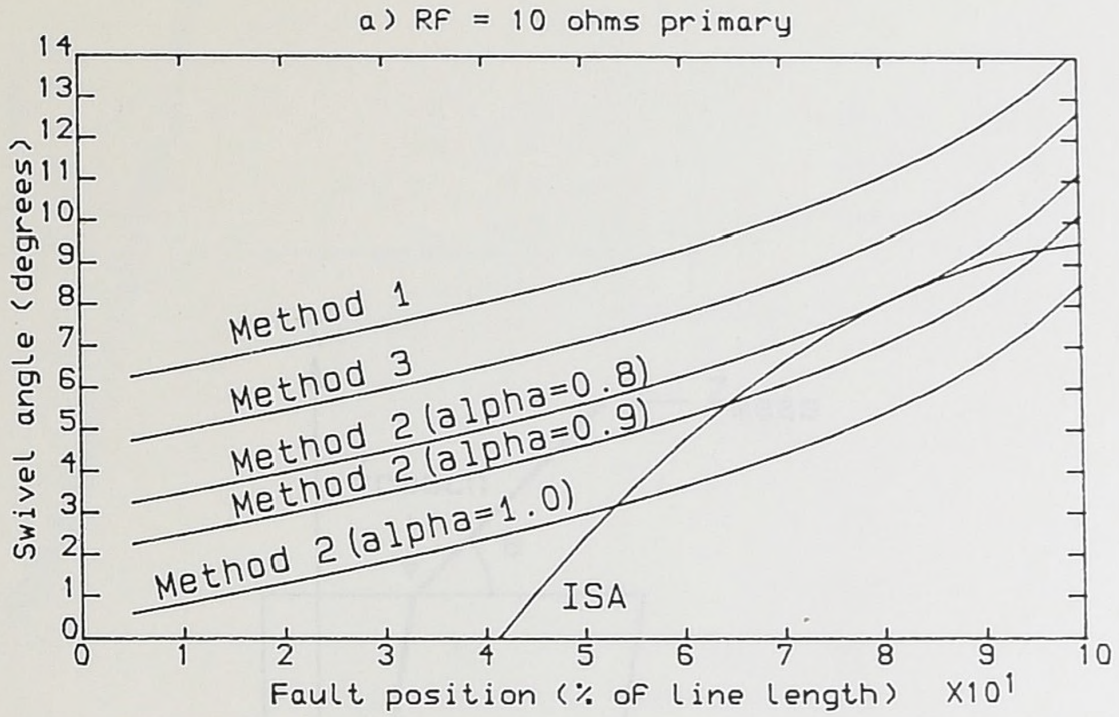


Figure 6.7

Performance of 3 methods of estimating the swivel angle on a 10km 220kV line. [Local & Remote SCL's=20GVA, full load importing]

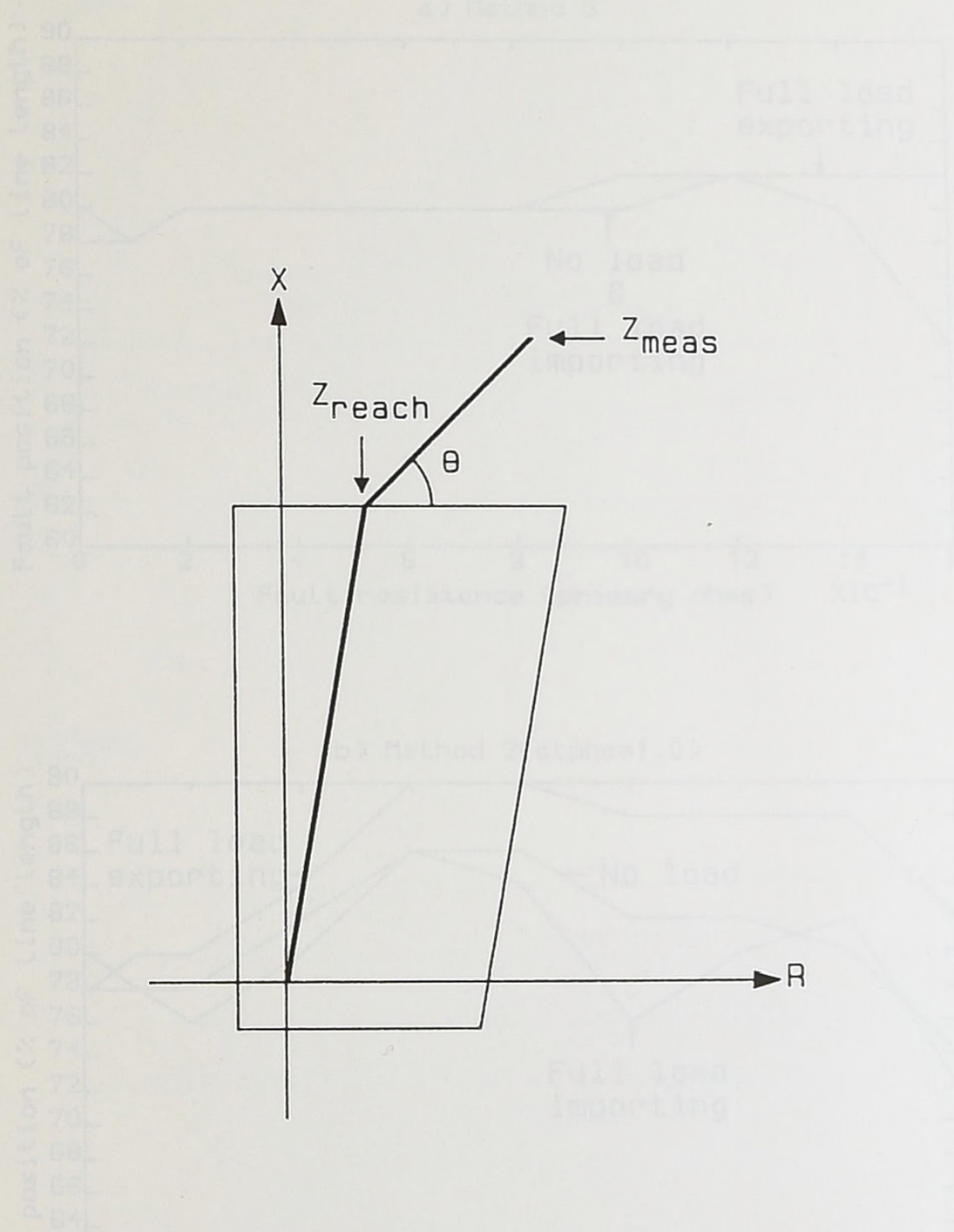


Figure 6.8 Component parts of impedance measured by earth element for resistive earth fault at the reach point.

Figure 6.9 Reach point accuracy of relay, for resistive earth fault, using 2 methods of estimating  $\theta$ . (Local SCL=20kVA, Remote SCL=200kVA)

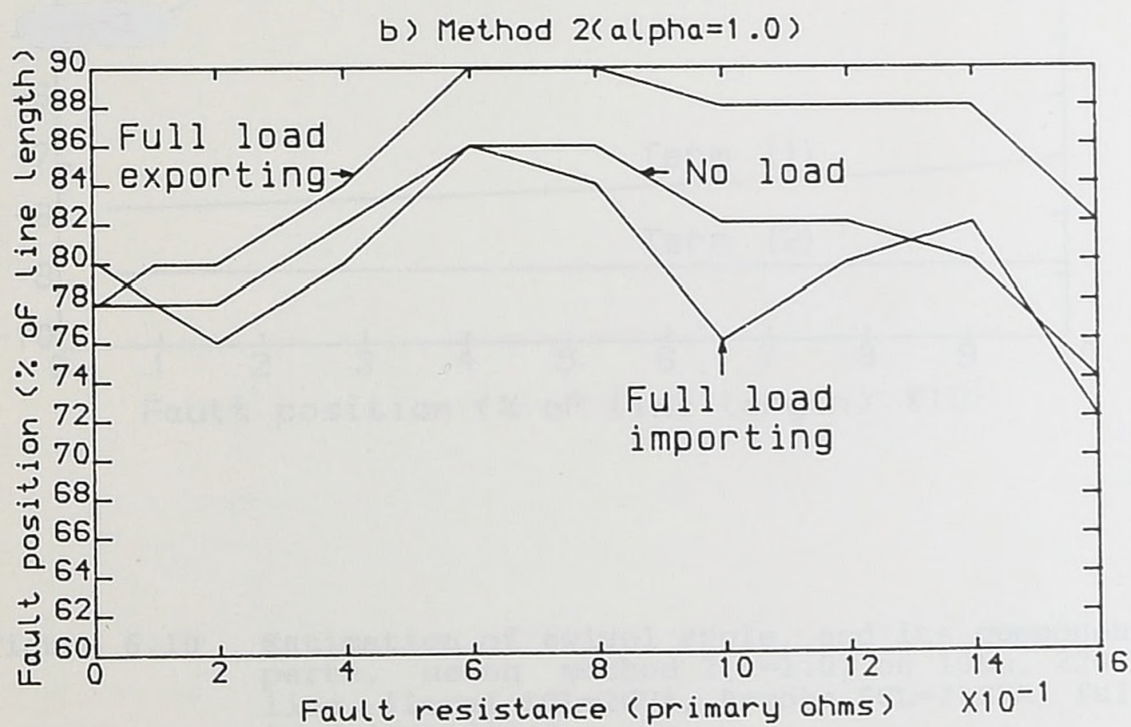
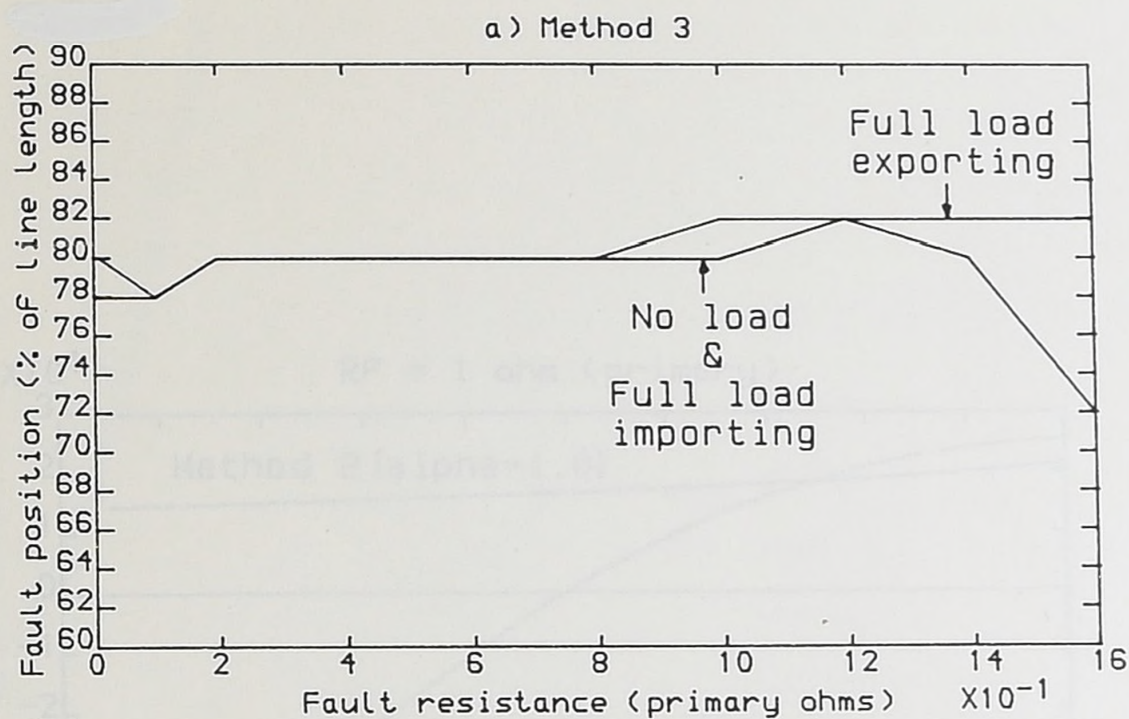


Figure 6.9 Reach point accuracy of relay, for resistive earth fault, using 2 methods of estimating  $\theta$ . [Local SCL=2GVA, Remote SCL=20GVA]

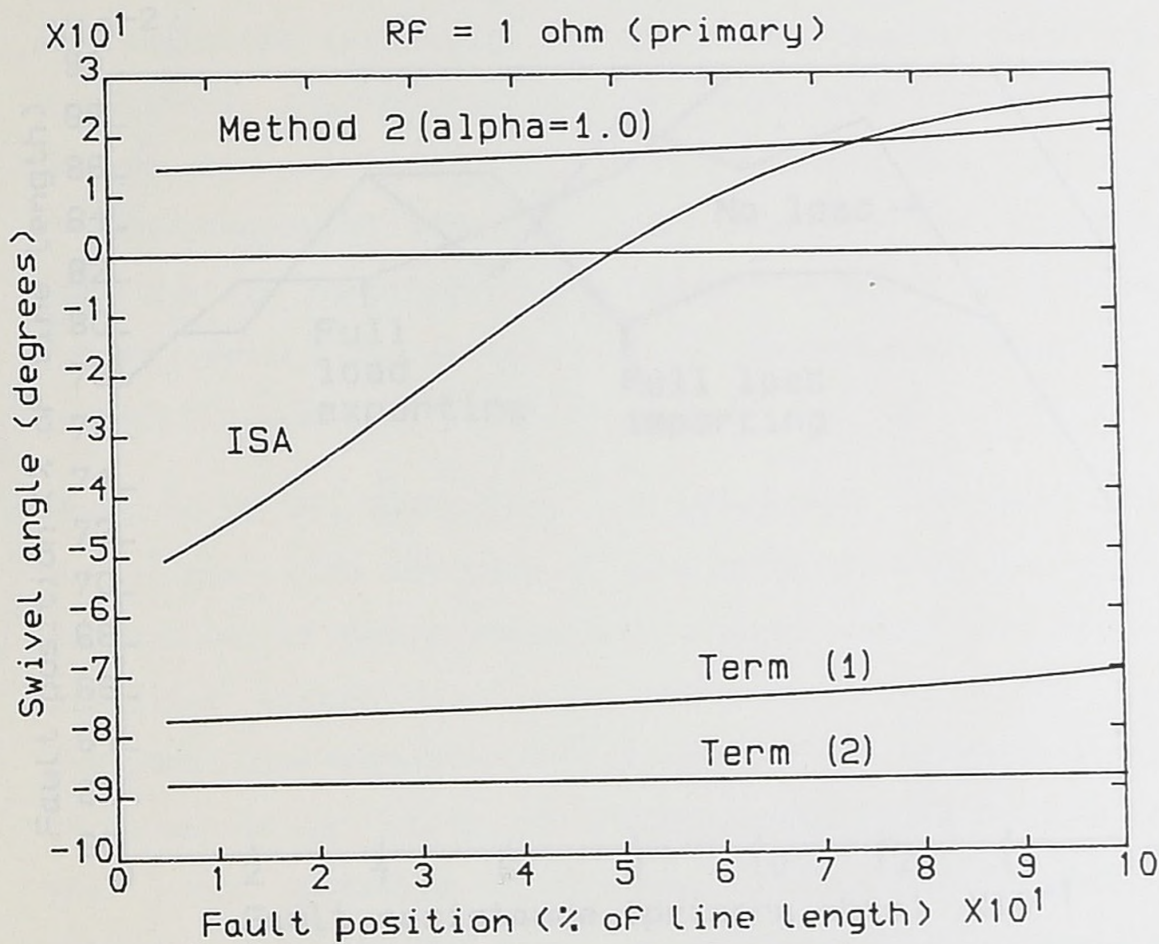


Figure 6.10 Estimation of swivel angle, and its component parts, using method 2( $\alpha=1.0$ ) on 10km, 220kV line. [Local SCL=2GVA, Remote SCL=20GVA, full load importing]

## SINGLE PHASE AND THREE-PHASE FAULTS

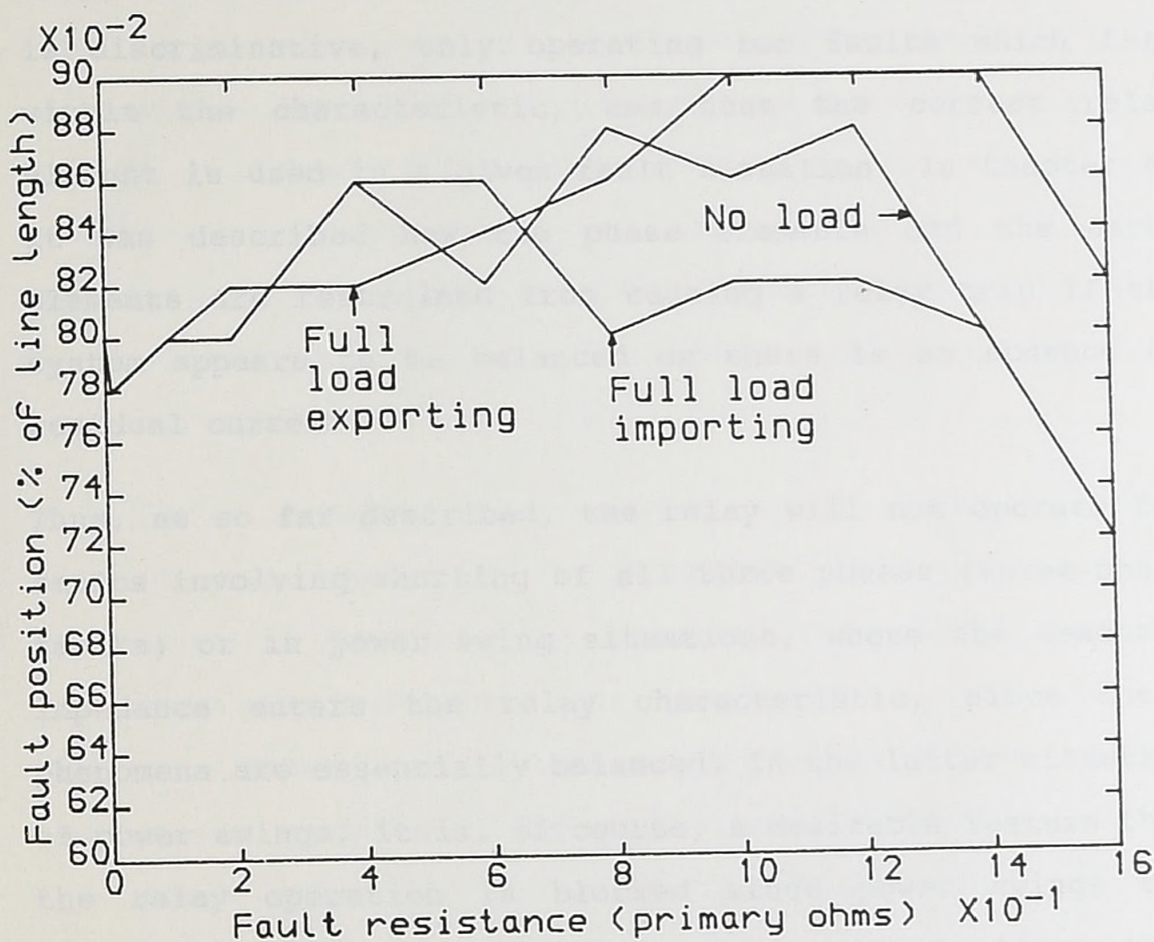


Figure 6.11 Reach point accuracy of relay, for resistive earth fault, using method2( $\alpha=1.0$ ), on 10km, 220kV line.  $2.8^\circ$  phase error between primary voltages and currents. [ Local SCL=2GVA, Remote SCL=20GVA]

## CHAPTER 7

### POWER SWINGS AND THREE-PHASE FAULTS

#### 7.1 INTRODUCTION

It has so far been discussed how the relay operates for single phase to earth and phase to phase faults. Further to this, attention has been focused on ensuring that the relay is discriminative, only operating for faults which fall within the characteristic, and that the correct relay element is used in a given fault situation. In Chapter 5, it was described how the phase elements and the earth elements are restrained from causing a relay trip if the system appears to be balanced or there is an absence of residual current.

Thus, as so far described, the relay will not operate for faults involving shorting of all three phases (three-phase faults) or in power swing situations, where the measured impedance enters the relay characteristic, since these phenomena are essentially balanced. In the latter situation of power swings, it is, of course, a desirable feature that the relay operation is blocked since power swings can eventually settle to normal system operation, there thus being no incentive for the protection to operate. The former case of three-phase faults, however, relative to phase to phase and phase to earth faults, presents a greater threat to system stability, and so it is imperative that the relay operates correctly.

Thus, it is necessary for the relay to be able to reliably differentiate between power swings and three-phase faults if correct operation is to be ensured. This Chapter will

describe the method used for detecting balanced faults and the technique used for preventing relay operation during power swings.

## 7.2 THREE-PHASE FAULTS

A typical cause of a three-phase fault is the situation where a line is energised, after maintenance, with the earthing clamps, which are used to ensure the safety of maintenance personnel during dead line working, still in position. Whilst great care is taken to avoid this situation, its occurrence must be catered for since the resulting effect on system stability could be potentially catastrophic. A fault of this nature can be expected to occur at any point on the line.

It will be recalled from section 5.4.3, that the earth elements are restrained by preventing any trip counter increments if there is an absence of residual current. Thus, the earth elements are not suited to the task of detecting three-phase faults since they will not operate under these conditions. The equivalent restraint process of the phase elements is shown in Figure 5.11, where individual phase elements are allowed to 'pick up', i.e. flag a fault, but without system imbalance the relay is prevented from tripping. Hence, a method of detecting balanced three-phase fault situations is to check if, simultaneously, all three of the phase elements are indicating a fault.

The flow diagram for the evaluation of a three-phase fault is shown in Figure 7.1. It is shown that relay operation is prevented if a power swing is in progress; how this is

ascertained will be discussed in the next section.

### 7.3 POWER SWINGS

#### 7.3.1 Causes of a power swing

Figure 7.2 shows an illustrative system scenario which can result in a power swing. A busbar P, with limited generating capacity is connected, via a two section transmission line, to a busbar R which is part of a large source network and maybe considered to be an infinite bus. A busbar Q is present between P and R and it is assumed that the relay is located here and is protecting line Q-R. Also connected to busbar R is a transmission line leading to busbar S. Under steady-state conditions, power is being transferred in the direction P-Q-R, and so the voltage at P,  $V_P$ , leads the voltage at R,  $V_R$ .

At some instant in time, a three-phase fault occurs, close to R, on line R-S. This may have been caused by the circuit breaker at R, on line R-S, being closed on to earthing clamps. Since power transfer between P and R is no longer possible, busbar R effectively being rendered at earth potential, the power that ordinarily would have been transferred from P now has the effect of increasing the angle of  $V_P$  with respect to  $V_R$ .

When the fault on R-S is removed, power transfer between P and R is, once again, possible. However, now that the angle between  $V_P$  and  $V_Q$  has exceeded its steady state full load value, an oscillation occurs in the rotor of the generating plant at P as it advances and retards in phase in an attempt to return to the steady state operating value. Since an oscillation of the rotor angle leads to a similar

variation in the transmitted power, this phenomenon is referred to as a **power swing**.

It can be seen that the increase in the rotor angle at P, as a result of the fault on R-S, increases with the fault clearance time. If the fault clearance time is long, then it is possible for the angle between P and R to become so large that synchronism is lost and a pole slip occurs.

### 7.3.2 Effect of power swings on distance relays

Consider, that at some instant in time, the voltages at P and R are in anti-phase. Therefore, there exists a point along P-Q-R where the voltage will appear to be zero. This point is referred to as the **electrical centre** of line P-R and is the point where the sum of the source and line impedances on one side of the point is equal to the sum of source and line impedances on the other side of the point. In this situation it will appear to the protection at Q that a three-phase fault exists at the point of the electrical centre; if this point lies in the relay characteristic then the relay will operate. It can be shown [36], that under these conditions, the locus of the impedance measured by a distance relay is circular and also a function of the ratio of the magnitudes of  $V_P$  and  $V_R$ . Whilst this effect has been described for what is essentially a pole slip condition, a similar effect can also occur when  $V_P$  and  $V_R$  are swinging relative to each other [36].

Using a frequency domain simulation of the system of Figure 7.2 [37], a study of the impedances seen by the phase elements of a relay situated at busbar Q has been made.

Details of this simulation are given in Appendix 13. Figure 7.3a shows the impedance seen by the 'b-c' element of the relay, situated at busbar Q, which was set to protect 80% of line Q-R. Figure 7.3a shows 10ms of prefault power transfer, 190ms of a fault close to busbar R and the ensuing power swing which resulted in two pole slips. The pole slips occur when the measured R and X values appear asymptotic at times 0.67 and 0.95 seconds.

A part of the power swing which adversely affects the protection occurs between the times 0.3 and 0.6 seconds. The locus of the measured impedance during this time is shown in Figure 7.4; this Figure also shows the relay characteristic which has a resistive to reactive reach ratio of 0.54. It can be seen that the locus of the measured impedance passes straight through the characteristic, implying that the electrical centre of the system is located approximately 20% from Q along line Q-R. The corresponding operation of the three-phase fault detection, as described in Section 7.2 but without any power swing blocking, is shown in Figure 7.3b. Similar relay maloperation is seen to occur at 0.85 seconds in Figures 7.3a and b. Note, from Figure 7.4, how the locus of the measured impedance appears to form part of a circle. The slow speed at which the impedance changes during a power swing, e.g. 300ms for the locus of Figure 7.4, is attributable to the mechanical time constants of the generating plant.

### 7.3.3 Zones of protection

Before discussing power swing blocking, it is advantageous

at this point to elaborate on the relay characteristics. Hitherto in this work, it has been described that the relay is provided with one characteristic, per element, which affords protection of the line on which the relay is situated, i.e. the local line. It is common practice [38] for distance relays to be provided with two extra characteristics which allow the relay to provide remote back-up protection for lines situated beyond the local line. Such characteristics are typically as shown in Figure 7.5.

The characteristic protecting the local line is referred to as zone 1, and the characteristics protecting the next two lines are referred to as zones 2 and 3. Zone 3, which provides forward and reverse remote backup, is larger than zone 2, which only provides remote backup in the forward direction. Generally, zone 1 is set to protect 80% of the local line, zone 2 is set to protect 50% of the shortest second line and zone 3 is set for 25% of the third line following the longest second line [38]. The additional characteristic, zone 6, of Figure 7.5 will be described in the next section.

Note that Figure 7.5 shows all the characteristics as being quadrilaterals. Whilst there are commercially available relays having quadrilateral characteristics [39], a large number of relays have offset mho and lenticular shaped characteristics.

#### 7.3.4 Conventional method of power swing blocking

Since power swing and pole slips are phenomena which are, in part, governed by the mechanical time constants of

generating plant, the time taken for the impedance to change from a load position to a point within the characteristic of the relay is correspondingly long. Thus, the conventional approach in power swing blocking is to introduce an additional characteristic to the relay, which completely envelopes the previously described characteristics, and to time the transition of the impedance crossing from one characteristic to the other [36,38]. If the transition is virtually instantaneous, then the disturbance must be due to a fault and relay operation is allowed. If a considerable time lag occurs between the impedance entering the additional characteristic and the conventional one, then the likelihood is that a power swing or pole slip is occurring and so relay operation is blocked. This additional characteristic is referred to as zone 6 and is shown in Figure 7.5.

Whilst this form of power swing blocking (PSB) has been used for many years, there are two fundamental disadvantages associated with its use. Firstly, the PSB is only reset when the impedance eventually exits from zone 6 and so, any genuine fault occurring during the time that the PSB is active will remain unnoticed by the distance protection.

Secondly, it is imperative for correct operation of the PSB, that zone 6 is set short of the load area. This, in consequence, imposes a further limitation on the setting of the resistive coverage of the relay characteristic. This limitation is further exacerbated when it is considered that zone 6 has to totally envelop zone 3.

### 7.3.5 A new method of power swing blocking

In order to develop a new technique of PSB that overcomes the limitations described in the previous section, it was necessary to examine the differences between a three-phase fault and a power swing. The single distinguishing feature, which is exploited in the conventional PSB, is that the change in impedance values during a power swing is, relative to a fault situation, slow.

In Section 5.3 it was described how the transient variation of the impedance estimates during the group delay, i.e. the period during which the prefilter contains both pre-fault and post-fault information, is used to delay the trip counter if the impedance passes through the characteristic but eventually converges outside of it. Since the prefilter group delay is 3ms in length, yet the time taken for the impedance to pass through the characteristic of Figure 7.4 is of the order of 150ms, it follows that the prefilter group delay is unlikely to produce any transient effects during a power swing and thus there will be minimal variation in the impedance over a 3ms interval.

In Section 5.3, which discusses the effect of varying the fault inception angle, the method used to effect the delay to the trip counter is to compare the value of  $d(D.X)/dt$ , the instantaneous impedance variation, with  $D.X_r$ , a variable which is a function of the reach point reactance. These variables are defined in Figure 5.6 and Section 5.2 respectively. To test the instantaneous impedance variation during power swings, the value of  $d(D.X)/dt$  is normalised, by dividing by  $D.X_r$ , to form the variable  $\sigma$ :

It is shown that  $\sigma = [d(D.X)/dt]/D.X_T \dots\dots\dots 7.1$

Since only the phase elements are involved in detecting three-phase faults and power swings, there are three instantaneous values of  $\sigma$ ;  $\sigma_{ab}$ ,  $\sigma_{bc}$  and  $\sigma_{ca}$ . Figure 7.6a shows the variation in  $\sigma_{bc}$  for the same power swing that is depicted in Figure 7.3.

In Figure 7.6a,  $\sigma_{bc}$  is observed to have values significantly greater than zero at point A, the inception of the three-phase fault, and points B and C, where a pole slip occurs. A slightly less significant effect occurs at point D where the three-phase fault is cleared. However, the important aspect of Figure 7.6a is that during the power swing, in the period 0.3 to 0.6 seconds when the impedance is observed from Figure 7.4 to pass through the relay characteristic, the value of  $\sigma_{bc}$  is virtually zero. Thus, on the evidence of Figure 7.4a, a method of differentiating between three-phase faults and power swings is to look for the presence of  $|\sigma| > 0$ . Note that, in the case of a three-phase fault,  $\sigma$  will always converge to zero at the end of the prefilter group delay; this is essential to relay operation since, from Section 5.3.2, if  $|\sigma| > 0.5$ , then the trip counter increment is zero and thus operation is inhibited.

In order to ascertain that, for all expected three-fault conditions, a significant value of  $\sigma$  is observed during the prefilter group delay, a detailed study of the behaviour of the peak values of  $\sigma_{ab}$ ,  $\sigma_{bc}$  and  $\sigma_{ca}$  under varying conditions of fault angle, fault position and SCL was conducted. The results are summarised in Appendix 14 where

it is shown that during the prefilter group delay of any expected three-phase fault, the value of  $\sigma$  for at least one of the phase elements will exceed 0.5.

Thus, with this result, it is now possible to propose a method of preventing relay operation during power swings. The method involves checking if, for any of the phase elements, the magnitude of  $\sigma$  exceeds 0.5. If this condition is found to be true immediately prior to the relay indicating a three-phase fault, then relay operation is allowed. If, however, a three-phase fault is indicated without  $|\sigma|$  recently exceeding 0.5, then operation is inhibited. This method differs from the conventional method of PSB in that it **enables** the relay to operate for three-phase faults rather than disables the relay for power swings.

### 7.3.6 Description of algorithm for new PSB method

The flow diagram of the algorithm used is shown in Figure 7.7. The algorithm will set the flag TPF E (Three-Phase Fault Enable) "true" if the magnitude of  $\sigma_{ab}$ ,  $\sigma_{bc}$  or  $\sigma_{ca}$  exceeds 0.5. TPF E, in the absence of any other effect, will remain "true" for 10ms; this is timed by the counter TCOUNT which is assigned an initial value of 40 (40 samples at 4kHz sampling frequency is equivalent to 10ms). The value of 10ms was chosen since it allows quick resetting in the event that the TPF E flag was set "true" due to some condition other than an in-zone three-phase fault, e.g. the pole slip shown at point B in Figure 7.6. In terms of the time taken for a power swing, 10ms is a relatively short time.

If, when TPF<sub>E</sub> is "true", there is a genuine three-phase fault, then the 10ms period is reset continually whilst any of the phase element averagers are invoked. TPF<sub>E</sub> then times out 10ms after the last averager is disabled. This arrangement allows for relay operation times which are greater than 10ms. Once the TPF<sub>E</sub> flag has been set "false", only the test for  $|\sigma|$  exceeding 0.5 can re-enable three-phase fault tripping.

In Figure 7.1, the operation of the relay for three-phase faults was seen to include a test for the presence of a power swing. Now that the methodology of the new method has been explained, the flow chart of Figure 7.1 is reproduced in Figure 7.8 where the conditional statement concerning power swings has been modified to reflect this new method.

### 7.3.7 Performance of new PSB method

The performance of the new method is shown in Figure 7.6. Figure 7.6c shows the behaviour of the TPF<sub>E</sub> flag; this can be seen to be set "true", as a function of  $\sigma$  of Figure 7.6a, in accordance to the previously described theory. Note that TPF<sub>E</sub> is "true" for approximately 30ms, after the three-phase fault has been removed, i.e. point D in Figure 7.6a, yet  $\sigma_{bc}$  is observed to not exceed 0.5. This is indicative that either  $\sigma_{ca}$  or  $\sigma_{ab}$  did exceed 0.5 at that point.

The three-phase trip flag, which represents when all the phase elements are indicating a fault, is seen not to coincide with TPF<sub>E</sub> being set "true", and thus, in accordance with Figure 7.8 no overall relay trip occurs for this power swing.

#### 7.4 CONCLUSION

This Chapter has discussed the cause and effects, on distance protection, of power swings. It has been shown that the relay will maloperate during certain power swing conditions when the measured impedance passes through the characteristic. Conventional power swing blocking techniques and their disadvantages have been described.

A new method of power swing blocking has been proposed which enables the relay to trip for three-phase fault conditions but disables the relay during power swings. It has been shown that this method will always correctly operate for the expected range of three-phase faults. The new method does not restrict the setting of any of the zones of the relay with respect to load encroachment. Further to this, the relay will operate correctly for an in-zone three-phase fault if it occurs during the time that a power swing is in progress.

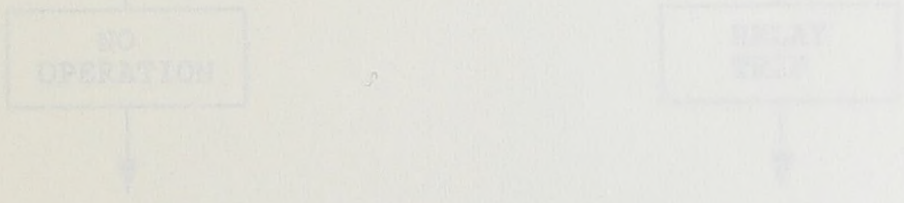


Figure 7.1 Flow chart for the detection of three-phase faults using the phase elements.

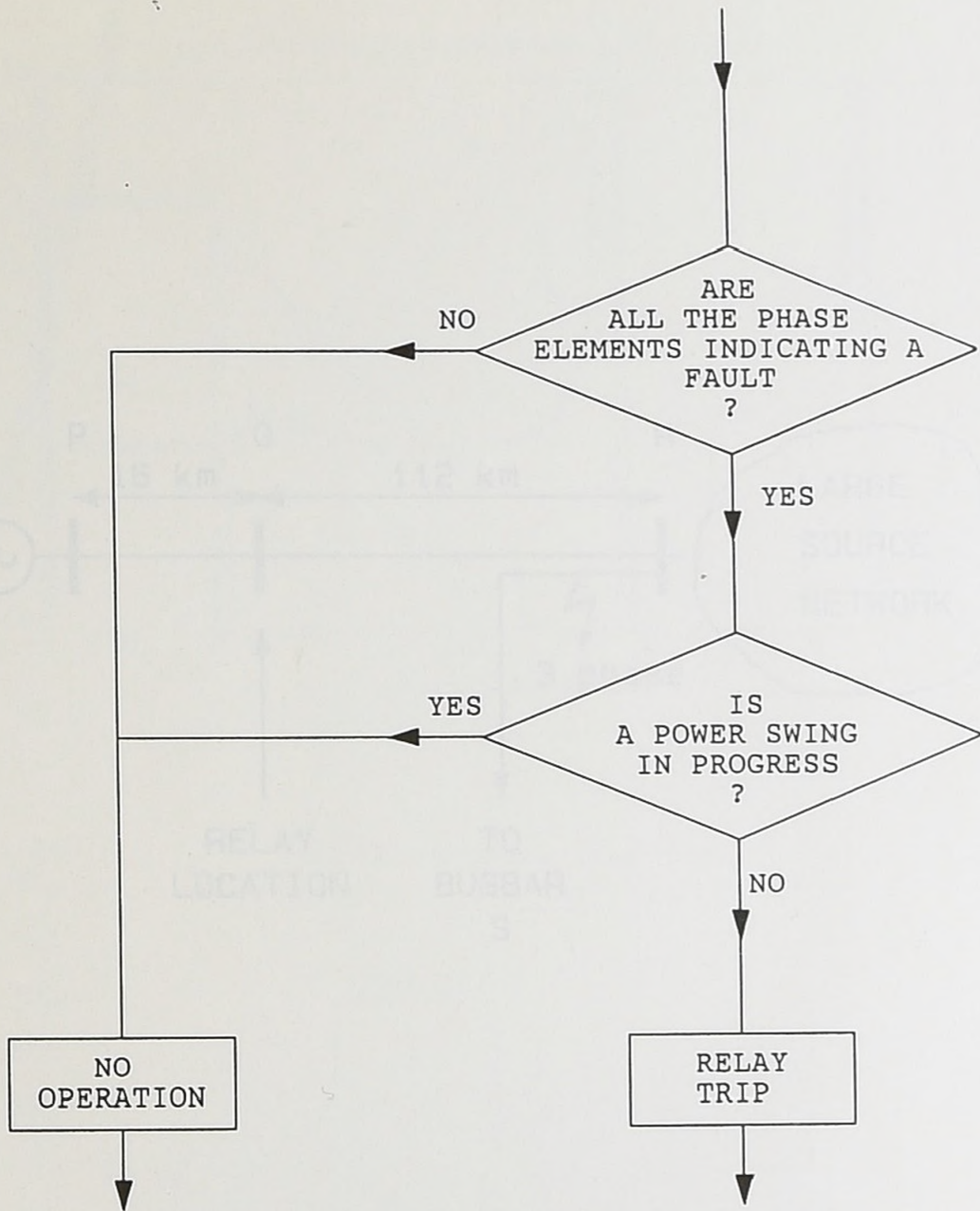


Figure 7.1 Flow chart for the detection of three phase faults using the phase elements.

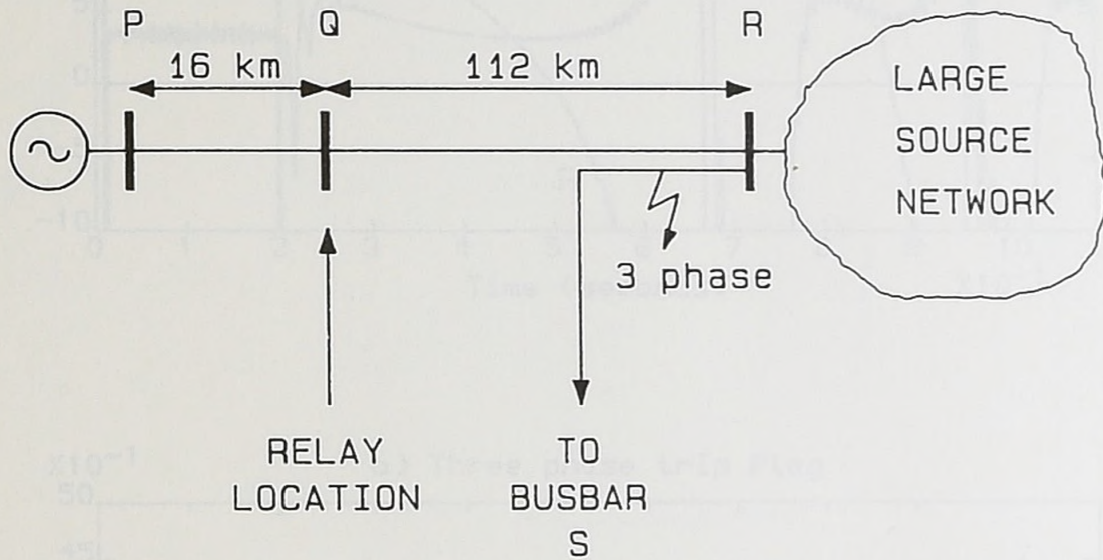


Figure 7.2 400kV system configuration used to study power swings.

Figure 7.3 Relay behaviour during power swing.

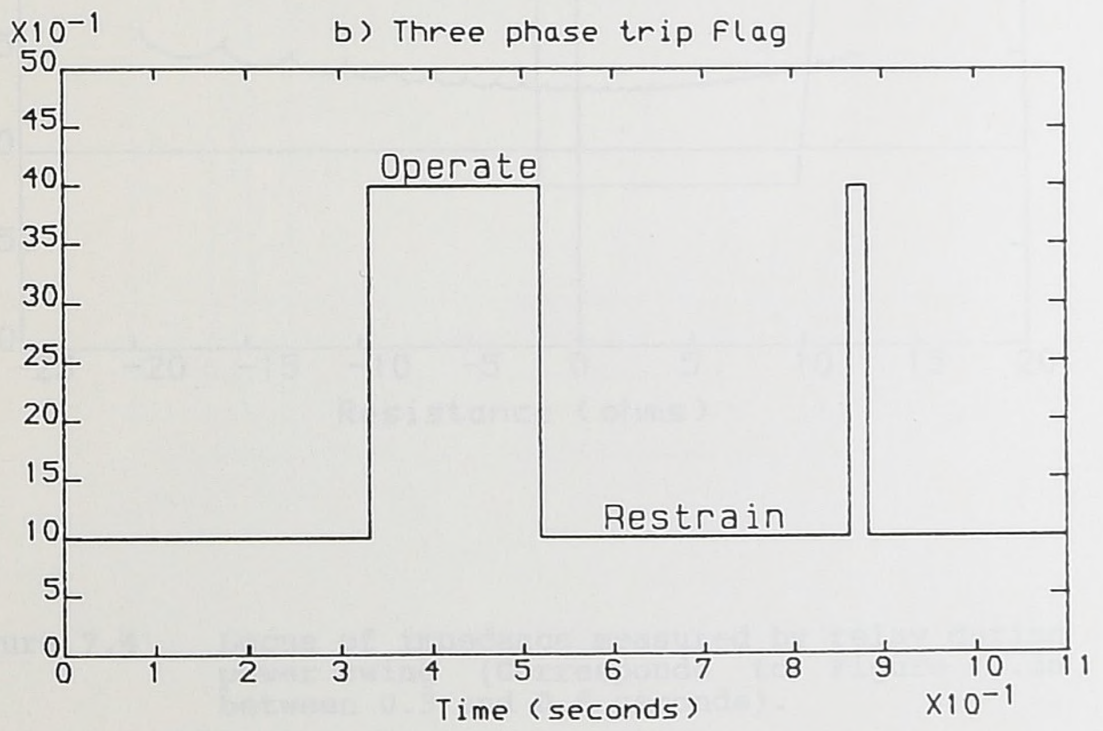
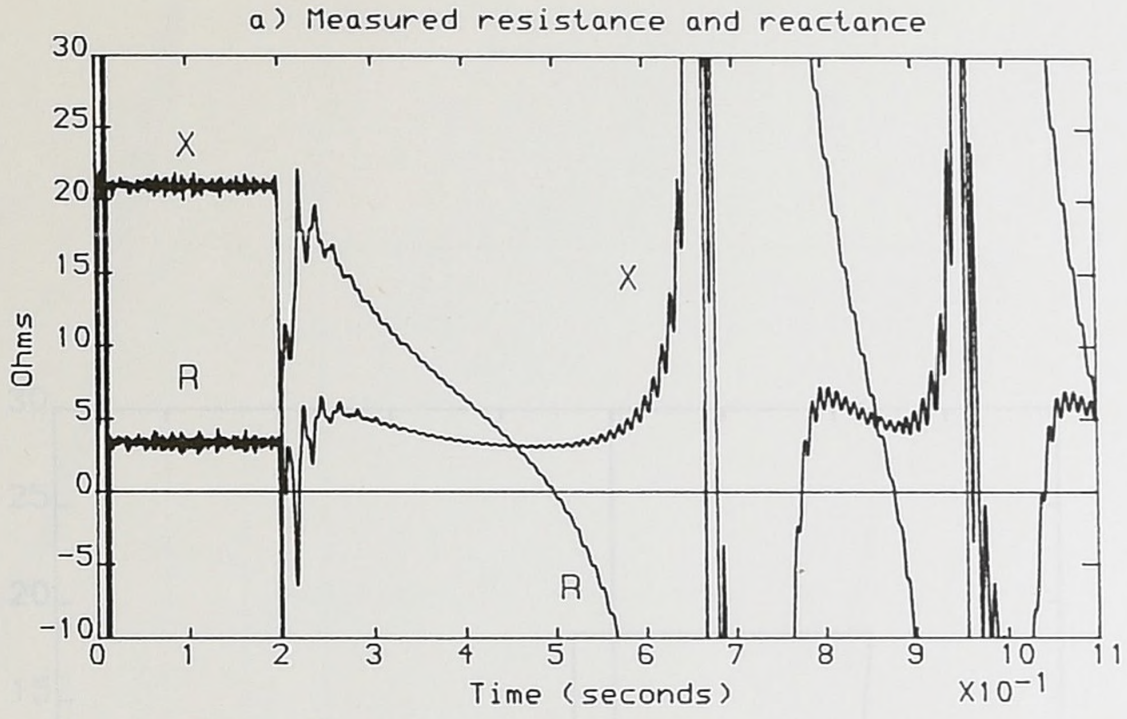


Figure 7.3 Relay behaviour during power swing.

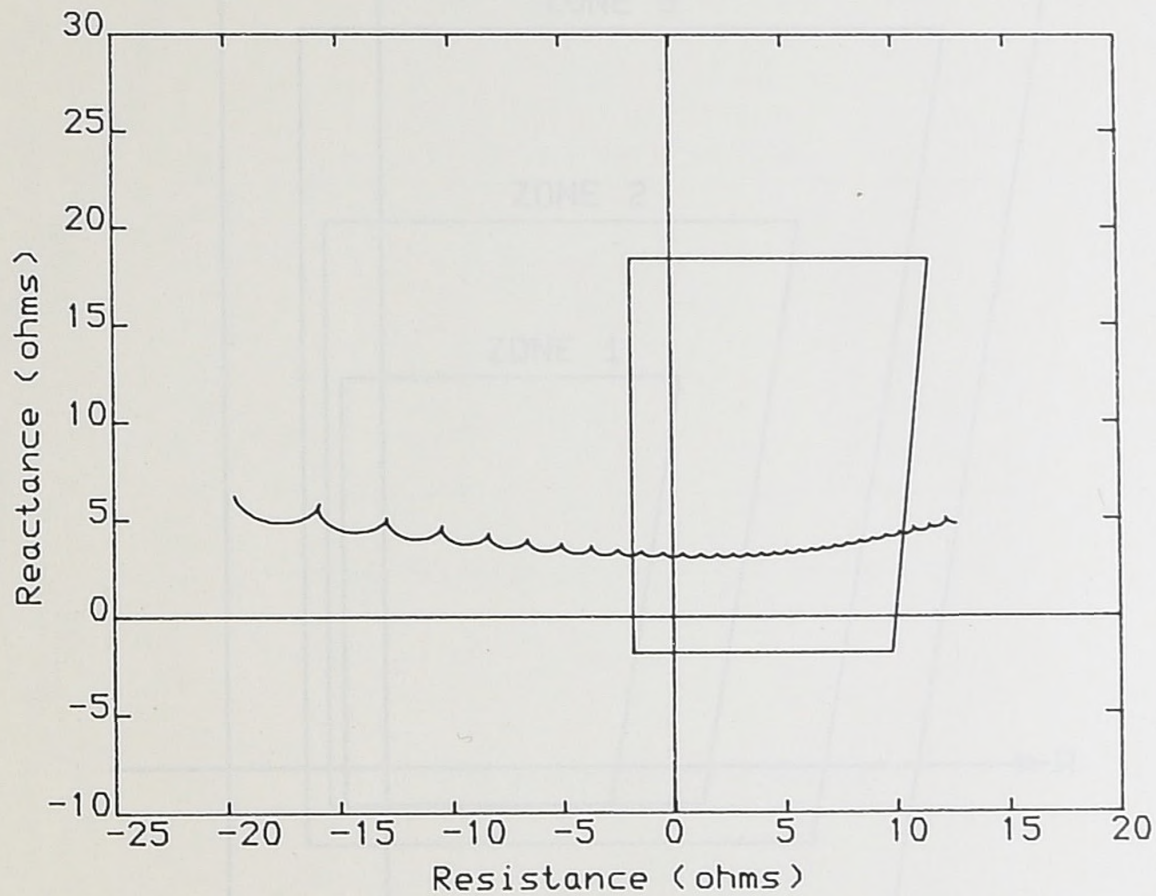


Figure 7.4 Locus of impedance measured by relay during power swing (Corresponds to Figure 7.3a between 0.3 and 0.6 seconds).

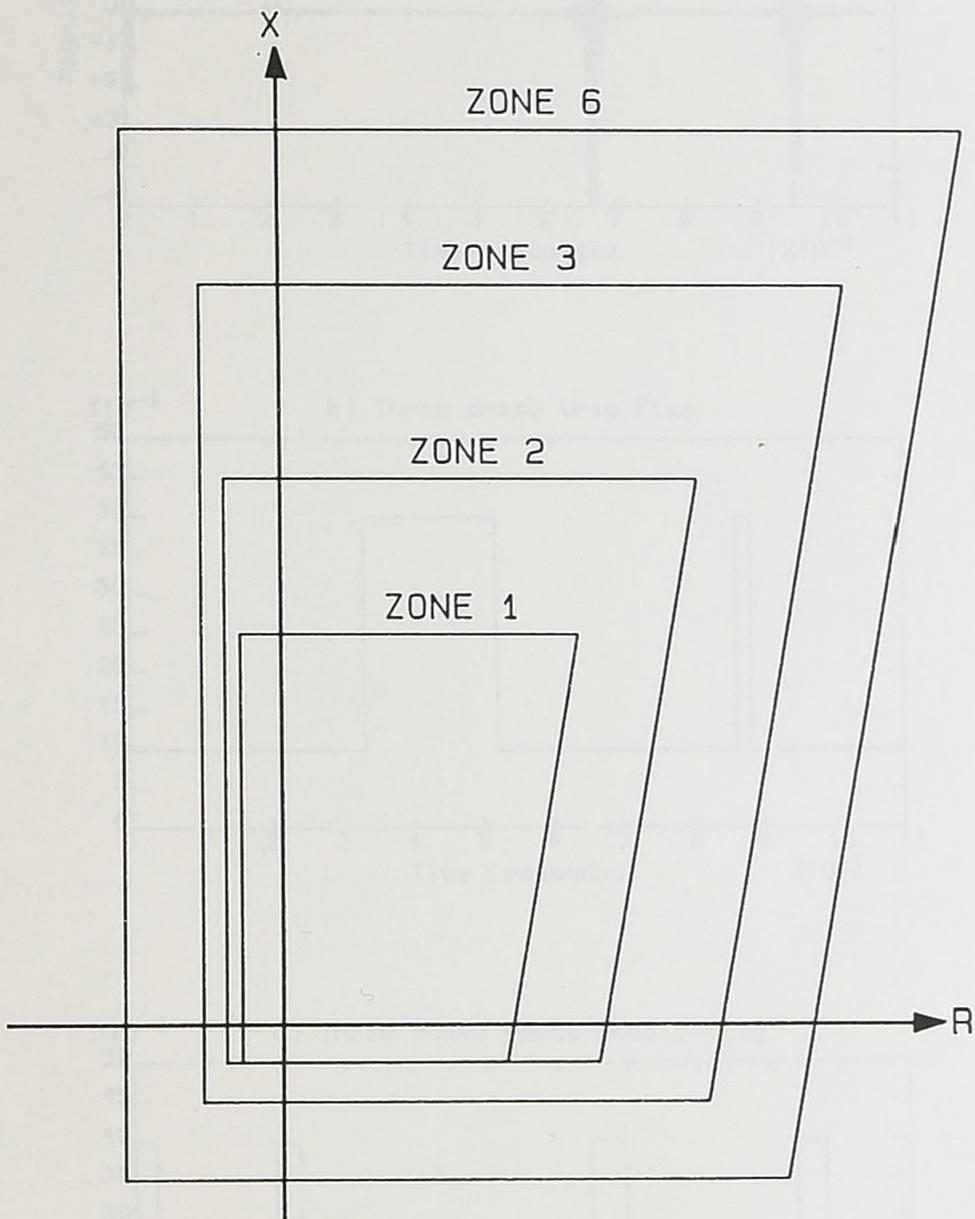


Figure 7.5 Zones of protection based on quadrilateral characteristics.

Figure 7.6 Behaviour of relay with new method of power swing blocking.

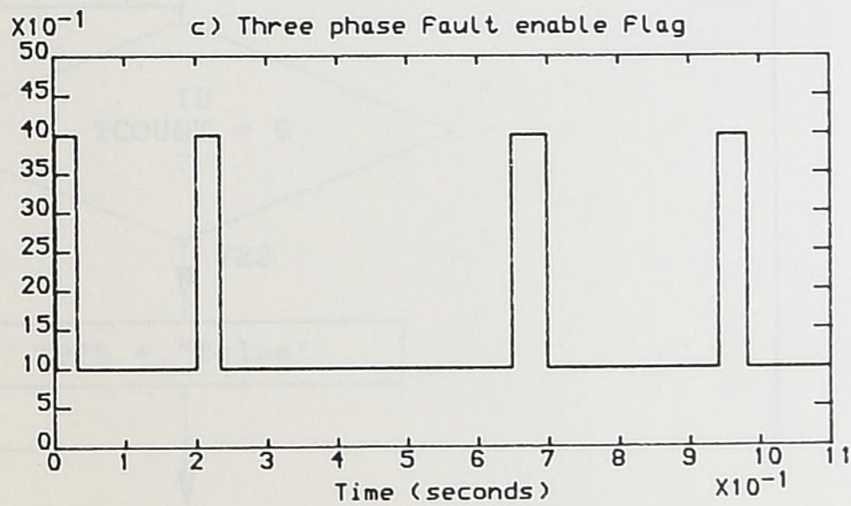
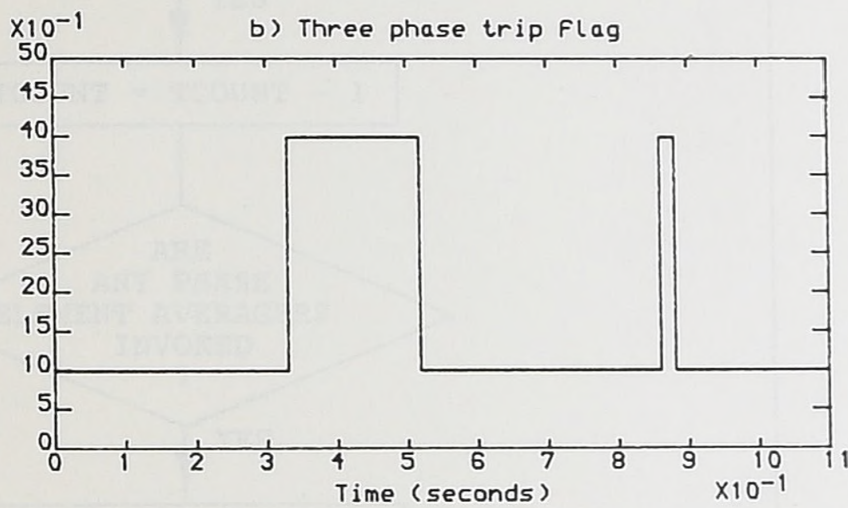
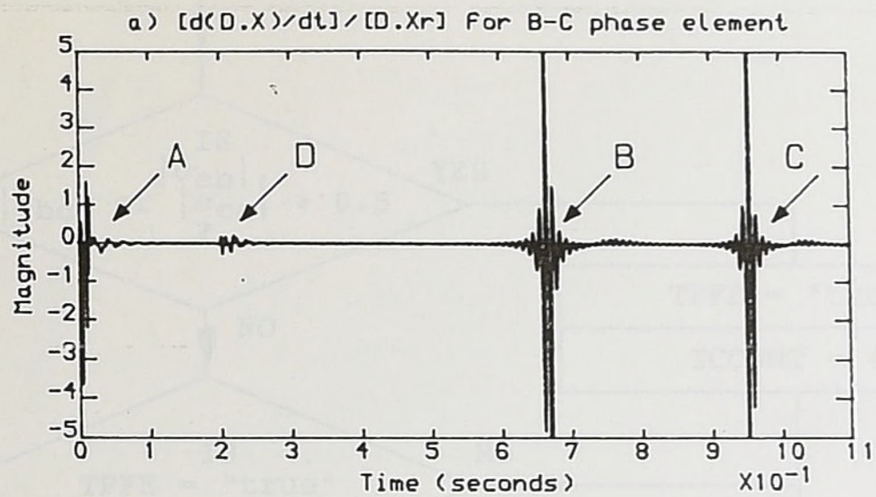


Figure 7.6 Behaviour of relay with new method of power swing blocking.

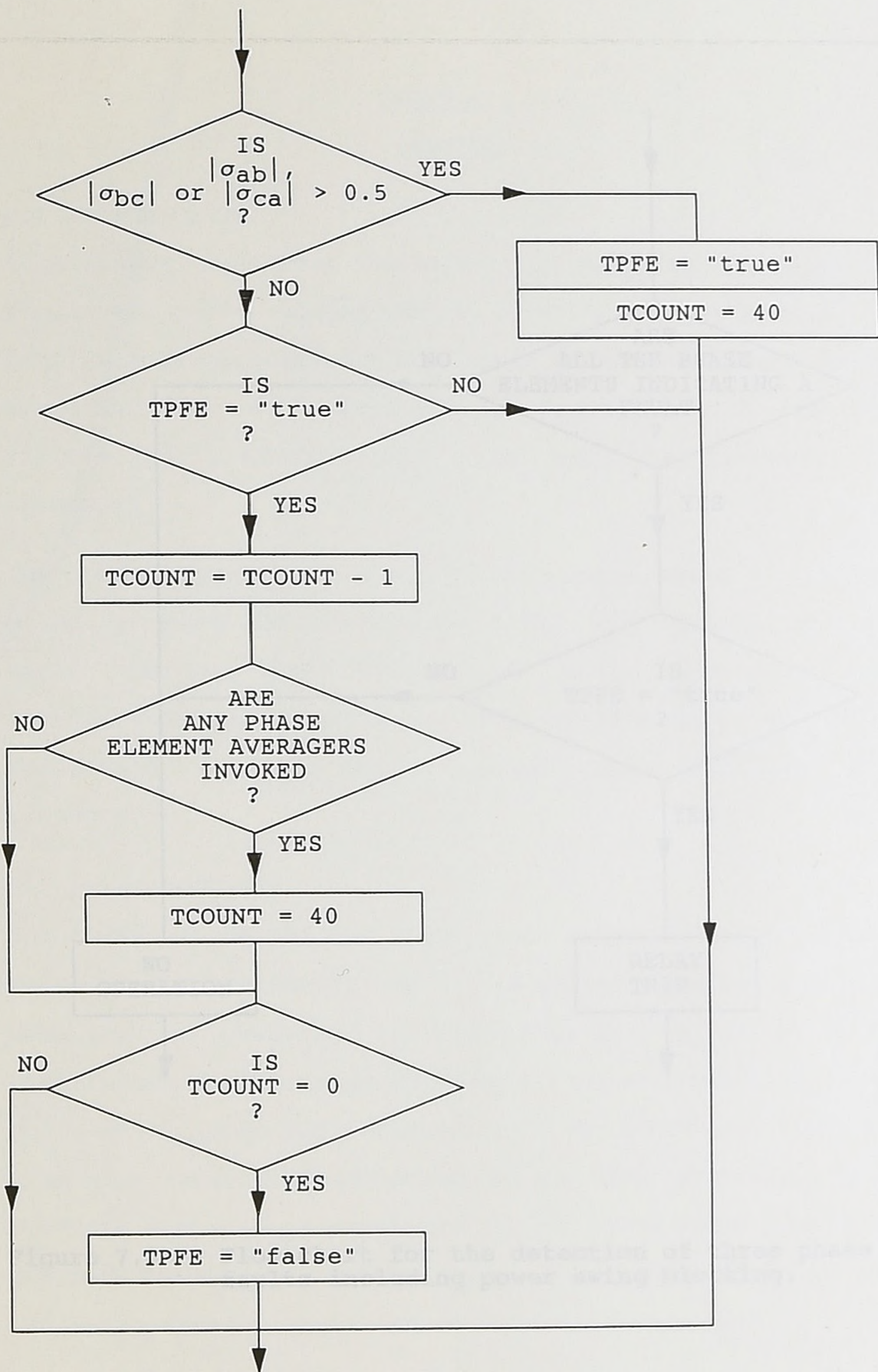


Figure 7.7 Flow chart for the algorithm used to differentiate between three phase faults and power swings.

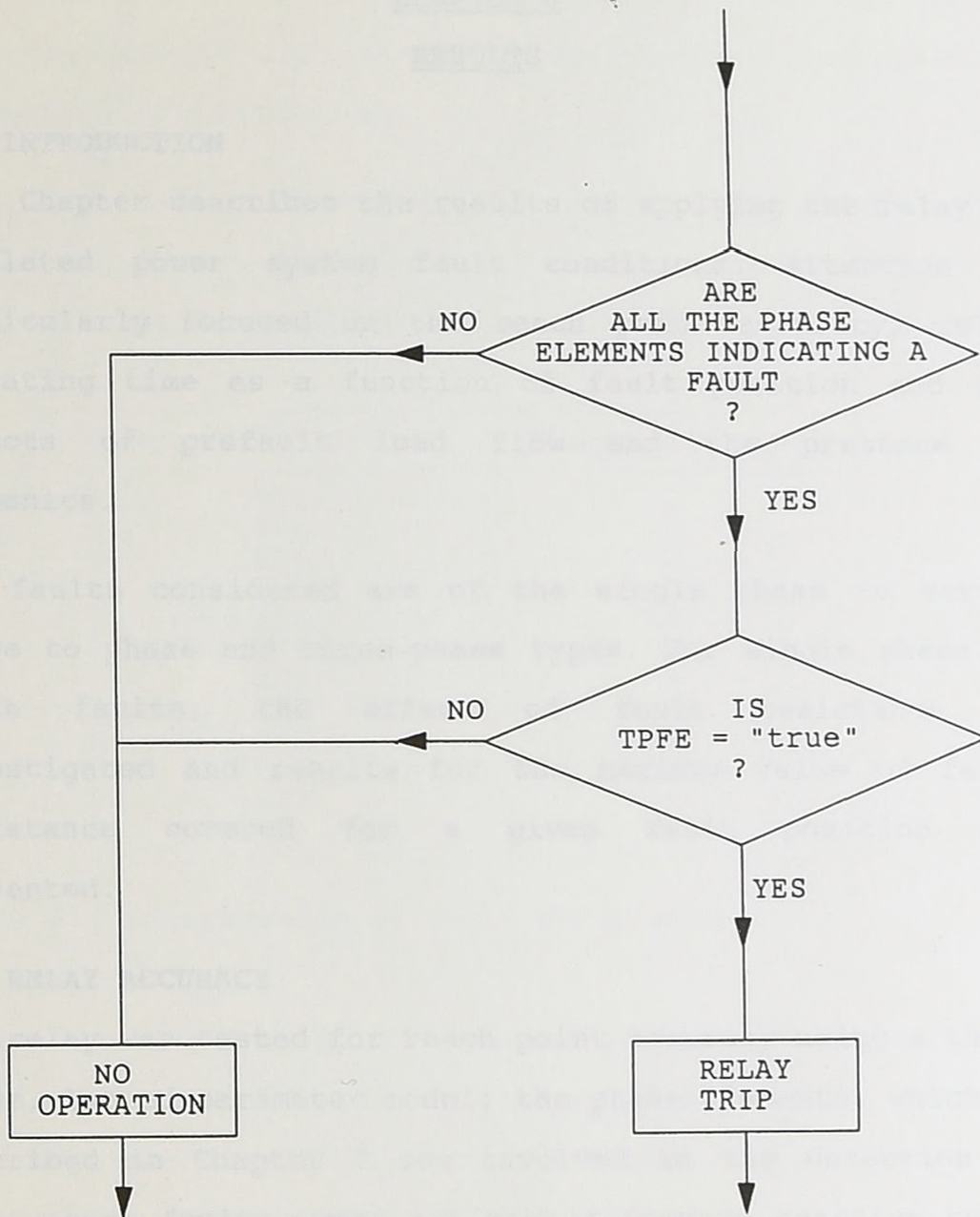


Figure 7.8 Flow chart for the detection of three phase faults including power swing blocking.

STP: 4.1, 1, 10, 30, 60

Fault angle: 0°, 15°, 30°, 45°, 60°, 75°, 90°

Harmonics: None, 0.5, 1.0, 5%, 10%, 15%

CHAPTER 8RESULTS**8.1 INTRODUCTION**

This Chapter describes the results of applying the relay to simulated power system fault conditions. Attention is particularly focused on the reach point accuracy, relay operating time as a function of fault position and the effects of prefault load flow and the presence of harmonics.

The faults considered are of the single phase to earth, phase to phase and three-phase types. For single phase to earth faults, the effect of fault resistance is investigated and results for the maximum value of fault resistance covered for a given fault position are presented.

**8.2 RELAY ACCURACY**

The relay was tested for reach point accuracy using a three phase, lumped parameter model; the phase elements, which as described in Chapter 7 are involved in the detection of three-phase faults, were set with a forward reactive reach point of  $4\Omega_{sec}$  and a resistive to reactive reach ratio of 0.5. The relay is considered to be 100% accurate if it operates for a  $4\Omega_{sec}$  fault but blocks for a fault having 1% greater impedance, i.e.  $4.04\Omega_{sec}$ . All combinations of the following system conditions were used in this test:

SIR:	0.1, 1, 10, 30, 60
Fault angle:	$0^\circ$ , $15^\circ$ , $30^\circ$ , $45^\circ$ , $60^\circ$ , $75^\circ$ , $90^\circ$
Harmonics:	None, 5% 3rd, 5% 5th, 5% 7th

Load: Full load, no load, reverse full load

Note that SIR is defined as source impedance (referred to secondary) divided by  $4\Omega$ .

Thus, a total number of 420 reach point cases were considered. The distribution of the cases considered against accuracy obtained is shown in Table 8.1:

Observed accuracy	Number of cases
91%	2
92%	5
93%	2
94%	2
95%	6
96%	0
97%	4
98%	0
99%	307
100%	85
101%	2
102%	5

Table 8.1 Distribution of reach point accuracy

Table 8.1 shows that, for the majority of the situations considered (93% of all the cases), the relay displays accuracy that is in the range 99 - 100%. It was felt that the results would be more meaningful if the cases that did not produce 99 - 100% accuracy were listed, rather than drawing accuracy curves. Thus, Tables 8.2 to 8.9 show the particular system conditions which did not give 99 - 100% accuracy.

Load	Harmonics	Fault Angle	SIR
None	5% 7th	30°	30
None	5% 7th	90°	30

Table 8.2 System conditions resulting in 91% accuracy

Load	Harmonics	Fault Angle	SIR
None	5% 7th	0°	30
None	5% 7th	15°	60
None	5% 7th	45°	30
None	5% 7th	60°	30
None	5% 7th	75°	60

Table 8.3 System conditions resulting in 92% accuracy

Load	Harmonics	Fault Angle	SIR
None	5% 7th	45°	10
None	5% 7th	45°	60

Table 8.4 System conditions resulting in 93% accuracy

Load	Harmonics	Fault Angle	SIR
None	5% 7th	15°	10
None	5% 7th	75°	10

Table 8.5 System conditions resulting in 94% accuracy

Load	Harmonics	Fault Angle	SIR
None	5% 7th	0°	10
None	5% 7th	0°	60
None	5% 7th	30°	60
None	5% 7th	60°	10
None	5% 7th	60°	60
None	5% 7th	90°	60

Table 8.6 System conditions resulting in 95% accuracy

Load	Harmonics	Fault Angle	SIR
None	5% 7th	15°	30
None	5% 7th	30°	10
None	5% 7th	75°	30
None	5% 7th	90°	10

Table 8.7 System conditions resulting in 97% accuracy

Load	Harmonics	Fault Angle	SIR
None	None	15°	60
None	None	75°	60

**Table 8.8 System conditions resulting in 101% accuracy**

Load	Harmonics	Fault Angle	SIR
None	None	0°	60
None	None	30°	60
None	None	45°	60
None	None	60°	60
None	None	90°	60

**Table 8.9 System conditions resulting in 102% accuracy**

Before analysing the results of Tables 8.2 to 8.9, it is worth recalling from Section 2.2 that the allowable tolerances in reach point accuracy are  $\pm 5\%$  for SIR's up to 30 and  $\pm 10\%$  for SIR's in the range 30 to 60. Further to this, the presence of 5% of any harmonic allows an extra  $\pm 5\%$  on top of the previous tolerances. It can be seen from Tables 8.2 to 8.9, that the performance of the relay falls well within these specifications.

Analysis of Tables 8.2 to 8.9 reveals that all situations where the accuracy is not 99 - 100% occur on an unloaded line; since, in practice, overhead transmission lines usually convey some flow of load, for the large majority of cases, the observed accuracy will be somewhat better than the results presented here.

For observed accuracies of greater than 100%, the SIR is 60. Since the voltage and current inputs to the relay are very small for SIR = 60 situations, the probable cause of

this effect is transient overreach. However, since the overreach is only 2%, this effect can be ignored.

All situations which resulted in the relay underreaching, are accompanied by the presence of 5% of 7th harmonic. It is seen from Figure 3.6c that the predicted error in the inductance measurement for the impedance measurement technique employed in the relay is only +1%. However, when the effect of the prefilter is considered, this error will be amplified. The frequency response of the prefilter is shown in Figure 4.4 where it can be seen that 7th harmonic, or 350Hz, represents almost the peak of the prefilter pass band and thus, any 7th harmonic in the input signals will have a gain of 5 to 6 times the gain of the 50Hz signal. Thus, the effective error in the inductance measurement for 7th harmonic signals is greater than +1% and, it will be appreciated, that positive errors of this nature will tend to make the relay underreach.

### 8.3 RELAY OPERATING TIME

#### 8.3.1 Single phase to earth faults

##### 8.3.1.1 100km line length

The earth fault operating times were observed for a variety of faults generated using the distributed parameter primary system simulation described in Section 2.5. The primary system simulation included the effect of the CVT. For these results, the 'a' phase was faulted with zero fault resistance; it will be seen from Appendix 7 that the 'a' phase lies closest to the ground for the single circuit, 400kV, vertical configuration considered.

Figure 8.1 shows the earth fault operating times, as a

function of the fault position, for a 100km line. The fault position is expressed as a percentage of the relay reach which was set to, nominally, 80% of the line length. Figure 8.1 shows 6 sets of results; these are for local SCL values of 0.5, 5 and 50GVA, and for fault inception angles, on the 'a' phase at the fault point, of  $90^\circ$  (voltage maxima faults) and  $0^\circ$  (voltage minima faults). All faults are shown for an unloaded line.

It can be seen from Figure 8.1 that the operating times are fairly constant over 75% of the relay reach. The increase in operating time for faults lying beyond 75% of the reach is due to the counting strategy discussed in Section 5.2. It is observed that the operating time decreases with increasing local SCL; for close-up faults at voltage maxima, the operating time is 6.25ms for a SCL of 50GVA and 10ms for a SCL of 0.5GVA. This increase in operating time for the 0.5GVA case is due to small primary system signal levels entering the relay which, due to quantisation errors, lead to poor resolution of the measured impedance. Despite this effect, the voltage maxima earth fault operating time at a SCL of 0.5GVA is less than 11.25ms for all faults up to 80% of the reach.

The results for faults occurring at the 'a' phase voltage zero crossing (voltage minima faults) show a tendency to be, approximately, 1ms less than the corresponding voltage maxima faults. At first sight, it may be expected that this effect is due to travelling wave distortion which will be present for the voltage maxima faults but not, to the same extent, for voltage minima faults. Note that a close-up

voltage maxima fault, due to the small distance between fault and source, does not lead to significant travelling wave distortion of the measured impedance since the travelling wave frequency will be high and its effects will be removed by the prefilter ( see Chapter 4). Since the reduction in operating time is seen to occur for close-up as well as mid-line faults it may be deduced that travelling wave distortion is not the prime cause. It is more likely that the prefilter transients, in the voltage minima fault cases, lead to a slightly faster convergence of the measured impedance and, thus, a faster relay operating time.

An important corollary of the observation that the voltage maxima fault operating times are constant over 75% of the relay reach, is that the filter filtering function is, evidently, removing some of the travelling wave induced distortion from the measured impedance. It may be further inferred that operating time results for application studies involving line lengths less than 100km will be, at worst, no greater than the operating time results for the 100km line case.

It will be noted that the relay exhibits good reach point accuracy for these faults. A small amount of transient overreach (3%) is observed for the voltage maxima, 0.5GVA case. Since this corresponds to the minimum limiting SCL considered, its effect is not significant.

It should be realised that similar reach point accuracy for faults occurring on either the 'b' or 'c' phases of the line configuration considered is unlikely to be observed.

Since the impedance per unit length is different for each phase, some overreaching is inevitable for 'b' or 'c' to earth faults.

### 8.3.1.2 250km line length

Figure 8.2 shows results, in the same format as Figure 8.1, for a 250km line length. For faults up to 50% of the relay reach the results can be seen to be similar to the 100km line cases. As the fault moves towards the reach point, however, the operating times are greatly increased over the corresponding 100km line results. This is due in part to the decreased signal level, and therefore increased quantisation errors, which are apparent for the 5GVA and 0.5GVA situations. Further to this, an increase in travelling wave noise can be expected for voltage maxima faults. Severe travelling wave distortion of the relay measurands will lead to oscillations in the measured impedance which will, in turn, slow down the counting strategy and lead to longer operating times. This effect is clearly shown for voltage maxima faults with a 0.5GVA SCL occurring at a fault position greater than 50% of the reach. The effect is less pronounced for the 5GVA SCL situation where operation times of less than 8.5ms result from voltage maxima faults lying within the first 75% of the reach.

The ability of the relay to afford good reach point accuracy and fast operation in situations, such as the 250km line cases, which involve severe travelling wave distortion can not be overstressed. Reference to Figure 4.2b, which shows the primary system waveform for a voltage

maxmima reach point fault on a 250km line, and Figure 4.6, which shows the reactance measured by the 'a' phase earth element for this fault, imply that it is the combination of signal filtering and counting strategy which, together, aid the overall performance of the relay.

Transient overreach is observed for the voltage minima, 5GVA situation, to the extent of 3%, which is within the allowable range given in the relay specifications, Section 2.2.

### 8.3.1.3 Effect of pre-fault load angle

Figure 8.3 shows operating time results for pre-fault full load, no load and reverse full load situations. The faults occur at voltage maxima on a 100km line with a local SCL of 5GVA. Scrutiny of Figure 8.3 reveals that faults occurring up to 75% of the reach result in operation times that are virtually independent of load flow. However, the interesting feature of Figure 8.3 is that the reach point accuracy is seen to be greatly affected by pre-fault load flow; full load and reverse full load is seen to result in overreach and underreach of approximately 6% respectively.

This effect is due to two factors. Firstly, it was discussed in Section 5.4.2 that there is an error associated with using a real, rather than complex, residual compensation factor. However, studies carried out using a lumped parameter model with ideal conductor transposition indicated that the error involved would not account for 5% of under or overreaching.

The second source of error is due to the non-ideal

transposition of conductors which is incorporated in the distributed parameter model used for these tests. It will be recalled from Appendix 9 that the residual compensation factor was derived using sequence components. Since the use of sequence components inherently assumes ideal transposition, it therefore follows that, even with perfect, complex residual compensation, there will be an error in earth fault impedance measurement on non-ideal transposed systems. Thus, it is concluded that reach point accuracy variation with prefault load flow is inevitable for any residually compensated earth fault relay and the results presented here represent the expected errors which occur in a true, albeit simulated, system.

The extent of the reach point accuracy variation with prefault load flow will be affected by the SCL at the remote end of the line. Situations where the remote SCL is greater than the value of 1GVA used for the results of Figure 8.3 may lead to even greater errors in reach point accuracy when there is significant prefault load flow.

#### 8.3.1.4 Detailed effect of fault inception angle

Figure 8.4 shows the variation in operating time as the fault inception angle is varied between  $0^\circ$  and  $360^\circ$ . The system is a 100km line with a SCL of 5GVA. Figure 8.4a shows results for faults occurring at 30km from busbar P. The operating time is observed to vary by 1.75ms overall being 9ms at most and having a minimum value of 7.25ms close to a zero crossing of the faulted phase voltage. It can be seen that the general shape of the graph repeats itself over any  $180^\circ$  interval.

Figure 8.4b shows the effect of the fault being 75km from the relay, this corresponds to 94% of the relay reach. It is noticed that a much larger deviation in the operation times occurs, the minimum being 10ms and the maximum being 19.5ms.

These effects are caused by the process described in Section 5.3.2 which prevents transient overreach due to adverse impedance trajectories for specific fault inception angles occurring during the prefilter group delay. The important feature of these results is that there is no great variation in operating time for faults where the relay is expected to operate fast, i.e. faults lying between the relay and the mid-point of the line.

### 8.3.2 Phase to phase faults

Relay operating times for phase to phase faults, clear of ground, are shown in Figure 8.5 for a 100km line. The primary system simulation used was, again, the distributed parameter model and the faults were simulated by short circuiting the 'a' and 'b' phases with zero fault resistance. Figure 8.5a shows results when the fault inception angle was such that the 'a' and 'b' phase voltages were equal in magnitude and opposite in polarity immediately prior to the fault (maximum voltage difference faults); this situation leads to maximum travelling wave effect. In figure 8.5b, the faulted phase voltages were equal in magnitude and polarity (minimum voltage difference faults), thus the travelling wave effect is minimised.

A similar trend to the earth fault results is seen in Figure 8.5. An increase in SCL at the relay point leads to

reduced operating times, and, the results for maximum voltage difference faults, Figure 8.5a, are typically 1ms slower than the corresponding results for zero voltage difference faults. It can be seen that the operating times for maximum voltage difference faults with a SCL of 0.5GVA are increased for faults occurring beyond 50% of the relay reach. This effect is due to the combination of small signal resolution and travelling wave noise. With the exception of this result, the phase elements are observed to operate in less than 10ms for all faults occurring up to 85% of the relay reach.

Notice that, in all cases, the relay overreaches by nearly 6%. This is not transient overreach but due to the differing impedances per unit length which are experienced on an untransposed line of this type. Since, it will be appreciated from Section 5.5, that, in the case of a phase fault, the relay effectively evaluates the total fault loop impedance and divides by 2, it is clear that overreaching due to unequal conductor impedances is inevitable.

### 8.3.3 Three-phase faults

Relay operating times for three-phase faults were evaluated using a lumped parameter model set to simulate the 400kV, 100km line application used earlier in this Chapter. The results are shown in Figure 8.6; the curves for a SCL of 0.5GVA are virtually identical to the 5GVA case and are therefore omitted.

In common with the earth and phase fault results, the relay is seen to operate faster for the SCL of 50GVA case. The effect of the counting strategy slowing the operating time

down for faults close to the reach point is clearly shown in Figure 8.6 and it will be observed that the relay exhibits perfect reach point performance.

The interesting feature of Figure 8.6 is the very fast operating times which occur for faults close to the reach point. This is due to the current clipping detection, described in Section 5.6.3, which trips the relay if 3ms of contiguous current clips is detected. Since the current clipping detection operates the relay without processing any impedance values, it is clear that relay operation due to this effect will be faster than the conventional impedance measurement approach. In Figure 8.6b, where the fault occurs at the zero crossing of the 'a' phase voltage and thus there is maximum offset in the 'a' phase current, it can be seen that the relay operates in 4.75ms for faults up to 20% of the relay reach which corresponds to a distance to fault of 16km from the relay busbar P. For faults occurring at the maximum value of the 'a' phase, minimum current offset will be present in the 'b' and 'c' phases and, it can be seen from Figure 8.6a, current clipping, and hence very fast operating times, are only seen for faults very close to busbar P.

#### **8.4 RELAY FAULT RESISTANCE COVERAGE**

The effects of remote source infeed for single phase to earth faults involving fault resistance were described in Chapter 6, and the impedances measured by the faulted earth element for a fault at the reach point were shown in Figures 6.4a to 6.4d for various values of fault resistance and prefault load. In Section 6.6 it was concluded that a

satisfactory method of swivelling the characteristic to prevent overreach was to set the swivelling angle according to the argument of the zero sequence current divided by the residually compensated line current.

This section shows the effect of using this method of adaptation on the fault resistance coverage for single phase to earth faults. The primary system simulation used was a lumped parameter model based up on the 200kV line configuration of Appendix 12. The line length was 10km and the relay was set to protect 80% of the line length with a resistive to reactive reach ratio of 3.

The results shown in Figures 8.7a to d represent the same local and remote SCL's used in Figures 6.4a to d. Each of Figures 8.7a to d show three curves representing the limiting case of relay operation for full load, no load and reverse full load respectively. The axes for these Figures are fault position and fault resistance (measured in primary ohms), thus the curves may be considered to represent, for a given fault position, the maximum value of fault resistance for which the relay will operate. Since the relay is set for 80% of the line length, the nominal reach point corresponds to a fault position of 8km.

It can be seen, for all Figures 8.7a to d, that the fault resistance coverage is a function of the prefault loading; maximum resistance coverage occurs when there is full prefault load flow from P to Q. The reach point behaviour of the adaptive relay, as a function of fault resistance, is seen to result in some overreach, but this is limited to a maximum fault position of 9km from the relay. Ironically,

the results for Figure 8.7d, where the remote source infeed is at its maximum, show the least amount of overreach amounting to only 0.3km.

Whilst this overreach is seen to exist, to put these results in some form of perspective, Figure 8.8 shows identical system conditions corresponding to Figure 8.7d, but the relay has a fixed characteristic. The performance of the fixed characteristic relay can be seen to afford overreaching, for a prefault full load exporting condition, up to the end of the line. It is possible, depending on source conditions, for the overreach to extend to the next line. However, for the adaptive relay, a small amount of overreaching is present, but this is limited to the local line and there is, thus, a distinct benefit associated with its use. Further to this, comparing Figures 8.7d and 8.8, it can be seen that the adaptive relay allows almost twice the fault resistance coverage of a fixed relay for a given prefault load and fault position.

Figures 8.9 and 8.10 show the performances of the adaptive and fixed characteristic relays on a 400kV, 100km line with local and remote SCL's of 5GVA and 50GVA respectively. The line type is the 400kV configuration shown in Appendix 7. These results show, again, that the adaptive characteristic does not allow the relay to grossly overreach for resistive earth faults when the prefault load flow is exporting from the relay busbar. For this application, however, the general increase in resistive coverage for faults well within the reach is not as great as the 10km, 220kV line application. For the prefault no load and full load

exporting situations, the resistive coverage is increased by approximately  $5\Omega_{pri}$ , but for the prefault importing situation, the resistive coverage is increased by nearly 2.5 times for faults at the mid point of the line. Hence, again, the adaptive relay is seen to provide a more discriminative and reliable protection function.

It is to be noted that a greater fault resistance coverage may be obtained by increasing the resistive reach of the relay. However, it is to be expected that the overreach shown, for example, in Figure 8.7c for fault resistances of approximately 2 to  $4\Omega_{pri}$ , will be increased if this action is taken. It is interesting to note that, for Figures 8.7a to d and Figure 8.9, the position of maximum overreach represents the point of transition between the relay restraining on the reactive reach line, and the relay restraining on the resistive reach line. Taking as an example, again, Figure 8.7c, faults with resistances up to approximately  $2\Omega_{pri}$  are restrained due to the adapted reactance exceeding the positive reactive reach point. However, for faults with resistances greater than approximately  $2\Omega_{pri}$ , the reactance is now less than the reach point reactance value and restraint of the relay occurs due to the measured resistance exceeding the positive resistive reach point value.

It is now apparent why the resistive coverage is a function of prefault load flow since, it was seen in Chapter 6, that the measured resistance is also a function of prefault load flow. Setting the relay with a resistive to reactive reach point ratio of 3 was considered to be the best compromise

between resistive coverage and overreach.

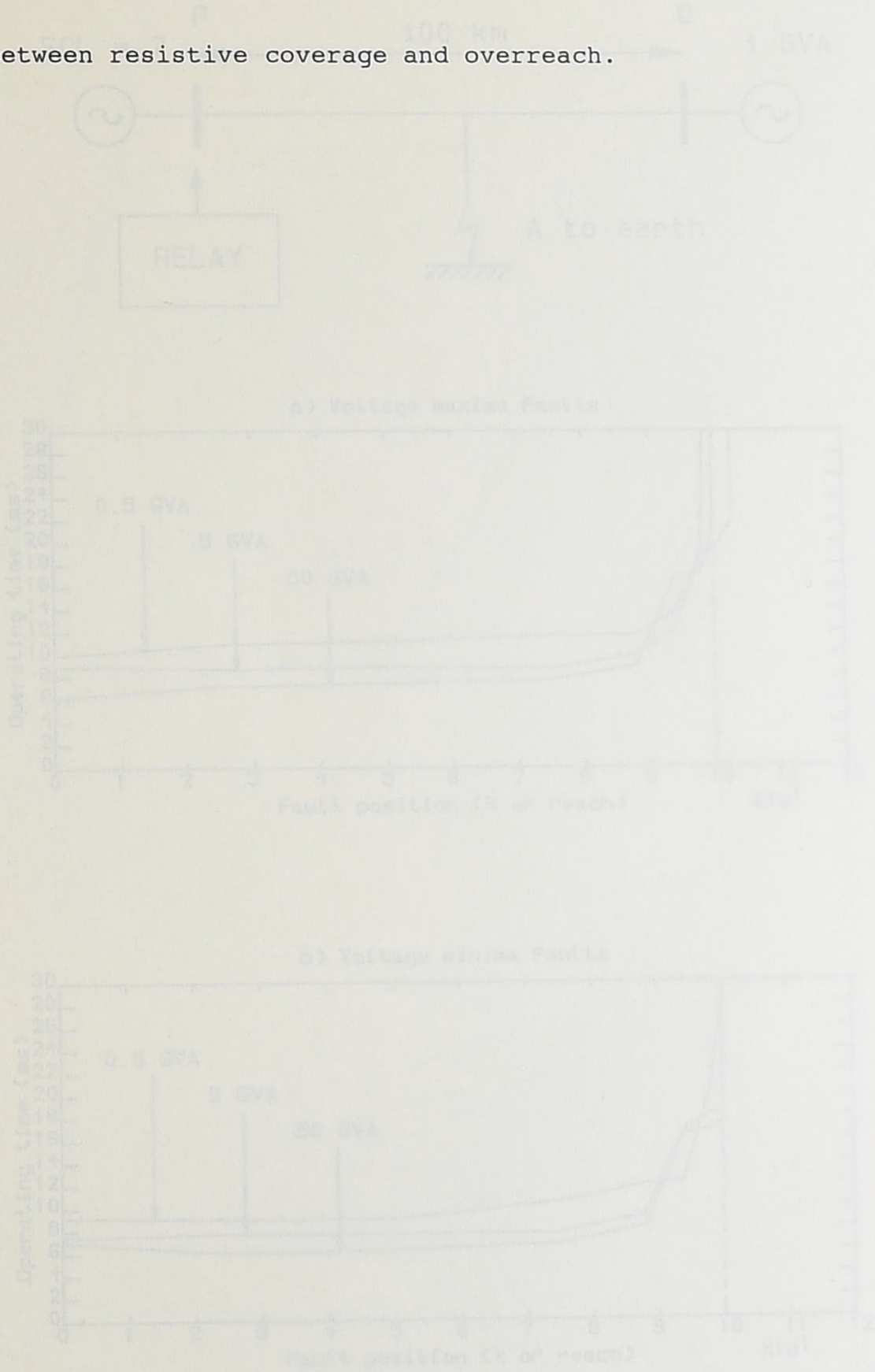


Figure 8.1 Earth fault operating times for 400kV, 100km line cases.

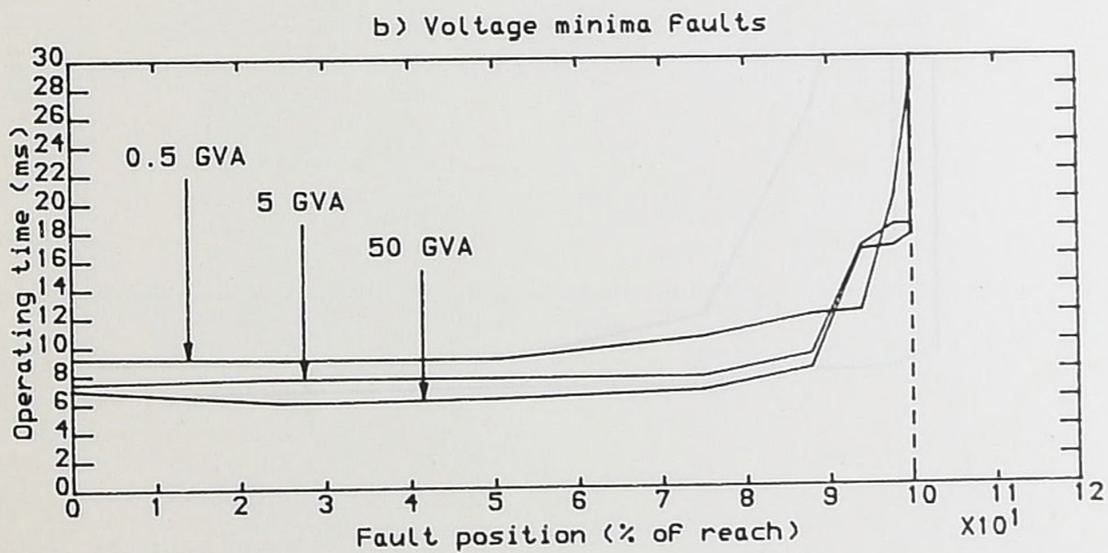
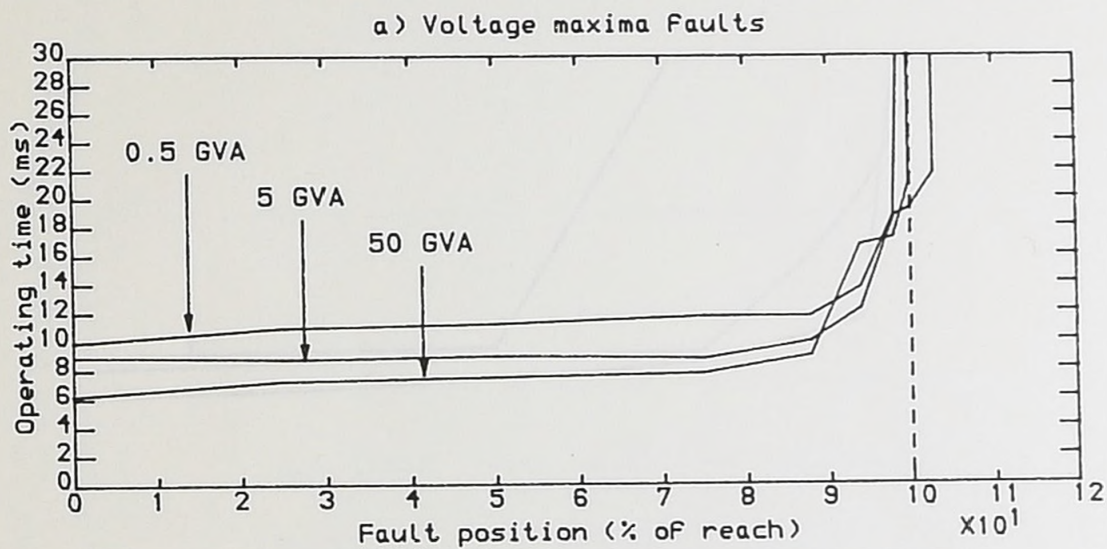
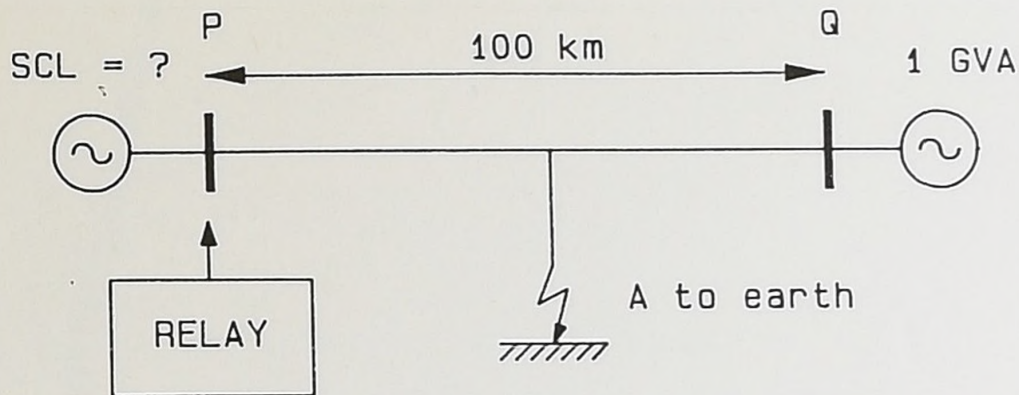


Figure 8.1 Earth fault operating times for 400kV, 100km line cases.

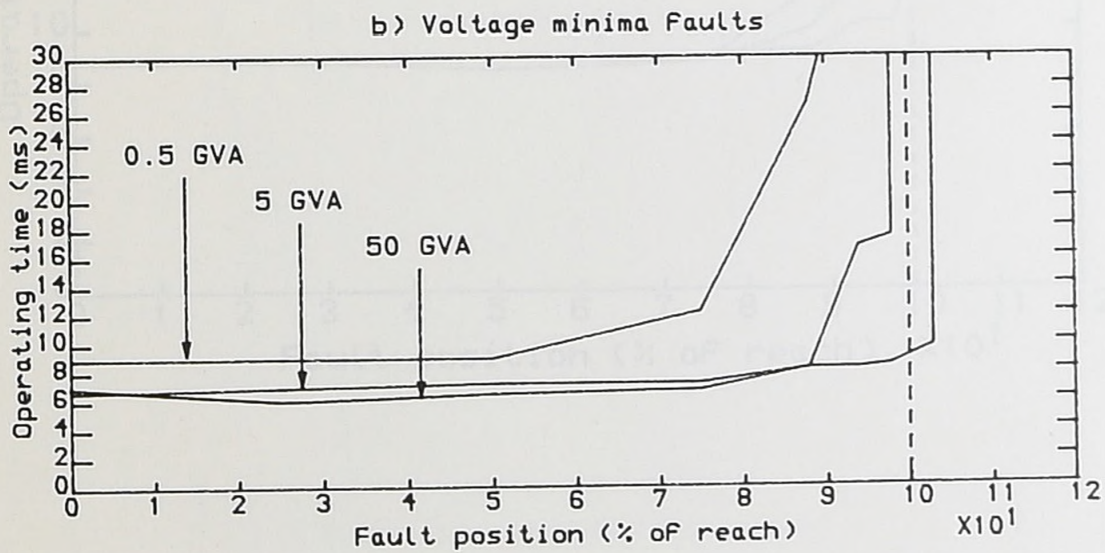
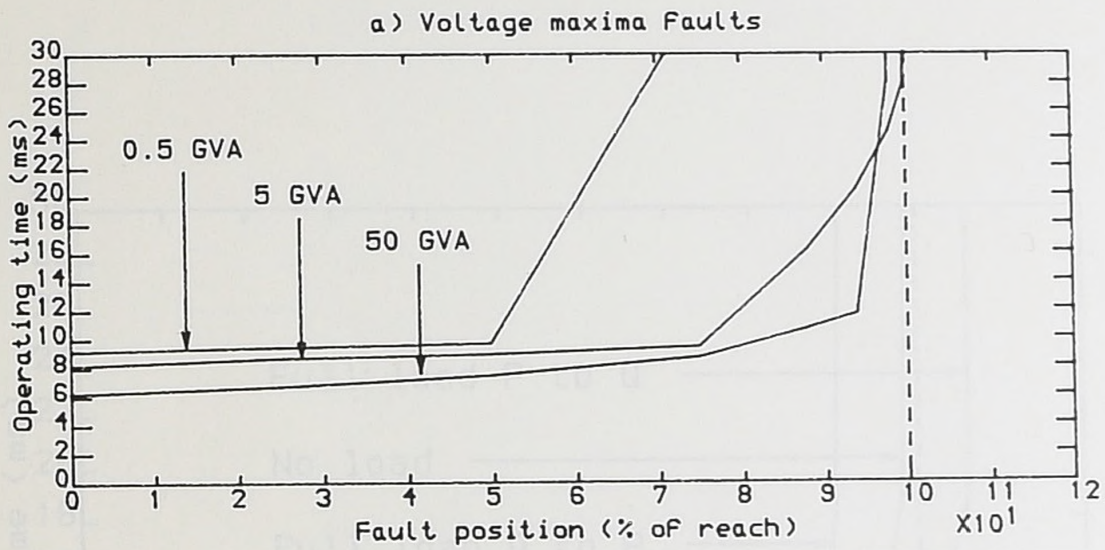
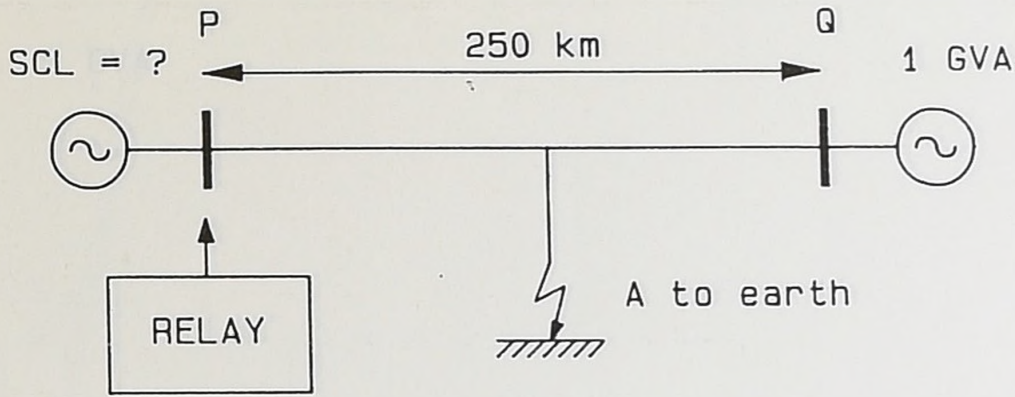


Figure 8.2 Earth fault operating times for 400kV, 250km line cases.

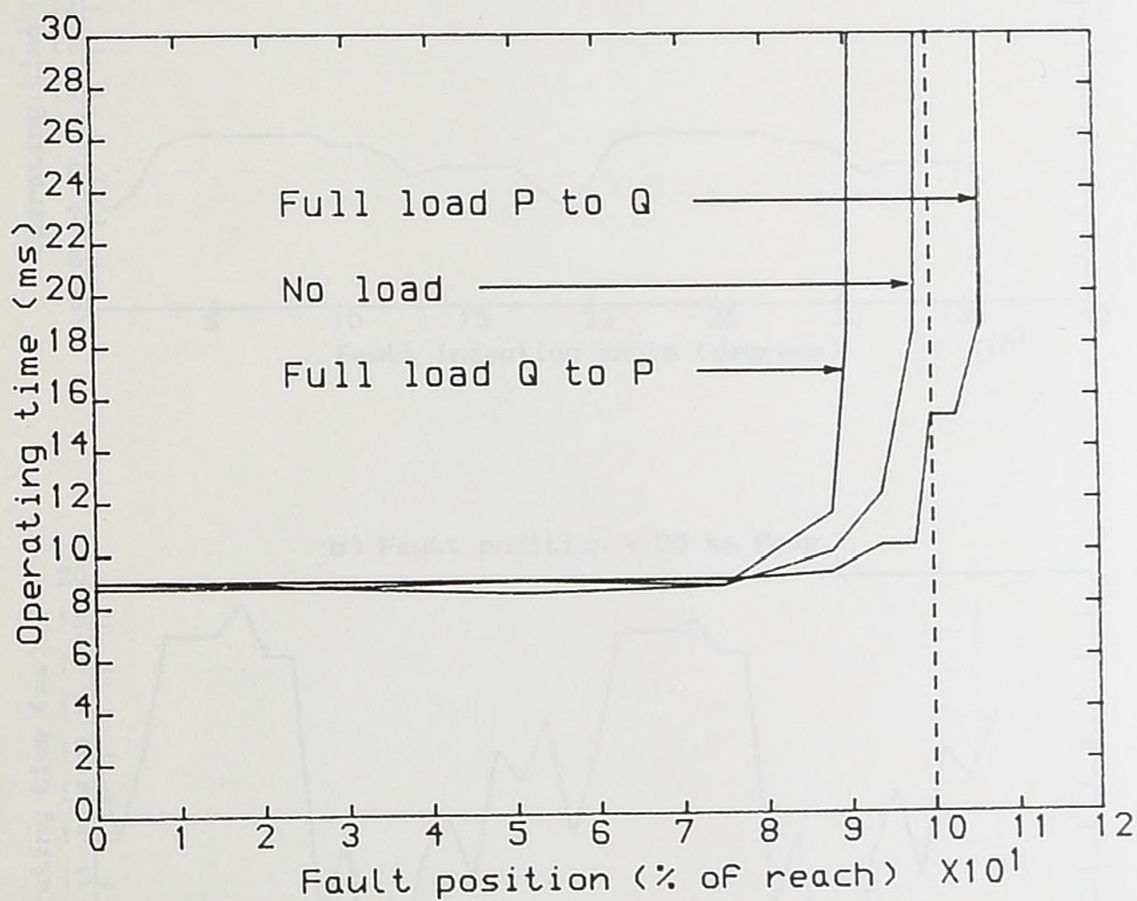
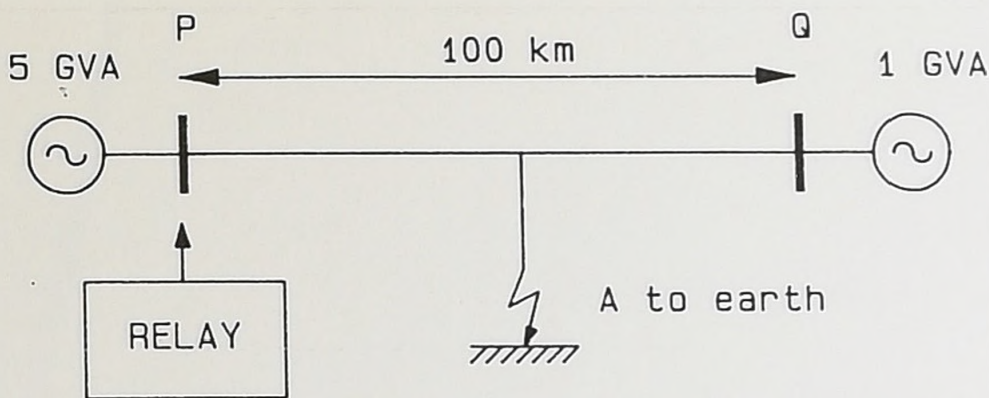


Figure 8.3 Effect of prefault load flow on earth fault operating time for 400kV, 100km line cases.

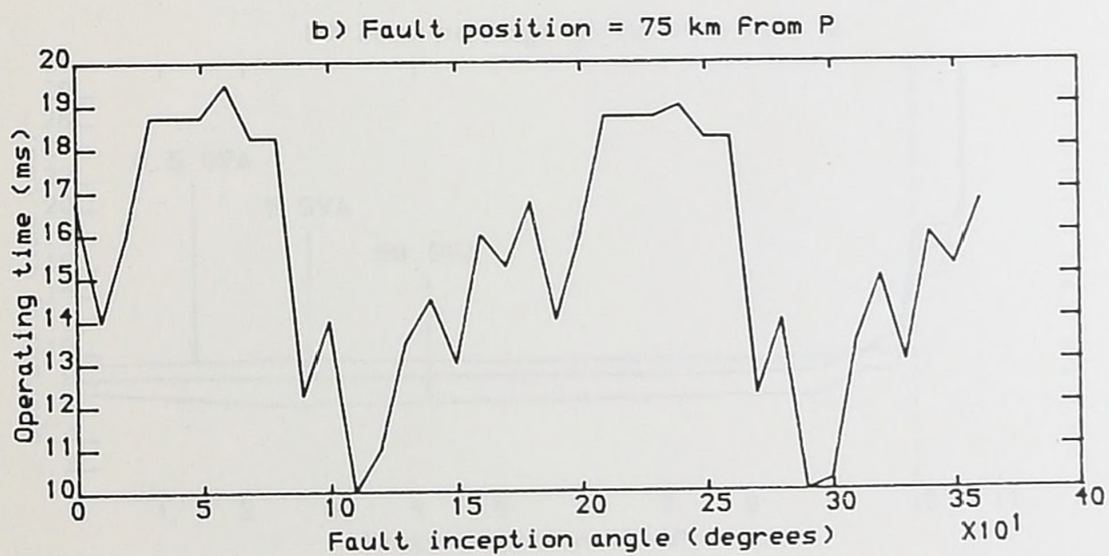
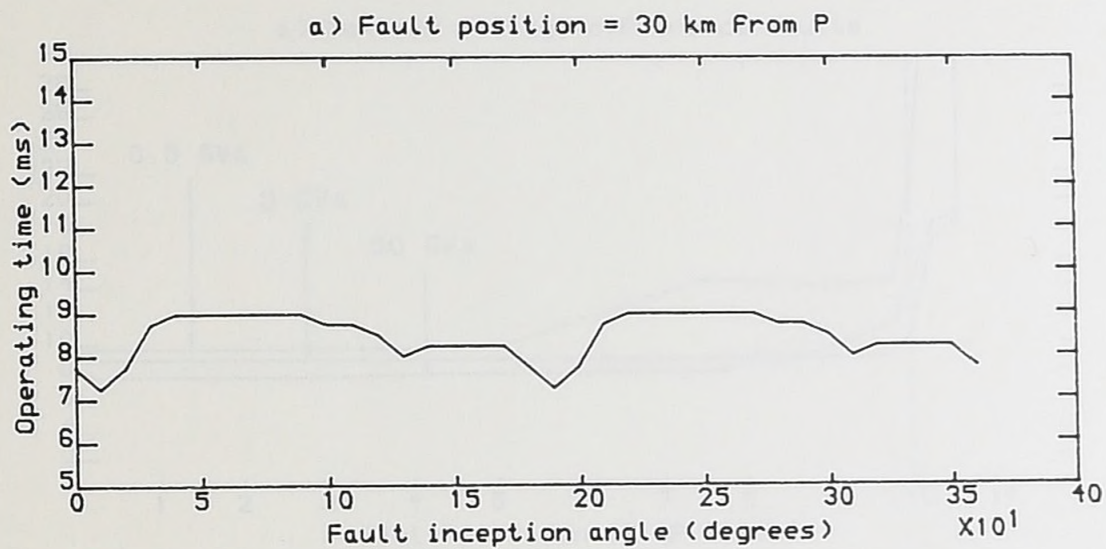
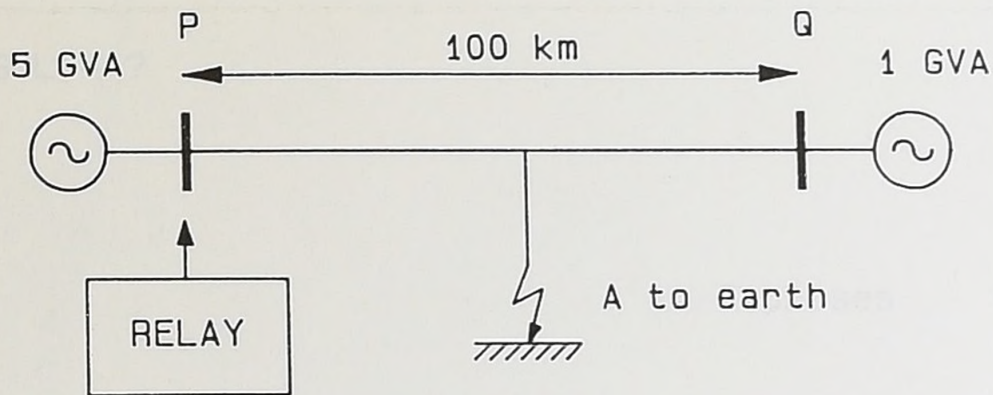


Figure 8.4 Earth fault operating time versus fault inception angle for 400kV, 100km line cases.

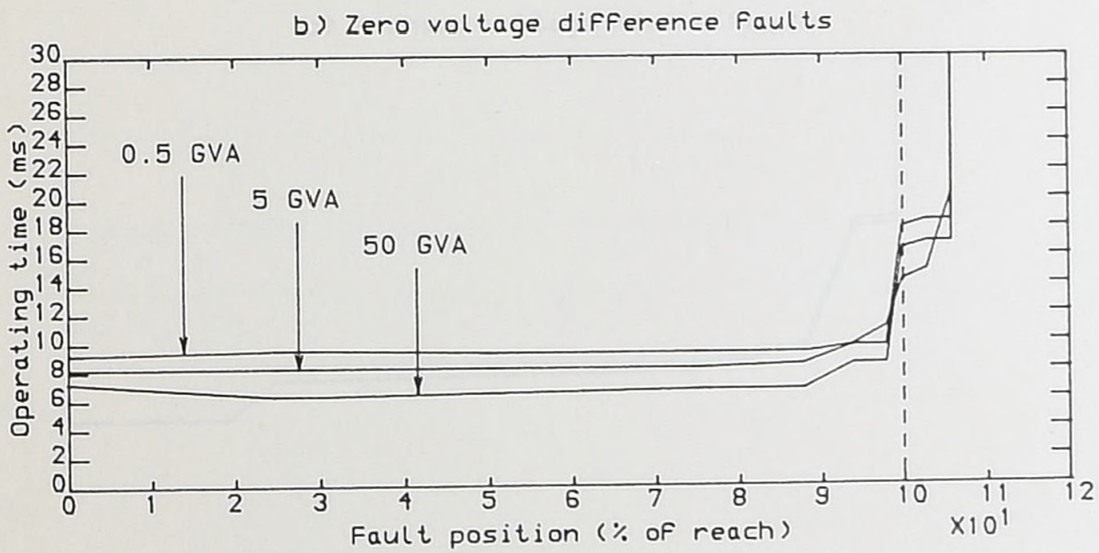
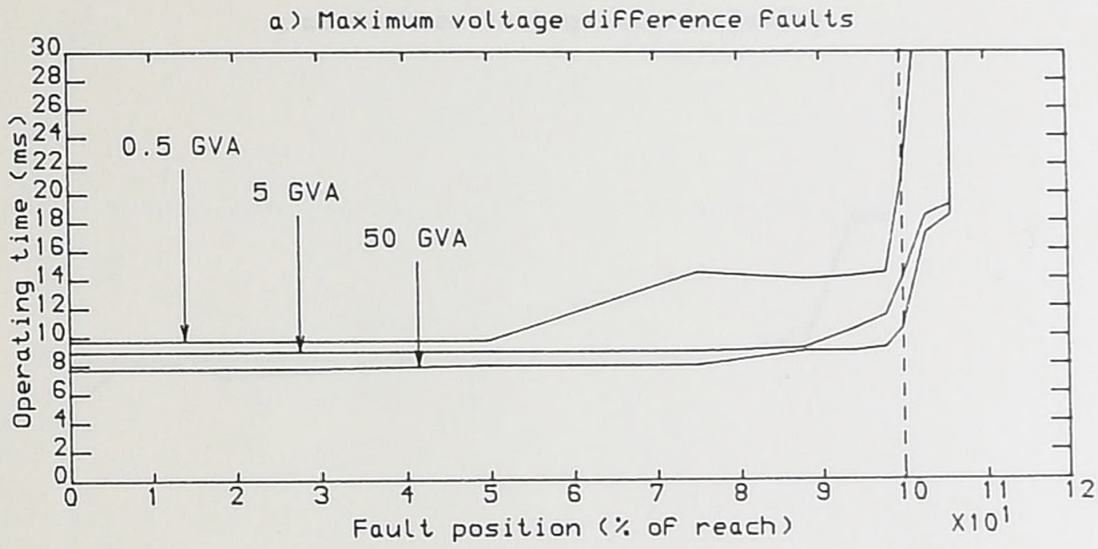
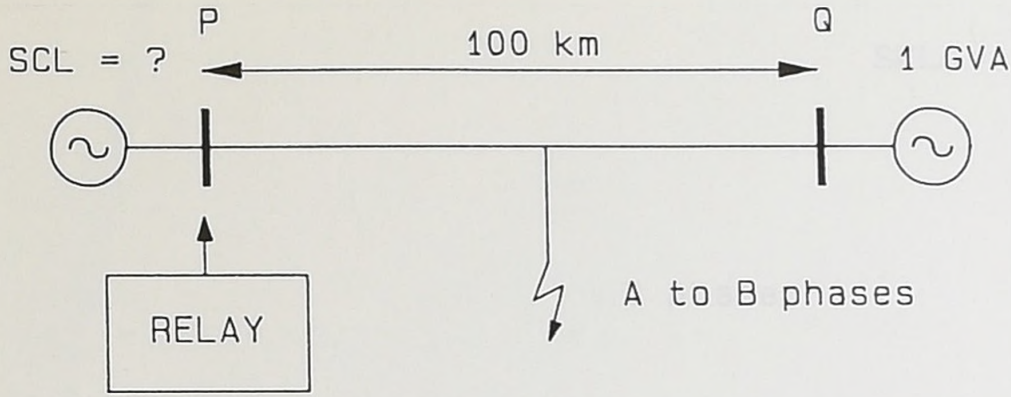


Figure 8.5 Phase fault operating times for 400kV, 100km line cases.

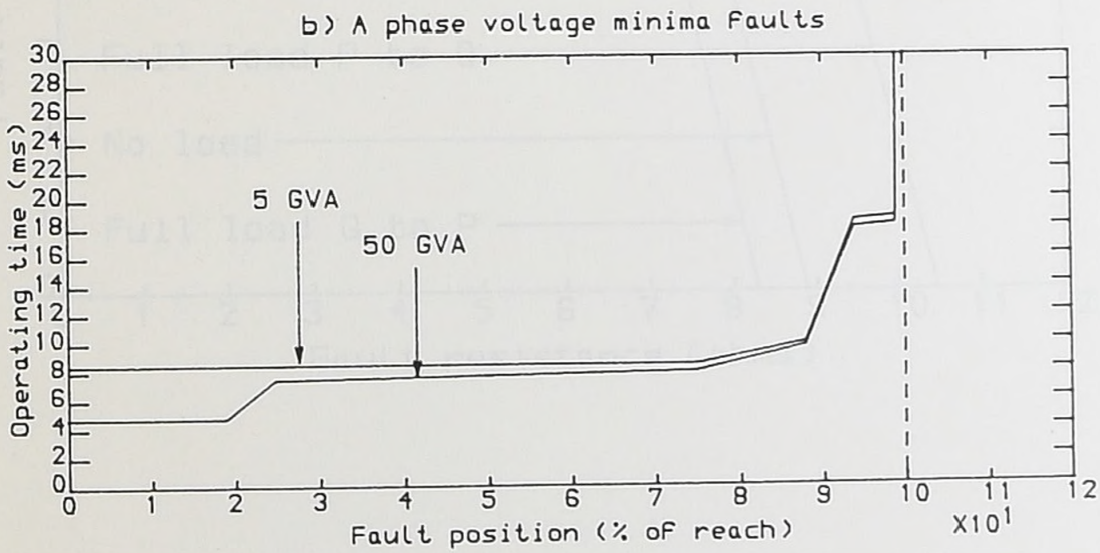
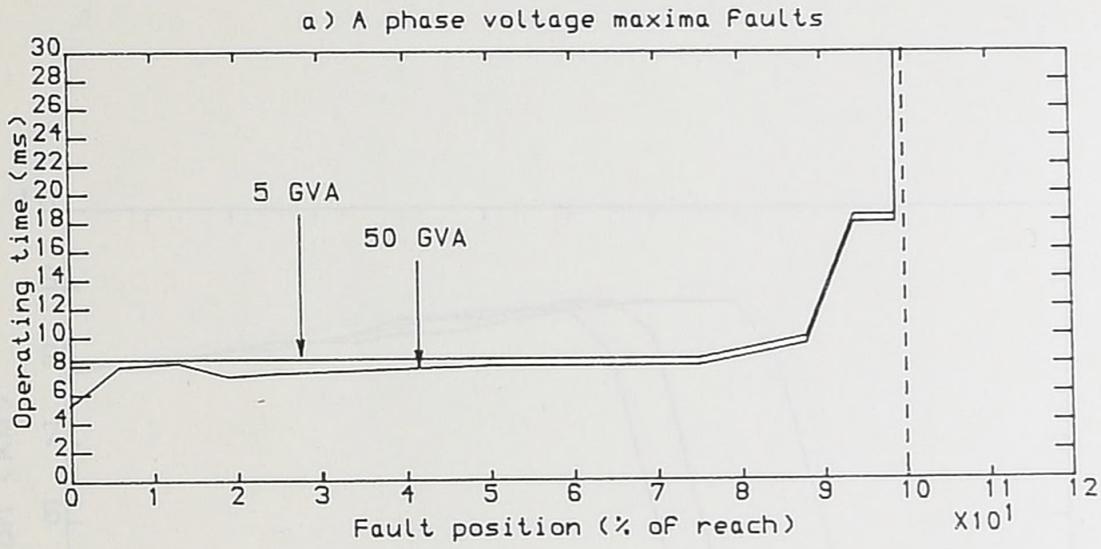
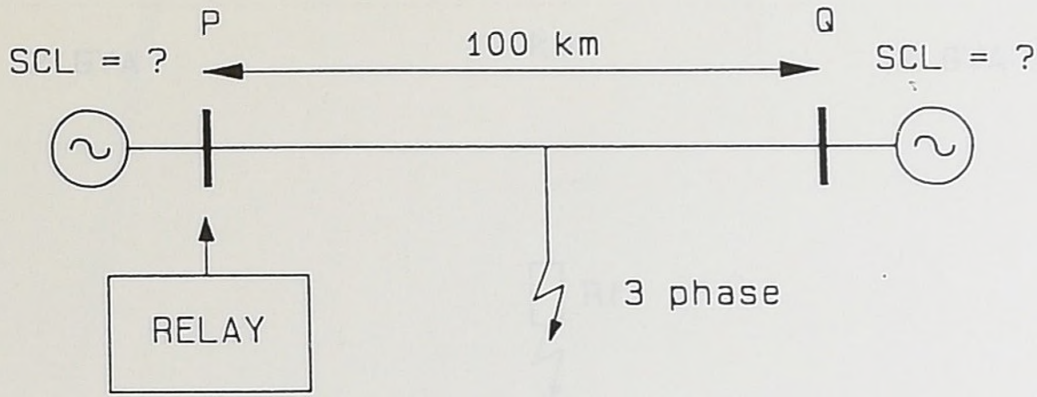


Figure 8.6 Three phase fault operating times for 400kV, 100km line cases.

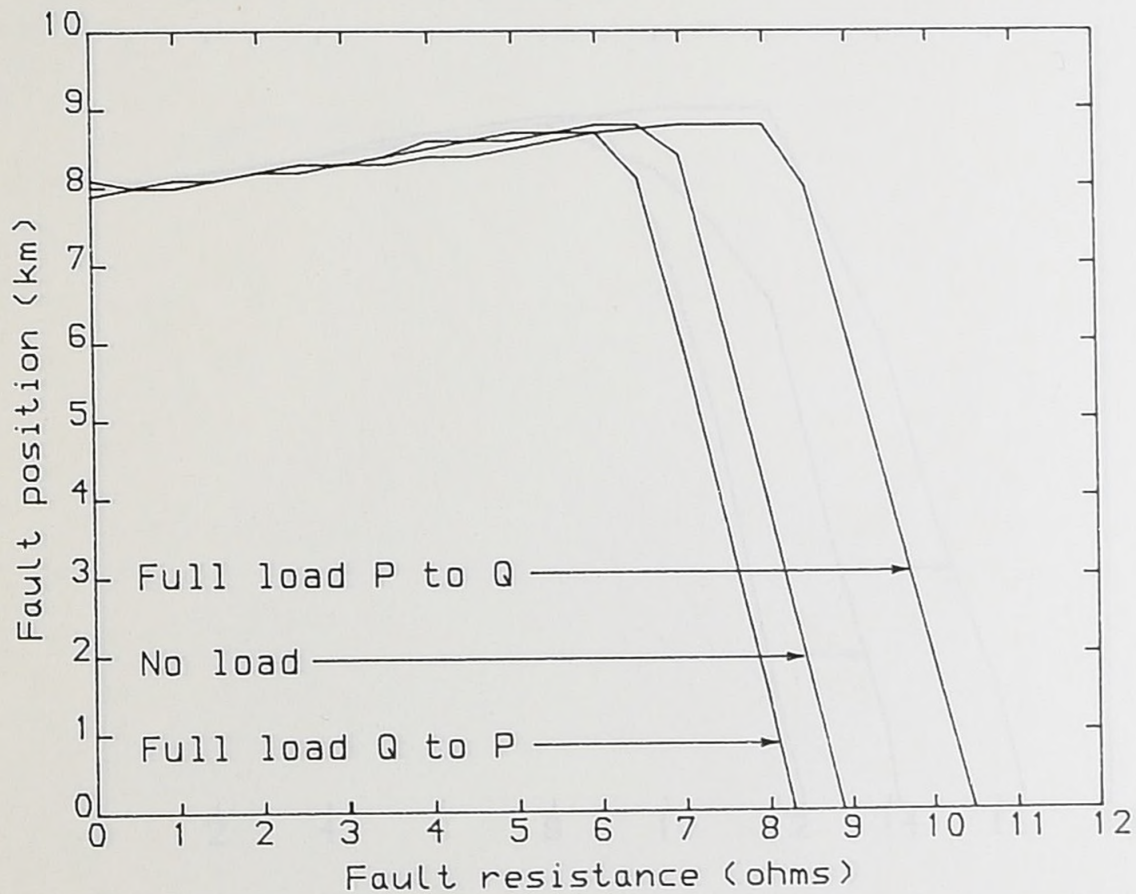
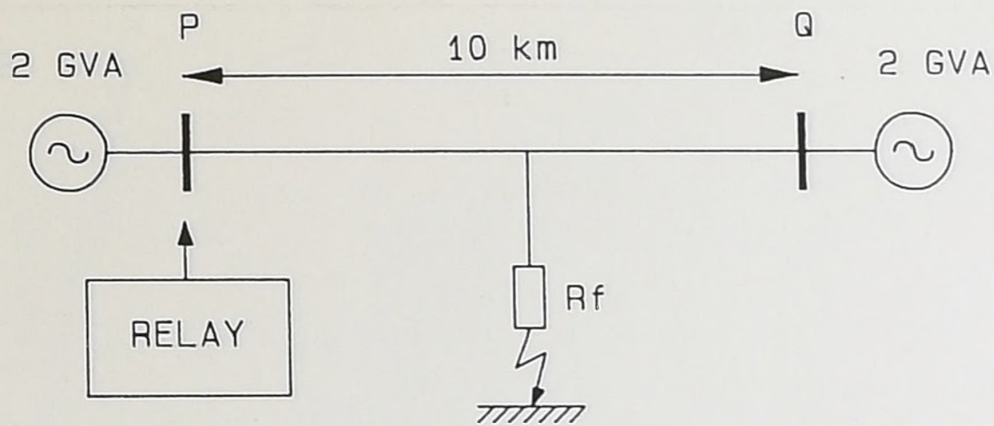


Figure 8.7a)

Resistive earth fault coverage for adaptive relay on 220kV, 10km line (Local SCL= 2GVA, remote SCL= 2GVA).

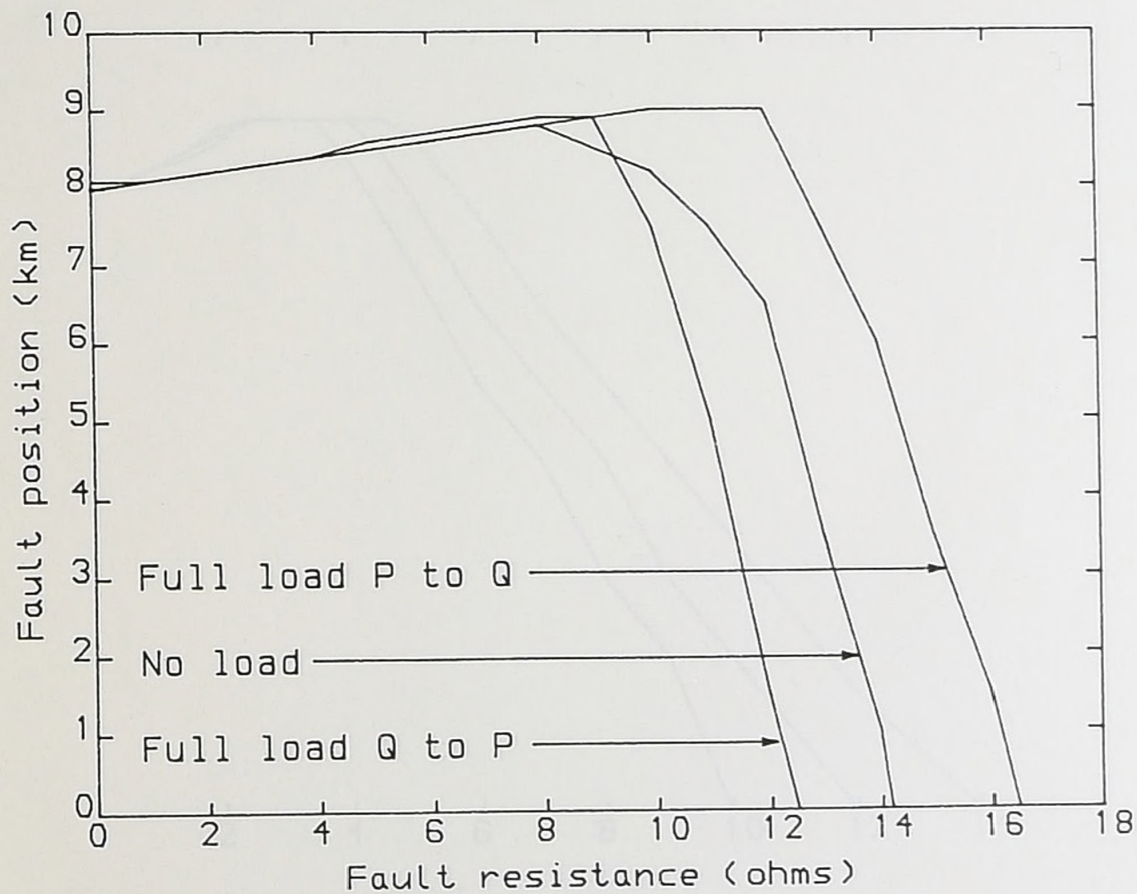
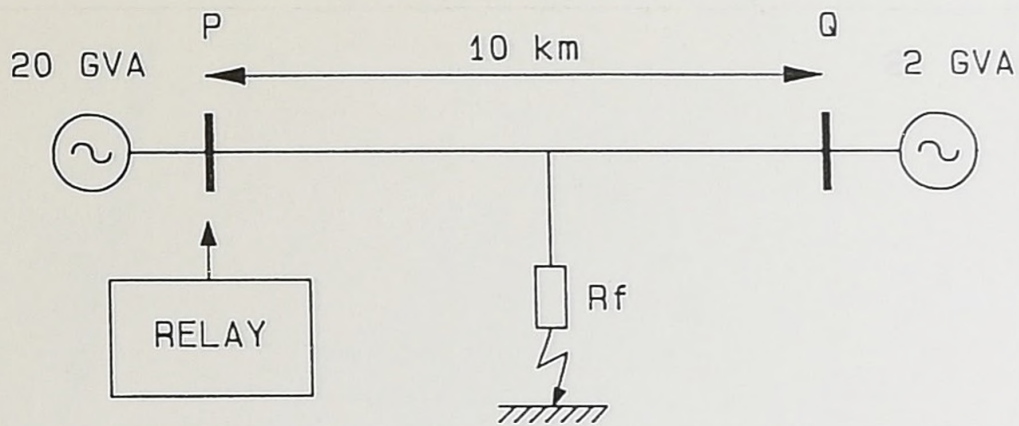


Figure 8.7b) Resistive earth fault coverage for adaptive relay on 220kV, 10km line (Local SCL=20GVA, remote SCL= 2GVA).

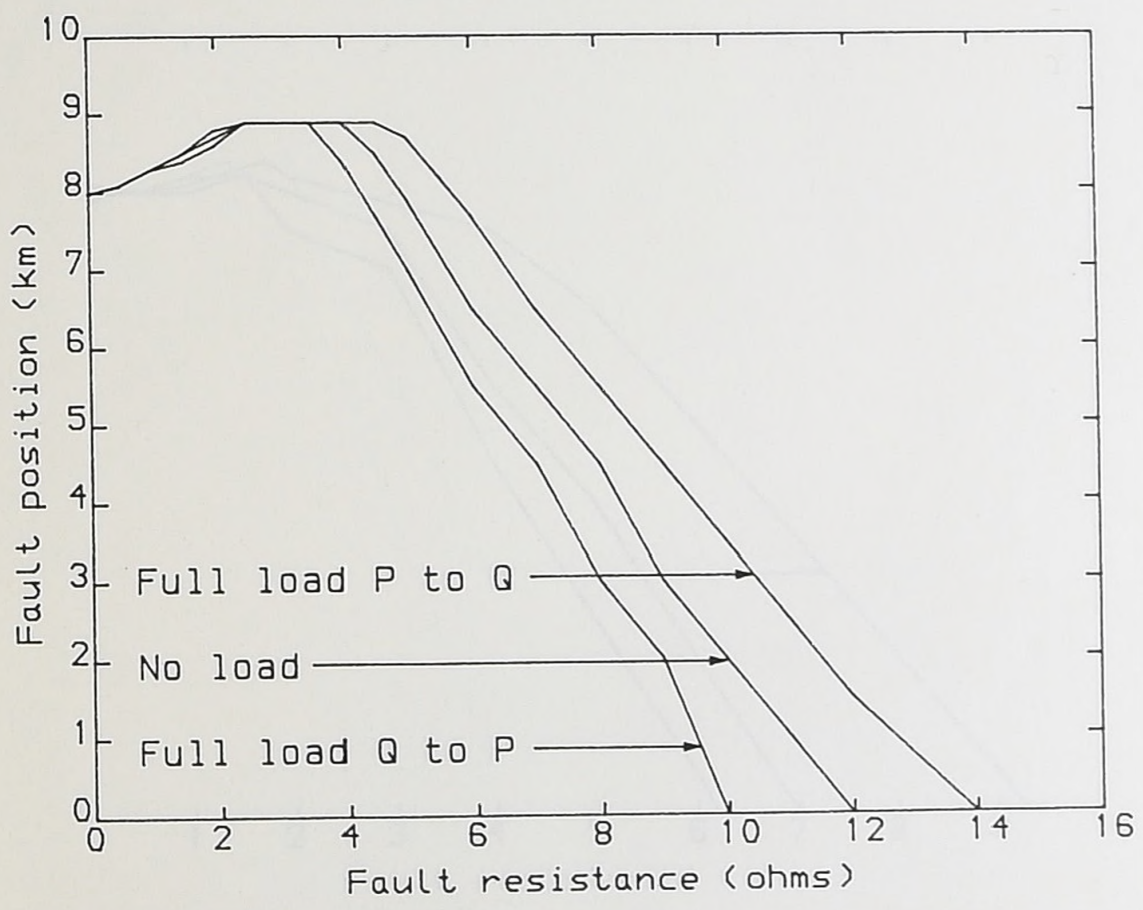
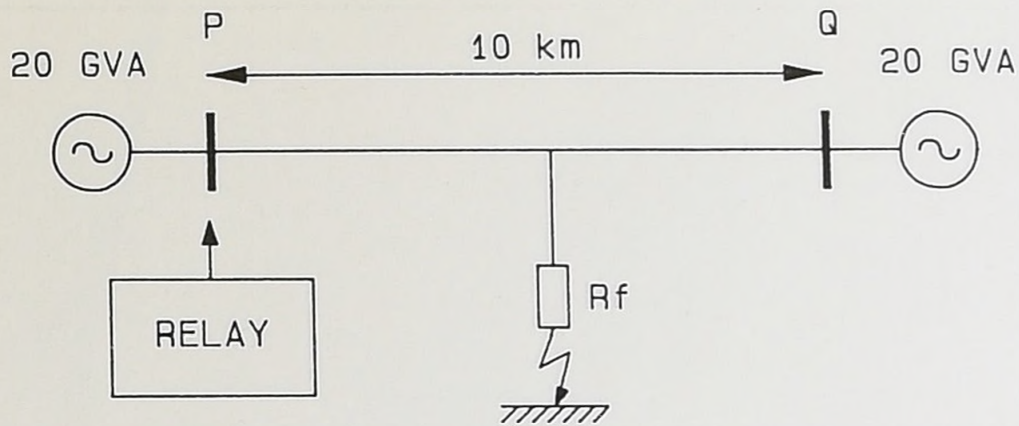


Figure 8.7c) Resistive earth fault coverage for adaptive relay on 220kV, 10km line (Local SCL=20GVA, remote SCL= 20GVA).

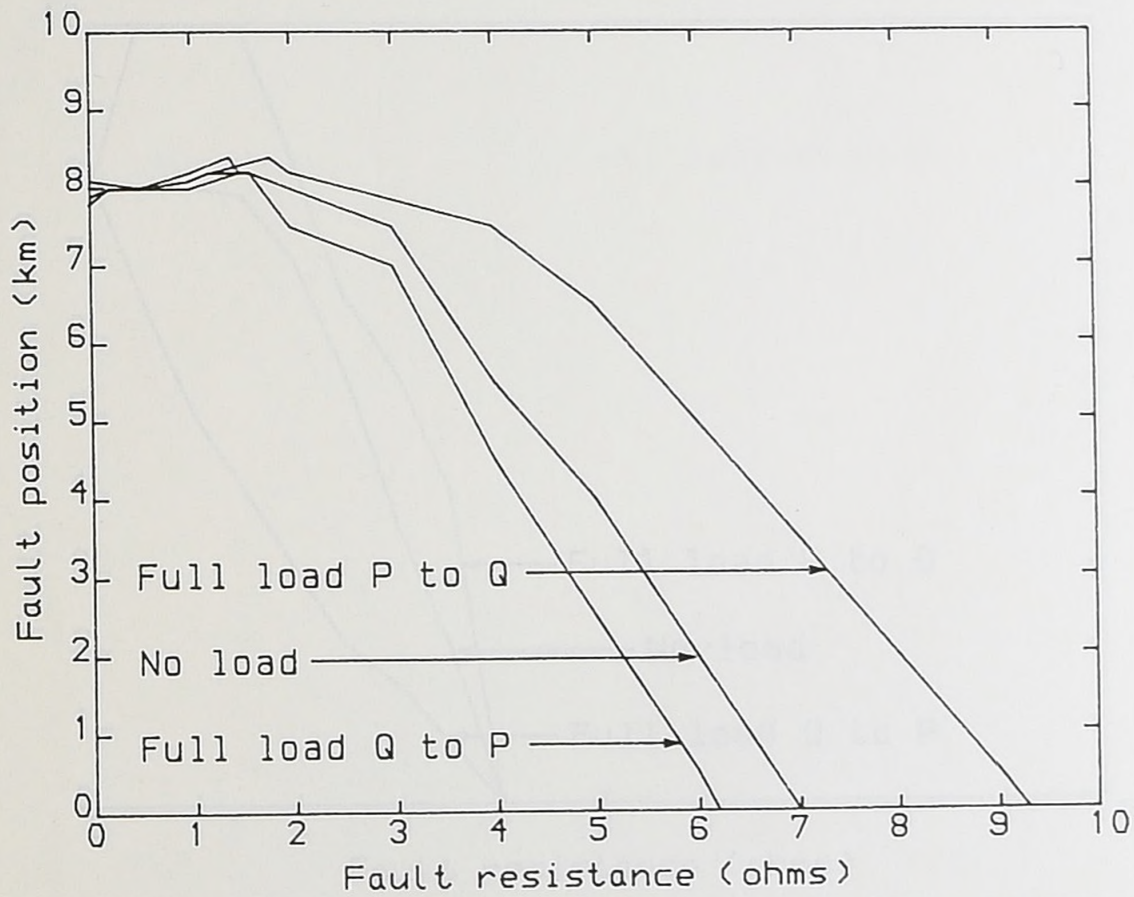
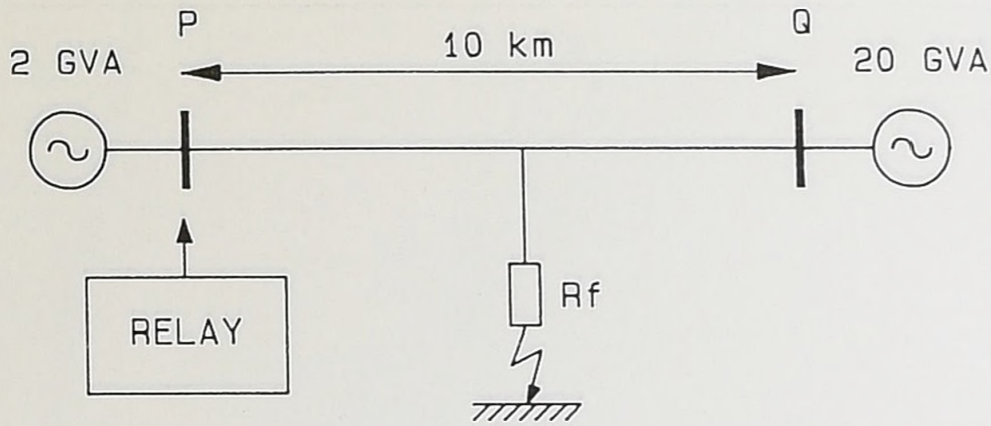


Figure 8.7d) Resistive earth fault coverage for adaptive relay on 220kV, 10km line (Local SCL= 2GVA, remote SCL= 20GVA).

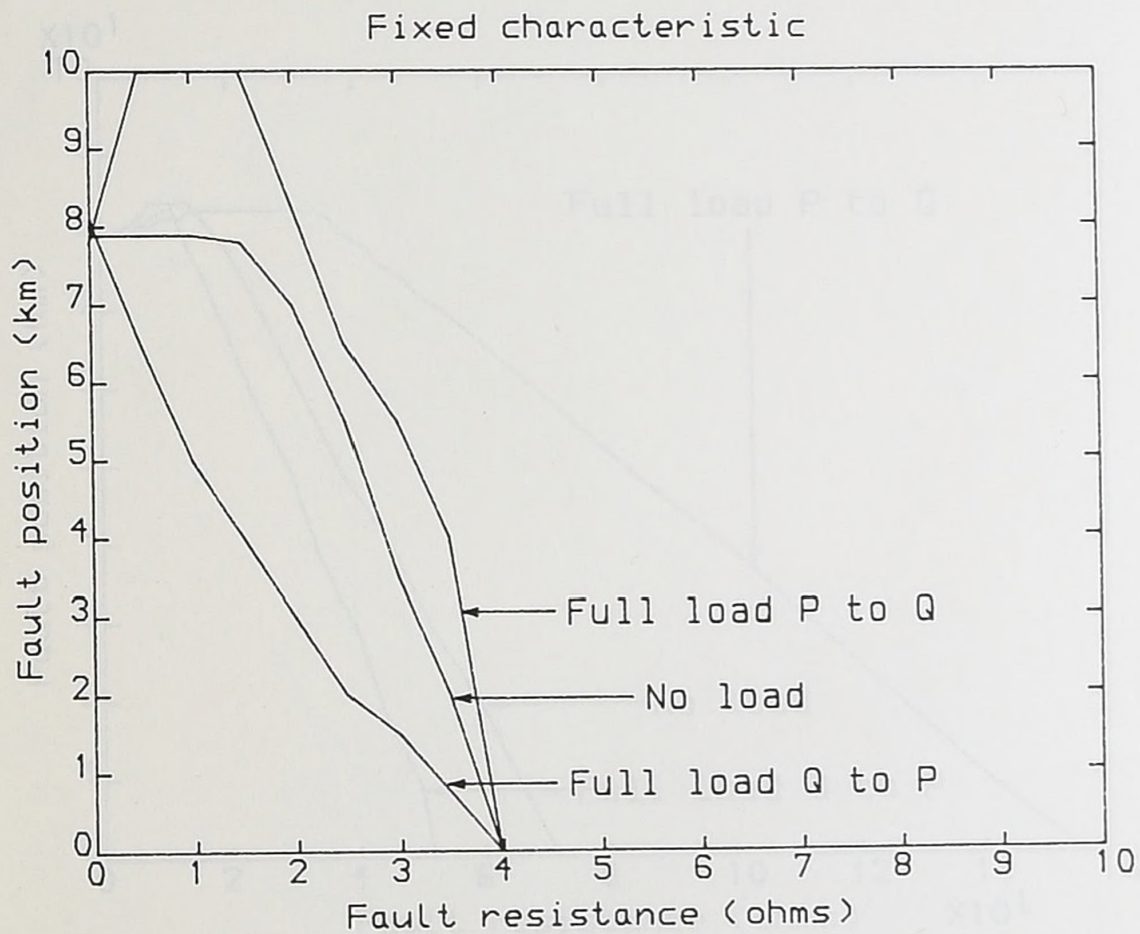
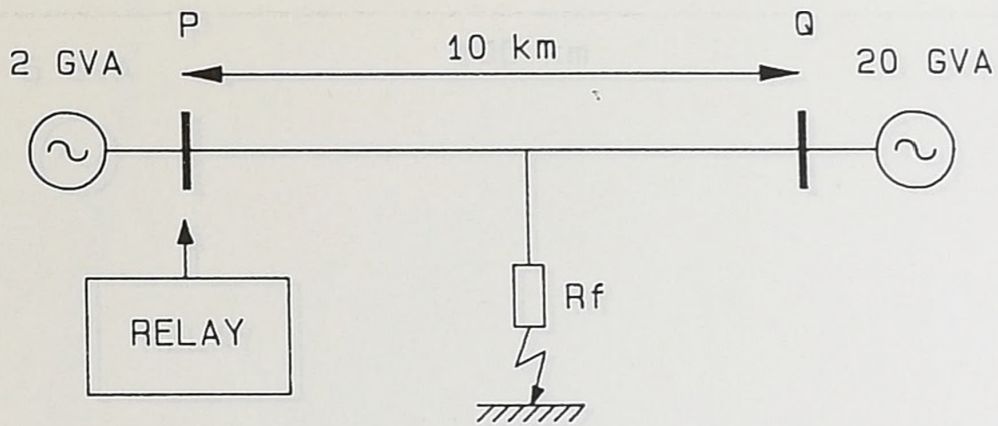


Figure 8.8 Resistive earth fault coverage for fixed characteristic relay on 220kV, 10km line (Local SCL = 2GVA, remote SCL = 20GVA).

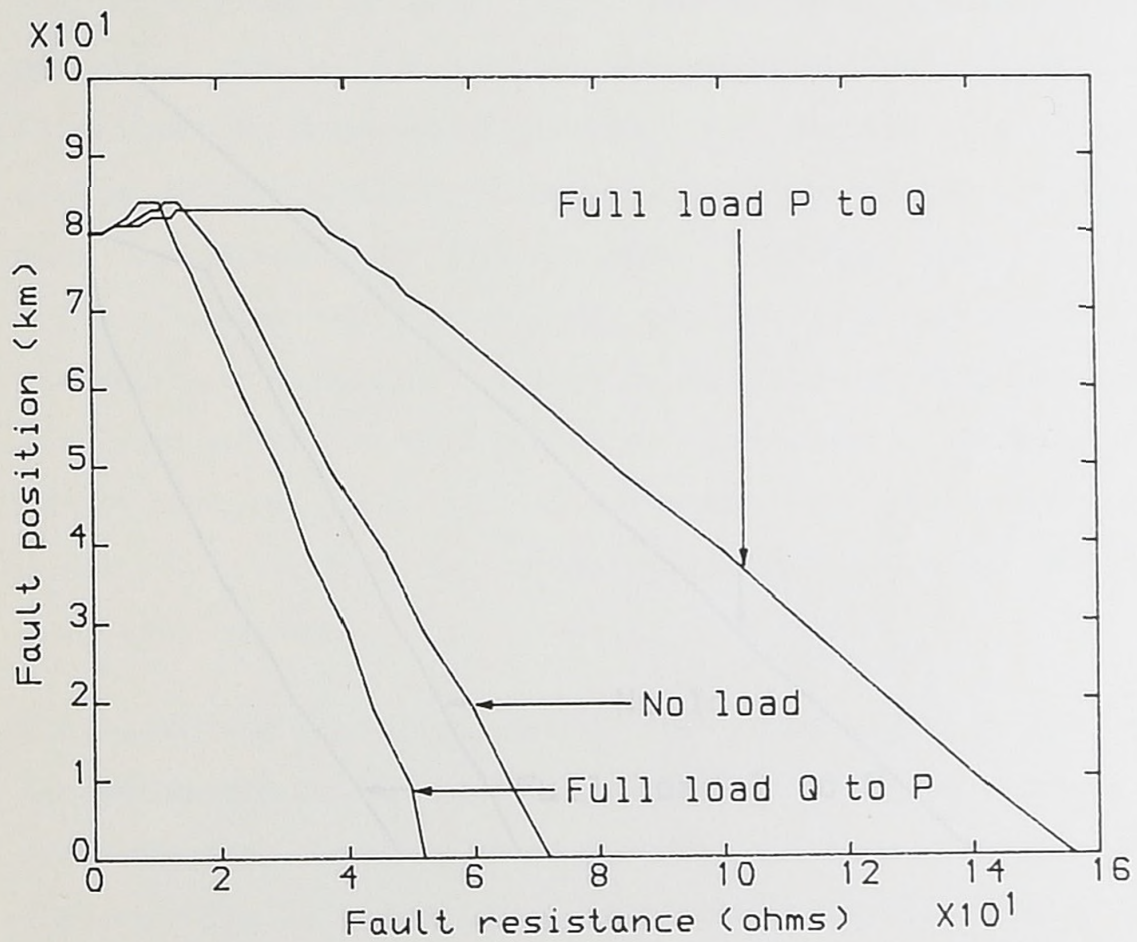
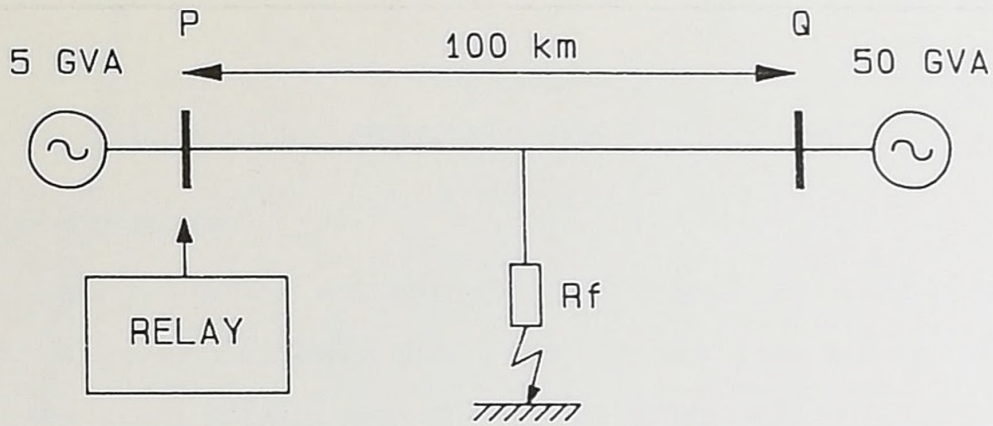


Figure 8.9 Resistive earth fault coverage for adaptive relay on 400kV, 100km line (Local SCL= 5GVA, remote SCL = 50GVA).

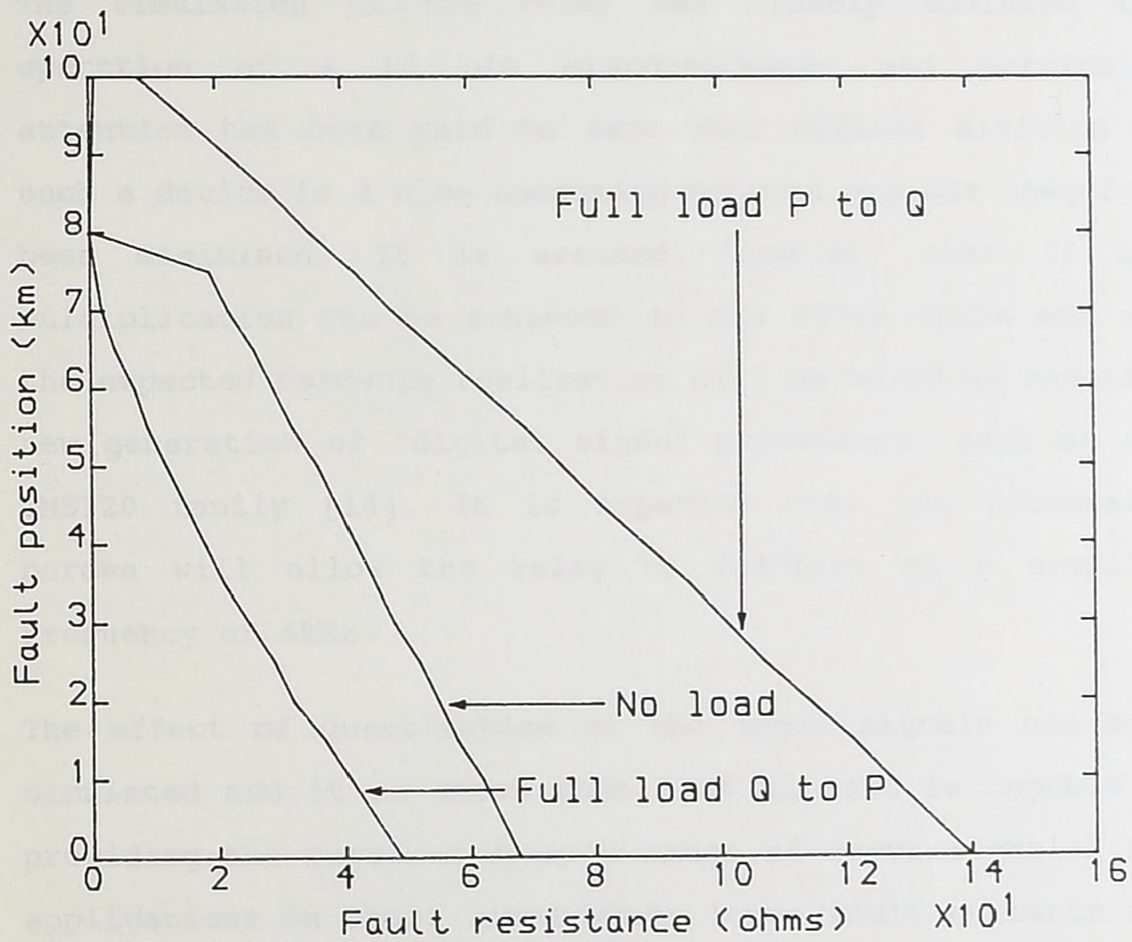
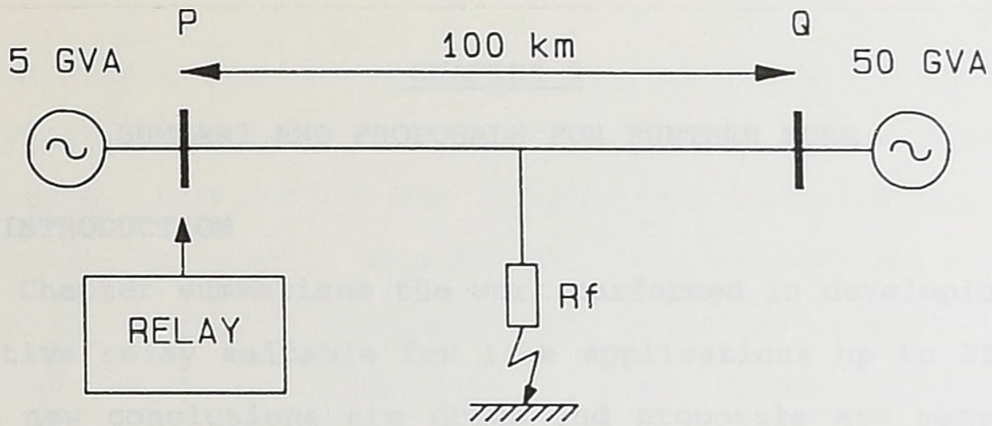


Figure 8.10

Resistive earth fault coverage for fixed characteristic relay on 400kV, 100km line (Local SCL = 5GVA, remote SCL = 50GVA).

## CHAPTER 9

### SUMMARY AND PROPOSALS FOR FURTHER WORK

#### 9.1 INTRODUCTION

This Chapter summarises the work performed in developing an adaptive relay suitable for line applications up to 250km. Some new conclusions are drawn and proposals are made for further work.

#### 9.2 SUMMARY

The simulation of the relay has closely emulated the operation of a 16 bit microprocessor and particular attention has been paid to fact that digital division in such a device is a time consuming process and has therefore been minimised. It is assumed, however, that 16 bit multiplication can be achieved in one clock cycle and so, the expected hardware realisation will be based on one of a new generation of 'digital signal processors' such as the TMS320 family [14]. It is expected that the processing burden will allow the relay to function at a sampling frequency of 4kHz.

The effect of quantisation of the input signals has been simulated and it is shown that a 14 bit ADC is capable of providing the required dynamic range of input signals. For applications on short lines where large fault currents are expected, the relay is provided with one adjustable setting, the current setting multiplier (CSM), which divides the current inputs by a factor of 4.

The algorithm used to convert voltage and current samples into measured resistance and reactances values has been

extensively evaluated from a number of potential options. The algorithm finally selected uses a time spaced solution technique which solves the first order differential line equation. The benefit of this algorithm over others is that it has a relatively flat frequency response close to power system frequency. This affords good relay response in situations where the power system frequency changes and situations where harmonics are present. Results on the relay reach point accuracy showed that the presence of 5% of 7th harmonic resulted, in some situations where there was no prefault load flow, in the relay underreaching although this was seen to be within the relay specifications.

The emphasis on this work has been to develop a distance relay which can be applied to any system without knowledge of the system source impedances or particular reference to the application line length. Indeed, with the exception of the reach point setting impedances, the only other adjustable setting is the CSM mentioned earlier. To develop a relay which is application independent puts a large burden on the relay filtering since, it was seen in Chapter 4, the expected frequency of travelling wave distortion arising from voltage maxima faults is a function of the distance to fault. The problem was overcome by the use of an adaptive filtering arrangement.

The adaptive filtering arrangement is as follows, firstly, a fixed length FIR prefilter having a group delay of 3ms, is used on all the voltage and current inputs. Such a filter is sufficient for situations where the threat to

system stability is at a maximum, and so, the relay exhibits fast operating times for close-up faults and situations where the SCL at the relay busbar is large. For a local SCL of 50GVA, the relay exhibits ultra high speed operation, i.e. operating times of 8ms and less, for all types of faults considered occurring up to the mid point of the line. For other situations, such as mid line faults on long transmission lines where the SCL is smaller, the sole use of the fixed length prefilter would not be sufficient to provide discriminative protection. Hence, and secondly, the fixed prefilter is supplemented by an adaptive filter, or signal averager, which is applied to the measured impedance values shortly after the fault has been detected. The adaptive filter, which has an initially small group delay, increases its group delay from the point of initiation. Thus the frequency domain function of the entire relay filtering process becomes more favourable to removing travelling wave effects as the time after the fault inception increases. The adaptive filter has been carefully designed so that its use does not incur any operating time penalty in situations where the fixed length prefilter alone would be sufficient. For lines with a local SCL of 5GVA the relay exhibits very high speed operation with operating times being less than, or equal to, 9ms for all types of fault occurring up to the mid line point.

The prefilter frequency response has a zero at dc thus facilitating the removal of offsets induced on either the voltage or current signals. The removal of voltage offsets is particularly relevant in relay applications involving a CVT since distortion of the measured impedance can arise.

Various relay applications using a distributed parameter primary system simulation, all of which incorporated a CVT simulation on the voltage channels, showed that no adverse relay behaviour occurred.

In order to solve the first order differential line equation, it is necessary to form a derivative of the current signal. Various equations were evaluated to this end, and, the equation chosen was shown to have the properties of good frequency responses and good resolution of small amplitude signals.

In common with some commercially available relays, the relay has a quadrilateral characteristic. The occurrence of a single impedance value falling within the characteristic was shown not to be a reliable situation to flag a fault and so, a counting strategy was proposed and implemented. Results for various types of fault showed that, whilst the reach point accuracy was good, the counting strategy had the effect of increasing the operating times for faults lying close to the reach point. This effect is not detrimental to the overall performance if it is assumed that each line is protected by two relays, one at each end; for this situation the important feature is the operating time up to the mid point of the line. Results showed that the relay operating time was fairly constant over 75% of the reach (60% of the line length) in all except very weak local source situations.

One aspect of the initial relay implementation which was observed not to promote good reach point accuracy, was the effect that the fault inception angle could have on the

trajectories of the measured impedance. It was shown that specific conditions of prefault load flow and fault inception angle resulted in the measured impedance proceeding through the relay characteristic and causing a relay trip, although the fault was out of zone. To prevent this condition from occurring, a technique of adapting the counter increment to reflect the certainty of the impedance measurement was developed. This technique was shown to completely eliminate overreaching due to fault inception angle variations.

To compensate the earth elements for changes in prefault load flows, a standard residual compensation technique was employed. It was shown that there were errors associated with this technique since the ideal residual compensation factor is a complex value and not entirely scalar, as used for this work. However, for overhead line applications, the use of a scalar residual compensation factor was shown to involve an error of only  $-1.2\%$  in the reactance measurement. When the relay was tested on an accurate simulation of a non-ideally transposed line, reach point accuracy was seen to be a function of prefault load flow. However, it was concluded that the residual compensation factor only played a small part in this error.

To prevent relay operation for faults that are clear of ground, the earth elements are restrained in the absence of residual current. This was achieved by forming a D term based on residual current quantities and comparing this term against a threshold value. It was shown that no operating time penalty resulted from this form of

restraint.

The phase elements were formed by taking the basic earth element structure and using the difference in voltages and difference in currents as the input measurands. It is possible to set the phase element characteristics independent of the earth elements. The phase elements are restrained from operating in any situation, but particularly power swings, where there is no perceived imbalance in the primary system. This restraint is based on the phase element D values.

The phase elements are also used for the detection of three-phase faults. A balanced three-phase fault does not lead to any imbalance in the primary system, and so, the relay detects such faults by checking if all three phase elements have, simultaneously, picked up.

To ensure that the relay maintains correct directionality during close-up faults, a reactance is formed based up on the postfault current and the prefault voltage. This reactance, referred to as the directional reactance, indicates the direction of the fault if the primary system voltage collapses. Examples were shown of relay operation for close-up faults and it was seen that the relay behaved correctly for both forward and reverse faults.

If the SCL on the relay busbar is high, it is possible that close-up faults may result in the current signal being clipped and, it was shown that this led to a detrimental effect on the relay operation time. It was also shown that current clipping could only ever occur for situations where

the relay is expected to operate. Thus, a technique was developed whereby current clipping is continually checked and, if it is found that clipping is occurring to the extent that the operating time will be affected, then the relay is tripped immediately. Results for three-phase faults that caused current clipping showed that the relay was capable of ultra high speed operation; relay operation times were typically 4.5ms. The technique of tripping for current clipping situations is effectively an overcurrent protection function.

It was shown in Chapter 6 that resistive earth faults result in the relay measuring an impedance value which does not accurately reflect the distance to the fault. Results showed that a fixed characteristic relay would grossly overreach for resistive faults occurring on a line with pre-fault exporting load flow and a SCL greater at the remote end than the local end. In order to prevent the relay overreaching for these situations, and, to generally improve the maximum fault resistance for which the relay will operate, a method of adapting the relay characteristic to suit the prospective fault condition was sought. This was achieved by swivelling the relay characteristic about its intersection with the solid fault impedance locus. Three methods of estimating the ideal swivelling angle were investigated and it was shown that the best method was to calculate the angle according to the argument of the residual current divided by the compensated line current. This method has the advantage of simple implementation. In applying this method to the fault evaluation process, the approach taken was to convert the measured impedance to a

value, set according to the measured resistance and calculated swivelling angle, that could then be used with the fixed characteristic. This approach was found to be simpler to implement than actually swivelling the boundary edges of the characteristic.

Results for a 220kV, 10km line application showed that the adaptive relay does not overreach, and gives almost twice the fault resistance coverage of a fixed characteristic relay, in the former situation of a strong remote source and a weak local one. For other situations it was observed that some overreaching occurred if the SCL of the local source was equal to, or greater than, the SCL of the remote source. The extent of the overreaching for these situations was noted to be a function of the resistive reach point setting. The best compromise between fault resistance coverage and overreach was seen to be when the resistive to reactive reach ratio was set to 3. For all the fault situations considered, there was never any operation by any element except the faulted earth element. Thus, it may be concluded that the method of adaptation does not cause the sound phase elements to see the fault.

An application study for a 400kV, 100km line showed, again, that overreaching was prevented under strong remote source situations and, the fault resistance coverage was improved, although not to the same extent as the 220kV, 10km line application.

If a system, part of which a distance relay is protecting, is subject to a power swing or pole slip, there is a possibility that the relay will measure an impedance which

lies within the characteristic. It was shown, for part of a 400kV system, that if the electrical centre of system lies within the relay characteristic then, during the period prior to a pole slip, the impedance measured by the phase elements would pass straight through the characteristic. Since the relay would perceive this situation as a three-phase fault, a technique was developed to enable the relay to differentiate between three-phase faults and power swings. The basis of this technique was to look for the occurrence of the prefilter group delay which will be present for a three-phase fault, but not for a power swing. A rigorous analysis for all expected conditions of three-phase faults showed that the technique proposed was sufficiently sensitive to correctly detect all three-phase faults. Tests on a simulated power swing showed that this technique was capable of blocking relay operation when the measured impedance entered the characteristic. The advantage that this technique brings over conventional methods of power swing blocking is that faults occurring during a power swing will be correctly detected and flagged.

Thus, an adaptive digital distance relay has been accurately simulated using the Fortran programming language. The relay has been tested for a variety of simulated power system fault conditions and has been shown to provide fast and discriminative protection performance. The relay has an adaptive characteristic which promotes good fault resistance coverage and incorporates a novel power swing blocking technique which allows faults to be detected during a power swing.

It is pointed out here, that conference publications arising from the work described in this thesis are included in Appendix 15.

### 9.3 PROPOSALS FOR FURTHER WORK

Further work is recommended in the following areas:

- a) Evaluation of the relay behaviour under earth fault conditions when compensated using a complex residual compensation factor. It is expected that a marginal improvement in reach point accuracy for earth faults will result from this, however, the effect on the fault resistance coverage may be more pronounced.
- b) Improving the fault resistance coverage by enhancing the described adaptation technique by the use of prefault load flow information. It was established that the fault resistive coverage is a function of prefault load flow. In particular, the two situations which result in worst case resistive coverage are prefault no load and full load importing. Since a fixed characteristic relay will not overreach at all in these situations, it may be possible to extend the fault resistance coverage, to that of the prefault full load exporting condition, by increasing the swivelling angle further if the prefault load flow is between the no load and full load importing conditions.
- c) Investigating the adaptive relay behaviour when used in a double circuit application. Faults involving dissimilar phases on a double circuit line, the so called cross country fault, can lead to incorrect distance relay operation. Adaptive techniques should be sought to promote discriminative relay operation for this situation. This

work would have particular relevance to the UK system where the use of double circuit lines is widespread.

d) The use of a least mean squares approach to adaptive filtering for distance protection. The adaptive filtering described in this thesis is seen to afford fast and reliable relay operation, however, the possibility exists for further increasing the operating time for faults which do not require extensive filtering of the input measurands. Work has already been carried out on the application of Kalman filtering for distance protection [9], but the use of a LMS adaptive filter [40] gives the potential advantage of being based on an FIR filter implementation, and thus the extent to which prefault information affects postfault decisions is minimised. This work would be timely in that digital signal processing hardware is now becoming available that would have the required processing capacity to perform a LMS algorithm in real time.

Hence,

$$I_{sec} = \frac{110 \cdot 1000}{400 \cdot 10^3} \\ = 0.55$$

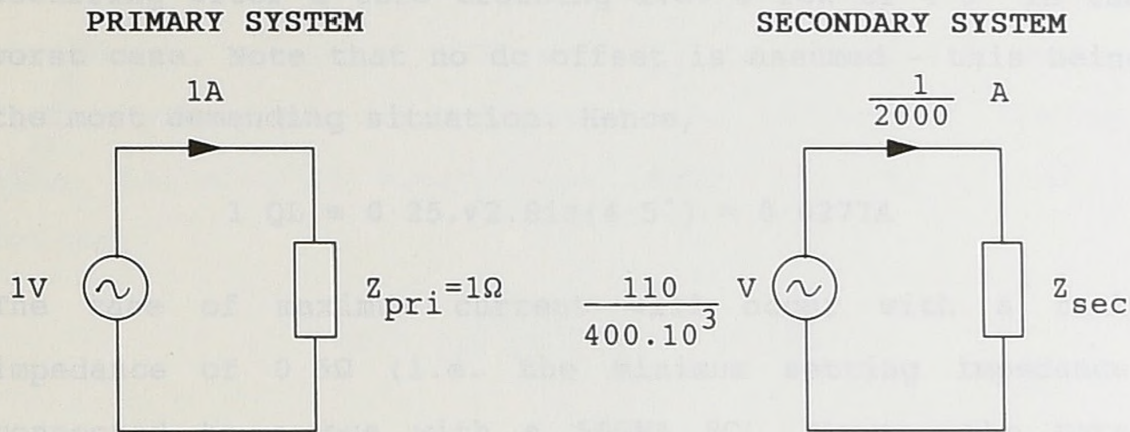
Therefore,

$$I_{sec} = 0.55 \cdot I_{pri}$$

## APPENDIX 1

### Relationship between primary and secondary impedances

Assuming the voltage transformation ratio to be 400kV/110V and the current transformation ratio to be 2000:1 between the primary and secondary systems, the impedance relationship may be derived as follows:



With a primary system voltage of, say, 1V and current of, say, 1A, the corresponding secondary system voltages and currents will be 110/400,000 V and 1/2000 A respectively.

Hence,

$$\begin{aligned} Z_{sec} &= \frac{110 \cdot 2000}{400 \cdot 10^3} \\ &= 0.55 \end{aligned}$$

Therefore,

$$\underline{\underline{Z_{sec} = 0.55 \cdot Z_{pri}}}$$

## APPENDIX 2

### Derivation of the required number of bits of the analogue to digital converter

The minimum current for which the relay is required to operate is, from section 2.1, 0.25 Arms. In order to give correct operation, the ADC must be able to discriminate at least 1 quantisation level (QL) for the first sample occurring after a zero crossing i.e. a POW of  $4.5^\circ$  in the worst case. Note that no dc offset is assumed - this being the most demanding situation. Hence,

$$1 \text{ QL} \equiv 0.25 \cdot \sqrt{2} \cdot \sin(4.5^\circ) = 0.0277 \text{ A}$$

The case of maximum current will occur with a fault impedance of  $0.5 \Omega$  (i.e. the minimum setting impedance) connected to a bus with a 50 GVA SCL. Hence, the total impedance in the fault path,  $Z_t$ , is given by,

$$Z_t = 0.55 \cdot 50 \cdot 10^9 / [400 \cdot 10^3]^2 + 0.5 = 0.6719 \Omega_{\text{sec}}$$

Thus, assuming a secondary line voltage of 110V, the peak value of the relay current,  $I_{\text{max}}$ , assuming it to be fully offset, is given by,

$$I_{\text{max}} = \frac{2 \cdot \sqrt{2} \cdot 110}{\sqrt{3}} \cdot \frac{1}{0.6719} \approx 268 \text{ A}$$

Hence, the number of bits,  $N$ , needed to digitise  $I_{\text{max}}$  is,

$$N = \log_2[268/0.0278] = 13.235$$

Thus, for a real device, the value of  $N$  would be 14. However, bearing in mind that the input signals are bipolar, the total number of bits required of the ADC will be 15.

### APPENDIX 3

#### Derivation of scaling factors for relay voltage and current transducers

**Voltage:** The relay input voltage,  $v_{in}$ , and the relay signal voltage,  $v_{sig}^V$ , are related by the following expression:

$$v_{sig}^V = K_V \cdot v_{in}$$

where  $K_V$  is the dimensionless scaling factor of the voltage transducer,  $v_{sig}^V$  is  $\pm 10V$  and  $v_{in}$  is the phase voltage corresponding to the secondary line voltage of 110Vrms. Thus, assuming an overvoltage factor of 1.8, it can be written,

$$K_V = \frac{10 \cdot \sqrt{3}}{110 \cdot \sqrt{2} \cdot 1.8} = 0.06186$$

**Current:** The relay input current,  $i_{in}$ , is converted by the current transducer to the relay signal voltage,  $v_{sig}^i$ .  $i_{in}$  and  $v_{sig}^i$  are similarly related by a factor,  $K_i$ , which has the units of ohms,

$$v_{sig}^i = K_i \cdot i_{in}$$

Since the magnitudes of relay input voltage and current are equalised, at the relay signal voltage level, for a 4 $\Omega$  fault, it follows that the peak input current value must correspond to the peak signal voltage under this condition. Hence,

$$K_i = \frac{10}{1.8} \cdot \frac{4 \cdot \sqrt{3}}{110 \cdot \sqrt{2}} = 0.2474$$

## APPENDIX 4

### Digital simulation of the anti-aliasing filter

The circuit of the anti-aliasing (AA) filter, shown in figure 2.3, consists of two R-C differentiator circuits separated by a unity gain buffer. Appendix 5 describes how a single R-C differentiator may be simulated using the recursive formula,

$$y(n) = \exp\{-T/CR\}.y(n-1) + (1/CR).x(n)$$

where T is the digital time step, y denotes the output and x the input. Thus, assuming the buffer to be ideal, the AA filter digital impulse response (IR) may be obtained by cascading two R-C filter simulations and observing the output when an impulse is fed in. An impulse is the input sequence of H(k) where H=1 for k=1 and H=0 otherwise.

The digital IR obtained from this method is shown in figure A4.1. In theory an analogue circuit has an infinite IR. However, by reference to figure A4.1, it can be seen that the IR tends to zero after 1ms. Thus the AA filter may be simulated using a finite impulse response structure and an IR truncated after 20 steps.

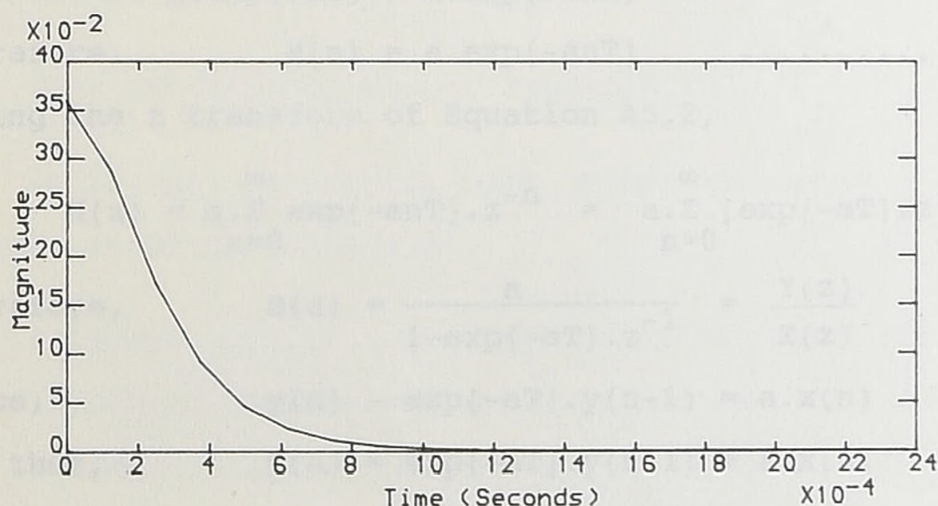
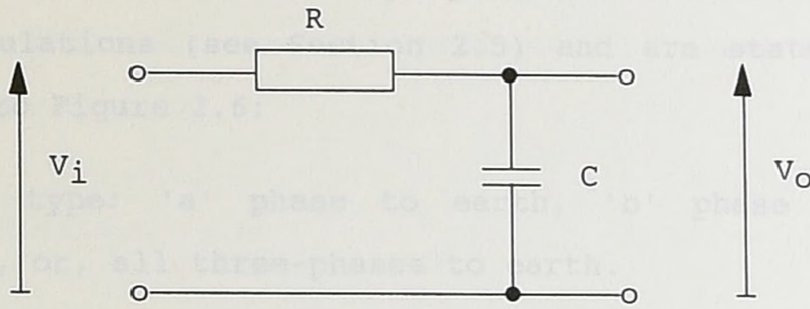


Figure A4.1 Impulse response of simulated AA filter

APPENDIX 5

Derivation of the recursive digital implementation  
of a simple R-C circuit



Analysing the above circuit,

$$\frac{V_i - V_o}{R} = C \cdot \frac{dV_o}{dt}$$

Therefore,

$$CR \cdot \frac{dV_o}{dt} + V_o = V_i \quad \dots\dots\dots A5.1$$

Taking the Laplace transform of Equation A5.1 gives,

$$V_o(sCR + 1) = V_i$$

Hence,  $H(s) = \frac{V_o}{V_i} = \frac{1}{sCR+1} = \frac{a}{s+a}$  where  $a = \frac{1}{CR}$

Transforming back into the time domain gives,

$$H(t) = a \cdot \exp\{-at\}$$

Setting the digital and analogue impulse responses equal,

$$a \cdot \exp\{-at\} = a \cdot \exp\{-anT\}$$

Therefore,  $H(n) = a \cdot \exp\{-anT\} \quad \dots\dots\dots A5.2$

Taking the z transform of Equation A5.2,

$$H(z) = a \cdot \sum_{n=0}^{\infty} \exp\{-anT\} \cdot z^{-n} = a \cdot \sum_{n=0}^{\infty} [\exp\{-aT\} \cdot z^{-1}]^n$$

Therefore,  $H(z) = \frac{a}{1 - \exp\{-aT\} \cdot z^{-1}} = \frac{Y(z)}{X(z)}$

Hence,  $y(n) - \exp\{-aT\} \cdot y(n-1) = a \cdot x(n)$

And thus,  $y(n) = \exp\{-aT\} \cdot y(n-1) + a \cdot x(n)$

## APPENDIX 6

### Programmable parameters for primary system simulations

The following parameters are programmable in both primary system simulations (see Section 2.5) and are stated with reference to Figure 2.6:

**Fault type:** 'a' phase to earth, 'b' phase to 'c' phase, or, all three-phases to earth.

**Line length:** measured in kilometres from P to Q.

**Source SCL:** specified individually at P and Q, measured in GVA.

**Distance to fault:** measured in kilometres from P.

**Load angle:** measured in degrees. A positive angle denotes that the voltage at busbar P leads the voltage at busbar Q. Thus, the power flow is from P to Q.

**Prefault time:** measured in ms. Normally 60ms or 3 cycles at 50Hz power system frequency.

**Source X/R ratio:** set to 15.

**Source  $Z_0/Z_1$  ratio:** set to 0.5.

The following parameters are programmable only in the distributed parameter simulation:

**Line configuration:** see Appendix 7.

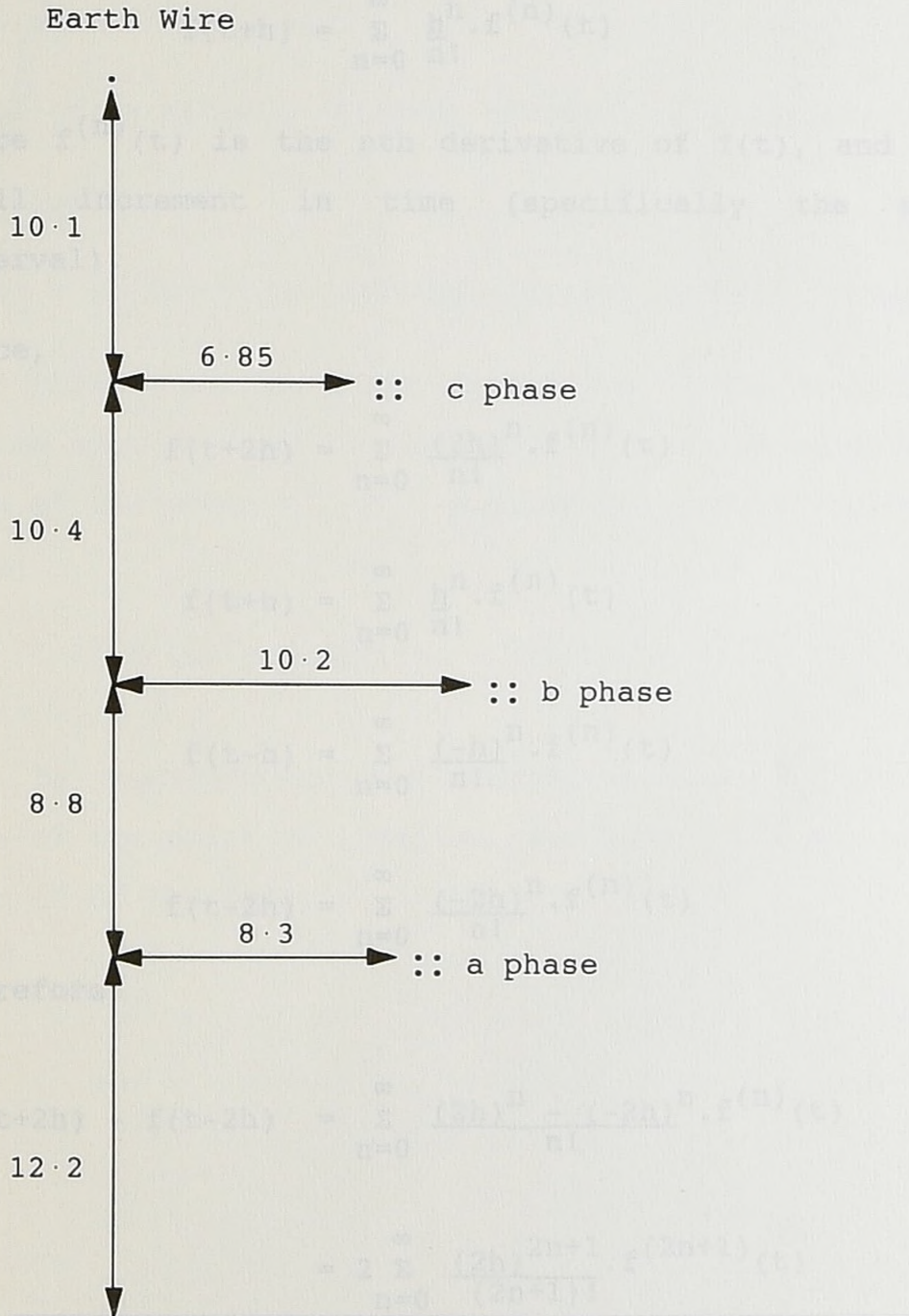
The following parameters are programmable only in the lumped parameter simulation:

**Harmonic level:** any combination of 3rd, 5th or 7th harmonic. Expressed as a percentage of the source voltage (i.e. not the busbar voltage) at P.

APPENDIX 7

400kV line configuration

The following 400kV, single circuit line configuration was used in the distributed parameter primary system simulation:



All dimensions in metres.

Similarly,

APPENDIX 8

## Formulation of the current derivative

For any infinitely differentiable function,  $f(t)$ , such as a power system current with or without harmonics, it can be written that:

$$f(t+h) = \sum_{n=0}^{\infty} \frac{h^n}{n!} \cdot f^{(n)}(t)$$

where  $f^{(n)}(t)$  is the  $n$ th derivative of  $f(t)$ , and  $h$  is a small increment in time (specifically the sampling interval).

Hence,

$$f(t+2h) = \sum_{n=0}^{\infty} \frac{(2h)^n}{n!} \cdot f^{(n)}(t)$$

$$f(t+h) = \sum_{n=0}^{\infty} \frac{h^n}{n!} \cdot f^{(n)}(t)$$

$$f(t-h) = \sum_{n=0}^{\infty} \frac{(-h)^n}{n!} \cdot f^{(n)}(t)$$

$$f(t-2h) = \sum_{n=0}^{\infty} \frac{(-2h)^n}{n!} \cdot f^{(n)}(t)$$

Therefore,

$$\begin{aligned} f(t+2h) - f(t-2h) &= \sum_{n=0}^{\infty} \frac{(2h)^n - (-2h)^n}{n!} \cdot f^{(n)}(t) \\ &= 2 \sum_{n=0}^{\infty} \frac{(2h)^{2n+1}}{(2n+1)!} \cdot f^{(2n+1)}(t) \\ &= 2 \left[ 2h \cdot f' + \frac{8h^3}{3!} \cdot f''' + K_1(t) \cdot h^5 \right] \end{aligned}$$

Similarly,

$$f(t+h) - f(t-h) = 2 \left[ h.f' + \frac{h^3}{3!}.f''' + K_2(t).h^5 \right]$$

Hence,

$$8\{f(t+h)-f(t-h)\} - \{f(t+2h)-f(t-2h)\} = 2[6h.f'(t) + K_3(t).h^5]$$

Thus,

$$12h.f'(t) = f(t-2h) - 8f(t-h) + 8f(t+h) - f(t+2h) - K_4(t).h^5$$

And finally,

$$f'(t) = \frac{1}{12h}\{f(t-2h) - 8f(t-h) + 8f(t+h) - f(t+2h)\} + K_5(t).h^4$$

This shows that the first derivative of the function  $f(t)$  may be approximated by the above expression with an error term of the order  $h^4$ . By a similar analysis it can be shown that:

$$f'(t) = \frac{1}{2h}\{f(t+h) - f(t-h)\} + K_6(t).h^2$$

i.e. by approximating the derivative using a point either side of the point of interest (see Equation 4.8), the error term is of the order  $h^2$ .

Thus, a distance relay may be compensated such that it measures only the positive phase sequence line impedance for an earth fault, by adding a factor,  $K_{res}$ , of the residual current to the line current.

## APPENDIX 9

### Derivation of the residual compensation factor

For a single phase to earth fault involving, say, the 'a' phase, the line current,  $I_a$ , measured by the relay is given by,

$$I_a = I_{a1} + I_{a2} + I_{a0}$$

and the measured phase voltage,  $V_a$ , is given by

$$V_a = \alpha Z_{11} \cdot I_{a1} + \alpha Z_{12} \cdot I_{a2} + \alpha Z_{10} \cdot I_{a0}$$

Since, for a transmission line,  $Z_{11} = Z_{12}$ , it may be written,

$$V_a = \alpha Z_{11} [I_{a1} + I_{a2} + I_{a0}] - \alpha Z_{11} \cdot I_{a0} + \alpha Z_{10} \cdot I_{a0}$$

And thus,

$$V_a = \alpha Z_{11} \cdot I_a + \alpha Z_{11} \cdot I_{a0} \cdot [(Z_{10}/Z_{11}) - 1]$$

Hence, letting,

$$K_{res} = 1/3 \cdot [(Z_{10}/Z_{11}) - 1]$$

and, 
$$I_{res} = 3 \cdot I_{a0} = I_{a0} + I_{b0} + I_{c0}$$

It follows that,

$$V_a = \alpha Z_{11} \cdot I_a + \alpha Z_{11} \cdot K_{res} \cdot I_{res}$$
$$\Rightarrow \frac{V_a}{I_a + K_{res} \cdot I_{res}} = \alpha Z_{11}$$

Thus, a distance relay may be compensated such that it measures only the positive phase sequence line impedance for an earth fault, by adding a factor,  $K_{res}$ , of the residual current to the line current.

APPENDIX 10

Relationship between D and the current magnitude

From Equation 3.4,

D = i\_r1.i\_r2' - i\_r1'.i\_r2

where i\_r1 and i\_r2 are time displaced instantaneous values of i\_r, and i\_r1' = d(i\_r1)/dt.

Let, i\_r1 = I\_max.Sin wt

and i\_r2 = I\_max.Sin(wt-phi)

where phi is the angular displacement between i\_r1 and i\_r2.

Hence, i\_r1' = omega . I\_max . Cos wt

and i\_r2' = omega . I\_max . Cos (wt-phi)

Thus, D = I\_max . Sin wt . omega . I\_max . Cos (wt-phi) - I\_max . Sin (wt-phi) . omega . I\_max . Cos wt

=> D = omega . I\_max^2 . Sin wt . [Cos wt . Cos phi + Sin wt . Sin phi] - omega . I\_max^2 . Cos wt . [Sin wt . Cos phi - Sin phi . Cos wt]

=> D = omega . I\_max^2 . Sin^2 wt . Sin phi + omega . I\_max^2 Cos^2 wt . Sin phi

Therefore,

D = omega . I\_max^2 . Sin phi .....A10.1

Note, from Section 3.3.3, phi, the angular displacement between solutions is given as 27°.

In order to relate D to a value of I\_max measured in secondary amperes, there are several factors to be considered. Firstly, it is necessary to calculate the value of 1 quantisation level (QL) for the current channel. The

## Appendix 10

scaling factor for the current channel was given in Appendix 3 as 0.2474; this relates the secondary current to the relay signal voltage level which is bounded in the range  $\pm 10V$ . The relay signal voltage is converted by a 14 bit ADC and thus +10V corresponds to  $2^{13}-1$  QLs. Hence,

$$1QL \equiv \frac{10}{0.2474 \cdot 8191} = 0.00493 \text{ Asec}$$

Secondly, before D is calculated, the current is filtered by the prefilter and thus, the gain of this filter must be taken into account. The 50Hz gain was measured to be 2.668. Note that this figure is different from the gain shown in Figure 4.4 since it takes into account an extra factor of 1.5, introduced to provide better resolution when the input signals are at their minimum level, and the effect of quantising the prefilter coefficients.

Thirdly, the current derivative, as described in Section 4.5, has a denominator term of  $12h$ , where  $h$  is the time interval between samples, implied in the calculation. This is to say that the current derivative value calculated by the relay should be divided by  $12h$  in order to conform to Equation 3.4 and, eventually, Equation A10.1. For a 4kHz sampling frequency,  $h$  is 0.00025 seconds.

Taking all the aforementioned points into consideration, and re-expressing Equation A10.1 with  $I_{\max}$  as the leading term measured in secondary amperes,

$$I_{\max} = \frac{\sqrt{D}}{\sqrt{(\omega \cdot \sin\phi \cdot 12h)}} \cdot \frac{0.00493}{2.668}$$

Hence,

$$\underline{\underline{I_{\max} = 0.002828 \cdot \sqrt{D} \text{ Asec}}}$$

APPENDIX 11

Impedance measured by relay for single phase to earth fault

From the sequence component diagram given in Figure 6.3, assuming the relay to be at busbar P and the fault to be on the 'a' phase, the faulted phase voltage,  $V_a$ , is given by,

$$V_a = V_{p1} + V_{p2} + V_{p0} \dots\dots\dots A12.1$$

Thus, summing the voltages comprising  $V_{p1}$ ,

$$V_{p1} = I_{p1} \cdot \alpha Z_{11} + I_{p2}(Z_{sp2} + \alpha Z_{12}) + I_{p0}(Z_{sp0} + \alpha Z_{10}) + 3I_f \cdot R_f \dots\dots A12.2$$

However, by inspection of the nps and zps networks, it is evident that,

$$V_{p2} = -I_{p2} \cdot Z_{sp2} \quad \text{and} \quad V_{p0} = -I_{p0} \cdot Z_{sp0} \dots\dots A12.3$$

Thus, substituting Equations A12.3 into Equation A12.2,

$$V_{p1} + V_{p2} + V_{p0} = I_{p1} \cdot \alpha Z_{11} + I_{p2} \cdot \alpha Z_{12} + I_{p0} \cdot \alpha Z_{10} + 3 \cdot I_f \cdot R_f$$

And hence, using Equation A12.1,

$$V_a = I_{p1} \cdot \alpha Z_{11} + I_{p2} \cdot \alpha Z_{12} + I_{p0} \cdot \alpha Z_{10} + 3 \cdot I_f \cdot R_f$$

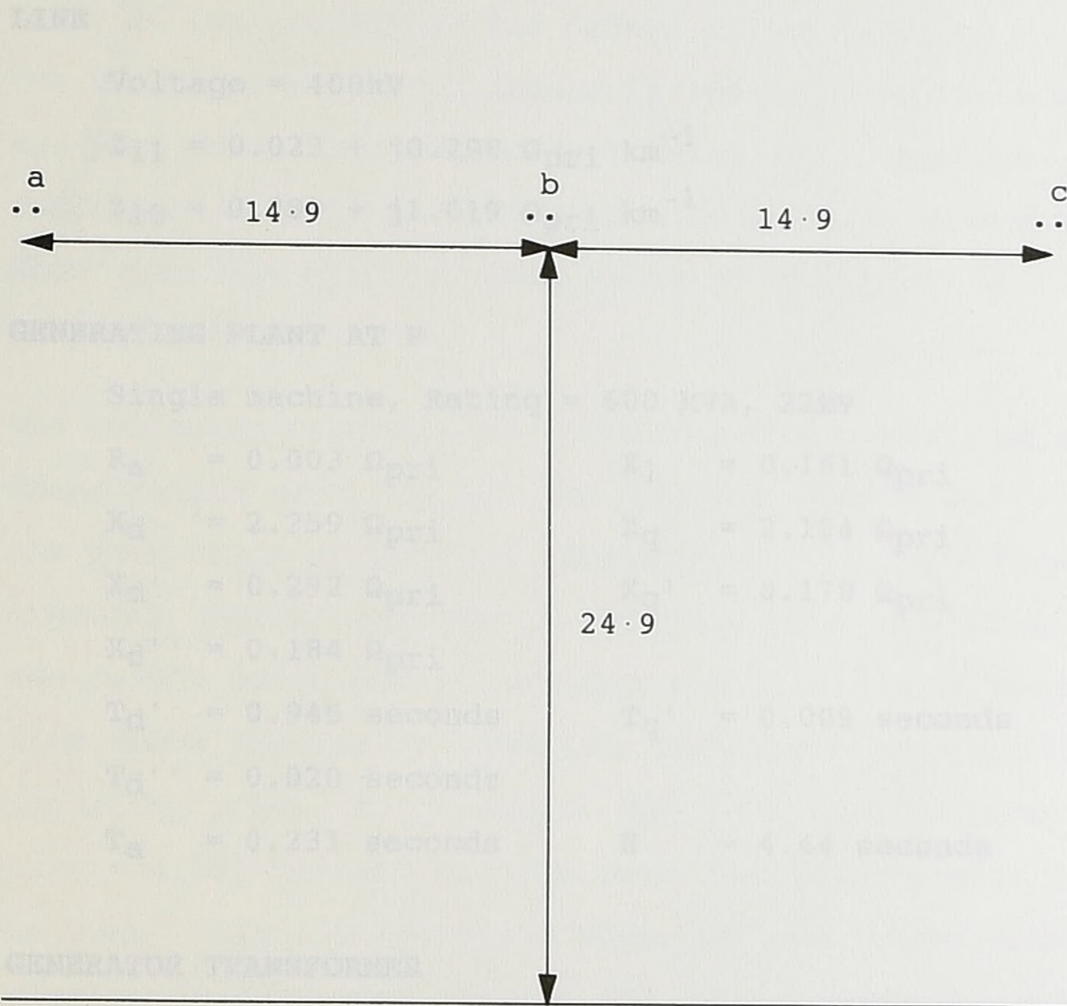
From Appendix 9, it was described that the relay is residually compensated for single phase to earth faults, and so, when fault resistance is included, the relay will measure,

$$\frac{V_a}{I_a + K_{res} \cdot I_{res}} = \alpha Z_{11} + \frac{3I_f \cdot R_f}{I_a + K_{res} \cdot I_{res}}$$

## APPENDIX 12

### 220kV line configuration

The application study used for examining the high resistance earth faults was based on a 220kV single circuit line with no earth wire [19]. The physical arrangement of the conductors is as follows:



All dimensions in metres.

A line of 10km in length was simulated using the lumped parameter simulation. The sequence parameters used were

$$Z_{11} = 0.408 + j3.86 \Omega_{\text{pri}}$$

$$Z_{10} = 1.818 + j12.1 \Omega_{\text{pri}}$$

## APPENDIX 13

### Parameters for power swing study

The system configuration used to study power swings is shown in Figure 7.2. The parameters used in the simulation program [37] are as follows.

#### LINE

Voltage = 400kV

$$Z_{11} = 0.023 + j0.298 \Omega_{\text{pri}} \text{ km}^{-1}$$

$$Z_{10} = 0.388 + j1.019 \Omega_{\text{pri}} \text{ km}^{-1}$$

#### GENERATING PLANT AT P

Single machine, Rating = 600 MVA, 22kV

$$R_a = 0.003 \Omega_{\text{pri}}$$

$$X_l = 0.161 \Omega_{\text{pri}}$$

$$X_d = 2.259 \Omega_{\text{pri}}$$

$$X_q = 2.194 \Omega_{\text{pri}}$$

$$X_d' = 0.292 \Omega_{\text{pri}}$$

$$X_q' = 0.178 \Omega_{\text{pri}}$$

$$X_d'' = 0.184 \Omega_{\text{pri}}$$

$$T_d' = 0.945 \text{ seconds}$$

$$T_q' = 0.009 \text{ seconds}$$

$$T_d'' = 0.020 \text{ seconds}$$

$$T_a = 0.231 \text{ seconds}$$

$$H = 4.44 \text{ seconds}$$

#### GENERATOR TRANSFORMER

Rating 600 MVA, 22kV/432kV(+2%, -15%)

$$Z = 0.0018 + j0.163 \text{ p.u.}$$

## APPENDIX 14

### Behaviour of $\sigma$ during three-phase fault conditions

In section 7.3.5, it is proposed that the relay differentiates between three-phase faults and power swings by checking for the maximum value that  $\sigma$ , a function of the change in instantaneous impedance, attains during the group delay of the prefilter. The change in the value of  $\sigma$  arises due to the prefilter transiently containing both prefault and post fault information just after the inception of the fault;  $\sigma$  is defined by Equation 7.1. This Appendix will show what the smallest peak value of  $|\sigma|$  is under three-phase fault conditions.

The following results were obtained from a study of three-phase faults on a 100 km, 400 kV line. Figure A14.1 shows the peak value of  $|\sigma|$ ,  $|\hat{\sigma}|$ , for each of the phase elements, observed during the group delay of the prefilter. The source SCL was 0.5GVA, the fault was located 30% along the line from the relay position and there was full load importing prior to the fault. The results of Figure A14.1 show how  $|\hat{\sigma}|$  varies with the fault inception angle; it can be seen that the general shape of the curve for each element is the same, but a  $60^\circ$  phase shift is observed between curves. Since all the elements are involved in indicating a three-phase fault, only the maxima of  $|\hat{\sigma}_{ab}|$ ,  $|\hat{\sigma}_{bc}|$  and  $|\hat{\sigma}_{ca}|$  need be considered at any point in time. For brevity, the following definition is introduced,

$$\hat{\sigma}_{\max} = \text{Maxima}(|\hat{\sigma}_{ab}|, |\hat{\sigma}_{bc}|, |\hat{\sigma}_{ca}|)$$

Figure A14.2a shows  $\hat{\sigma}_{\max}$  calculated from the results of

Figure A14.1. Figures A14.2b and c show  $\hat{\sigma}_{\max}$  for source SCL's of 5GVA and 50GVA; the fault position and prefault load flow remain the same as for Figure A14.1. Note how the mean value of  $\hat{\sigma}_{\max}$  decreases with increasing source SCL. The minimum value of  $\hat{\sigma}_{\max}$  from Figure A14.2 is 0.54. This is observed at a fault inception angle of  $45^\circ$  when the SCL was at the maximum value considered in this work of 50GVA.

The sensitivity of  $\hat{\sigma}_{\max}$  versus prefault load flow is shown in Figure A14.3a for a fault angle of  $45^\circ$ , SCL of 50GVA and fault position of 30%. It can be seen from Figure A14.3a that the minimum value of  $\hat{\sigma}_{\max}$  occurs at a load angle of  $-13^\circ$  which is equivalent to full load importing to the relay location and is the prefault load flow condition considered earlier.

All the results so far have been carried out at a fault position of 30% of the line length from the relay. Using the system conditions which have previously resulted in the minimum value of 0.54 for  $\hat{\sigma}_{\max}$ , a check was made on how the fault position changes this minimum; this is shown in Figure A14.3b. It will be evident from Figure A14.3b that moving the fault closer to the relay location leads to a decrease in  $\hat{\sigma}_{\max}$ .

Results are not shown for close-up faults since current clipping was observed to occur if the fault was closer than 16% of the line length from the relay;  $\hat{\sigma}_{\max}$  is 0.5 at this point. It was described in Section 5.6.3 how the relay operates under current clipping conditions. It is assumed here that a power swing will not result in current clipping. With this point in mind it may further be assumed

that a relay trip initiated by the current clipping mechanism of Section 5.6.3 is not inhibited by the power swing blocking approach discussed in Section 7.3.5. Thus, in evaluating the minimum value of  $\hat{\sigma}_{\max}$  which will enable the relay to differentiate between a three-phase fault and a power swing, it is not necessary to consider values of  $\hat{\sigma}_{\max}$  which are also accompanied by current clipping.

Hence, it may be concluded from the foregoing that the minimum value of  $\hat{\sigma}_{\max}$  observed during the prefilter group delay of any three-phase fault, which does not cause current clipping, is 0.5.

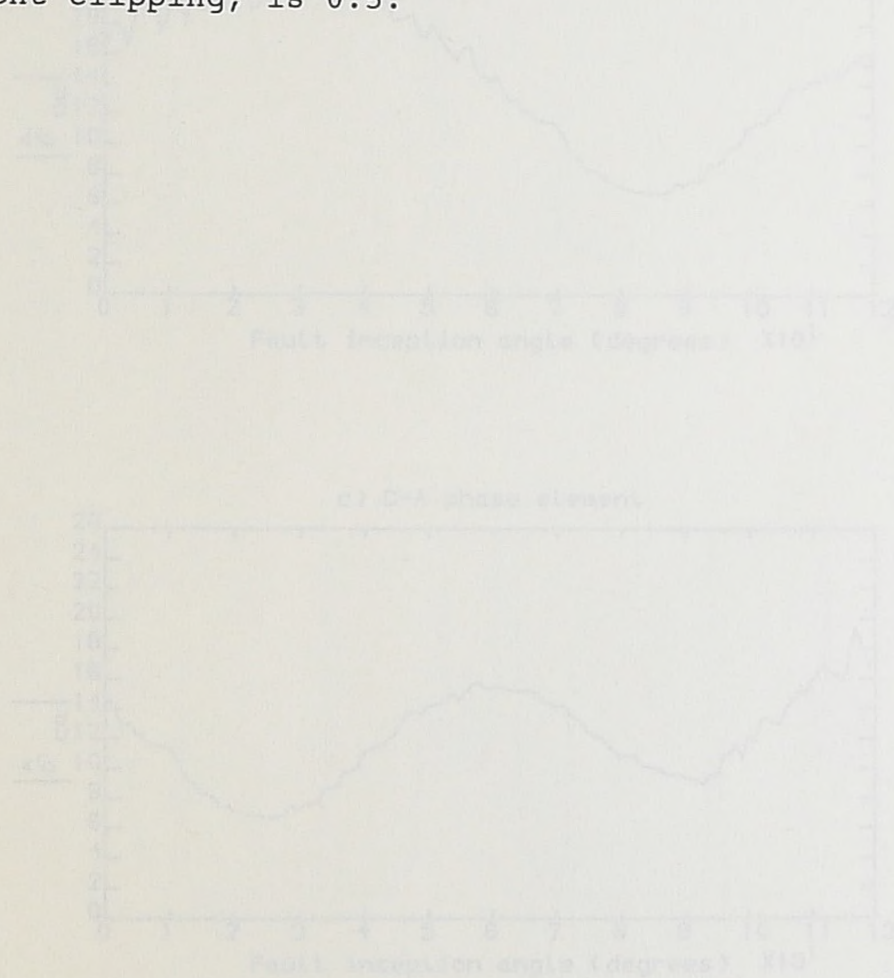


Figure A14.1 Variation of  $\delta$  versus fault angle for each phase element.

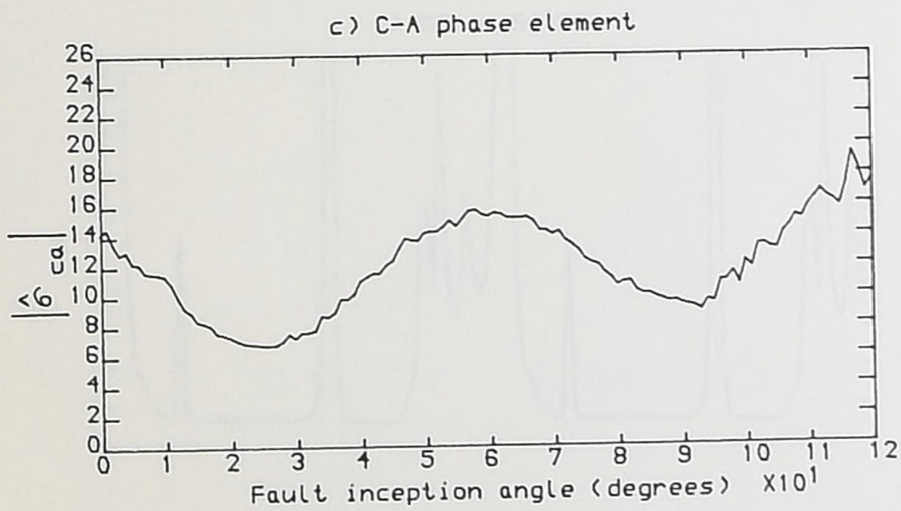
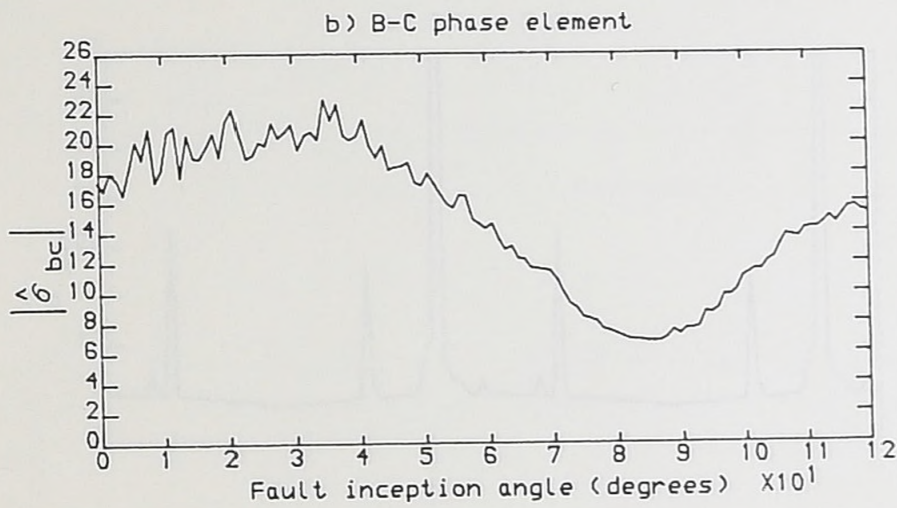
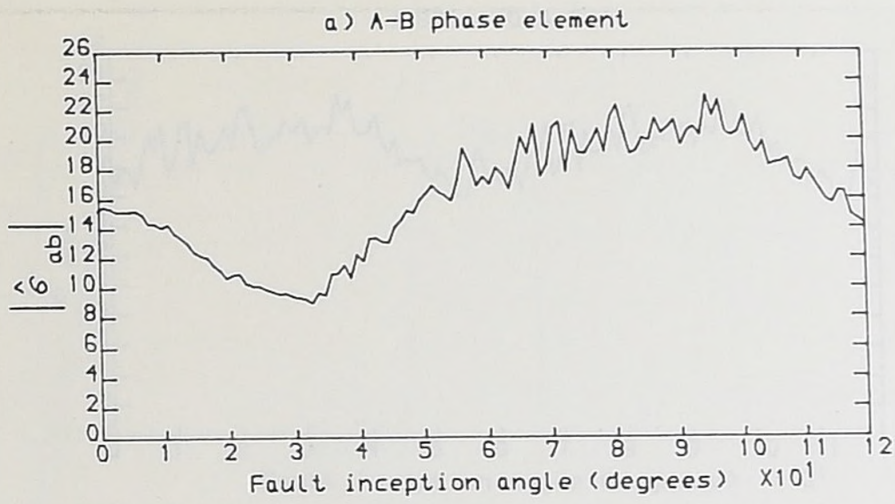


Figure A14.1 Variation of  $\hat{\sigma}$  versus fault angle for each phase element.

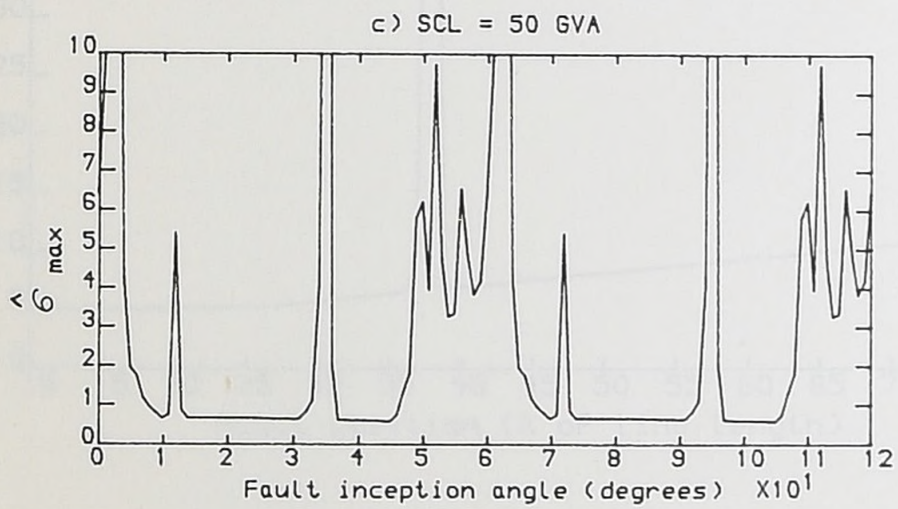
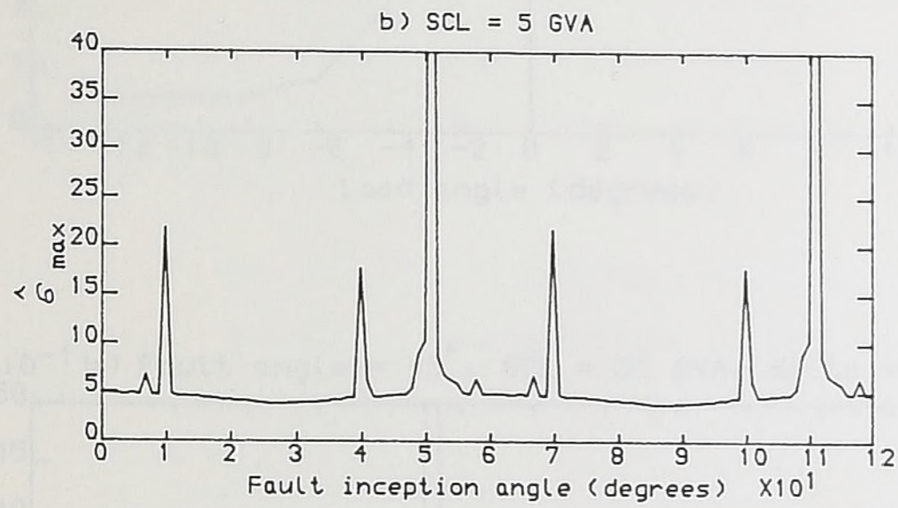
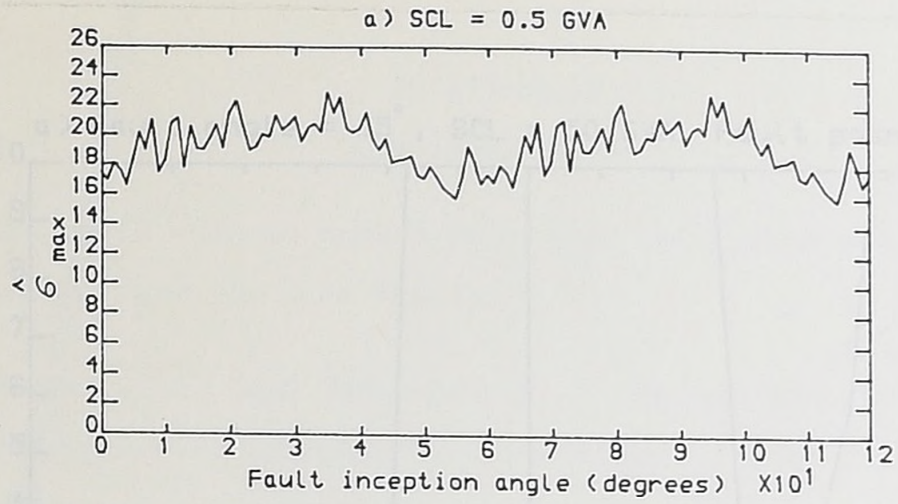


Figure A14.2 Variation of  $\hat{\sigma}_{max}$  versus fault angle for different values of SCL.

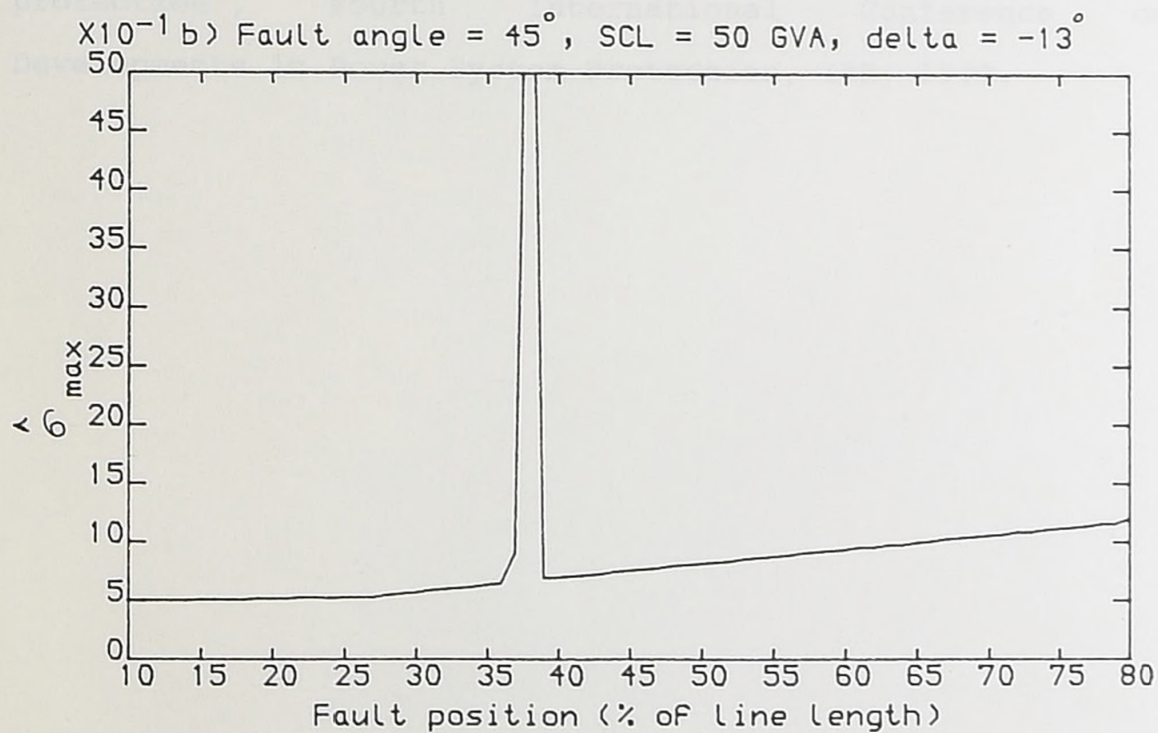
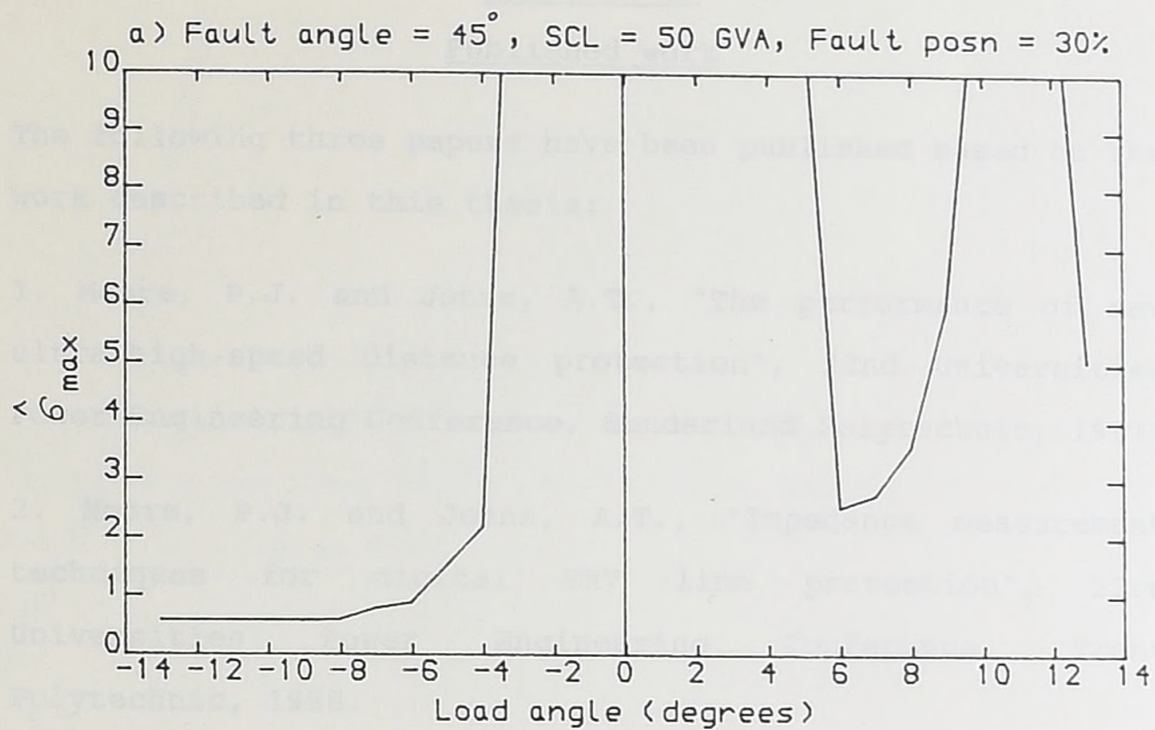


Figure A14.3 Variation of  $\hat{\sigma}_{\max}$  versus a) Load angle, and b) Fault position.

APPENDIX 15

Published work

The following three papers have been published based on the work described in this thesis:

1. Moore, P.J. and Johns, A.T., "The performance of new ultra-high-speed distance protection", 22nd Universities Power Engineering Conference, Sunderland Polytechnic, 1987.
2. Moore, P.J. and Johns, A.T., "Impedance measurement techniques for digital EHV line protection", 23rd Universities Power Engineering Conference, Trent Polytechnic, 1988.
3. Moore, P.J. and Johns, A.T., "Adaptive digital distance protection", Fourth International Conference on Developments in Power System Protection, IEE, 1989.

The published works described on p.156  
have been removed for copyright reasons



UNIVERSITY OF SHEFFIELD, SHEFFIELD, S10 2TN

F. J. BERRY AND A. T. JONES

City Road, London, W1

ABSTRACT

The following paper was presented to the 23rd Universities Power Engineering Conference at Trent Polytechnic, 20th - 22nd September 1988.

INTRODUCTION

While conventional static state predictor models are usually based on linear models, several researches have pointed out that it is not possible to model the system with an accuracy which is high enough to allow the use of such models. In order to overcome this difficulty, it is suggested that the impedance prediction is made as a function of the system state.

The approximate method of calculating the  $Z$  and  $X$  components of the system impedance is to solving the matrix equation described by Jones and Berry (1):

$$Z = Z_0 + \frac{1}{s} \frac{dZ_0}{ds}$$

where  $Z_0$  is the impedance at  $s=0$  and  $s$  is the Laplace transform variable.

The  $Z$  and  $X$  values can be calculated as:

$$Z = \frac{1}{s} \frac{dZ_0}{ds} + Z_0$$

$$X = \frac{1}{s} \frac{dX_0}{ds} + X_0$$

The derivatives  $\frac{dZ_0}{ds}$  and  $\frac{dX_0}{ds}$  can be calculated by the method of residues. Note that the calculation of  $Z$  is really a calculation of the line impedance,  $Z$  being found using an assumed value of power factor transient.

This paper will describe, and compare the results of, the method of solving equation (1). The first method uses orthogonal filters to provide the derivatives and the second method uses a series of approximations.

THE APPROXIMATION

The first method described has been described as a fast computer using infinite series. The approximation has been explained such that it enables the analysis of  $Z$  in the microprocessor which will be considered the hardware realization of the system. The paper compares the phase voltages and the line currents at a rate that the line voltage samples is 0.75  $\mu$ s.

REFERENCES

1. Jones, F. J. and Berry, A. T. (1988)

Further developments in the prediction of the system impedance. In Proceedings of the 23rd Universities Power Engineering Conference, Trent Polytechnic, 20th - 22nd September 1988.

APPENDIX

Fig. 1

It will be shown in Fig. 1, a typical system impedance response is obtained by using the method.

Reference 1 shows that the impedance  $Z$  is a function of the system state. The method of solving equation (1) is to solve the matrix equation described by Jones and Berry (1):

To calculate the  $Z$  and  $X$  values and compare the results of the method. The method uses the form of orthogonal filters and the results are compared with the results of the method. The results are compared with the results of the method. The results are compared with the results of the method.



Figure 1. Comparison impedance using orthogonal filters

The following paper was presented to the IEE Fourth International Conference on Developments in Power System Protection at the University of Edinburgh, 11th - 13th April 1989.

## REFERENCES

1. MANN, B.J., "Real time computer calculation of the impedance of a faulted single-phase line", Elec. Engg. Trans. I.E.Aust., Vol. EE5, No.1, March, 1969, pp26-8.
2. McINNES, A.D., and MORRISON, I.F., "Real time calculation of resistance and reactance for transmission line protection by digital computer", Elec. Engg. Trans. I.E.Aust., March 1971, pp.16-23.
3. RANJBAR, A.M., and CORY, B.J., "An improved method for the digital protection of high voltage transmission lines", IEEE Trans. on Power Apparatus and Systems, Vol. PAS-94, No.2, March/April 1975, pp.544-550.
4. HOPE, G.S. and UMAMAHESWARAN, V.S., "Sampling for computer protection of transmission lines", IEEE Trans. on Power Apparatus and Systems, Vol. PAS-93, No. 5, Sept/Oct 1974, pp. 1522-1534.
5. HOPE, G.S., MALIK, O.P. and RASMY, M.E., "Digital transmission-line protection in real time", IEE Proc., Vol. 123, No. 12, December 1976.
6. RANJBAR, A.M. and CORY, B.J., "Filters for digital protection of long transmission lines", IEEE PES Summer Meeting, Vancouver, British Columbia, Canada, July 15-20, 1979.
7. JOHNS, A.T., and MARTIN, M.A., "New Ultra-High-Speed distance protection using Finite-Transform Techniques", IEE Proc., Vol.130, Pt.C, No.3, May 1983.
8. JEYASURYA, B., and SMOLINSKI, W.J., "Identification of a best algorithm for digital distance protection of transmission lines", IEEE Trans on Power Apparatus and Systems, Vol.PAS-102, No.10, October 1983, pp.3358-69.

## References

9. ALEGRIA, C.M., MALIK, O.P., and COSTA, E., "Performance comparison of fourier and Kalman filter techniques for transmission line impedance calculation", IEE "Third International conference on developments in power system protection", London, April 17 - 19, 1985.
10. HOROWITZ, S.H., PHADKE, A.G. and THORP, J.S., "Adaptive transmission system relaying", IEEE PES Summer Meeting, San Francisco, California, July 12 - 17, 1987.
11. ROCKEFELLER, G.D., WAGNER, C.L., LINDERS, J.R., HICKS, K.L. and RIZY, D.T., "Adaptive transmission relaying concepts for improved performance", IEEE PES Summer Meeting, San Francisco, California, July 12 - 17, 1987.
12. SHAH, K.R., DETJEN, E.R. and PHADKE, A.G., "Feasability of adaptive distribution protection system using computer overcurrent relaying concept", IEEE Rural Electric Power Conference, San Antonio, Texas, May 3 - 5, 1987.
13. IEEE Tutorial Course, Microprocessor Relays and Protection Systems, IEEE Publication No. 88EH0269-1-PWR, 1987.
14. THE TMS32025 USERS GUIDE, Texas Instruments, 1985.
15. "Fiber optic channels for protective relaying", A report prepared for the IEEE Power System Relaying Committee by the Fiber Optics Relay Channels Working Group, IEEE PES Winter Meeting, January 31 - February 5, 1988.

## References

16. HICKS, K.L. and BUTT, W.H., "Feasability and economics of ultra-high-speed fault clearing", IEEE Trans. on Power Apparatus and Systems, Vol. PAS-99, No. 6, Nov/Dec, 1980, pp. 2138-2145.
17. ZHANG, Z. and CHEN, D., "An adaptive approach in digital distance protection", IEEE PES Winter Meeting, New York, New York, January 31 - February 5, 1988.
18. BENMOUYAL, G., "An adaptive sampling-interval generator for digital relaying", IEEE PES Winter Meeting, New York, New York, January 29 - February 3, 1989.
19. JOHNS, A.T. and EL-ALAILY, A.A., "New distance protective relay with improved coverage for high-resistance earth faults", Proc. IEE, Vol. 124, No. 4, April 1977, pp. 349-355.
20. WISZNIEWSKI, A., "Accurate fault impedance locating algorithm", Proc. IEE, Vol. 130, No. 6, Nov 1983, pp. 311-314.
21. LIAN, B.Z., "Digital distance protection for resistive earth fault", IEE Second International Conference on "Developments in Distribution Switchgear", London, 14-16 May, 1986.
22. IEEE Tutorial Course, Computer Relaying, IEEE Publication No. 79EH0148-07-PWR, 1979.
23. TERRELL, T.J., "Introduction to digital filters", MacMillan, 1985.
24. LYNN, P.A., "An introduction to the analysis and processing of signals", MacMillan, 1984.
25. BOZIC, S.M., "Digital and Kalman filtering", Edward Arnold, 1979.

## References

26. RABINER, L.R. and GOLD, B., "Theory and application of digital signal processing", Prentice-Hall, 1975.
27. JOHNS, A.T. and AGGARWAL, R.K., "Digital simulation of faulted ehv transmission lines with particular reference to very-high-speed protection", Proc. IEE, Vol. 123, No. 4, April 1976, pp. 353-359.
28. BARKER, A., "Wave differential protection of ehv transmission lines", PhD thesis, University of Bath, September 1984.
29. D'AMORE, D., and FERRERO, A., "A simplified algorithm for digital distance protection based on fourier techniques", IEEE/PES 1988 Winter Meeting, New York, New York, Paper no. 88 WM 117-4.
30. BARRETTA, L., D'AMORE, D., and FERRERO, A., "Analysis and simulation of algorithms for digital distance relays", L'Energia Elettrica (Italy), Vol. 63, No. 5, 1986, pp.221-230 (In Italian).
31. HORTON, J.W., "The use of Walsh functions for high speed digital relaying", IEEE PES Summer Meeting, San Francisco, USA, July 1975.
32. CROSSLEY, P.A. and MCLAREN, P.G., "Distance protection based on travelling waves", IEEE Trans. on Power Apparatus and Systems, PAS-102, No. 9, Sept 1983, pp. 2971-2983.
33. SWIFT, G.W., "The spectra of fault-induced transients", IEEE Trans. on Power Apparatus and Systems, Vol. PAS-98, No.3, May/June 1979, pp.940-947.
34. HUGHES, M.A., "Distance protection as affected by capacitor voltage transformers", Proc. IEE, Vol. 121, No. 12, Dec 1974, pp. 1557-1566.

## References

35. BRIGHAM, ORAN E., "The Fast Fourier Transform", Prentice Hall, 1974.
36. COOK, V., "Analysis of distance protection", Research Studies Press, 1985.
37. ELKATEB, M.M., "Machine fault analysis for power swing studies", Internal report no. MK0101, Power Systems Research Lab., Dept. of Electrical, Electronic and Information Engineering, City University, 1988.
38. PROTECTIVE RELAYS APPLICATION GUIDE, GEC Measurements, 1975.
39. 'QUADRAMHO' STATIC DISTANCE PROTECTION RELAY, GEC Measurements, Publication R-5580.
40. WIDROW, B. and STEARNS, S.D., "Adaptive signal processing", Prentice-Hall, 1985.